

Kinetic Removal of Various Organic Pollutants from Aqueous Solution by Adsorption on to Activated Fly Ash and Supported Catalysts

A Thesis

Submitted for the Award of

Doctor of Philosophy

Degree

In Chemistry

(Faculty of Science)

to the

UNIVERSITY OF KOTA, KOTA

By

Swarnima Agarwal



Under the supervision of

Prof. Ashu Rani

Department of Pure and Applied Chemistry
University of Kota
Kota (Rajasthan)

2017



*Dedicated
to
my family*

CERTIFICATE

I feel great pleasure in certifying that the thesis entitled “**Kinetic Removal of Various Organic Pollutants from Aqueous Solution by Adsorption on to Activated Fly Ash and Supported Catalysts**” by **Swarnima Agarwal** under my guidance.

She has completed the following requirement as per Ph.D. regulations of the University:

- a) Course work as per the university rules.
- b) Residential requirement of the university (200 days).
- c) Regularly submitted annual progress reports.
- d) Presented his work in the departmental committee.
- e) Published/accepted minimum of one research paper in a referred research journal.

I recommend the submission of thesis.

Date:

Prof. Ashu Rani
Department of Pure & Applied Chemistry
University of Kota, Kota

Candidate's Declaration

I hereby certified that the work, which is being presented in the thesis entitled **“Kinetic Removal of Various Organic Pollutants from Aqueous Solution by Adsorption on to Activated Fly Ash and Supported Catalysts”** in partial fulfillment of the requirement for the award of the Degree of Doctor of Philosophy, carried under the supervision of **Professor Ashu Rani** and submitted to the **Department of Pure & Applied Chemistry, University of Kota, Kota** represent my idea in my own words and where others ideas or words have been included, have adequately cited and referenced the original sources. The work presented in this thesis has not been submitted elsewhere for the award of any other degree or diploma from any Institutions. I also declare that I have adhered to all principles of academic honesty and integrity and have not misrepresented or fabricated or falsified any idea/data/fact/source in my submission. I understand that any violation of the above will be cause for disciplinary action by the University and can also evoke penal action from the sources which have thus not been properly cited or from whom proper permission has not been taken when needed.

Date:

Swarnima Agarwal

This is to certify that the above statement made by **Swarnima Agarwal** (Enrolment No. **F-6 ()/Res/UOK/2013/16608-09**) is correct to the best of my knowledge.

Date:

Prof. Ashu Rani
Department of Pure & Applied Chemistry
University of Kota, Kota

ACKNOWLEDGMENT

Words are often less to reveals one's deep regards. With an understanding that work like this can never be the outcome of a single person, I take this opportunity to express my profound sense of gratitude and respect to all those who helped me through the duration of this work.

First and foremost, praises and thanks to “[God](#)” for his showers of blessings, for leading me in the right path and for giving me strength to cross the toughest situations.

I avail this opportunity to extend my hearty indebtedness to my research supervisor [Prof. Ashu Rani](#) (Professor, Department of Pure and Applied Chemistry and Dean, P.G. Studies) for her inspiring guidance, untiring efforts, patience, constant motivation and regular monitoring and meticulous attention at all stages of my research work. I would also like to convey my deep regards for her apart from the subject of my research. I learnt a lot from her, which I am sure, will be useful in different stages of my life. She has provided many opportunities for me to increase my abilities as a researcher and responsibilities as a team member.

I am grateful to [Prof. P.K. Dashora](#), Vice Chancellor, [Sh. Onkar Singh](#), [Prof. Madhusudhan Sharma](#), former Vice Chancellor, [Dr. O.P. Rishi](#), Director (Research), University of Kota, Kota for allowing me to carryon my research work in his respective institute.

With the deepest sense of gratitude, I would like to thank [Dr. Manju Bala Yadav](#) and [Dr. Arun Kumar](#) (Lecturers, Government Collage, Kota) for her generous support, friendly nature, pleasant behavior. They inspired me in all the stages of my research work.

I would like to thank faculty members of Department of Pure & Applied Chemistry, University of Kota, [Dr. Niloo Chauhan](#), [Dr. Bhawani Singh](#), [Dr. Sweta Vyas](#), [Mr. Ankit Sharma](#), [Dr. Sushil Sharma](#), [Dr. Shweta Saxena](#), [Dr. Bhartiya](#)

[Sharma](#) and official staff of department, Research section and Accounts section of University of Kota, for immediate help and timely cooperation.

I am grateful to my ex-colleagues [Dr. Deepti](#), [Dr. Anita](#), [Dr. Shefali](#), my lab-mates [Sakshi](#), [Renu](#), [Khushboo](#), [Niharika](#), [Hari Om](#), [Priyanka](#), [Niranjan](#), [Rajesh](#), [Kiran](#), [Deepak](#) and [Honey](#) for their unconditional support and friendly atmosphere in the lab throughout my research career.

I would like to acknowledge, [Mr. S.N. Tiwari](#), Officer-in-Charge and [Dr. Vyom Saxena](#) former Officer-in-Charge Environmental Survey Lab, BARC, Rawatbhata for providing laboratory and analytical facilities. Special thanks to [Mr. Sourajyoti Chowdhury](#), Scientific Officer 'F', NPCIL, Rawatbhata for supporting in analytical work.

I would like to thanks Director, [CSMCRI, Bhavnagar, Gujarat](#) for Surface area and Porosimetry analysis, Director, [ISM, Dhanbad](#) for SEM(EDX) and [Mr. Tejbeer Singh](#), [Sophisticated Analytical Instrument Facility \(SAIF\), Chandigarh](#) for XRF & XRD studies.

I would like to express my sincere thank to [University Grant Commission, New Delhi, India \(UGC\)](#) for giving me [Junior and Senior Research Fellowship](#) for providing me financial and analytical support.

My deepest love to my son '[Hardik](#)' and '[Ritwik](#)', who have been marooned of all my care & attention during my research, and instead complaining for it, consoled me, motivated me, motivated me and recharged me by the divine touch of her tender fingers whenever I had felt low. If 'child is the father of man, both are my parents.

I cannot express enough thanks to my dearest and most beloved soul mate '[Ajay Garg](#)' [Scientific Officer 'F', Nuclear Power Corporation of India Ltd.], who has helped me to nurture to environment of creativity and support, without him I would have simply been unable to write this today, It was him only always standing beside me during all the moments and shades of life. It is once again the matter of

expressing emotion, feeling and gratitude in available few limited words. These words truly represent my expression, devotion and respect for my life partner.

The highest gratitude goes to my family. My family has always been a source of inspiration and encouragement. I Wish to thanks my father [Mr. Vinod Kumar Agarwal](#) and my mother [Mrs. Urmila Devi](#), whom love, teaching and support have bought me this far. I wish to thanks my younger brother [Dr. Shailesh Agarwal](#) and my loving sisters [Sweta Agarwal](#), [Dr. Shalini Agarwal](#) and [Ruchi Agarwal](#) for their affection, understanding, unconditional support and help. I would also like to express a debt of gratitude to my mother-in-law [Mrs. Shakuntala Devi](#) and father-in-law [Mr. Harish Chandra Gupta](#) for their kind support, love and wishes.

And everyone else, who kept asking me all these times ‘Have you finished your theist yet?’. Silencing that question was a prime motivation when life’s other intellectual enticements kept signing me.

Most importantly, I would like to thank again [God](#), for this blessing throughout the work.

[Swarnima Agarwal](#)

INDEX

Chapters	Page No.
Chapter 1: The Perspective	1-52
Abstract	1
1.1 Classification of organic pollutants	2
1.2 Main categories of organic pollutants, Sources & their toxic effects	4
1.3 Various treatment technologies for waste water	13
1.4 Various Adsorbents Used for Water Treatment	26
1.5 Scope of the work	40
1.6 References	41
 Chapter 2: Materials, methods and characterization techniques	 53-86
Abstract	53
2.1 Chemicals and Solutions	54
2.2 Adsorbent Materials	56
2.3 Minor Equipments	57
2.4 Characterization Techniques and Major Equipments	58
2.5 Analytical Measurements	73
2.6 Batch Experimental Programme	74
2.7 Adsorption Mechanism and Kinetics	75
2.8 Thermodynamic Studies	82
2.9 References	84
 Chapter 3: Kinetics of Adsorptive Removal of Dyes (Methylene Blue and Brilliant Green) from Aqueous Solution over Various Types of Fly Ash: Equilibrium, Kinetics, Thermodynamics and Modeling	 87-139
Abstract	87
3.1 Introduction	88
3.2 Materials and methods	90
3.3 Result and discussion	92
3.4 Conclusion	136
3.5 References	137

Chapter 4: Adsorption of Resorcinol from Aqueous Solution onto Low Cost Fly Ash (FA) and NaOH Treated Fly Ash (NaFA): Equilibrium, Kinetics, Thermodynamics and Modeling

		140-190
	Abstract	140
4.1	Introduction	141
4.2	Materials and methods	144
4.3	Result and discussion	147
4.4	Conclusion	187
4.5	References	187

Chapter 5: Adsorption of Resorcinol from Aqueous Solution onto CTAB / NaOH / Fly Ash Composites: Equilibrium, Kinetics, Thermodynamics and Modeling

		191-232
	Abstract	191
5.1	Introduction	192
5.2	Materials and methods	194
5.3	Result and discussion	196
5.4	Conclusion	230
5.6	References	231

Chapter 6: Adsorption of Tannic acid from Aqueous Solution onto Chitosan / NaOH / Fly Ash Composites: Equilibrium, Kinetics, Thermodynamics and Modeling

		233-277
	Abstract	233
6.1	Introduction	234
6.2	Materials and methods	236
6.3	Result and discussion	238
6.4	Conclusion	274
6.5	References	275

**Chapter 7: Adsorption of 4-chloro-2-methyl phenoxyacetic acid (MCPA)
from aqueous solution onto CTAB / NaOH / Fly Ash Composites:
Equilibrium, Kinetics, Thermodynamics and Modeling**

278-304

	Abstract	278
7.1	Introduction	279
7.2	Materials and methods	281
7.3	Result and discussion	282
7.4	Conclusion	302
7.5	References	302

Publications

Conferences



Chapter-1

The Perspective

ABSTRACT

Present chapter gives a review on various types of organic pollutants with a brief discussion of different techniques to remove these pollutants from effluents of many industries namely textile, paper & pulp, rubber, petrochemical and leather etc. A collection of several references is presented with details of some important adsorbent like silica, clay, zeolite, polysaccheride, low cost materials such as industrial waste viz. bottom ash, deoiled soya, baggase fly ash, red mud and coal fly ash etc. The chapter intended to give a complete survey of all published work on removal of organic pollutants from waste water by adsorption, also give a background and summary of recent important development of adsorbents by waste materials. The scope of the present work has been outlined at the end of this chapter.

Advances in technology have resulted in greater water demands for industry therefore volume of wastewater from the industries has increased tremendously, which needs treatment for economical use of industrial waste water. This wastewater contains a variety of suspended solids, oils, metals, and organics [1] making it unusable for potable and agricultural purposes. Water pollution due to organic contaminants is another serious issue because of acute toxicities and carcinogenic nature of the pollutants [2]. Presence of various hazardous contaminants like, pesticides, phenols, herbicides, organic acids, dyes, fluoride, arsenic, nitrate, sulfate, other heavy metals etc. in underground water as well as surface water has been reported from different parts of India [3-6]. In many cases, the water sources have been rendered unsafe not only for human consumption but also for other activities such as irrigation and industrial needs.

Organic pollutants is the term used when large quantities of organic compounds originates from domestic sewage, urban run-off, agriculture wastewater, sewage treatment plants and industrial effluents including food processing, pulp and paper making and aquaculture [7-9]. During the decomposition process of organic pollutants the dissolved oxygen in the receiving water may be consumed at a greater rate than it can be replenished, causing oxygen depletion and having severe consequences for the stream biota. Wastewater with organic pollutants contains large quantities of suspended solids which reduce the light available to photosynthetic organisms and, on settling out, alter the characteristics of the river bed, rendering it an unsuitable habitat for many invertebrates. Organic pollutants include pesticides, fertilizers, hydrocarbons, phenols, plasticizers, biphenyls, detergents, oils, greases, pharmaceuticals, proteins and carbohydrates. Most organic pollutants are either ionizable or non-ionizable compounds. Phenolic compounds (phenol, p-chlorophenol, bis phenol A etc.) are typical ionizable chemicals which are weakly acidic while non-ionizable organic pollutants are permanently electrically neutral because they do not possess an ionizable group like aniline, nitrobenzene, naphthalene etc [10]. Phenol and its derivatives appear to be the major organic pollutants globally in this century [11]. They, derived from industrial effluent

discharge, present an ongoing and serious threat to human health and to natural water.

1.1 Classification of organic pollutants

Organic pollutants can be broadly divided into following categories:

1.1.1 Oxygen Demanding Wastes

The wastewaters such as, domestic and municipal sewage, wastewater from food processing industries, canning industries, slaughter houses, paper and pulp mills, tanneries, breweries, distilleries, etc. have considerable concentration of biodegradable organic compounds either in suspended, colloidal or dissolved forms. These wastes undergo degradation and decomposition by bacterial activity. The dissolved oxygen available in the water body will be consumed for aerobic oxidation of organic matter present in the wastewater. Hence, depletion of the DO will be a serious problem adversely affecting aquatic life, if DO falls below 4.0 mg/L. This decrease of DO is an index of pollution due to oxygen demanding wastes [12].

1.1.2 Synthetic Organic Compounds

Synthetic organic compounds are also likely to enter the ecosystem through various manmade activities such as production of these compounds, spillage during transportation, and their different application in material production. These include synthetic pesticides, synthetic detergents, food additives, pharmaceuticals, insecticides, paints, synthetic fibers, plastics, solvents and volatile organic compounds (VOCs). Most of these compounds are toxic and bio refractory organics i.e., they are resistant to microbial degradation. Even concentrations of some of these in traces make water unfit for different uses. The detergents can form foams and volatile substances may cause explosion in sewers.

The most common organic pollutants named persistent organic pollutants (POPs). POPs are compounds of great concern due to their toxicity, persistence, long-range transport ability and bioaccumulation in animals [13], travel long distances and persist in living organisms. POPs are carbon-based chemical compounds and mixtures (twelve pollutants) that include industrial chemicals

such as polychlorinated biphenyls (PCBs) [14, 15], polychlorinated dibenzo-p-dioxins and dibenzofurans (PCDD/Fs) [16], and some organochlorine pesticides (OCPs) [17], such as hexachlorobenzene (HCB) or dichloro-diphenyl-trichloroethane (DDT) [18]. PCDD/Fs are released to the environment as by-products of several processes, like waste incineration or metal production. Polychlorinated biphenyls (PCBs) are used in the industries since 1930s which are complex mixtures of chlorobiphenyls [19]. These compounds are exceedingly persistent and their stability to chemical reagents is also high. Many of these compounds have been or continue to be used in large quantities and due to their environmental persistence, have the ability to bioaccumulate and biomagnify. The organic compounds constitute a very large group of pollutants in the wastewater.

1.1.3 Oil

Oil is a natural product which results from the plant remains fossilized over millions of years, under marine conditions. It is a complex mixture of hydrocarbons and degradable products under bacterial action, the biodegradation rate is different for different oils, tars being one of the slowest. Oil enters in to water through oil spills, leak from oil pipes, wastewater from production and refineries. Being lighter than water it spreads over the surface of water, separating the contact of water with air, hence resulting in reduction of DO. This pollutant is also responsible for endangering water birds and coastal plants due to coating of oils and adversely affecting the normal activities [20]. It also results in reduction of light transmission through surface waters, thereby reducing the photosynthetic activity of the aquatic plants. Oil includes polycyclic aromatic hydrocarbons (PAH), some of which are known to be carcinogenic [21].

1.2 Some organic Pollutants, Sources and Their Toxic Effects

There are various type of organic compound like Polycyclic aromatic hydrocarbons (PAHs), Polychlorinated Biphenyls (PCBs), pesticides, phenolic compounds, herbicides, organic acids, dyes etc. which are drain from many industries as effluent water causing several environmental issues and health hazards are well known organic pollutants. They can originate from food and

household related products, such as long chain fatty acids and their methyl and ethyl esters, originating from faeces, soaps and food oils. Being relatively hydrophobic these compounds are attached to particles, the concentration of fatty acids and esters in the unfiltered influent is more than 500µg/l. Other organic pollutants from domestic origin are the sterols from animal foods and faeces and indol from faeces. Caffeine is also found from discharges from coffee processing. Some major out of large number of organic pollutant are described in brief as follows:

1.2.1 Polycyclic Aromatic Hydrocarbons (PAHs)

Polycyclic aromatic hydrocarbons (PAHs) arise from incomplete combustion or pyrolysis of organic substances such as wood, carbon or mineral oil [22]. Such combustion processes include food preparation in households and food shops, discharge of certain petroleum products (from garages, vehicle washing and maintenance, fuel stations), discharge of storm runoff with PAHs from car exhaust particles and road runoff, and also from incomplete combustion processes in urban landfills. PAHs concentrate in sewage sludge due to their low biodegradability. Cancer, skin, lung, bladder, liver, and stomach cancers are human health risk of exposure to PAHs [23]. It has also been linked with cardiovascular disease as well as poor fetal development.

1.2.2 Polychlorinated Biphenyls (PCBs)

PCBs are another toxic compounds directly manufactured by chlorination of biphenyls for use as hydraulic liquids (hydraulic oils), emollients for synthetic materials, lubricants, impregnating agents for wood and paper, flame protective substances, carrier substances for insecticides and in transformers and condensers. These may be retained in service until the end of their useful life.

The other main sources of PCBs in the environment are combustion processes, from waste incineration plants, fossil fuel burning and to other incomplete combustion processes [24]. PCBs are adsorbed by solids and therefore they accumulate in sewage sludge. According to the U.S. Environmental Protection Agency (EPA), PCBs cause cancer in animals and are probable human

carcinogens [14]. Ortho-PCBs can disrupt thyroid hormone transport by binding to transthyretin [25].

1.2.3 Di-(2-ethylhexyl) phthalate (DEHP)

DEHP is used as emollient in synthetic materials. 90 % of DEHP is used in PVC and about 10% in laquers and paints. It is common to use DEHP as antifoaming agent in paper production, as an emulsifier for cosmetics, in perfumes and pesticides. They aid in the production of different synthetic materials such as dielectric in condensers, and substitute for substances such as PCBs and pump oil. DEHP has specific emissions from various human activities like cellulose/paper production, DEHP production, plastisol-coating process, PVC production and processing, leaching from PVC products, leaching from waste in landfills and waste incineration and uncontrolled combustion etc. DEHP is found regularly in municipal wastewater and, because of its lipophilic properties, it concentrates in sewage sludge, show many toxic effects, including increased cell proliferation, carcinogenic, decreased apoptosis, oxidative damage, and selective clonal expansion of the initiated cells; all of which take place in multiple sites of the human body [26].

1.2.4 Detergents and Foams (Anionic and Non-ionic Surfactants)

One of the main sources of organic pollution is detergents. Detergents are mainly made up by surfactants and surface-active agents, which tend to produce stable, copious foams in rivers. These foams generally form a thick and dense layer over the surface of the water, extending over several hundreds of meters of the river and sea water. These foams also prove to be an unhygienic source of domestic water. Detergents sometimes can contain suspected carcinogens, and ingredients that do not fully biodegrade.

Detergents also contain oxygen-reducing substances (“i.e.” a chemical compound that readily transfer oxygen atoms) that may cause severe damage to the fishes and marine animals. This may also lead to eutrophication, a process by which a water body becomes enriched in dissolved nutrients (e.g., phosphates, calcium and magnesium). It has negative impacts on environment, especially on aquatic animals because water rich in nutrients stimulates the growth of aquatic

plant life, resulting in depletion of oxygen. It can cause the water to grow murky thus blocking out light and disrupting the growth of plants. Turbidity also clogs the respiratory system of some species of fishes. Pathogens from these toxic water bodies bring about in human or animal hosts diseases, which may be fatal. Drinking water contaminated by detergents can be hazardous to human health [27]. Humans become ill with a range of symptoms such as skin irritation, sore throat, nausea, stomach cramps, and liver damage. This can be poisonous and accounts to death in several cases. Such contaminated water is also not preferable for the growth of crops e.g., rice, wheat and soybean.

1.2.5 Polychlorinated Dibenzop-dioxins and Dibenzofurans (PCDD/PCDF)

The generic term "dioxins" represents a mixture of 219 different polychlorinated dibenzo-p-dioxins and furans. The most well known and hazardous dioxin, is the tetrachlorodibenzo-p-dioxin (TCDD). Dioxin concentrations are calculated as sum of the toxicity equivalents (TEQ) relative to the most toxic dioxin [TCDD]. The main sources of polychlorinated dibenzo-p-dioxins and dibenzofurans are as follows [28]:

- Chemical reactions or chemical reaction processes: Dioxins arise as unwanted by products from the production or use of many organo-chlorine compounds, such as chlorine bleaching of cellulose in paper production and chlorine alkali electrolysis.
- Combustion processes or thermal processes: Dioxins arise by thermal processes like waste incineration plants and incomplete combustion processes in landfills, combustion plants, iron smelting, petrol and diesel engines and are released into the atmosphere.

The inhalation of high dose of Dioxins may cause developmental abnormalities in the enamel of children's teeth, central and peripheral nervous system pathology, thyroid disorder, damage to the immune system and diabetes in humans [29, 30].

1.2.6 Plasticisers and flame retardants

Plasticisers and flame retardants are used in many products for household and industrial applications. The organic pollutants present in these products are benzenesulphonamides, adipates (esters of hexandioic acid), phthalates (esters of phthalic acid, among which DEHP is the most common), several phosphate esters (2-chloroethanol phosphate) and TBP (tri-n-butyl phosphate) are used in flame-retardant, compositions in textiles, plastics as well as in other products. Many brominated flame retardants with aromatic rings, are reported thyroid hormone disruptors [31] and whereas plasticizers cause potential endocrine disruptors, diabetes, obesity with some developmental toxicity as reported earlier [32].

1.2.7 Preservatives and antioxidants

Preservatives and antioxidants are constituents of household and industrial products, and among the organic pollutants linked with these compounds are parabens (esters of hydroxybenzoic acid), substituted phenols and quinones. Some antioxidant supplements may promote disease and increase mortality in humans under certain conditions [33, 34].

1.2.8 Solvents

Solvents both chlorinated and non-chlorinated (alcohols, ethers, ketones) are present in a large range of products such as car shampoos, household cleaners and degreasing agents from vehicle maintenance and production. Chlorinated solvents, such as trichloroethylene and trichloroethane, are in increasingly wide use. The principal sources of diffuse pollution from chlorinated solvents are due to artisanal activities such as metal finishing activities and dry cleaners. Almost all organic solvents are poisonous if swallowed or inhaled in sufficient quantity, and most cause dermatitis after sufficient skin contact. High concentrations of most solvents can cause narcosis (dizziness, nausea, fatigue, loss of coordination, coma, and the like).

1.2.9 Pharmaceutical products

The pharmaceutical industrial discharge of active pharmaceutical ingredients (APIs) from manufacturing is considered as pharmaceutical waste. In 2007, the first in a series of papers was published showing very high emissions of

pharmaceuticals from drug manufacturers in Patancheru, near Hyderabad, India [35-37]. The concentration of ciprofloxacin, which is a broad-spectrum antibiotic, was as high as 31 mg l^{-1} [35], which is approximately one million times greater than the levels that are regularly found in treated municipal sewage effluents [38] and toxic to a range of organisms. These discharges have led to pollution of river sediment [37], surface, ground and drinking water [36] and high concentrations of degradation products from penicillin were observed at another factory [39]. The concentration of ethinyloestradiol in the treated effluent from yet another Chinese plant was 51 mg l^{-1} [40], which is considerably greater than the concentrations found in sewage effluents and is clearly high enough to disturb reproduction in aquatic vertebrates.

1.2.10 Dyes

Dyes may be defined as substances that, when applied to a substrate, provide color by a process. Such substances with considerable coloring capacity are widely employed in the textile, pharmaceutical, food, cosmetics, plastics, photographic and paper industries. Due to ever-growing demands in textiles, synthetic organic dyes are widely used for dyeing textile fibers such as cotton and polyester. Approximately 10,000 different dyes and pigments are used for industries and over 7×10^5 tons of these dyes are annually produced worldwide [41]. Dyes and pigments represent one of the problematic groups; they are emitted into wastewaters from various industrial branches, mainly from the dye manufacturing and textile finishing [42] and also from food colouring, cosmetics, paper and carpet industries. Synthetic dyes have complex aromatic structures which provide them physico-chemical, thermal and optical stability [9]. Dyes in effluents, if not removed, cause disturbance to the ecological systems of the receiving waters. These materials also pose certain health hazards and environmental pollution. The dye is considered highly toxic to humans and animals and can cause permanent injury to the eyes of humans and animals [43]. Oral consumption of the dye can cause irritation to the gastrointestinal tract and symptoms like nausea, vomiting, and diarrhea. Dyes are broadly classified as anionic, cationic, non-ionic and zwitterionic depending on the ionic charge on the dye molecules. Cationic dyes are more toxic than anionic dyes [41].

1.2.11 Phenolic Compounds

A large group of pollutants in the wastewater are of aromatic compounds especially phenol and its derivatives such as resorcinol, catechol, nitrophenols, Ortho-chloro phenol, 2,4-Dichloro phenol and cresols are widely found in the effluent of many industries [44,45]. Phenol is present in the surface water of industrial effluents such as coal tar, petrochemical, oil refineries, leather, gasoline, plastic, paint, rubber-proofing, coking, pharmaceutical and steel industries, domestic wastewaters and chemical spillage [46]. Resorcinol is found in the effluents of many industries such as textile, paper and pulp, steel, petrochemical, petroleum refinery, rubber, dyes, plastics, pharmaceutical, cosmetics etc., and in synthetic coal fuel conversion process wastewater [10]. Tannic acid is a component of natural organic matter (NOM) in surface and ground water, which is derived from the breakdown of plant biomass [47, 48]. Tannic acid is also found in wastewater discharged from coir and cork process, plant medicine, paper and leather industries [48, 49].

Phenolic compounds are very harmful to organisms even at very low concentration due to their toxicity, foul odour and carcinogenic properties [50]. The health effects following repeated exposure to low levels of phenol in water include liver damage, kidney damage, headache, fainting, diarrhoea, mouth ulcers, dark urine, impaired vision, mental disturbances and hemolytic anemia [50]. The lethal blood concentration for phenol is around 4.7-130 mg/L. Tannic acid may cause a serious problem for drinking water production because TA can form carcinogenic disinfection by-products (DBTs) such as trihalomethanes (THMs) during chlorination process [47, 48], which currently are regulated by U.S. Environmental Protection Agency (EPA) under the stage 1 Disinfectants and Disinfection By-Products (D/DBP) Rule. In addition, as a water soluble polyphenolic compound, tannic acid has toxicity for aquatic organisms such as algae, phytoplankton, fish and invertebrates [47]. Ministry of Environment and Forest (MOEF), Govt. of India, New Delhi and United States Environmental Protection Agency (USEPA) has listed phenol and phenolic compound under priority pollutants list. As per the Bureau of Indian Standards, New Delhi, India, the allowable limit of phenol in drinking water is 1mg/L while MOEF (Govt. of

India) has set a maximum concentration level of 1 mg/L of phenol in the industry effluents for safe discharge into inland surface water and 5 mg/L for safe discharge into public sewers and marine coastal areas [50]. The World Health Organization (WHO) recommended 0.001 mg/L as the permissible phenolic concentration in portable water. It is therefore necessary to reduce or to eliminate phenols from water and wastewater before discharge or reuse.

1.2.12 Organic Acid

Organic acids like Salicylic acid (o-hydroxybenzoic acid), Acetic acid, Benzoic acid etc., containing wastewater presents a serious environmental problem due to their high toxicity and accumulation in the environment [51]. Salicylic acid is widely used in many pharmaceutical, manufacturing activities of paper milling; cosmetic industries landfill leachate and cosmetic formulations, being easily produced from hydrolytic deacetylation of the common drug acetylsalicylic acid (aspirin) [52]. Salicylic acid is also a key ingredient in many skin-care ointments, creams, gels and transdermal patches. This aromatic organic compound is very toxic and can stimulate skin and mucous membrane, and reacts with protein, and can bring about tinnitus, qualm, naupathia and electrolytic turbulence [53]. Thousands of tons of pharmaceutical drugs are consumed yearly worldwide in human and veterinary medicine. Due to the inefficient destruction of these wastewaters in sewage treatment plants, these compounds have been recently detected in surface, ground and even drinking waters up to micrograms per liter [54]. The possible interactions of these pollutants with living beings in the environment indicate that some drugs can affect the endocrine system of fishes, can make toxic effects on algae and invertebrates, promote the development of multi-resistant strains of microorganisms [55] and potential adverse health effects on animals and human beings.

1.2.13 Pesticides and Herbicides

Pesticides are the major input in today's intensive agriculture. Wide spread use of these agricultural inputs has caused contamination of ground and surface water resources due to their leaching and runoff losses. Improper disposal of the empty pesticide containers, washing of spray instruments and unregulated

discharge from manufacturing units are other causes of water contamination. Many commonly used pesticides are resistant to natural degradation in the environment, hence, pose human health problems and ecotoxicity [56]. Pollutants are the triazine group, phenyl urea group (e.g. chlorotoluron, isoproturon and diuron), phenoxy acid group (eg. Mecoprop and 2,4-D) and glyphosate, DDD, DDE [57], Lindane, Malathion [58], Carbofuran [59] and TCB [60] etc. Herbicides such Diuron has been detected in surface and ground waters at levels that exceed the health-based standards. Diuron (3-[3,4-(dichlorophenyl)-1,1dimethylurea]) a substituted urea herbicide, has been widely used since the 1950s to control a variety of annual and perennial broadleaf and grassy weeds, as well as mosses [61]. Its presence in water has to be carefully controlled since it was designated as persistent organic pollutant in EU legislation [62].

Chlorophenoxy herbicides, which have potential toxicity toward humans and animals and are suspect mutagens and carcinogens, are used worldwide on a large scale as plant growth regulators for agricultural and nonagricultural purposes. Among them, 4-chloro-2-methylphenoxyacetic acid (MCPA) is used in amounts exceeding 2000 tons per year in Western European countries [63]. Furthermore, this herbicide has been classified by the U.S. Environmental Protection Agency (EPA) as a potential groundwater contaminant [64]. It is used as the dimethylammonium, potassium, or sodium-potassium salt in commercial preparations, very often formulated together with other chlorophenoxy pesticides (2, 4-D, dicamba, MCPB) and is widely used for controlling broad leaf weeds mainly in cereals, grasses, plants, tobacco and cotton [65]. However, when MCPA is used in the agricultural area, only a minor proportion reaches the target [66]. Most of it penetrates in the soil and enters the surface water as a result of runoff from agricultural land [67]. Hence, it has potential toxicity for humans and animals, such as irreversible damage to the nervous system, causes dizziness and cough after inhalation [68].

Water pollution by organic chemicals is a major problem over decades. Owing to this, there is growing concern over the removal of organic compounds from water. Due to their toxic nature and harmful effect on environment and

human beings it is necessary to understand their removal from industrial waste water. There are several methods for treatment of industrial waste water and to remove pollutants. Some of them are given below:

1.3 Various Treatment Technologies for Waste Water

A range of conventional treatment technologies for organic compounds removal have been investigated extensively, such as ultra filtration, activated sludge, ion exchange, chemical coagulation, precipitation, distillation, gas stripping, solvent extraction, chemical oxidation, complexation, bioremediation, carbon adsorption, electrochemical treatment, reverse osmosis and hydrogen peroxide catalysis. However, most of the above methods suffer from one or more limitations and none of them were successful in completely removing the organic contaminants from wastewater. The removal of all organics in an economic way remains an important problem, although a number of systems have been developed with adsorption techniques. Some of the techniques are briefly described as follows:

1.3.1 Solvent extraction method

Solvent extraction is a process for separating a substance from one or more others by using a solvent and is widely used to clean or extract harmful materials or chemical pollutants. PCBs, grease or oil are the chemicals which do not dissolve in water. But they stick or remain absorbed to the soil, sludge or sediment which pollutes the surface. The chemicals used in solvent extraction dissolve these chemical pollutants and clean the site. It relies on variations in the solubility of different compounds in different substances. In most cases, the substance to be extracted, which may be a solid, a liquid or a gas, is dissolved in a liquid, along with other substances, and a liquid solvent is used for the extraction, this is sometimes called liquid-liquid extraction. The technique may also be applied to solid materials that contain compounds that need to be extracted. This method is widely used in industry, and in the laboratory for refining, isolating and purifying a variety of useful compounds.

A solvent will be chosen that does not mix with the compound in which the substance of interest is currently dissolved, so that, when left undisturbed, they will form two separate layers, as with oil and water. It is also important that the compound to be extracted should have greater solubility in the solvent that has been added, and that this should not dissolve any unwanted substances in the original mixture. Once added, the two liquids may be shaken together for a time then allowed to stand for a while, so that they separate out. The choice of solvent to be used will depend on the chemical and physical properties of all the substances in the mixture. The process may need to be carried out in several stages, using different solvents.

One of the most widespread industrial uses of this technique is in the petrochemical refining industry. As petroleum products are processed, impurities remain in the raw products. Using suitable solvents, the useful material can be separated from the unwanted substances, and then further extraction can be used to separate out the different grades of hydrocarbons according to their uses, which may be as fuels, lubricants, or as raw materials for the chemical industry. Solvent extraction is also used in the refining of uranium for nuclear reactors. The removal of model pollutants bromocresol green and phenol from water is demonstrated via two liquid–liquid extraction methods [69].

Heavy crude oil removal from contaminated soils by the hexane - acetone solvent mixture is another application of solvent extraction technique. The mixtures of hexane and acetone (25 volume %) were demonstrated to be the most effective in removing petroleum hydrocarbons from contaminated soils and approximately 90% of saturates, naphthene aromatics, polar aromatics, and 60% of nC(7)-asphaltenes were removed [70].

Advantages

- Separation of components widely varying in their boiling points
- Extraction of thermally sensitive components
- Helpful in separation of azeotropic mixture
- Separation of single component from the multicomponents

Disadvantages

- High cost of extracting
- Appreciable solubility of solvents in water results in high solvent loss.
- The method itself can result in pollution

1.3.2 Membrane Technology

The main force of membrane technology is the fact that it works without the addition of chemicals, with a relatively low energy use and easy and well-arranged process conduction. Membrane technology is a generic term for a number of different, very characteristic separation processes. These processes are of the same kind, because in each of them a membrane is used. Membranes are used more and more often for the creation of process water from groundwater, surface water or wastewater. Membranes are now competitive for conventional techniques. The membrane separation process (Figure 1.1) is based on the presence of semi permeable membranes.

There are various methods to enable substances to penetrate a membrane. Examples of these methods are the applications of high pressure, the maintenance of a concentration gradient on both sides of the membrane and the introduction of an electric potential. Membranes occupy through a selective separation wall. Certain substances can pass through the membrane, while other substances are caught. Membrane filtration can be used as an alternative for flocculation, sediment purification techniques, adsorption (sand filters and active carbon filters, ion exchangers), extraction and distillation.

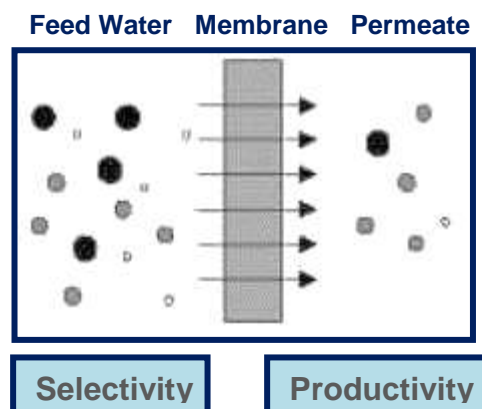


Figure 1.1: Membrane Filtration

Membrane filtration can be divided between micro and ultra-filtration on the one hand and nano filtration and Reverse Osmosis (RO or hyper filtration) on the other hand. When membrane filtration is used for the removal of larger particles, micro filtration and ultra-filtration are applied. Because of the open character of the membranes the productivity is high while the pressure differences are low. When salts need to be removed from water, nano filtration and reverse osmosis are applied. Nano filtration and RO membranes do not work according to the principle of pores; separation takes place by diffusion through the membrane. The pressure that is required to perform nano filtration and reverse osmosis is much higher than the pressure required for micro and ultra-filtration, while productivity is much lower. Application of membrane techniques for the removal of organic micro pollutants from water and wastewater are well reported [71, 72]. Different types of filtration required for separation of particles of varying sizes are shown in Figure 1.2.

Advantages:

- It is a process that can take place at low temperatures so that it enables the treatment of heat-sensitive matter.
- It is a process with low cost.
- Widely used in the food, beverage industries and dairy products.
- It is a simple and efficient technology.

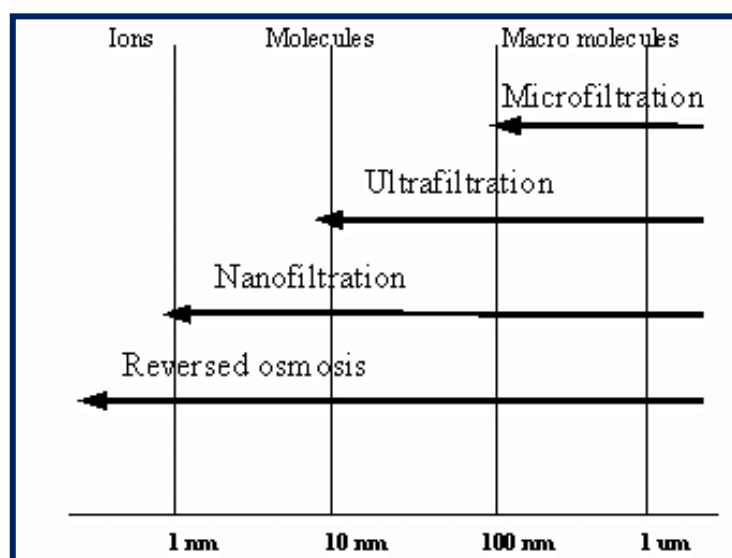


Figure 1.2: Type of filtration

Disadvantages:

- High capital cost
- Inefficient at low concentrations
- Fouling by organic materials

1.3.3 Ion exchange processes

Ion exchange is a water treatment method where one or more undesirable ionic contaminants are removed from water by exchange with another non-objectionable, or less objectionable ionic substance (Figure 1.3). Both the contaminant and the exchanged substance must be dissolved and have the same type of electrical charge (positive or negative). A typical example of ion exchange is water softening aiming to reduce calcium and magnesium content. Ion exchange process can also remove various charged atoms or molecules (ions) such as nitrates, fluoride, sulphates, perchlorate, iron and manganese ions as well as toxic metals (radium, uranium, chromium, etc.) from water.

The most typical application of ion exchange is the preparation of high purity water for industrial applications, water softening, recovery or removal of metals in the chemical industry. Synthetic and industrially produced ion exchange resins consist of small, microporous beads that are insoluble in water and organic solvents. The most widely used base-materials are polystyrene and polyacrylate.

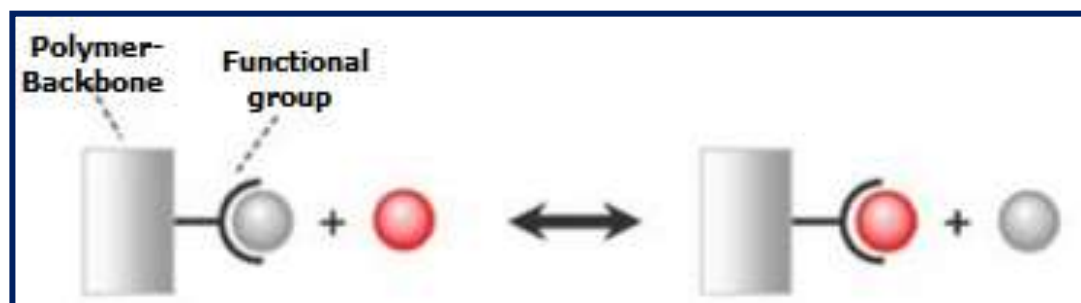


Figure 1.3: Ion Exchange Process

The binding force between the functional group and the attached ion is relatively weak. The exchange can be reversed by another ion passing across the functional group. This process can be repeated continually, with one exchange reaction following another [73].

Advantages

- One of the most appropriate technologies to removes dissolved inorganic ions effectively
- Possibility to regenerate resin
- Relatively inexpensive initial capital investment
- Use in water softening (remove calcium and magnesium ions), water demineralisation (removal of all ions), and de-alkalisation (removal of bicarbonates)
- Anionic exchange units can remove nitrate, sulfate, and other negatively charged atoms [74]
- Cation exchange resins can also remove most positively charged ions in water such as iron, lead, radium, barium, aluminium and copper among others

Disadvantages

- The process of regenerating the ion exchange beds dumps salt water into the environment (regeneration)
- Does not remove bacteria effectively
- High operation costs over long-term
- High cost of ion exchange resins
- Ineffective for nonionic pollutants

1.3.4 Biological Wastewater Treatment

Biological treatments (Figure 1.4), which use organisms to break down organic substances in wastewater, are widely used around the world. Unlike other wastewater treatments, which use only mechanical or chemical processes, biological treatments include the use of bacteria, nematodes, or other small organisms [75]. Over time, scientists have been able to control and refine both

aerobic and anaerobic biological processes to achieve the optimal removal of substances from wastewater.

Secondary Wastewater Treatment

Biological wastewater treatment is often used as a secondary treatment process, which means it is used to remove material remaining after primary treatment (the stage in which sediments or substances such as oil are removed from the wastewater). Several types of biological processes can be used to treat wastewater, including activated sludge process, constructed wetlands, and various types of filtration. These methods can be divided into aerobic and anaerobic processes.

Aerobic Wastewater Treatment

Aerobic wastewater treatment processes include treatments such as activated sludge, oxidation ditches, trickling filter, lagoon-based treatments, and aerobic digestion. Aeration is one of the first stages in the process since bacteria and other organisms require oxygen to break down organic substances in the wastewater being treated. It is particularly well suited for treating waste streams high in organic or biodegradable content. It is most often used to treat municipal sewage, wastewater generated by pulp and paper mills, food-related industries such as meat processing and any industry producing waste streams containing carbon molecules. It can be used on challenging chemicals such as methane, ammonia, iron, and manganese, as well as biodegradable organic compounds.

Anaerobic Wastewater Treatment

Anaerobic treatment is a process that uses bacteria to break down organic material in an oxygen-free environment. Lagoons and septic tanks are example implementations of these types of anaerobic treatment methods. The best known type of anaerobic treatment is anaerobic digestion. Anaerobic digestion is used for effluent treatment in food and beverage manufacturing, as well as for treatment of municipal wastewater, chemical effluent, and agricultural waste. Once the anaerobic digestion treatment process is completed, the wastewater can undergo additional treatments. For example, the remaining wastewater tends to require

additional treatment for high levels of biochemical oxygen demand (BOD) and chemical oxygen demand (COD).

Advantages

- Low capital, operation and maintenance cost
- Easy to operate and maintain
- Require relatively lesser land area
- Removes up to 70% of solids and bacteria

Disadvantages

- Incapable of effectively treating organic waste
- Ineffective in removing color, as most dyes are toxic to the organisms used
- Required large space area



Figure 1.4: Biological Water Filtration

1.3.5 Advanced oxidation process

Advanced oxidation processes (AOPs), are a set of chemical treatment procedures designed to remove organic (and sometimes inorganic) materials in water and wastewater by oxidation through reactions with hydroxyl radicals

(•OH) [76]. In real-world applications of wastewater treatment, however, this term usually refers more specifically to a subset of such chemical processes that employ ozone (O₃), hydrogen peroxide (H₂O₂) and/or UV light [77]. One such type of process is called in situ chemical oxidation.

AOPs rely on in-situ production of highly reactive hydroxyl radicals (•OH). These reactive species are the strongest oxidants that can be applied in water and can virtually oxidize any compound present in the water matrix, often at a diffusion controlled reaction speed. Consequently, •OH reacts unselectively once formed and contaminants will be quickly and efficiently fragmented and converted into small inorganic molecules. Hydroxyl radicals are produced with the help of one or more primary oxidants (e.g. ozone, hydrogen peroxide, oxygen) and/or energy sources (e.g. ultraviolet light) or catalysts (e.g. titanium dioxide). Precise, pre-programmed dosages, sequences and combinations of these reagents are applied in order to obtain a maximum •OH yield. In general, when applied in properly tuned conditions, AOPs can reduce the concentration of contaminants from several-hundred ppm to less than 5 ppb and therefore significantly bring COD and TOC down, which earned it the credit of “water treatment processes of the 21st century” [78].

The AOP procedure is particularly useful for cleaning biologically toxic or non-degradable materials such as aromatics, pesticides, petroleum constituents, and volatile organic compounds in wastewater.[79] Additionally, AOPs can be used to treat effluent of secondary treated wastewater which is then called tertiary treatment[80]. AOPs generally means application of either advanced oxidation technologies using UV/O₃, O₃/H₂O₂, UV/H₂O₂ or the photo Fenton reaction (UV/H₂O₂/Fe²⁺ or Fe³⁺). Peyton gave a detailed overview and description of AOPs [81]. Photo-Fenton processes could be applied in treating many industrial wastewaters, i.e. wastewater from plastic industry, landfill leachate, dye house industry [82], quinoline (aromatic compound) [83], pesticides [84], organic compounds and phenolic wastes [85], trichloroethylene trihalomethanes [86], and wastewater from paper industry.

Advantages

- It can effectively eliminate organic compounds in aqueous phase.
- It can remove various type of organic pollutants at the same time due to the remarkable reactivity of $\bullet\text{OH}$.
- Some heavy metals can also be removed in forms of precipitated $\text{M}(\text{OH})_x$.

Disadvantages

- Difficult to scale up
- Expensive method
- Formation of by-product
- Secondary treatment is required for complete waste water treatment

1.3.6 Coagulation-flocculation process

In water treatment, coagulation is a process that occurs when a coagulant is added to water to "destabilize" colloidal suspensions. Conversely, flocculation involves the addition of polymers that clump the small, destabilized particles together into larger aggregates so that they can be more easily separated from the water. Coagulation is a chemical process that involves neutralization of charge whereas flocculation is a physical process and does not involve neutralization of charge. The coagulation-flocculation process can be used as a preliminary or intermediary step between other water or wastewater treatment processes like filtration and sedimentation. Iron and aluminium salts are the most widely used coagulants but salts of other metals such as titanium and zirconium have been found to be highly effective as well [87, 88]. Coagulation is affected by the type of coagulant used, its dose and mass; pH and initial turbidity of the water that is being treated; and properties of the pollutants present [89]. The effectiveness of the coagulation process is also affected by pretreatments like oxidation [87].

In a colloidal suspension, particles will settle very slowly or not at all because the colloidal particles carry surface electrical charges that mutually repel each other. A coagulant (typically a metallic salt) with the opposite charge is added to the water to overcome the repulsive charge and "destabilize" the suspension. For example, the colloidal particles are negatively charged and alum

is added as a coagulant to create positively charged ions. Once the repulsive charges have been neutralized (since opposite charges attract), the van der Waals force will cause the particles to cling together (agglomerate) and form micro floc.

Disadvantages

- Considerable amount of sludge is generated, which cause problem of disposal.
- Fails work for soluble pollutants
- Chemicals need to be added on a continues basis
- Other processes like oxidation, filtration and sedimentation are necessary for complete raw water or wastewater
- Running cost is effectively high

1.3.7 Adsorption Process

Adsorption is the adhesion of atoms, ions, or molecules from a gas, liquid, or dissolved solid to a surface . It is the phenomenon of accumulation of large number of molecular species at the surface of liquid or solid phase in comparison to the bulk. The process of adsorption arises due to presence of unbalanced or residual forces at the surface of liquid or solid phase. These unbalanced residual forces have tendency to attract and retain the molecular species with which it comes in contact with the surface. Adsorption is essentially a surface phenomenon. It is a physio-chemical treatment process in which dissolved molecules are attached to the surface of an adsorbent by physical/chemical forces. Adsorption is mass transfer operation in which constituents in one phase is transferred to the other phase.

Adsorption is a surface-based process (Figure 1.5) whereas absorption means uniform distribution of the substance throughout the bulk, adsorption essentially happens at the surface of the substance. When both Adsorption and Absorption processes take place simultaneously, the process is called sorption. While desorption is the reverse of it. Adsorption process involves two components Adsorbent and Adsorbate. Adsorbent is the substance on the surface of which adsorption takes place. Adsorbate is the substance which is being adsorbed on the

surface of adsorbent. Adsorbate gets adsorbed. Adsorption occurs in following three steps:

- Step 1: Diffusion of adsorbate (film diffusion) in which adsorbate diffuses from the major body of the stream to the external surface of the adsorbent particle.
- Step 2: Migration into pores of adsorbent surface (pore diffusion) in which adsorbate migrates from the relatively small area of the external surface to the pores within each adsorbent particle. The bulk of adsorption usually occurs in these pores because there is the majority of available surface area.
- Step 3: Layer Build up on adsorbent in which contaminant molecules adhere to the surface in the pores.

Some typical applications of adsorption technique in waste water treatment include removal of specific contaminants, which are resistant to biodegradation and are toxic e.g. phenols, metals ions and color additives as well as advanced treatment of waste water for improved removal of organic materials over that of biological counterpart [91]. Adsorption technology is currently used extensively for the removal of organic and inorganic micro-pollutants from aqueous solution [92].

Advantage

- Low initial cost
- Simplicity of design
- Capability for adsorbing a broad range of different types of adsorbents efficiently
- Easy operation
- Insensitivity to toxic substances
- Reusability of adsorbent

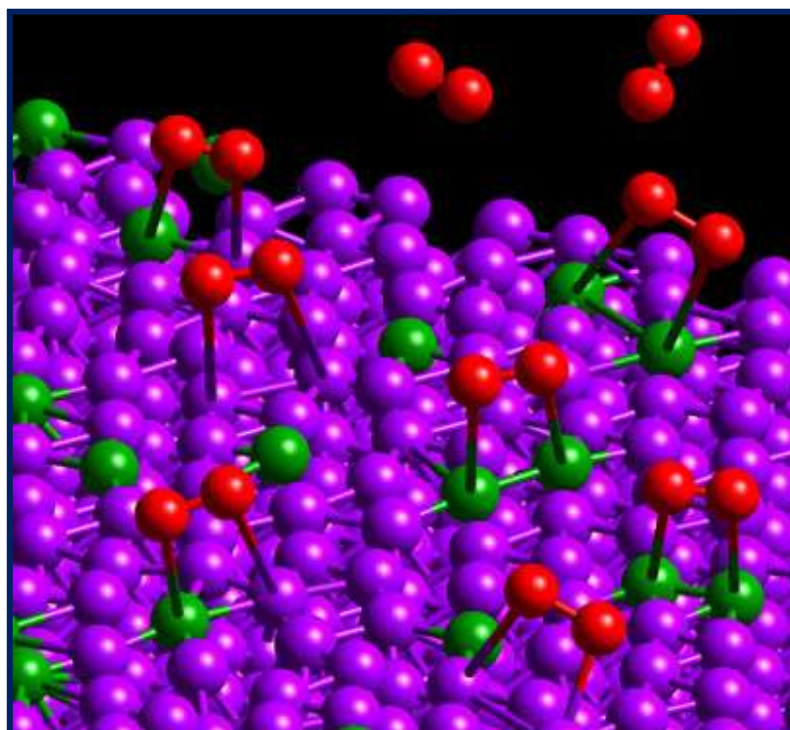


Figure 1.5: Oxygen molecules (red) adsorb on a bimetallic surface of platinum (purple) and cobalt (green) [90]

Adsorption is considered to be cost effective method for quickly lowering the concentration of organics from an effluent. Adsorption is not specific to only one type of contaminants and removes most of the contaminants. It is an economic way to remove pollutants. So it is proven to be one of the most attractive and effective techniques for purification and separation in wastewater treatment due to the high concentrating ability and reusability of adsorbent. Some important adsorbents widely used in waste water treatment are described briefly in the next topics.

1.4 Various Adsorbents Used for Water Treatment

Different types of adsorbents are classified into natural adsorbents and synthetic adsorbents. Natural adsorbents include charcoal, clays, clay minerals, red mud, zeolites, chitosan and ores. These natural materials, in many instances are relatively of low cost, abundant in supply and have significant potential for modification and ultimately enhancement of their adsorption capabilities. Synthetic adsorbents are adsorbents prepared from Agricultural products and wastes, house hold wastes, Industrial wastes, sewage sludge and polymeric adsorbents. Each adsorbent has its own characteristics such as porosity, pore structure and nature of its adsorbing surfaces. Many waste materials include fruit wastes, coconut shell, scrap tires, bark and other tannin-rich materials, sawdust, rice husk, petroleum wastes, fertilizer wastes, fly ash, sugar industry wastes, blast furnace slag, seafood processing wastes, seaweed and algae, peat moss etc.

Characteristics and General Requirements

Adsorbents are used usually in the form of spherical pellets, rods, moldings or monoliths with hydrodynamic diameters between 0.5 and 10 mm. They must have high abrasion resistance, high thermal stability and small pore diameters which results in higher exposed surface area and hence high surface capacity for adsorption.

Most industrial adsorbents fall into one of three classes:

- Oxygen-containing compounds: These are typically hydrophilic and polar and include materials such as silica gel and zeolites.
- Carbon-based compounds: These are typically hydrophobic and non-polar and include materials such as activated carbon and graphite.
- Polymer-based compounds: These are compounds containing polar or non-polar functional groups in a porous polymer matrix.

Some of the most widely used adsorbents are described below:

1.4.1 Activated Carbon

Activated carbons can be further divided into commercially available and synthetic activated carbons.

i) Commercial activated carbon

Commercially available activated carbon, also called activated charcoal or activated coal, is a form of carbon that has been processed to make it extremely porous and thus to have a very large surface area (500 m²/g) available for adsorption or chemical reaction. It is amorphous solid consisting of microcrystallites with a graphite lattice and non-polar.

Adsorption on to carbon had been used for water treatment as early as 2000 B.C. [93]. Cheremisinoff and Ellerbush presented the use of activated carbon in the water and wastewater industry as a standard adsorbent for the reclamation of municipal and industrial wastewater to a potable water quality in 1940's [94]. It is used for adsorption of organic substances, non-polar adsorbates and for waste gas (and waste water) treatment. It is the most widely used adsorbent since most of its chemical (e.g. surface groups) and physical properties (e.g. pore size distribution and surface area) can be tuned according to what is needed. Adsorption on activated carbon is currently the most frequently used technology for removing organic pollutants from aqueous industrial sludge, surface waters and drinking water. The recent reports on various activated carbon materials capable of pollutant removal is given in literature review [95-99].

ii) Synthetic activated carbons

Precursors to the activated carbons are either of degraded and coalified plant matter (e.g., all ranks of coal, lignite and peat) or of botanical origin (e.g., nut shells, wood, and coconut shells). Agricultural wastes are considered as very important feed stocks in virtue of two facts: they are renewable and low-cost materials. The most commonly used feed stocks include corncob [100], lignin [101], apricot stone shell [102], activated sludge [103], bagasse ash and charcoal [95], coffee grounds [104], paper mill sludge [105], and coconut shell [106]. Schemes for the production of activated carbons are either thermal procedures (physical) or chemical routes. The former involves primary carbonization of the raw materials ($< 700\text{ }^{\circ}\text{C}$) followed by controlled gasification at higher temperatures ($850\text{ }^{\circ}\text{C}$) in a stream of an oxidizing gas (steam, CO_2 , N_2 , air, or a mixture). The chemical route is done by impregnation of the precursor with H_2SO_4 , H_3PO_4 , ZnCl_2 , or HNO_3 [100-106] and then by heat treatment at moderate temperatures ($400\text{--}600\text{ }^{\circ}\text{C}$) in a one-step process.

1.4.2 Silica Gel

Silica gel (Figure 1.6) is a chemically inert, nontoxic, polar and dimensionally stable ($< 400^{\circ}\text{C}$) amorphous form of SiO_2 , possess structure consisting of tetrahedral units of SiO_4 connected by siloxane bridges Si-O-Si [107]. It poses high superficial area, porous structure. Silica gel is mostly employed as support among the inorganic adsorbents [108].

The silica surface under normal condition is recovered with reactive hydroxyl groups Si-OH, called silanol groups, while its interior is connected by siloxane groups (Si-O-Si). These silanol groups (Si-OH) determine the behavior of its surface, exercising an important function in the adsorption processes [109]. Silica gel is used as adsorbent for the drying of gases [110], organic solvents [111] and transformer oils [112].

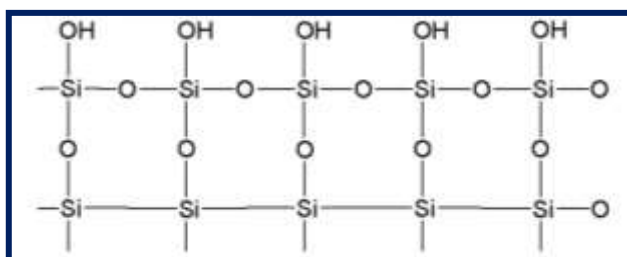


Figure 1.6: Structure of Silica Gel

1.4.3 Clays

Natural clay minerals are well known and familiar to mankind from the earliest days of civilization. Because of their low cost, abundance in most continents of the world, promising sorption properties, high specific area and potential for ion-exchange, clay materials are strong candidates as adsorbents. Clay materials possess a layered structure and are considered as host materials. They are classified by the difference in their layered structures shown in Figure 1.7. There are several classes of clays such as kaolinite $[\text{Al}_4\text{Si}_4\text{O}_{10}(\text{OH})_8]$ (Figure 1.8), smectite (montmorillonite, saponite) $[\text{Al}_2\text{Si}_4\text{O}_{10}(\text{OH})_2 \cdot n\text{H}_2\text{O}]$ (Figure 1.9), mica (illite) $[\text{K}_2 \text{Al}_4(\text{Si}_6\text{Al}_2)\text{O}_{20}(\text{OH})_4]$, serpentine, bentonite (Figure 1.10), diatomite, pyrophyllite (talc), vermiculite, sepiolite and chlorite $[(\text{Mg,Fe})_5 (\text{Al,Fe}^{111})_2 \text{Si}_3\text{O}_{10}(\text{OH})_8]$ [113]. Out of the four types, montmorillonite clays have the smallest crystallite size, large surface area and highest cation exchange capacity. The adsorption capabilities result from a net negative charge on the structure of minerals. This negative charge gives clay the capabilities to adsorb positively charged species. Their sorption properties also come from their high surface area and high porosity [114]. Clay minerals exhibit a strong affinity for both heteroatomic cationic and anionic dyes. They possess a wide pore size distribution, ranging from micro ($< 20\text{A}^0$) to mesopores ($20\text{-}500\text{A}^0$). The clay minerals consist of two silicon-oxygen tetrahedral sheets that sandwich an aluminium - oxygen - hydroxyl tetrahedral sheets as shown in Figure 1.7. Several extensive studies have been carried out on the adsorption capacity of clay for waste water purification, including sepiolite [115], kaolinite [116], montmorillonite [117], smectite [118] and benonite [119]. The ionic charges on the clay surface can also increase the adsorption capacity by attracting oppositely charged polluting substances and convert them into harmless or easily removed

forms. Bekci et al. [120] investigated montmorillonite as adsorbent in the removal of trimethoprim, one of the main antibacterial agents used in human and veterinary medicine worldwide. Modified clays were reported to adsorb environmental toxicants such as phenols, chlorophenols [121] etc. Moreover the use of different forms of clay is also accounted in adsorption of radionuclides like Cs^+ , Sr^+ [122], dyes [123], organic and inorganic pollutants such as humic acid [124], aniline [125] from waste water.

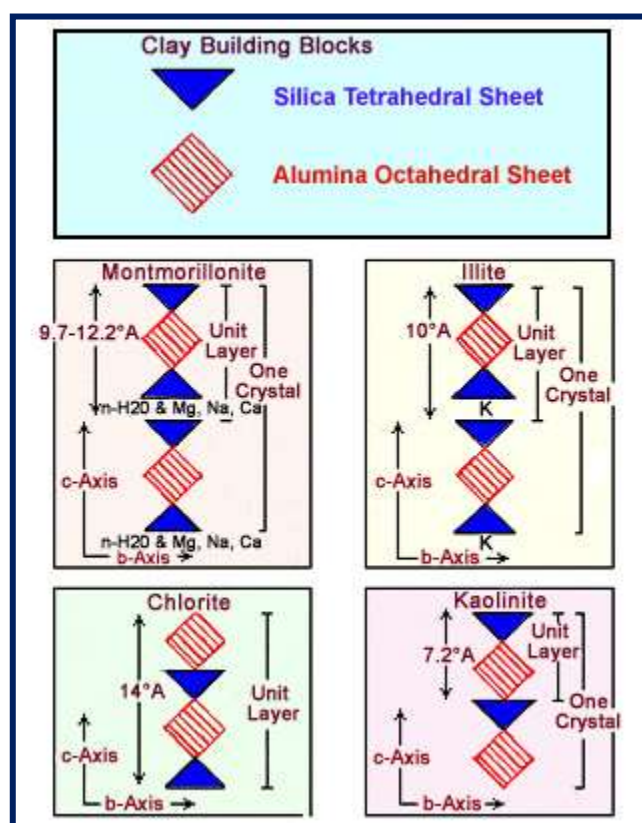


Figure 1.7: Crystal structure of common clay minerals

(i) *Kaolin*

Kaolin [$\text{Al}_4\text{Si}_4\text{O}_{10}(\text{OH})_8$] (Figure 1.8) is one of the very common low costs natural clay adsorbent with ionic crystalline structure. Kaolinite is a 1:1 aluminosilicate crystalline structure consists of stacked pairs of tetrahedral silica sheets and octahedral alumina oxygen atoms, and successive pairs are held together by hydrogen bonding between silica–oxygen and aluminum–hydroxyl groups. Adsorption experiments kaolin as an adsorbent have been reported on acidic dye [126] basic dyes such as methylene blue and malachite green [127].

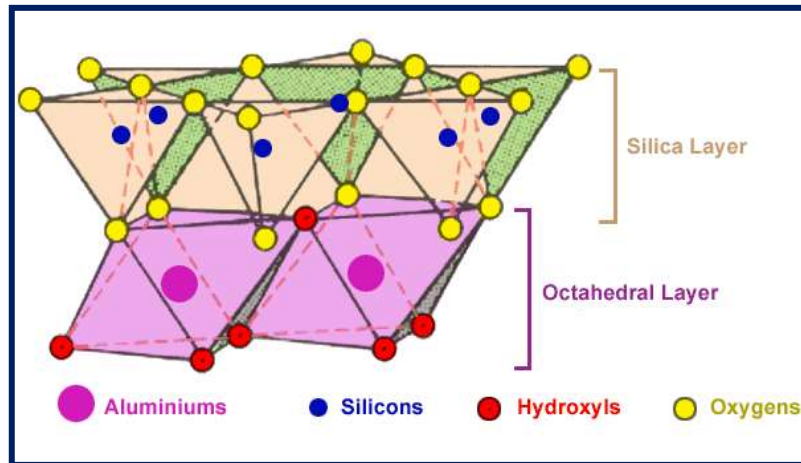


Figure 1.8: Structure of Kaolinite

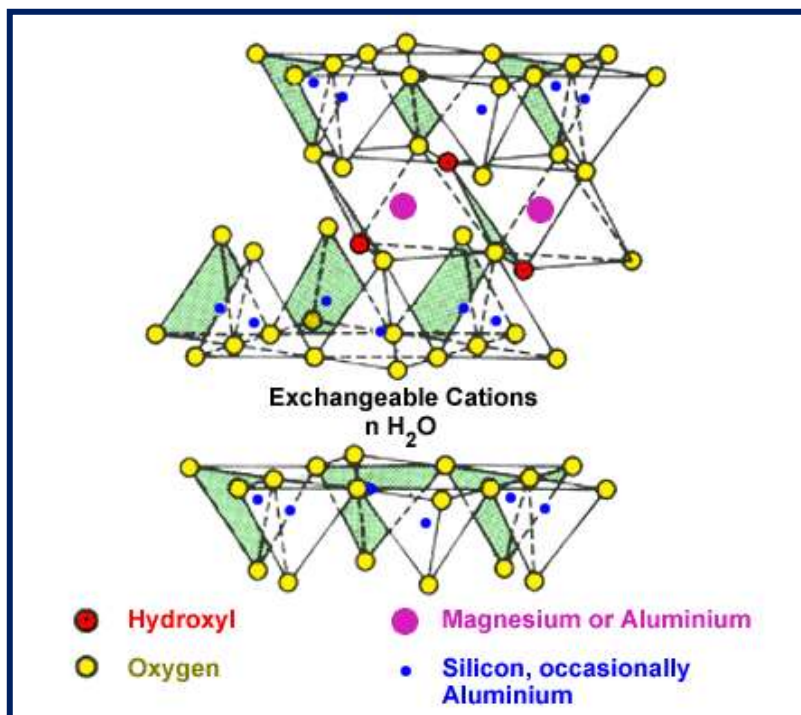


Figure 1.9: Structure of Montmorillonite (Smectite)

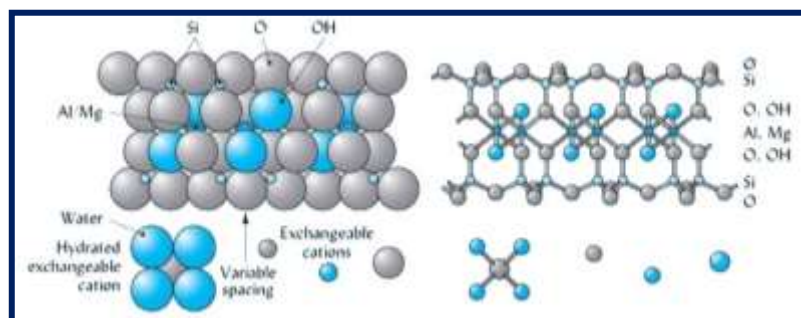


Figure 1.10: Structure of bentonite

(ii) *Sepiolite*

Sepiolite is a hydrous magnesium silicate characterized by its fibrous morphology and intra crystalline channels, having the ideal structural formula $\text{Si}_{12}\text{Mg}_8\text{O}_3(\text{OH})_4(\text{OH}_2)48\text{H}_2\text{O}$ for the half unit cell [128]. Sepiolite has a common industrial application due to its molecular sized channels and large specific surface (more than $200 \text{ m}^2\text{g}^{-1}$). It is an effective sorbent in the removal of compounds like aromatic amines, diquat, paraquat and methyl green from aqueous solutions [129].

1.4.4. Industrial waste/by-product

(i) *Red mud*

Among various industrial by-products, red mud is a solid waste residue formed after the caustic digestion of bauxite ores during the production of alumina. Each year, about 90 million tonnes of red mud are produced globally [130]. Depending on the origin, quality and composition of the bauxite, the amount of red mud left over from alumina refining can vary widely. It is mainly composed of fine particles containing aluminum, iron, silicon, titanium oxides and hydroxides. The red colour is caused by the oxidized iron present, which can make up to 60% of the mass of the red mud. Red mud residues as unconventional adsorbents for water and wastewater treatment are motivated by the fact that red mud is a fine-grained mixture of oxides and hydroxides, capable of removing several contaminants, as well as being widely available. Efforts have been made to convert red mud into a low-cost adsorbent, and the final material has been used for the removal of phenol, 2-CP, 4-CP, and 2,4-DCP from wastewater [131].

(ii) *Bagasse fly ash*

Sugar cane bagasse is an industrial waste which is used worldwide as fuel in the same sugar-cane industry. The combustion yields ashes containing high amounts of unburned matter, silicon and aluminium oxides as main components. These sugar-cane bagasse ashes have been used as a cement-replacing material in the concrete industry and as an adsorbent in wastewater treatment. Removal of lindane and malathion [132], Quinoline [133], Para-nitro phenol [134] etc. from wastewater have been reported using bagasse fly ash.

(iii) *Rice husk*

Rice husks are agricultural waste, accounting for about one-fifth of the annual gross rice production (545 million metric tons) of the world [135]. Rice husk is burned in the boiler of various industries to produce steam, thus, conserving both energy and resources. During the burning of rice husk, a waste called rice husk ash (RHA) is collected from the particulate collection equipment attached upstream to the stacks of rice husk-fired boilers. Chemical content of rice husk consists of 50% cellulose, 25-30% lignin, and 15-20% silica. It has been used as an absorbent to remove metal ions [136], dye [137], oil [138] and arsenic [139] from aqueous solution.

(iv) *Bottom ash*

Bottom ash is a granulated waste material obtained from thermal coal-fired power generation plants. It appears as dark grey black sand size granules and is composed of SiO_2 , Al_2O_3 , Fe_2O_3 with smaller percentages of CaO , MgO , sulfates and other compounds. Disposal of the ash is always a matter of concern to the authorities, because it makes agricultural land uncultivable and infertile [140]. Bottom ash is reported to be used for the removal of dye brilliant green, from the water [141].

(v) *Deoiled soya*

Deoiled soya is a by-product of soyabean oil extracting mills. In our country there has been a phenomenal increase in the production of soyabean particularly in the last two decades and India has become one of the leading producers of the soyabean crop. Deoiled soya is a dry, brownish white, porous, flaky material, which is obtained after extracting all possible nutrients of soyabean. At one time it was widely used as animal and fish feed but now it is a banned edible substance due to its bitter taste and toxicity. Deoiled soya is reported to be used for the removal of hazardous dye, brilliant green, from the water [141].

(vi) *Sewage sludge*

Sewage sludge are by-products derived from regular activities of wastewater treatment plants. An average production of 40–60 g dry matter /

inhabitant / day is typical for urban sewage plants, to which must be added a corresponding amount produced by industrial sewage plants. The sludge contained approximately 50% organic matter and 1–4% inorganic C. Organic and inorganic C, organic N, inorganic P, and Ca and Mg. Researchers have prepared the adsorbent from sewage sludge by pyrolysis (or carbonization) process for different industrial applications [142]. M. Otero et al. [143] have used the adsorbents produced from sewage sludge in organic pollutant (methylene blue) removal. After chemical activation and pyrolysis treatment, sewage sludge provided materials of great porosity and high surface area.

(vii) *Saw dust*

Sawdust or wood dust is a by-product of cutting, grinding, drilling, sanding, or otherwise pulverizing wood or any other material with a saw or other tool, composed of fine particles of wood. It is also the byproduct of certain animals, birds and insects which live in wood. It was used as an adsorbent for removing 2-Nitro phenol, 4-Nitro phenol, phenol [144], from aqueous solution.

1.4.5 Synthetic resins

Resins have macroporous structure shown in Figure 1.11. Removal of phenolic compounds from industrial wastewater was studied by adsorption in fixed-bed with polymeric resins [145]. Kujawski et al. reported that Amberlite XAD-4 had the better properties in decontamination of phenol from solutions [146]. There are many types of Resins like cationic, anionic, chelating etc. shown in Figure 1.12. It was shown that regeneration of the resin bed could be effectively performed with NaOH solution (Figure 1.13). Streat and Sweetland have studied the removal of 2-CP, 3- CP, and 4-CP from potable water using Hypersol-Macronet resins (MN-100, MN-150, MN-200) [147]. Vinylpyridine-DVB copolymer was found to have an excellent capacity for removing phenol from water [148].

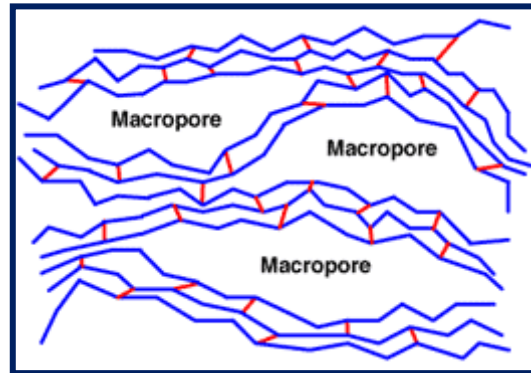


Figure 1.11: Macroporous structure of resin

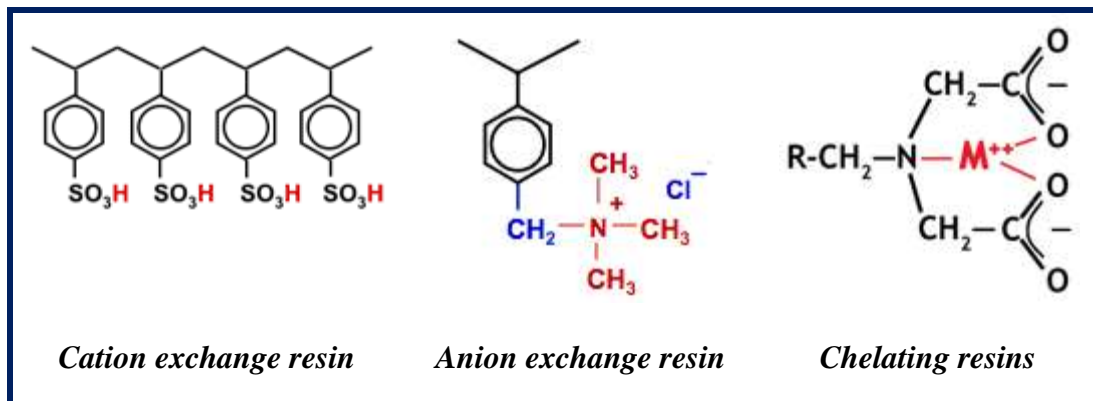


Figure 1.12: Type of resin

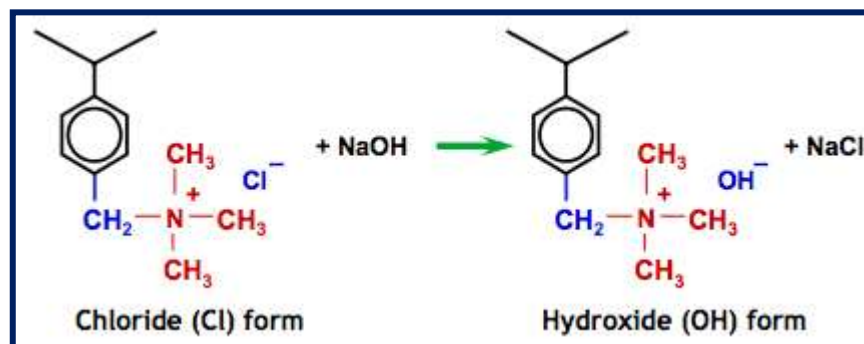
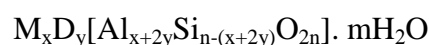


Figure 1.13: Regeneration of resin

1.4.6 Zeolites

Zeolites are microporous crystalline solids with well-defined structures. Zeolites are polar in nature and have a micro-porous structure. Generally they contain silicon, aluminium and oxygen in their frame work and cations, water and other molecules within their pores. The silicon and aluminium atoms are tetrahedrally coordinated with each other through shared oxygen atoms. zeolites have a rigid, 3-dimensional crystalline structure (similar to a honey comb) consisting of a network of interconnected tunnels and cages (Figure 1.14). Water moves freely in and out of these pores but the zeolite framework remains rigid. Another special aspects of the structure is that the pore and channel sizes are nearly uniform, allowing the crystal to act as a molecular sieve. The porous zeolite is host to water molecules and ions of potassium and calcium, as well as a variety of other positively charged ions, but only those of appropriate molecular size to fit into the pores are admitted creating the sieving properties. Because of their regular and reproducible structure, they behave in predictable fashion. The zeolite composition is follows [149]:



Where,

M = Monovalent cation (viz. Na, K, Li)

D = Divalent cation (viz. Mg, Ca, Sr, Ba)

m = number of water molecules in relation to the total volume ($n/2 < m < n$)

n = number of monovalent cations

y = number of divalent cations

Zeolites are widely used in a variety of application, as ion-exchange beds in domestic and commercial water purification [150], softening [151], separation and removal of gases and heavy metal [152], air separation, catalytic cracking, petrochemical cracking and catalytic synthesis [153] and reforming. Zeolites are used for adsorption and separation due to its shape selective properties, they have been applied as chemical sieve, water softener and adsorbents [154], in mine water remediation [155].

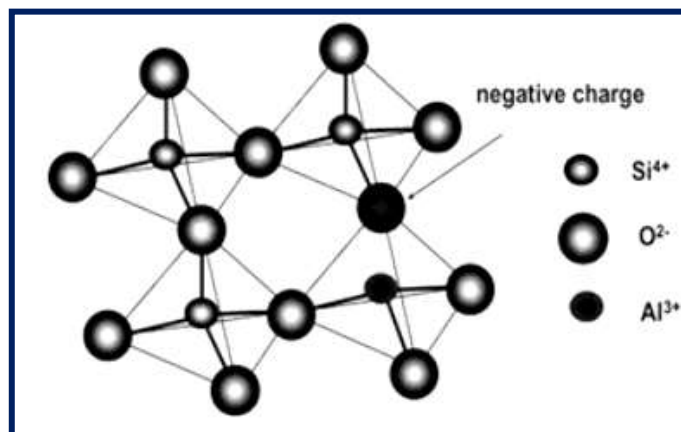
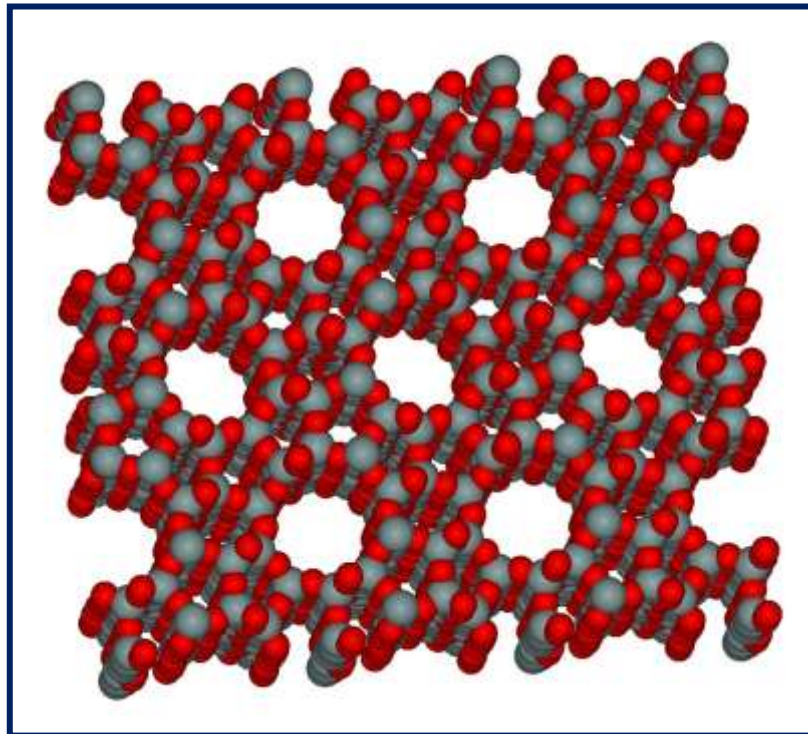


Figure 1.14: Basic structure of Zeolite

1.4.7 Polysaccharide

The recent developments in the synthesis of adsorbents containing polysaccharides, in particular modified biopolymers derived from chitin, chitosan and cyclodextrin. New polysaccharide based materials are used [156] for the removal of pollutants from the wastewater. The recent reports on various crosslinking polysaccharide materials capable of pollutant removal are given in Table 1.1.

Table 1.1: Recent report on various crosslinking polysaccharide materials capable of pollutant removal

Polysaccharides	Cross linking agents	Material obtained	Pollutants	References
Chitosan	EPI	Beads	Dyes	[157]
	GLA, EGDE	Beads	Dyes	[158]
Starch	EPI	Gels	Phenols	[159]
	EPI	Gels	Dyes	[160]
	EPI	Beads	Dyes	[161]
Cyclodextrin	EPI	Gels	Phenols	[162]
	EPI	Gels	Beta-naphtol	[163]
	EPI	Gels	Dyes	[164]

GLA - Glutaraldehyde, EPI – Epichlorohydrin, EGDE - Ethyleneglycoldiglycidylether

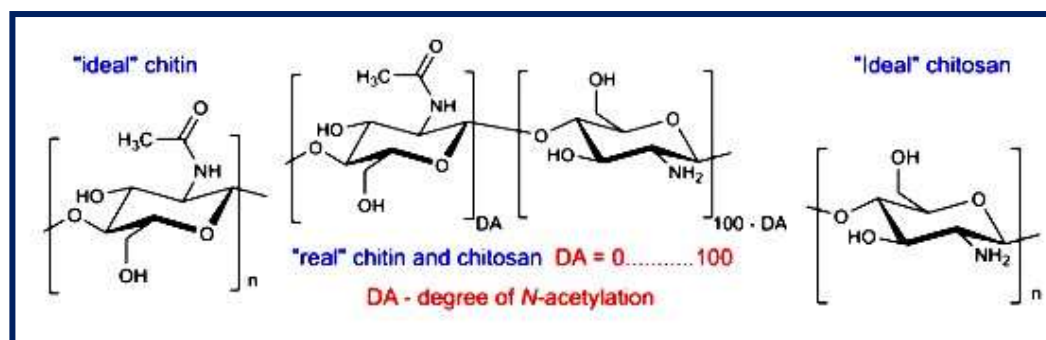


Figure 1.15: Structure of chitin and Chitosan

Chitosan (Figure 1.15), a natural biopolymeric cation and cheap material has been widely used as an adsorbent for the heavy metal like Cu [165] and neutral or positively charged organic species like reactive dyes [166], because the amino ($-NH_2$) and hydroxyl ($-OH$) groups on the biopolymer chain can act as the coordination and reaction sites. The electrolytic nature and chelating ability of the biopolymer is mainly governed by the protonation degree of the NH_3^+ group ($pK_a = 6.3$), which is dependent on pH [167].

1.4.8 Fly ash as low cost Adsorbent

Since wide scale coal firing for power generation began in the 1920s, many millions of tons of ash and related by-products have been generated. The current annual production of coal ash worldwide is estimated around 600 million tones, with fly ash constituting about 500 million tons at 75–80% of the total ash produced [168]. Thus, the amount of coal waste (fly ash), released by factories and thermal power plants has been increasing throughout the world. The economically viable solution to this problem should include utilization of waste materials for new products rather than land disposal. Fly ash is generally grey in color, abrasive, mostly alkaline, and refractory in nature.

Pozzolans, which are siliceous or siliceous and aluminous materials that together with water and calcium hydroxide form cementitious products at ambient temperatures, are also admixtures. Fly ash from pulverized coal combustion is categorized as such a pozzolan. Fly ash also contains different essential elements, including both macronutrients P, K, Ca, Mg and micronutrients Zn, Fe, Cu, Mn, B, and Mo for plant growth. The chemical composition of fly ash like high percentage of silica (60–65%), alumina (25–30%), magnetite, Fe_2O_3 (6–15%) enables its use for the synthesis of zeolite, alum, and precipitated silica. The other important physicochemical characteristics of fly ash, such as bulk density, particle size, porosity, water holding capacity, and surface area makes it suitable for use as an adsorbent.

The conversion of fly ash into zeolite has also been widely examined [169]. Another interesting possibility might be use as a low-cost adsorbent for gas and water treatment. Several investigations are reported in the literature on the

utilization of fly ash for the removal of heavy metals [170], flue gas cleaning [171], toxic inorganic ions [172, 173] and organics from industrial wastewater. A brief review of studies on use of fly ash as low cost adsorbent for organic pollutants is given in Table 1.2.

Table 1.2: A brief review of studies on use of fly ash as low cost adsorbent for organic pollutants

Type of organic pollutants	Name of compounds	References
Phenolic compounds	Phenol	[174]
	Phenol, Cresol, and their mixtures	[175]
	Phenol, 3-chlorophenol, 2,4-dichlorophenol	[176]
Dyes	Congo red	[177]
	Chrysoidine R	[178]
	Acid Orange 7	[179]
	Methylene blue	[180]
	Rhodamine B	[181]
Pesticides	Carbofuran	[182]
	Indole-3-acetic acid, Beta Naphthalene acetic acid	[183]
	PCBs	[184]
Other organic compounds	o-xylene	[185]
	TNT	[186]
	Aldehydes, Ketones	[187]
	Aromatics, Alcohols	[188]
	Oxalic acid	[189]

1.5 Scope of the work

The aim of this work is to study the preparation and characterization of innovative fly ash supported adsorbents and to evaluate their adsorption capacity for removal of various organic pollutants from waste water. Fly ash is siliceous and carboneous waste materials, non toxic and external surface which can be activated during the chemical activation. In this study adsorbents are prepared by

activating with NaOH, surfactant cetyltrimethylammonium bromide (CTAB), poly saccheride chitosan over mechanically and thermally supported materials, characterized by using different analytical techniques such as x-ray fluorescence (XRF), x-ray diffraction (XRD), field emission scanning electro-microscope (FE-SEM), N₂ adsorption-desorption, surface area and porosity measurement, Fourier transform infrared (FT-IR) etc. The effects of several experimental parameters such as contact time, initial adsorbate dosages, initial adsorbent concentration, temperature, ionic strength and solution pH for different organic pollutants adsorption onto fly ash and its supported adsorbents were investigated. The experimental results were analyzed by kinetic and isotherm models. Thermodynamic parameters such as Gibbs free energy change (ΔG°), enthalpy change (ΔH°) and entropy change (ΔS°) were calculated. The prepared adsorbents serves potential solid base supported adsorbents for various organic pollutants removal from waste water. Thus the present research study reports new supported adsorbents for the replacement of commercial adsorbents for cost effective waste water treatment technologies.

1.6 References

- [1] R. Hammer, In Fracking's Wake: New Rules are needed to Protect Our Health and Environment from Contaminated Wastewater. NRDC Document, D:12-05-A (2012) 4-16.
- [2] I. Ali, M. Asim, T. A. Khan, J. Environ. Manage., 113 (2012) 170-183.
- [3] Central Pollution Control Board. Status of water quality in India 2007, New Delhi, India: CPCB, (2008) 13-30.
- [4] S.Z. Lari, N.A. Khan, K.N. Gandhi, T.S Meshram, and N.P. Thacker, J. Environ. Health Sci. Eng., 12 (2014) 11.
- [5] P.K. Kumar, M.M. Pacha, Curr. World Environ., 10 (1) (2015).
- [6] M. Velusamy, A. Pandiyarajan, M.S .Dheenadayalan, Int. J. of Chem. and Phy. Sci., 4 (2015) 71-78.
- [7] M.M. Kowska, M. Spycha, Pol. J. Environ. Stud., 23(1) (2014) 131-37.

- [8] G. Mckay, S.J. Allen, I.F. Meconney, M.S. Ottrburn, J. of Colloid Inter. Sci., 80 (1981) 323-39.
- [9] A. Kumar, S. Kumar, S. Kumar, Carbon, 41 (2003) 3015-25.
- [10] J. Xie, W. Meng, D. Wu, Z.Zhang, H. Kong, J. of Hazard. Mater.231–232 (2012) 57-63.
- [11] S.H. Lin, R.S. Juang, J. of Environ. Manag., 90(3) (2008) 1336-49.
- [12] J.N. Munyasya, K.K. Juma, M.W. Burugu, D.N. Mburu, E.O. Okuku, J. Environ. Anal. Toxicol., S7 (2015) 1-6.
- [13] J. Jacob, Inter. J. of Bioscience, Biochemistry and Bioinformatics, 3(6) (2013) 657-61.
- [14] Health Effects of PCBs, U.S. Environmental Protection Agency, 13 June 2013.
- [15] K. Chauhan, P.R. Kodavanti, J.D. McKinney, Toxicology and Applied Pharmacology, 162(1) (2000) 10-21.
- [16] M. R. Beychok, Atmospheric Environment. 21(1) (1987) 29-36.
- [17] U. Ali, J.H. Syed, R.N. Malik, A. Katsoyiannis, J. Li, G. Zhang, K. C. Jones, Sci. of the Total Environ., 476-77 (2014) 705-17.
- [18] Lear, Linda, Rachel Carson, Witness for Nature. Mariner Books, ISBN 978-0-547-23823-4 (2009).
- [19] Polychlorinated Biphenyl and the Environment, Interdepartmental Task Force on PCBs, Washington D.C., May 1972.
- [20] G. Dunnet, D. Crisp, G. Conan, W. Bourne, Philosophical Transactions of the Royal Society of London., B297 (1982) 413-27.
- [21] I. Hussein, Abdel-Shafy, Mona S.M. Mansour, Egyptian Journal of Petroleum, 25 (2016) 107-23.
- [22] Polycyclic aromatic hydrocarbons, National Pollutant Inventory, Deptt. Of Environ. & Energy, Australian Govt., 2014.
- [23] C.E. Bostrom, P. Gerde, A. Hanberg, B. Jernstrom, C. Johansson, T. Kyrklund, A. Rannug, M. Tornqvist, K. Victorin, R. Westerholm, Environ. Health Perspectives, 110 (2002) 451-88.

- [24] H.D. Patrick, PCB and PAH Releases from Incineration and Power Generation Processes R&D Technical Report, ISBN: 1857 05895 X, P4-052 (1998) 28-31
- [25] K. Chauhan, P.R. Kodavanti, J.D. McKinney, Toxicology and Applied Pharmacology, 162(1) (2000) 10-21.
- [26] I. Rusyn, J. Corton, Christopher Mutation Research / Reviews in Mutation Research, 750(2) (2012) 141-58.
- [27] B. Tsyntsarski, B. Petrova, T. Budinova, N. Petrov, D. K. Teodosiev, A. Sarbu, Desalination and Water Treatment, 52 (2014) 16-18.
- [28] M.D.S. Pereira, PCDD, PCDF and PCB: main sources, environmental behaviour and risk to man and biota Quím. Nova, 27 (2004) 1-10.
- [29] S. Alaluusua, P. Calderara, P.M. Gerthoux, P.L. Lukinmaa, O. Kovero, L. Needham, D.G. Patterson, J. Tuomisto, P. Mocarelli, (Environ. Health Perspect, 112(13) (2004) 1313-18.
- [30] R.E. Peterson, H.M. Theobald, G.L. Kimmel, Crit. Rev. Toxicol. 23(3) (1993) 283-93.
- [31] S.D. Shaw, A. Blum, R. Weber, K. Kannan, D. Rich, D. Lucas, C.P. Koshland, Reviews on Environmental Health, 25(4) (2010) 261-305.
- [32] Plastics and Health Risks Annual Review of Public Health, 31(2010) 179-94.
- [33] G. Bjelakovic, D. Nikolova, L.L. Gluud, R.G. Simonetti, C. Gluud, JAMA, 297(8) (2007) 842-57.
- [34] M. Ristow, K. Zarse, Experimental Gerontology, 45(6) (2010) 410-18.
- [35] D.G.J. Larsson, C. de Pedro, N. Paxéus, J. Hazard. Mater., 148 (2007) 751-55.
- [36] J. Fick, H. Soderstrom, R.H. Lindberg, C. Phan, M. Tysklind, D.G.J. Larsson, Environ. Toxicol. Chem., 28 (2009) 2522-27.
- [37] E. Kristiansson, J. Fick, A. Janzon, R. Grabic, C. Rutgersson, B. Weijdegard, H. Soderstrom, D.G.J. Larsson, Pyrosequencing of antibiotic-contaminated river sediments reveals high levels of resistance and gene transfer elements. PLoS ONE 6, e17038 (2011).

- [38] R.H. Lindberg, P. Wennberg, M.I. Johansson, M. Tysklind, B.A. Andersson, *Environ. Sci. Technol.*, 39 (2005) 3421-29.
- [39] D. Li, M. Yang, J. Hu, Y. Zhang, H. Chang, F. Jin, *Water Res.*, 42 (2008) 307-17.
- [40] C.W. Cui, S.L. Ji, H.Y. Ren., *Environ. Monit. Assess.*, 121 (2006) 409-19.
- [41] H. Zollinger, *Color Chemistry Synthesis*, (1987) 92-102.
- [42] P. Janos, H. Buchtova, M. Ryznarova, *Water Res.*, 37 (2003) 4938-44.
- [43] B.K. Singh, P.S. Nayak, *Adsorption Sci Technol.*, 22 (2004) 295-309.
- [44] R.K. Singh, S. Kumar, S. Kumar, A. Kumar, *J. Hazard. Mater.*, 155 (2008) 523-35.
- [45] S. Kumar, M. Zafar, J.K. Prajapati, S. Kumar, S. Kannepalli, *J. Hazard. Mater.*, 185 (2011) 287-94.
- [46] S.H. Lin, R.S. Juang, *J. Environ. Manage.*, 90 (2009) 1336-49.
- [47] J.H. Wang, S.R. Zheng, J.L. Liu, Z.Y. Xu, *Chem. Eng. J.*, 165 (2010) 10-16.
- [48] J.N. Wang, A.M. Li, L. Xu, Y. Zhou, *J. Hazard. Mater.*, 169 (2009) 794-800.
- [49] J.H. Wang, C.L. Zheng, S.L. Ding, H.R. Ma, Y.F. Ji, *Desalination*, 273 (2011) 285-91.
- [50] R.M. Aghav, S. Kumar, S.N. Mukherjee, *J. Hazard. Mater.*, 188 (2011) 67-77.
- [51] A. Monique, K.K. Ravi, B. Stephen, *Appl. Clay Sci.*, 13 (1998) 13-20.
- [52] R. Andreozzi, R. Marotta, P. Nicklas, *Chemosphere*, 50 (2003) 1319-30.
- [53] X.M. Chen, D.R. Silva, C.A. Martinez-Huitle, *Chin. Chem. Lett.*, 21 (2010) 101-4.
- [54] N. Nakada, T. Tanishima, H. Shinohara, K. Kiri, H. Takada, *Water Res.*, 40 (2006) 3297-303.
- [55] A.I. Balcioglu, M. Otker, *Chemosphere*, 50 (2003) 85-95.
- [56] R. Grover, A.J. Cessna, (Eds.), *CRC Press, Boca Raton, FL*. (1991).
- [57] V.K. Gupta, I. Ali, *Water Res.*, 35 (2001) 33-40.

- [58] V.K. Gupta, C.K. Jain, I. Ali, S. Chandra, S. Agarwal, *Water Res*, 36 (2002) 2483-90.
- [59] K. Kumari, S.K. Saxena, *Colloids Surf.*, 33 (1988) 55-61.
- [60] H.Nollet, M.Roels, P. Lutgen, P.Van Der Meeren, W. Verstraete. *Chemosphere*, 53 (2003) 655-65.
- [61] S. Giacomazzi, N. Cochet, *Chemosphere*, 56 (2004) 1021-32.
- [62] E.M. Thurman, K.C. Bastian, T. Moolhagen, *Sci. Total Environ.*, 148 (2000) 189-200.
- [63] M. Fielding, D. Barcelo, A. Helweg, L. Torstenson, P. Van Zoonen, G. Angeletti, *Water Pollution Research Report 27*. Commission of the European Communities, Brussels, (1992) 1-136.
- [64] M.M. Walker, L.H. Keith, , *EPA's Pesticide Fact Sheet Database*. Lewis Publishing, Chelsea, M.I., (1992).
- [65] I. Vergili, H. Barlas, *Desalination*, 249 (2009) 1107–14.
- [66] A. Zertal, M. Jacquet, B. Lavedrine, T. Sehili, *Chemosphere*, 58 (2005) 1431-37.
- [67] P. Vizcaino, A. Pistocchi, *Environ. Pollut.*, 158 (2010) 3017-27.
- [68] M.A. CrespIn, M. Gallego, M. Valcarcel, *Environ. Sci. Technol.*, 35 (2001) 4265-70.
- [69] C. Juan. L. Montilla, S. Pandey, D.O. Shah, D.C. Oscar, *Water Research*, 39 (2005) 1907-13.
- [70] X. Li, Y. Du, G. Wu., Z. Li, H. Li, H. Sui, *Chemosphere*, 88 (2012) 245-49.
- [71] O. Ojajuni, D. Saroj, G. Cavalli, *J. Environ. Techno. Reviews*, 4 (2015).
- [72] M. Bodzek, *Copernican Letters*, 6 (2015) 1-10.
- [73] S. Neumann, Fatula, *Principles of Ion Exchange in Wastewater Treatment*. In: *Asian Water*, 2009.
- [74] J. Gregory, *Water Research*, 6 (1972) 681-84.
- [75] A. Mittal, *Biological wastewater treatment method*, *Water Today*, 2011.
- [76] J.Q. Jiang, *Separation engineering*, 8 (2015) 36-44.

- [77] L. Chekli, C. Eripret, S.H. Park, S.A.A. Tabatabai, O. Vronska, B. Tamburic, J.H. Kim, H.K. Shon, *Separ. and Purifi. Techno.*, 175 (2017) 99-106.
- [78] Ramavandi, Bahman, *Water Resources and Industry*, 6 (2014) 36-50.
- [79] C.Y.P. Ayekoe, D. Robert, D.G. Lancine, *Catalysis Today*, 281(1) (2017) 2-13.
- [80] W. Glaze, J.W. Kang, D.H. Chapin, *Ozone: Science & Engineering*, 9(4) (1987) 335-52.
- [81] E. E. Ebrahiema, M. N. Al-Maghrabib, A. R. Mobarkia, *Arabian Journal of Chemistry*, (2013) 1-6.
- [82] Bauer, H. Fallmann *Res. Chem. Intermediate*, 23(4) (1997) 341-54.
- [83] D. Sundstorm, B. Wier, H. Klie, *Environ. Prog.*, 8 (1989) 6-11.
- [84] S. Chiron, A.A. Fernandez, A. Rodriguez, E.G. Calvo, *Water Res.*, 34(2) (2000) 366-77.
- [85] I.G. Rashed, M.A. Hanna, H.F. El-Gamal, A.A. Al-Sarawy, F.K.M. Wali, *Eng. Res. J.*, 92 (2004) 97-107.
- [86] L.T. Amy, R. Christopher, D. Warberg, A. Atkinson, *Richard Water Res.*, 35(4) (2001) 977-84.
- [87] A. Koohestanian, M. Hosseini, Z. Abbasian, *American-Eurasian J. Agric. & Environ. Sci.*, 4(2) (2008) 266-73.
- [88] P.A. Beltrán, J.A.M. Roca, A.B. Piá, M.G. Melon, P. Ruiz, *J. of Hazar. Mater.*, 164(1) (2009) 288-95.
- [89] Oladoja, N. Abiola, *Sustainable Chemistry and Pharmacy*, 3 (2016) 47-58.
- [90] P.B. Balbuena, D. Altomare, L. Agapito, J. M. Seminario, *J. Phys. Chem., B* 107(49) (2003) 13671-80.
- [91] P. Cooper, *Color in Dye houses effluents*, Alden Press, Oxford, 1995.
- [92] I.H. Suffert, M.J. Mcgurie, *Ann Arbor Science*, Michigan, 1980.
- [93] W.T. Tsai, C.Y. Chang, M.C. Lin. *Microporous Mat.*, 45 (2001) 51-58.
- [94] P.N. Cheremisibonoff, *Ann Arbor science*, Michigan, 1979.
- [95] S. Mukherjee, S.A. Kumar, K. Misra, M. Fan, *Chem. Eng. J.*, 129 (2007) 133-42.

- [96] A. Martins, N. Nunes, *J. Chem. Educ.*, 92(1) (2015) 143-47.
- [97] U. Kouakou, A. S. Ello, J. A. Yapo and A. Trokourey, *J. of Environ. Chem. and Ecotoxicology*, 5(6) (2013) 168-71.
- [98] P. Chingombe, B. Saha, R.J. Wakeman, *Carbon*, 43 (2005) 3132-43.
- [99] L. Monser, N. Adhoum, *Separ. and Purifi. Techno.*, 26(2002) 137-46.
- [100] A.N.A. El-Hendawy, S.E. Samra, B.S. Girgis, *Colloids Surf. A: Physico chem. Eng. Asp.*, 180 (2001) 209-21.
- [101] E. G. Serranoa, T. Corderoa, J. R. Mirasola, L. Cotorueloa, J.J. Rodriguez, *Water Res.*, 38 (2004) 3043-50.
- [102] A.A. Daifullah, B.S. Girgis, *Water Res.*, 32 (1998) 1169-77.
- [103] M.J. Martin, E. Serra, A. Ros, M.D. Balaguer, M. Rigola, *Carbon* 42 (2004) 1383-88.
- [104] A. Namane, A. Mekarzia, K. Benrachedi, N.B. Bensemra, A.J. Hellal, *J. Hazard. Mat.*, B119 (2005) 189-94.
- [105] N.R. Khalili, J.D. Vyas, W. Weangkaew, S.J. Westfall, S.J. Parulekar, R. Sherwood, *Sep. Purif. Technol.*, 26 (2002) 295-304.
- [106] M. Radhika, K. Palanivelu, *J. Hazard. Mat.*, B138 (2006) 116-24.
- [107] P.D. Maniar, Y.A. Navrotsk, *J. Non cryst. Solids*, 120 (1990) 20-25.
- [108] A. Bagreev, J.A. Menendez, I. Dukhno, Y. Tarasenko, T. Bandosz, *J. Carbon*, 43 (2005) 208-10.
- [109] C.G. Armistead, A.J. Tyler, F.A. Hambleto, *J. Phys. Chem.*, 73 (1969) 3947-52.
- [110] D.L. Wood, E.M. Rabinovich, *Appl. Spectrosc.*, 43 (1989) 263-67.
- [111] O.V. Krokhim, N.V. Svintsova, O.N.O. Brezkov, O.A. Shpingun, *Anal. Chem.*, 52 (1997) 1066-668.
- [112] D.R. Kepp, U.G. Sidelmann, J. Tjornelund, S.H. Hansen, *J. Chromatography*, B 696 (1997) 235-41.
- [113] L.T. Kubota, F. Gouvea, A.N. Andrada, B.G. Milagres, G.O. Neto, *Electrochim. Acta*, 41 (1996) 1465-69.
- [114] T. Shichi, K. Takagi, *J. Photochem. Photobiol. C: Photochem.*, Rev.1 (2000) 113-30.

- [115] M. Alkan, O. Demirbas, S. Celikcapa, M. Dogan, *J. Hazard. Mater.*, 116 (2004) 135-45.
- [116] M. Alkan, O. Demirbas, M. Dogan, *Mater.*, 101 (2007) 388-96.
- [117] M.M. Kamal, B.M. Youssef, *Dyes Pigments*, 15 (1991) 175-82.
- [118] C.C. Wang, L.C. Juang, T.C. Hsu, C.K.Lee, J.F. Lee, F.C. Huang. *J. Colloid Interf. Sci.*, 273 (2004) 80-86.
- [119] I.K. Tonle, E. Ngameni, H.L. Tcheumi, V. Tchieda, S. Carteret, A. Walcarius, *The dye, Talanta*, 74 (2008) 489-97.
- [120] V. Vimonses, S. Lei, B.Jin, C.W.K. Chow, C. Saint. *Chem. Eng. J.*, 148 (2009) 354-64.
- [121] Z. Bekei, Y. Seki, M.K. Yurdakoc, *J. Hazard Mater.*, B 133 (2006) 233-42.
- [122] M.M. Mortland, S. Shaobai, S.A. Boyd, *Clay and Clay Minerals*, 34 (1986) 581-85.
- [123] J. Bors, S. Dultz, B. Riebe, *Appl. Clay Sci.*, 16 (2013) 1-13.
- [124] M.A. Mumin, M.M.R. Khan, K.F. Akhter, M.J. Uddin, *Int. J. Environ. Sci. Tech.*, 4 (2007) 525-32.
- [125] J.Q. Jiang, C. Cooper, *Environ. Eng. Sci.*, 20 (2003) 581-86.
- [126] B.K. Nandi, A. Goswami, M.K. Purkreit, *Journal of Hazardous Materials*, 161 (2009) 387-95.
- [127] R.G. Harris, J.D. Wells, B.B. Johnson, *Colloids Surf. A: Physicochem. Eng. Aspects*, 180 (2001) 131-40.
- [128] E. Sabah, M. Turan, M.S. Celik, *Water Res.*, 36 (2002) 3957-64.
- [129] M. Ugurlu, A.S. Hazrbulan, *Fresenius Environ. Bull.*, 16(8) (2007) 887-95.
- [130] S. Kumar, R. Kumar, A. Bandopadhyay, *Resour. Conserv. Recycl.*, 48 (2006) 301-14.
- [131] V.P. Gadepalle, S.K. Ouki, R. Van Herwijnen, T. Hutchings, *Soil Sediment Contam.*, 16 (2007) 233-51.
- [132] V.K. Gupta, C.K. Jain, I. Ali, S. Chandra, S. Agarwal, *Water Research*, 36 (2002) 2483-90.

- [133] D. Rameshraj, V.C. Srivastava, J.P. Kushwaha, I. D. Mall, Chem. Eng. Jol., (2012) 343-51.
- [134] V.K. Gupta, S. Sharma, I.S. Yadav, D. Mohan J. Chem. Technol. Biotechnol., 71 (1998) 180-6.
- [135] V.C. Srivastava, M.M. Swamy, I.D. Mall, B. Prasad, I.M. Mishra, Colloids Surf. A: Physicochem. Eng. Asp., 272 (2006)
- [136] Q. Feng, Q. Lin, F. Gong, S. Sugita, M.J. Shoya, J. of Colloid and Inter. Sci., 1-8 (2004) 278.
- [137] V.C. Srivastava., I.D. Mall, I.M. Mishra, J. of Hazard. Mater., B134 (2006) 257-67.
- [138] V.S. Mane, I.D. Mall, V.C. Srivastava, J. of Environ. Manag., 84 (2007) 390-400.
- [139] K.S. Chou, J.C. Tsai, C.T. Lo, Bioresource Technology, 78(2) (2001) 217-19.
- [140] N.L. Hecht, D.S. Duvall, vol. III, Utility Coal Ash, National Environmental Research Center, U.S. Environmental Protection Agency, 1975.
- [141] A. Mittal, D. Kaur, J. Mittal, J. of Colloid and Inter. Sci., 326 (2008) 8-17.
- [142] S. Rio, C.F. Brasquet, L.L. Coq, P.L. Cloirec, Environ. Sci. Technol., 39 (2005) 4249-57.
- [143] M. Otero, F. Rozada, L.F. Calvo, A.I. Garca, A. Moran, Dyes Pigm., 57 (2003) 55-65.
- [144] S. Larous, A.H. Meniai, Energy Procedia, 18 (2012) 905-14.
- [145] B.C. Pan, F.W. Menga, X.Q. Chen, B.J. Pan, X.T. Li, Zhang, W.M. Zhang, X.J.L. Chena, Q.X. Zhang, Y. Sun, J. Hazard. Mat., B124 (2005) 74-80.
- [146] W. Kujawski, A. Warszawski, W. Ratajczak, T. Porebski, W. Capala, I. Ostrowska, Sep. Purif. Technol., 40 (2004) 123-32.
- [147] M. Streat, L.A. Sweetland, 1997. React. Funct. Polym., 35 (1997) 99-109.
- [148] N. Kawabata, K. Ohira, Environ. Sci. Technol., 13 (1979) 1396-1402.
- [149] F.A. Dawodu, G.K. Akpomie, M.E. Ejikeme, P.C.N. Ejikeme, Int. J. Multidisciplinary Sci. Eng., 3 (2012) 13-18.

- [150] D.W. Breck, Zeolite Molecular Sieve: Structure, Chemistry, and Use, first ed., Wiley, New York, 1974.
- [151] L.B. Sand, F.A. Mumpton, 1st ed., Pergamon Press, Oxford, 1978.
- [152] K.S. Hui, C.Y.H. Chao, S.C. Kot, J. Hazard. Mater. B127 (2005) 89-101.
- [153] S.H. Chung, S.S. Kim, Y.M. Nam, S.M. Kim, B.J. Lee, J. Ind. Eng. Chem., 9 (2003) 181-87.
- [154] H. Ghobarkar, O. Schaf, U. Guth, Prog. Solid State Chem., 27(1999) 29-73.
- [155] V.R.K. Vadapalli, W.M. Gitari, A. Ellendt, L.F. Ptryk, G. Balfour, S. Afr. J. Sci., 106 (2007) 1-7.
- [156] M. Singh, R. Sharma, U.C. Banerjee. Biotechnol. Adv., 20 (2002) 341-59.
- [157] M. Ruiz, A.M. Sastre, E. Guibal, React. Funct. Polym., B45 (2000) 155-73.
- [158] B.J. Mcafee, W.D. Gould, J.C. Nadeau, A.C.A. DaCosta, Sep. Sci. Technol., 36 (2001) 3207-22.
- [159] M.S.Chiou, H.Y.Li, Chemosphere, 50 (2003) 1095-105.
- [160] W.S.W. Ngah, C.S. Endud, R. Mayanar, React. Funct. Polym., 50 (2002) 181-90.
- [161] F. Delval, J. Vebrel, P. Pont, M. Morcellet, L. Janus, G. Crini, Polym. Recycl., 5 (2000) 137-43.
- [162] W.E. Baille, W.Q. Huang, M. Nichifor, X.X. Zhu, J.M.S. Pure Appl. Chem., A 37 (2000) 677-90.
- [163] G. Crini, M. Morcellet, J. Sep. Sci., 25 (2002) 789-813.
- [164] L. Janus, B. Carbonnier, A. Deratani, M. Bacquet, G. Crini, Laureyns, J. Etal. New J. Chem., 27 (2003) 207-312.
- [165] F.C. Wu, R.L. Tseng, R.S. Juang, Ind. Eng. Chem. Res., 38 (1999) 270-75.
- [166] F.C. Wu, R.L. Tseng, R.S. Juang, J. Hazard. Mater., B 81 (2001) 167-77.
- [167] L. Dambies, C. Guimon, S. Yiacoumi, E. Guibal, Colloids Surf. A Physicochem. Eng. Asp., 177 (2001) 203-14.

- [168] R.C. Joshi, R.P. Lothia. Fly ash in concrete: production, properties and uses. In: *Advances in concrete technology*, vol. 2. Gordon and Breach Science Publishers, 1997.
- [169] X. Querol, N. Moreno, J.C. Umana, A. Alastuey, E. Hernandez, A. Lopez-Soler., *Int. J. Coal Geol.*, 50 (2002) 413-23.
- [170] G.P. Dasmahapatra, T.K. Pal, A.K. Bhadra, B. Bhattacharya, *Sep. Sci. Technol.*, 31 (1996) 2001-9.
- [171] G.Q. Lu, D.D. Do, *Fuel Process Technol.*, 27 (1991) 95-107.
- [172] J.F. Hollis, R. Keren, M. Gal, *J. Environ. Qual.*, 17 (1988) 181-4.
- [173] N.M. Agyei, C.A. Strydom, *Cem. Concr. Res.*, 32 (2002) 1889-97.
- [174] S.K. Khanna, P. Malhotra, *Ind J. Environ. Health*, 19 (1977) 224-37.
- [175] S. Kumar, S.N. Upadhyay, Y.D. Upadhyay. *J. Chem. Technol. Biotech.*, 37 (1987) 281-90.
- [176] A. Akgerman, M.J. Zardkoohi, *Chem. Eng. Data*, 41 (1996) 185-7.
- [177] B.J. Acemioglu. *Colloid. Interface Sci.*, 274 (2004) 371-9.
- [178] M. Matheswaran, T. Karunanithi. *J. Hazard Mater.*, 145 (2007) 154-61.
- [179] V.K. Gupta, A. Mittal, V. Gajbe, J. Mittal. *Ind. Eng. Chem. Res.*, 45(4) (2006) 1446–53.
- [180] J.X. Lin, S.L. Zhan, M.H. Fang, X.Q. Qian, H. Yang. *J. Environ. Manage.*, 87(1) (2008) 193-200.
- [181] K. Yamada, K. Haraguchi, C.C. Gacho, P.W. Bussakorn, M.L. Pena. In: *International Ash Utilization Symposium*. Centre for Applied Energy Research, University of Kentucky, 2003. Paper No. 116.
- [182] K. Kumari, S.K. Saxena. *Colloids Surf.*, 33 (1988) 55-61.
- [183] H.S. Rathore, S.K. Sharma, M. Agarwal. *Environ. Pollut. Series B. Chem. Phys.*, 10 (1985) 249-60.
- [184] H. Nollet, M. Roels, P. Lutgen, P. Van Der Meeren, W. Verstraete. *Chemosphere*, 53 (2003) 655-65.
- [185] K. Banerjee, P.N. Cheremisinoff, S.L. Cheng. *Water Res.*, 31 (1997) 249-61.

- [186] V. Solin, M. Kustka. Scientific Papers from Institute of Chemical Technology, 2 (1958) 247.
- [187] R. Bhargava, R.P. Mathur, P. Khanna. Ind. J. Environ. Health, 16 (1974) 109-20.
- [188] K. Banerjee, P.Y. Horng, P.N. Cheremisinoff, M.S. Sheih, S.L. Cheng In: Proceedings of 43rd industrial waste conference. West Lafayette: Purdue University, (1988) 397-406.
- [189] K.K. Jain, G. Prasad, V.N. Sinah. Ind. J. Chem., 19 (1980) 154-6.



Chapter-2

***Materials, Methods and Characterization
Techniques***

ABSTRACT

The current chapter describes the details of various chemicals and reagents, equipment, fundamental experimental details of the studies concluded in this thesis. Procedures for studying adsorption kinetics, adsorption isotherms models, thermodynamic study and error analysis equations have been discussed in this chapter. Description of various characterization techniques like XRF, XRD, FE-SEM with EDX, FTIR, pH_{ZPC} , Cation exchange capacity, organic carbon content, surface area and porosimetry etc. are briefly given.

The present chapter describes the instrumentation and methods used for adsorption process for removal of various organic compounds over raw fly ash (FA), NaOH treated fly ash (NaFA), surfactant cetyltrimethylammonium bromide (CTAB) modified fly ash (CTAB / NaOH / fly ash composite) and chitosan modified fly ash (Chitosan / NaOH / fly ash composite). Procedure for studying adsorption kinetics, adsorption isotherms, thermodynamic study, error analysis equations and characterization techniques for synthesized adsorbent materials have also been described in this chapter.

2.1 Chemicals and Solutions

(i) Resorcinol

Resorcinol of AR grade from S.D. Fine Chemical Limited was used as phenol source. For standard solution one gram of the resorcinol was dissolved in one litre double-distilled water to prepare stock solution (1000 mg/l). Experimental solutions of the desired concentrations were obtained by successive dilutions with distilled water.

(ii) Tannic Acid

Tannic acid of AR grade from S.D. Fine Chemical Limited was used as poly phenol source. Solution of tannic acid was prepared as discussed above.

(iii) MCPA (4-chloro-2-methylphenoxyacetic acid)

MCPA [(C₉H₉ClO₃) 98% (M.W.200.62) of Sigma–Aldrich, CAS no. 94-74-6] was used as pesticide or herbicide source.

(iv) Brilliant Green Dye (BG) (MW: 462.65)

Brilliant green of AR grade from S.D. Fine Chemicals Limited was used as dye source.

(v) Methylene Blue Dye (MB) (MW: 373.91)

Methylene blue of AR grade from S.D. Fine Chemical Limited was used as dye source.

(vi) Surfactant

N-Cetyl-N, N, N-Trimethyl Ammonium Bromide ($C_{19}H_{42}BrN$) 98% (M.W.364.46) of LOBA Chemi. (CAS no.59-09-0) was purchased for the synthesis of new adsorbent, surfactant modified fly ash.

(vii) Chitosan

Chitosan ($C_6H_{11}NO_4$) AR grade from Himedia, (Degree of De-acetylation > 75% CAS no. 9012-76-4) was used for the synthesis of chitosan modified fly ash.

(viii) Sodium Hydroxide (NaOH)

NaOH of AR grade from B.D.H. Fine Chemicals was used for maintaining pH of solution and synthesis of new adsorbent, NaOH treated fly ash.

(ix) Hydrochloric Acid (HCl)

HCl of AR grade from B.D.H. Fine Chemicals was used for maintaining pH of solution.

(x) Sodium Chloride (NaCl)

NaCl of AR grade from Ranbaxy was used for maintaining ionic strength of solution.

(xi) Potassium Nitrate (KNO_3)

KNO_3 of AR grade from B.D.H. Fine Chemicals was used for preparation of solutions of desired pH strength. A solution of 0.1 N KNO_3 was prepared by dissolving 10.11 gram of KNO_3 in 100 ml. of double distilled water.

(xii) Potassium Hydroxide (KOH)

Concentrated KOH of AR grade from B.D.H. Fine Chemicals was used for preparation of solutions of desired pH strength. A solution of 0.1 N KOH was prepared by dissolving 5.61 gram of KOH in 100 ml. of double distilled water.

(xiii) Nitric Acid (HNO_3)

Concentrated HNO_3 of AR grade from B.D.H. Fine Chemicals was used for preparation of solutions of desired pH strength and maintaining the pH of adsorbing solution.

(xiv) KCl

KCl of AR grade from Ranbaxy was used for estimation of Total Cation Exchange Capacity.

(xv) Acetic Acid Glacial (CH_3COOH)

Acid of AR grade from Ranbaxy was used for the preparation of buffer solution.

(xvi) Sodium Acetate (CH_3COONa)

Sodium Acetate of AR grade from Ranbaxy was used for the preparation of buffer solution.

(xvii) Ammonium Hydroxide (58% NH_4OH)

Ammonium hydroxide of AR grade from Ranbaxy was used for the preparation of ammonium acetate solution.

(xviii) Ethyle Alcohol (95%)

Ethyle alcohol of AR grade from Ranbaxy was purchased and used for washing of adsorbent.

2.2 Adsorbent Materials

2.2.1 Fly ash

Fly ash (FA) samples were collected from different coal based industrial units in India, which are given as below:

1. Sri Ram Fertilisers & Chemical Ltd., Kota, Rajasthan - FA_{10} , FA_{30} , FA_{35} and FA_{40} (From Four different types of Boilers according to their capacity 10 MW, 30 MW, 35 MW and 40 MW respectively)
2. Kota Super Thermal Power Station, Kota, Rajasthan - FA_{KT}
3. Lehra Mohabbat Thermal Power Plant, Bhatinda, Punjab - FA_{BT}

4. Tata Thermal Power Plant, Jamshedpur, Jharkhand - FA_{JM}
5. Suratgarh Thermal Power Station, Ganganagar, Rajasthan - FA_{ST}
6. Talchar Super Thermal Power Station, Angul, Orissa - FA_{TR}
7. Vindhyachal Super Thermal Power Station, Singrauli, Madhya Pradesh - FA_{VL}
8. Giral Lignite Thermal Power Station, Barmer, Rajasthan - FA_{BM}

The collected samples were used as adsorbents after suitable treatments for removal of organic pollutants. The details of various adsorbents are described in respective chapters

2.3 Minor Equipments

(i) UV/Vis Spectrophotometer

Concentration of all organic compounds were determined by finding out the absorbance at the characteristic wavelength using a double beam **UV/Vis spectrophotometer (model Spectrscan UV 2600/02)**.

(ii) pH Meter

The Syntonic digital pH meter model, 335 was used for measuring pH of the reaction mixtures and for calculating pH_{ZPC} .

(iii) Temperature-Controlled Orbital Shaker

Temperature controlled orbital shaker (Anand and Anand, New Delhi) was used for shaking solution and preparing fly ash supported adsorbents.

(iv) Electronic Balance

Citizen electronic balance (**Model: Cx 200**) with least count of 0.0001 mg was used for weighing purposes.

(v) Stirrer

Remi 2LH stirrer was used for stirring to make supported adsorbent from fly ash at a fixed and suitable rpm.

(vi) Planetary Ball Mill

High energy Planetary ball mill (**Retsch PM-100, Germany**) was used for ball milling of fly ash and supported adsorbents to grind them in to fine particles for improving adsorption capacity and surface area.

(vii) Centrifuge Machine

Centrifuge machine (**MBL-20 make**) was used to obtained supernatant liquid from solution.

(viii) Muffle Furnace

Ambassador Muffle furnace with maximum temperature upto 1200 °C was used for heating, drying and calcinations of fly ash and supported adsorbent made from fly ash.

(ix) Flame Atomic Absorption Spectrophotometer

The Na, K, Ca present in samples were analysed by Flame Atomic Absorption Spectrophotometer model 128, make Systronics.

2.4 Characterization Techniques and Major Equipments

(i) X-Ray Fluorescence (XRF) and Energy Dispersive X-Ray (EDX)

The chemical analysis of fly ash is carried out by X-ray fluorescence (XRF), inductively coupled plasma and flame atomic absorption spectrophotometer and other fly ash supported adsorbents analysed by Energy dispersive X-ray (EDX) due to small amount is required in EDX study. As fly ash is ensembles of elements, therefore a multi elemental technique capable of determining elements with accuracy is preferred.

X-Ray Fluorescence (XRF)

In XRF, major elements were analysed on a fused glass bead at 50 kV and 50 mA tube operating conditions. The intensity obtained for the elements were calibrated by using standards for both major and minor elemental analysis [1]. XRF Analysis is a widely used method of elemental analysis and chemical analysis providing both quantitative and qualitative compositional information.

XRF can measure the wide range of measurable elements covering nearly the entire periodic system. X-ray fluorescence model **WD-XRF (S8 Tiger Bruker, Germany)** at was used for the present work. It is the wave length dispersive X-Ray fluorescence (WD-XRF), which separates the characteristic wavelengths with a very high degree of resolution. Optimized analyser, crystals and detectors are used to separate and count the emitted X-rays. WD-XRF is unsurpassed in terms of analytical accuracy and precision. In this method, the sample is excited with a primary X-ray beam, causing the sample to have fluorescence. The primary X-ray ejects electrons out of the inner atomic shells (K- and L-shell). The resulting “vacancy” is filled by an electron from an outer electronic shell. This electron transition takes place only between the inner shells of the atom, which are not involved in chemical bonding. Hence the samples could be analyzed directly without advanced sample preparation.

Energy-dispersive X-ray spectroscopy

Energy-dispersive X-ray spectroscopy (EDS, EDX, EDXS or XEDS), sometimes called energy dispersive X-ray analysis (EDXA) or energy dispersive X-ray microanalysis (EDXMA), is an analytical technique used for the elemental analysis or chemical characterization of a sample. It relies on an interaction of some source of X-ray excitation and a sample. Its characterization capabilities are due in large part to the fundamental principle that each element has a unique atomic structure allowing a unique set of peaks on its electromagnetic spectrum emission [2].

To stimulate the emission of characteristic X-rays from a specimen, a high-energy beam of charged particles such as electrons or protons, or a beam of X-rays, is focused into the sample being studied. At rest, an atom within the sample contains ground state (or unexcited) electrons in discrete energy levels or electron shells bound to the nucleus. The incident beam may excite an electron in an inner shell, ejecting it from the shell while creating an electron hole where the electron was. An electron from an outer, higher-energy shell then fills the hole, and the difference in energy between the higher-energy shell and the lower energy shell may be released in the form of an X-ray. The number and energy of

the X-rays emitted from a specimen can be measured by an energy-dispersive spectrometer. As the energies of the X-rays are characteristic of the difference in energy between the two shells and of the atomic structure of the emitting element, EDS allows the elemental composition of the specimen to be measured [2]. **EDX (FE-SEM SUPRA 55 attached with Energy Dispersive Microanalysis)** was used for the present work.

(ii) X-ray Diffraction Study (XRD)

X-ray powder diffraction (XRD) is a rapid analytical technique primarily used for structural properties viz. Phase identification of a crystalline material, crystallinity, crystalline size and can provide information on unit cell dimensions. The analyzed material is finely ground, homogenized, and average bulk composition is determined. The crystalline phase(s) in the fly ash and fly ash supported adsorbent materials were identified by powder X-ray diffraction analysis on a **X' Pert Pro, X-ray diffractometer using Ni filtered Cu-K α radiation (40 kV, 40 mA and $\lambda = 1.54056 \text{ \AA}$)**. For typical powder patterns, data is collected at 2θ from $\sim 5^\circ$ to 70° , angles that are preset in the X-ray scan. In XRD the parallel planes inside the crystal called lattice planes are designated by their integers h , k and l called miller indices, which are of the reciprocals of the intersection between the lattice plane and the three crystallographic axis that span the unit cell of the crystal. A given set of planes with indices h , k and l cut the a-axis of the unit cell in h section, b-axis in k sections and the c-axis in l sections. The incident X-ray beam and the lattice planes have to be oriented in a certain angle (θ) to allow diffraction. Beams reflected at parallel lattice planes in the distance (d_{hkl}) interfere and give intensity maximum, which occurs as a peak in X-ray diffractogram, if their path difference $2d_{hkl}$ is an integer of wavelength (λ). This relationship can be expressed mathematically in Bragg's law [3, 4] which is expressed as:

$$n\lambda = 2 d \sin \theta \quad (2.1)$$

Where λ is the wavelength of x-rays, d is the interplanar spacing, θ is the x-ray angle, n is an integer. The X-ray diffractogram consists of a plot of reflected intensity versus the diffracted angle 2θ . In powder samples with randomly

oriented crystallite, the same amount of the crystallite has the right orientation for the diffraction for all lattice planes. If instead, a certain pattern is preferred the intensity of some reflection is lowered or increased, Information about the lattice parameters is available from peak position. The sharpness of the diffraction lines is determined from their intensity together with their breadth, which is called the full width at half maximum (FWHM). The breadth of the peak is increased with decreasing crystalline size. The XRD pattern of a sample shows the intensity of X-ray diffracted by different planes of the crystal at different angles. The crystal phase identification is based on the comparison of the set of reflections of the specimen with that of pure references phases or with database [5]. X-ray diffraction line broadening analysis is used to determine crystallite size of the crystalline phase using the Scherrer formula [6] as in equation 2.2 where,

$$\text{Crystallite size} = K\lambda / W.\cos\theta \quad (2.2)$$

Where K = shape factor, λ = wavelength of x-rays radiation, W = difference of broadened profile width of the experimental sample (W_b) and standard profile width of the reference sample (W_s), θ = angle of diffraction.

(iii) Fourier Transform Infrared Spectroscopy (FT-IR)

Fourier Transform Infrared Spectroscopy, also known as FTIR Analysis or FTIR Spectroscopy, is an analytical technique used to identify chemical bonding and molecular structure of materials like organic, polymeric, inorganic, presence of various groups, structure, hydrogen bonding, etc. The FTIR analysis method uses infrared light to scan test samples and observe chemical properties. The technique works on the fact that bonds and groups of bonds vibrate at characteristic frequency. The interactions of IR radiation with molecules results to vibration in the dipole moment and therefore, the transitions take place in vibrational energy levels of the molecules, which are quantized. The activation of the molecule leads to different mode of fractional motions such as stretching (symmetric and asymmetric) and bending, promotes the molecule in higher vibrational energy level. The energy of the stretching vibrational motion is higher than that of the bending vibration and the asymmetric stretching motion

(asymmetrical stretching frequency) is higher than symmetric stretching (symmetrical stretching frequency). The transition in vibrational energy levels of the molecule gives IR spectrum, which is the graph between the wave number and the % transmittance or absorbance. The test is performed in absorbance, but can be converted to transmittance. Both qualitative and quantitative information about the test sample can be provided. The FTIR spectra were recorded with a **Bruker FT-IR spectrophotometer (Tensor-27)** with **DRS (Diffuse Reflectance Spectroscopic)** using the KBr method for analyzing the bonding structure of the samples. FT-IR was performed by mixing the samples with KBr in 1:20 weight ratio. Spectra were recorded in the range 400-4000 cm^{-1} with a resolution of 4 cm^{-1} . The overall spectrum of FTIR is divided into two general regions: 4000-1300 cm^{-1} (the functional group region) and 1300-400 cm^{-1} (the fingerprint region). The frequency assignment approach is used for the interpretation of the spectrum.

(iv) **Scanning Electron Microscopy (SEM)**

The Morphological and Topographical studies were carried out using electron microscope, which is a straight forward technique useful for the determination of the morphology and size of solid catalyst. Two important electron microscopic techniques viz. Scanning Electron Microscopy (SEM) and Transmission Electron Microscopy (TEM) were explored in this section.

Scanning Electron Microscope (**FE-SEM SUPRA 55 attached with Energy Dispersive Microanalysis**) is being used to determine the morphology of different samples used in this study. A portion of sample was sprinkled onto double sided tape mounted on a SEM stub, which enables to determine the particle morphology, external surface structure of particles.

Transmission Electron Microscopy (TEM) resembles optical microscopy, except that electromagnetic instead of optical lenses are used to focus an electron beam on the sample. Two modes are available in TEM, a two dimensional image of the density or thickness of the sample, and a dark field mode where the electron diffraction pattern is recorded [7]. Since TEM has a higher resolution than SEM, it is often used to image under nano sized catalysts such as metals oxide particles, supported metals and catalysts with nanopores [8].

(v) **BET Surface Area and Pore Size Distribution**

Specific surface area, pore diameter and pore volume in the samples were determined from N₂ adsorption –desorption isotherms and the pore-size distribution obtained from **ASAP 2010 from Micrometric** by fitting the amount of N₂ adsorbed at -196⁰C for the BET equation and the pore-size analyzer. BET and BJS approaches were used to calculate surface area and pore size distribution respectively [9]. BET theory aims to explain the physical adsorption of gas molecules on a solid surface and serves as the basis for an important analytical technique for the measurement of the specific surface area of a material [10]. The concept of the theory is an extension of the Langmuir theory which is a theory for monolayer molecular adsorption, to multilayer adsorption with the following hypotheses: (a) gas molecules physically adsorb on a solid in layer infinitely; (b) there is no interaction between each adsorption layer; and (c) the Langmuir theory can be applied to each layer. The resulting BET equation is expressed by (2.3).

$$\frac{1}{v\left[\left(\frac{P_0}{P}\right)-1\right]} = \frac{c-1}{v_m c} \left(\frac{P}{P_0}\right) + \frac{1}{v_m c} \quad (2.3)$$

P and P₀ are the equilibrium and the saturation pressure of adsorbates at the temperature of adsorption, v is the adsorbed gas quantity (for example, in volume units), and v_m is the monolayer adsorbed gas quantity, c is the BET constant, The BET method is widely used in surface science for the calculation of surface areas of solids by physical adsorption of gas molecules. A total surface area S_{total} and a specific surface area S are evaluated by using equations (2.4) and (2.5):

$$S_{\text{BET, total}} = (v_m N S) / V \quad (2.4)$$

Where v_m is in units of volume which are also the units of the molar volume of the adsorbate gas

$$S_{\text{BET}} = S_{\text{total}} / a \quad (2.5)$$

N – Avogadro s number,

S – Adsorption cross section of the adsorbing species,

V – Molar volume of adsorbate gas,

a – mass of adsorbent (in g)

The N₂ adsorption –desorption isotherms of FA₄₀, NaFA, CTAB / NaOH / fly ash composite and Chitosan / NaOH / fly ash composite at liquid nitrogen temperature (77 K) and gas saturation vapor tension range were measured as per following procedure-Approximately 0.3 to 0.5 g of powder were placed in a test tube and allowed to degas for 2 hours at 175 °C in flowing nitrogen. This removes contaminants such as water vapor and adsorbed gases from the samples. The static physisorption isotherms were obtained with N₂ in liquid nitrogen, the amount of liquid nitrogen adsorption, or desorption from the materials as a function of pressure ($P/P_0 = 0.025-0.999$). Data were obtained by admitting or removing a known quantity of adsorbing gas in or out of a sample cell containing the solid adsorbent maintained at a constant temperature (77.35 K). As adsorption or desorption occurs, the pressure in the sample cell changes until equilibrium is established. From the N₂ static physisorption isotherms of the samples to obtain the single layer adsorption capacity, the specific surface area of the sample was calculated from the BET adsorption equation. Based on the BJH academic model, the properties of the cumulative pore specific surface area, cumulative pore volume, average pore diameter, and BJH desorption pore distribution curves of the samples were estimated by BJH analysis method. An adsorption is the source of information about properties, such as the porous structure of the adsorbent, heat of adsorption and physical and chemical characteristics.

Most analysis of adsorption equilibria begins with classification of the isotherms. The IUPAC classification scheme has six types of isotherms for vapour / solid equilibria [11] as shown in Figure 2.1 and interpretation is given in Table 2.1. It is based on an earlier classification by Brunauer [12] which had five types of isotherms. A type I isotherm ‘approaches a limiting value’ [13] and usually is used to describe adsorption on microporous adsorbents. Types II and III describe adsorption on macroporous and non-porous adsorbents with strong and weak adsorbate–adsorbent interactions respectively [11]. Types IV and V show hysteresis for strongly and weakly adsorbing surfaces. This hysteresis behaviour has been attributed to capillary condensation [14]. Type VI, which was not

included in the Brunauer classification, illustrates that the adsorption isotherms can have one or more steps [15]. Recently, Rouquerol et al. [16] extended this scheme by considering the shapes of isotherms with adsorption hysteresis in more detail. The IUPAC classification of adsorption behaviour reflects the ideas of Brunauer [12] based on knowledge in the 1940s and 1950s.

There also have been classifications of hysteresis loops [13]. As seen from Figure 2.2, hysteresis loops may exhibit different shapes. In type H-1, the hysteresis loop is narrow, the adsorption and desorption branches are almost vertical and nearly parallel. It has been associated with porous materials made from agglomerates or compacts of approximately uniform spheres and having a narrow pore-size distribution. The type H-2 loop is broad with the desorption branch being much steeper than the adsorption branch. It can be found in many porous adsorbents and is believed to occur [16] in systems where the distribution of pore sizes and pore shapes are broad. It is believed that this kind of loop results when there is a difference in mechanism between condensation and evaporation and that this occurs in pores with narrow necks and wide bodies or when the porous material has an interconnected pore network [16]. The type H-3 loop does not exhibit any limiting adsorption at high p/p_0 . It is believed [16] that this type of isotherm occurs with aggregates of plate-like particles giving rise to slit-shaped pores. The type H-4 loop is nearly horizontal and parallel over a wide range of p/p_0 . It is often associated with narrow slit-like pores [16].

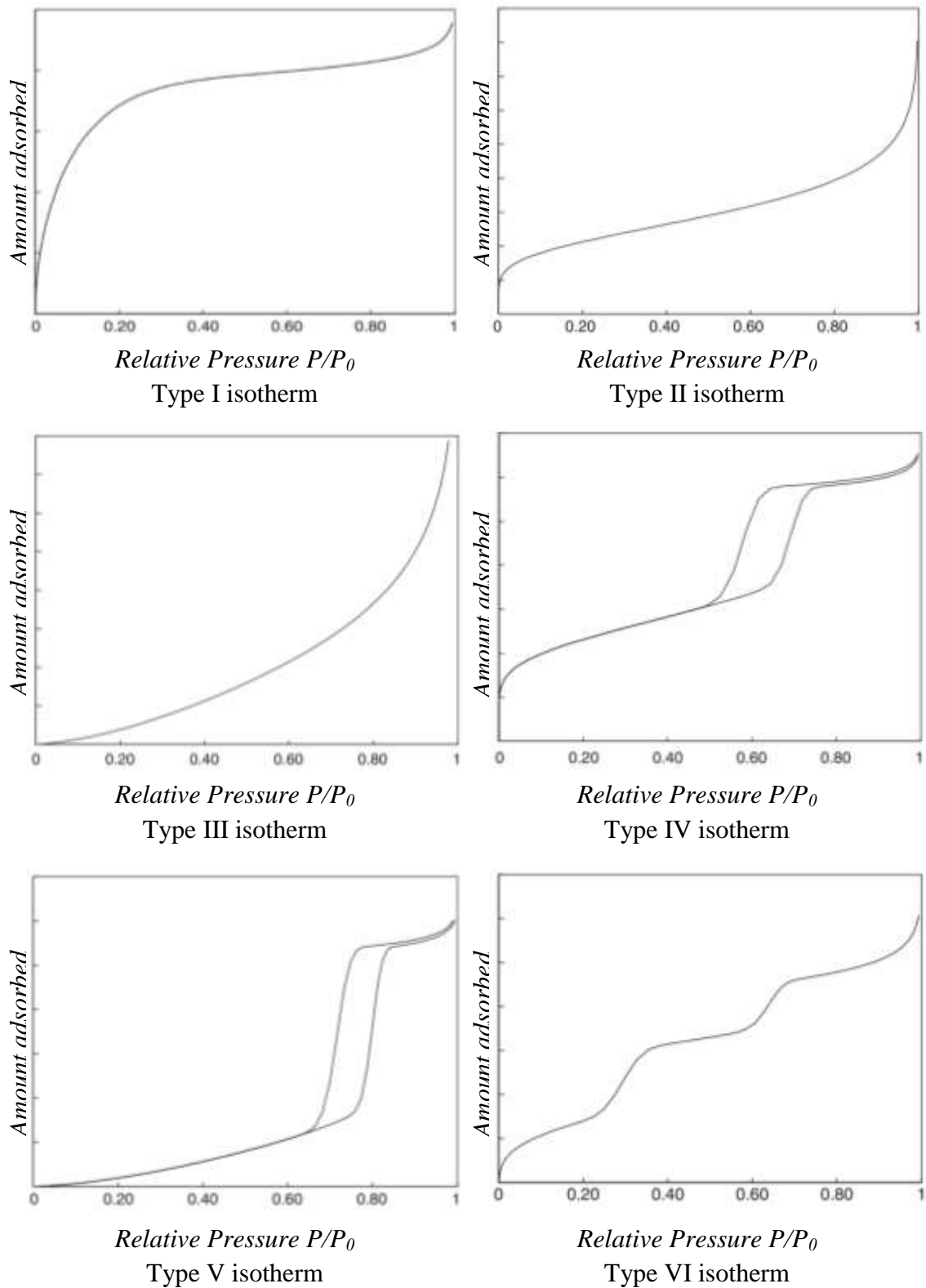


Figure 2.1: The IUPAC classification of adsorption isotherms for gas–solid equilibria

Table 2.1: Classifications of physical adsorption isotherms

Type	Interpretation
I	This is characteristic of either a chemisorption isotherm (in which case the final upswing at high pressures may not be present) or physisorption on a material that has extremely fine pores (micropores).
II	This is characteristic of a material, which is not porous, or possibly macroporous, and has a high energy of adsorption.
III	This is characteristic of a material, which is not porous, or possibly macroporous, and has a low energy of adsorption.
IV	This is characteristic of a material, which contains mesoporosity and has a high energy of adsorption. These often contain hysteresis attributed to the mesoporosity.
V	This is characteristic of a material, which contains mesoporosity and has a low energy of adsorption. These often contain hysteresis attributed to the mesoporosity.
VI	This type of isotherm is include multiple pore sizes. If the steps are at the low pressure portion of the isotherm, then the steps may be due to two or more distinct energies of adsorption. If the steps are at the high pressure part of the isotherm, then the steps might be due to sharp steps on the adsorbate surface.

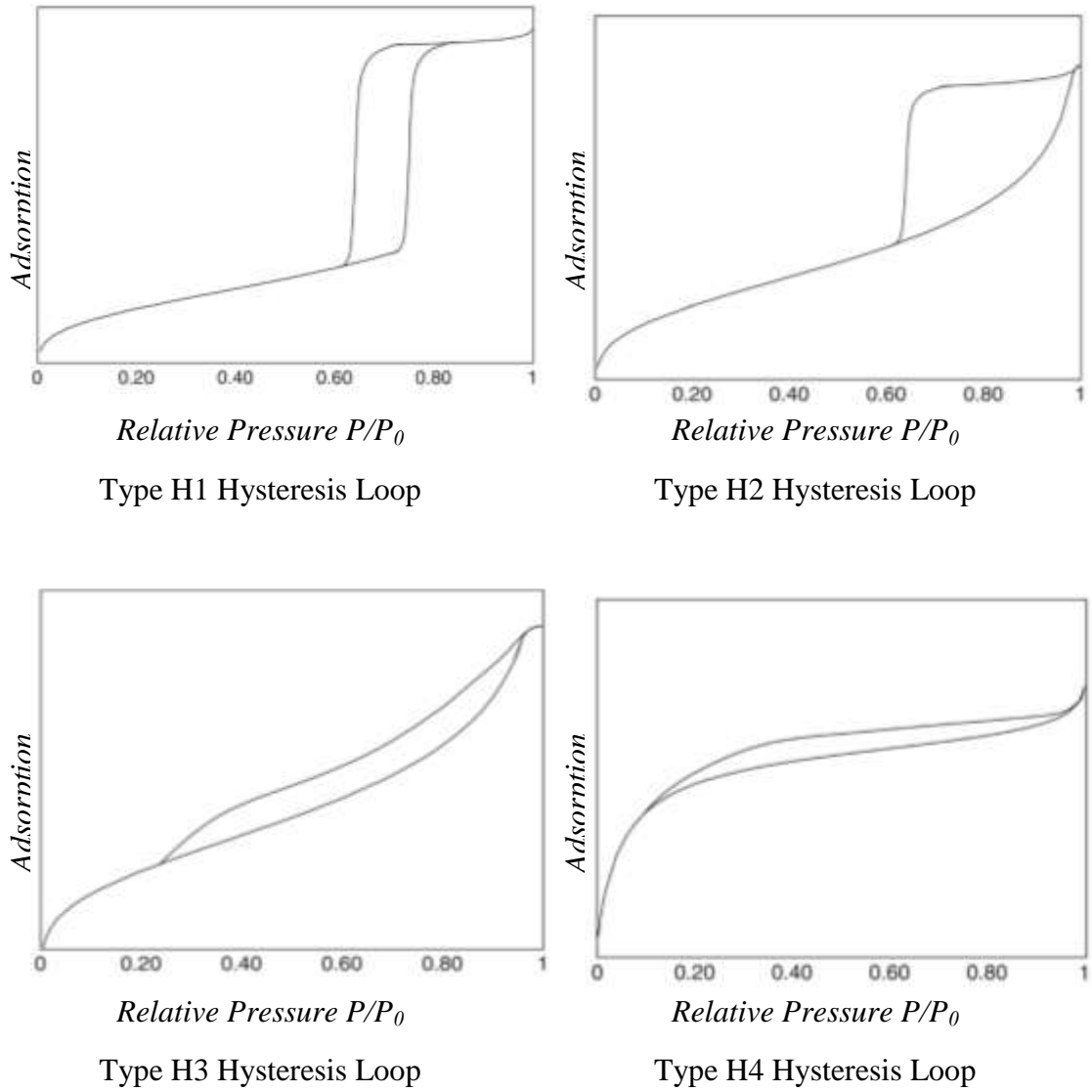
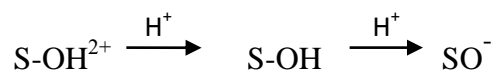


Figure 2.2: Modern classification of hysteresis loops

(vi) Point of Zero Charge (pH_{zpc})

Most of solid surfaces have pH dependant surface charges, when in contact with the aqueous solutions. Surfaces can have positive or negative charges or both depending upon the pH, temperature, background electrolyte concentration and presence of cations and anions present in the aqueous solution [17], following is the mechanism



Where S represents the solid surface, the pH at which the net charge on the surface is zero is called Zero Point Charge (ZPC) or point of zero charge. The pH of zero point charge (pH_{zpc}) plays an important role in the adsorption process. The point of zero charge of the adsorbent is determined by the solid addition method [18, 19]. For this purpose, 50 ml of 0.1 M KNO₃ solution was placed in a 100 ml in sealed cap conical flask. The pH was adjusted to successive initial value between 2 and 12, by using either 0.05 N HNO₃ or 0.1 N KOH. Then 1.0 g adsorbents were added to the solution. After shaking for 24 hours in thermostatic shaker, the final pH was measured. A plot is drawn between Δ pH and initial pH₀. The pH at Δ pH = 0 is taken as the pH_{zpc}.

The pH of the solution affects the surface charge of the adsorbents as well as the degree of ionization and speciation of different pollutants. Changes in the pH affect the adsorptive process through dissociation of functional groups as the active sites on the surface of the adsorbent. This subsequently leads to a shift in the reaction kinetics and the equilibrium characteristics of the adsorption process. Adsorption of the various anionic and cationic species on such adsorbents can be explained on the basis of the competitive adsorption of H⁺ and OH⁻ ions with the adsorbate. It is a common observation that the surface adsorbs anions favourably at lower pH due to presence of H⁺ ions, whereas the surface is active for the adsorption of cations at higher pH due to deposition of OH⁻ ions [20].

(vii) Cation Exchange Capacity (CEC)

Cations are positively charged ions such as calcium (Ca^{2+}), magnesium (Mg^{2+}), and potassium (K^+), sodium (Na^+), hydrogen (H^+), aluminum (Al^{3+}), iron (Fe^{2+}), manganese (Mn^{2+}), zinc (Zn^{2+}) and copper (Cu^{2+}). The capacity of the fly ash to hold on to these cations called the cation exchange capacity (CEC). These cations are held by the negatively charged fly ash and organic matter particles in the fly ash through electrostatic forces (negative soil particles attract the positive cations). The cations on the CEC of the fly ash particles are easily exchangeable with other cations. Thus, the CEC of a fly ash represents the total amount of exchangeable cations that the fly ash can adsorb.

CEC is the number of exchangeable cations per dry weight that a fly ash is capable of holding, at a given pH value, and available for exchange with the fly ash water solution. The CEC is the number of positive charges (cations) that a representative sample of soil can hold. It is usually described as the number of hydrogen ions (H^+) necessary to fill the soil cation holding sites per 100 grams of dry soil. Alternatively, an equivalent amount of another cation (Al^{3+} or Ca^{2+}) can be used in the measure. In soil science, an equivalent is defined by the number of charges in terms of a given number of hydrogen ions. As hydrogen ions have only one positive charge (H^+), this makes calculations relatively simple. An equivalent of Al^{3+} that could be held would amount to one third as many of those ions, and Ca^{2+} would have half as many ions.

Translation from meq / 100g to an applicable unit, for instance lbs/acre of available nutrients, can be calculated, but must consider the atomic weight, the ion's valence, and using a reasonable estimate of soil depth and density. cation exchange capacity is of two type:

- (a) External cation exchange capacity (ECEC)
- (b) Total cation exchange capacity (TCEC)

(a) External Cation Exchange Capacity (ECEC)

The external cation exchange capacity (ECEC) was determined by adsorption of methylene blue from aqueous solution [21, 22].

Determination of ECEC (Methylene Blue Titration Method)

In this method a spectrophotometer is used to determine the amount of methylene blue (remaining in the solution). Spectrophotometer improves the accuracy of determining the adsorbed methylene blue. The test procedure is described as follows: Two gram of oven dried adsorbent was mixed with 200 ml of deionised water in a 600 ml flask. The methylene blue solution was added to adsorbent suspension (the concentration was 1g/L of MB). The suspension was mixed continuously for about 2h with shaker, and allowed to sit over night to reach adsorption equilibrium and allow particle settlement. Then 5 ml of fluid was removed, and it was centrifuged (the remain concentration of MB) in the fluid was determined by UV-visible spectrophotometer, at wavelength of 660 nm. The CEC was derived from the point of complete cation replacement determined on the titration curve. When the curve deviate from 45⁰ line it means that added MB cannot adsorbed by the adsorbent completely. In other words, all the exchangeable sites of the adsorbent are covered by MB molecules. The assumption is that MB dye is capable of attaching itself to exchange sites on the adsorbent surface by replacing the cations. Plotting the adsorbed MB against the added MB shows a deviation from 45⁰ straight lines in the titration method. At this point CEC is determined by the following formula

$$C = 100V_{cc} N_{mb} / m_s \quad (2.6)$$

Where C = the cation exchange (meq/100g adsorbent),

m_s = weight of the adsorbent,

V_{cc} = the volume of the MB titrant, and

N_{mb} = the normality of the MB substance, meq / mL.

$N_{mb} \%$ = weight of methylene blue (g)/320 100-X/100

Where X = the moisture content of the MB substance, %

(b) Total Cation Exchange Capacity (TCEC)

The total cation exchange capacity (TCEC) was determined from the amount of retained ammonium by the ammonium acetate method [23].

Determination of TCEC (ammonium acetate method)

- For preparation of 1 M NH_4OAc at pH 7.00 (10 litre): The solution was prepared in a fume hood to avoid breathing vapors of ammonia and acetic acid. 580 mL of glacial acetic acid (99.5%) was added to approximately 5 L of water, 680 mL of concentrated ammonium hydroxide (58% NH_4OH) and dilute with distill water to yield a volume of approximately 1900 ml. pH was adjusted to 7.00 with drop wise additions of either ammonium hydroxide or acetic acid. Than dilute to 10 L.
- 10 grams of air-dried adsorbent placed into a 250 ml beaker.
- 25 mL of NH_4OAc was added to the adsorbent. Refrain from mixing the beaker in a circular fashion to avoid adsorbent wicking onto the sides of the beaker. Covered and left it for overnight.
- For each sample, a 7 cm Buchner funnels was prepared by fitting it with a 7 cm Whatman #42 filter paper. The filter was wet with a minimum amount of NH_4OAc . The funnel was inserted into a 250 ml suction flask. Turned on vacuum pump to seat the moistened filter. Stir and transfer the adsorbent - NH_4OAc mixture into the filter.
- 75 mL NH_4OAc was measured for each sample into a plastic squirt bottle with one bottle for each sample. Use about 10 mL of the NH_4OAc in the bottle to transfer all of the adsorbent to the Buchner funnel.
- The adsorbent was covered with a 7.0 cm What man #1 filter paper to keep it moist between leaching's.
- The adsorbent was leached 5 to 7 times with 10 to 15 ml increments of NH_4OAc .
- The leachate was transferred to a 250 mL volumetric and brought to volume with 1 M NH_4OAc .

- The adsorbent was leached with about 25 mL portions of ethanol and 25 mL portions of 1 M KCl five to six times for a total volume of about 150 ml to remove excess NH_4OAc and adsorbed NH_4 respectively in the adsorbent.
- The leachate was transferred to a 250 mL volumetric flask and brought to volume using 1 M KCl. The solution was analyzed for NH_4 concentration using colorimetry.

(viii) Carbon Content

Organic carbon content was measured by the difference in weight loss between 105 and 750 °C.

2.5 Analytical Measurements

Concentration of all organic compound were determined by finding out the absorbance at the characteristic wavelength using a double beam UV/VIS spectrophotometer (model Spectrscan UV 2600/02). A standard solution of the organic compound was taken and the absorbance was determined at different wavelengths to obtain a plot of absorbance versus wavelength. For standard solution an accurately weighed quantity of the organic compound was dissolved in double-distilled water to prepare stock solution (1000 mg/l). Experimental solutions of the desired concentrations were obtained by successive dilutions with distilled water.

The wavelength corresponding to maximum absorbance (λ max) as determined from this plot was 625 nm for Brilliant green (BG), 660 nm for Methylene blue (MB), 225 nm for 4-chloro-2-methyl phenoxyacetic acid (MCPA), 212 nm for Tannic acid and 313 nm for Resorcinol. This wavelength was used for preparing the calibration curves between absorbance and the concentration of the organic compound solution. The calibration plot of absorbance versus concentration for all organic compounds showed a linear variation up to 20 mg/l concentration. Therefore, the samples with higher concentrations of organic compound (> 20 mg/l) were diluted with distilled water, whenever necessary, to make the concentration less than 20 mg/l, for

the accurate determination of the organic compound concentration with the help of the linear portion of the calibration curve.

2.6 Batch Experimental Programme

To study the effect of important parameters like pH, effect of adsorbent (m), initial concentration of adsorbate (C_0) and contact time (t) on the adsorptive removal of organic compounds, batch experiments were conducted. For each experimental run, 50 ml of solution of known concentration and a known amount of the adsorbent were taken in a 250 ml stoppered conical flask. This mixture was agitated in a temperature-controlled orbital shaker at a constant speed of 200 rpm. Samples were withdrawn at appropriate time intervals. Some FA (adsorbent) particles remain suspended and do not settle down easily. Therefore, all the samples were centrifuged at 2000 rpm for 4 min and analyzed for the residual pollutant concentration. The effect of pH on organic compounds removal was studied over a pH range of 3-11. pH was adjusted by the addition of dilute aqueous solutions of HCl or NaOH (0.10 M). For the optimum amount of adsorbent per unit mass of adsorbate, a 50 ml organic compound solution was contacted with different amounts of FA till equilibrium was attained. Blank experimental runs, with only the adsorbent in 50 ml of double-distilled water, were conducted simultaneously at similar conditions to account for any colour leached by the adsorbents and adsorbed by glass containers. .

The amounts of solute adsorbed per unit mass of adsorbent (q_e) were calculated from the differences between the initial and the final solute concentrations in solution before and after adsorption:

$$q_e = \frac{(C_0 - C_e)V}{W} \quad (2.7)$$

Where V is the sample volume in litre (L), C_0 is the initial solute concentration in mg L^{-1} , C_e is the equilibrium concentration in mg L^{-1} , and W is the dry weight of adsorbent in gram. Blank determinations including determinations for adsorbent in the absence of adsorbates were always carried out. All experiments were conducted in duplicate and the mean data are reported.

2.7 Adsorption Mechanism and Kinetics

The study of adsorption kinetics is markedly important since it provides informative reaction pathways and mechanism involved in the adsorption process. The obtained Kinetics rate is used to determine the feasible exploitation of adsorption. A slow adsorption rate often presents serious limitations for the practical application of the adsorption process. Adsorption is a physio-chemical reaction process. The molecules adhere to a surface of adsorbents with which they come into contact, due to force of attraction at the surface. The use of surface energy to attract and hold molecules can be carried out by either physical or chemical attraction. The Adsorption mechanism occurs in three basic steps which are bulk diffusion, pore diffusion, and adhesion of the solute molecule of the adsorbate through the particle surface film .Pore diffusion involves the migration of solute molecule adhere to the pore surface. It is noteworthy that the rate of adsorption of a particular molecule depends upon its mobility in the solution phase, the sorbent pore structure, the particle size and the hydrodynamics of contact between the solution and particle phase [24].

For a solid liquid adsorption process, the solute transfer is usually characterized by either external mass transfer (boundary layer diffusion) or intra particle diffusion or both. The adsorption dynamics can be described by the following three consecutive steps:

- Transport of solute from bulk solution through liquid film to adsorbent exterior surface.
- Solute diffusion into pore of adsorbent except for a small quantity of sorption on external surface; parallel to this is intra particle transport mechanism of surface diffusion.
- Adsorption of solute on interior surfaces of the pores and capillary spaces of adsorbent.

The last step is an equilibrium reaction. Of the three steps, the third step is rapid and negligible. The overall rate of adsorption will be controlled by the slowest step that would be either film diffusion or pore diffusion controlled.

2.7.1 Kinetic Models

The kinetics of adsorption was determined by analyzing adsorptive uptake of the organic compound from the aqueous solution at different time intervals. Various kinetic models have been suggested [25, 26,29] for adsorption, including the Lagergren pseudo-first order kinetics, the pseudo second order kinetics, Bangham equation and intra particle diffusion model, which are expressed in Equations (2.8 - 2.14) as listed below:

(i) **Lagergren pseudo-first order kinetics**

The linearized form of pseudo-first-order kinetic model is given in equation 2.8 follows:

$$\ln(q_e - q_t) = \ln(q_e) - k_1 t \quad (2.8)$$

Where q_e (mg/g) and q_t (mg/g) are the organic compounds adsorption capacities for fly ash and fly ash supported adsorbent at equilibrium and at any time t (min), respectively. k_1 (1/min) is the rate constant of pseudo-first-order kinetic model. The linear plot of $\ln(q_e - q_t)$ versus t was used to calculate the rate constant k_1 and R^2 is the determination coefficient.

(ii) **Pseudo second order kinetics**

The linearized form of pseudo-second-order kinetic model is given in equation 2.9

$$\frac{t}{q_t} = \frac{1}{k_2 q_e^2} + \frac{t}{q_e} \quad (2.9)$$

Where k_2 (g/mg min) is the rate constant of pseudo-second-order kinetic model. It can be rearranged as equation 2.10

$$q_t = \frac{t k_2 q_e^2}{1 + t k_2 q_e} \quad (2.10)$$

The initial sorption rate, h (mg/g min), at $t \rightarrow 0$ is defined as equation 2.11

$$h = k_2 q_e^2 \quad (2.11)$$

Eq. (2.10) can be rearranged to obtained equation 2.12

$$q_t = \frac{t}{1/h + (1/q_e)t} \quad (2.12)$$

The values of equilibrium adsorption capacity q_e and initial sorption rate h , calculated from the intercept and slope of the line at plot of t/q_t versus t , k_2 rate constant are determined from the value of h , along with the value of determination coefficient R^2 . If the R^2 value obtained was very high ($R^2 > 0.999$), and the calculated q_e value was in good agreement with the experimental one, suggesting the applicability of that kinetic model to describe the adsorption kinetics data.

If linear plots of q_e and h against C_0 were regressed to obtain these values in terms of C_0 with high a coefficient of regression. Therefore, q_e and h can be express as a function of C_0 . A comparison of experimental data points and the surface predicted by the Eq. (2.12) are used to derive the sorption capacity, q_t at any given C_0 and t [26].

(iii) **Bangham's equation**

Bangham's equation [26, 27] is given as equation 2.13

$$\log \log \left(\frac{C_0}{C_0 - q_t m} \right) = \log \left(\frac{k_0 m}{2.303V} \right) + \alpha \log(t) \quad (2.13)$$

Where V is the volume of the solution (mL), and α (< 1) and k_0 are constants. The double logarithmic plot, of Eq. (2.13), it show that the diffusion of adsorbate into the pores of the adsorbent is the not only rate-controlling step [26, 27]. It may be that both the film and pore diffusion are important to different extents in the removal process.

(iv) **Intra particle diffusion model**

An adsorption reaction is said to be intra-particle diffusion controlled if the reaction sites are internally located in the porous adsorbents and the external resistance to diffusive transport process is much less than the internal resistance. Intra particle diffusion given by Weber & Morris [28] is expressed in equation 2.14

$$q_t = k_{diff} t^{0.5} + C \quad (2.14)$$

Where q_t is as defined in Eq. (2.8), k_{diff} is the intra-particle diffusion rate constant ($\text{mg min}^{-1/2}\text{g}^{-1}$) and C is the intercept constant. If the graphical plot of q_t versus $t^{0.5}$ is a straight line passing through the origin, then the sorption process fits to the intra-particle diffusion kinetic model. If the intra-practical diffusion plot is found in two steps than it indicates that adsorption occur in two steps. In first step, the adsorption of adsorbates occurs on an external surface of adsorbents, while in second step, the adsorbates penetrate through the pores of the adsorbents indicating that intra-practical diffusion is the rate limiting step [30]. The values of rate parameters are lower indicating that organic compound diffuses more into the interior pores of the sorbents. If in intra-practical diffusion model, the coefficient values (R^2) are nearer to that of the other kinetic model, which denote that the intra-practical is not only the rate controlling step concluding that the film diffusion and intra-practical diffusion both are occurring simultaneously.

2.7.2 Adsorption Isotherms

Adsorption isotherm is a graphical representation between the equilibrium concentration of the adsorbate and the adsorbed amount at constant temperature. It characterizes the distribution of adsorbed species between liquid and adsorbent at various equilibrium concentrations, based on a set of assumptions that are mainly the heterogeneity of the adsorbent, the type of coverage and the type of interaction between the adsorbate species. Analysis of the adsorption isotherms is of fundamental importance to describe how adsorbate molecules interact with the adsorbent surface. Equilibrium studies determine the capacity of the adsorbent and describe the adsorption isotherms by content whose value express the surface properties and affinity of the adsorbents. The relationship between equilibrium data and either theoretical or practical equation is essential for interpretation and prediction of the adsorption. [31]

Several adsorption isotherms have been investigated for the adsorption process and are summarized by foo and hameed [32], among those, the Langmuir [33] and Freundlich [34] models are the most common isotherms due to their simplicity and capability to describe experimental results in wide ranges of concentrations.

For adsorption isotherms, organic compound solution of different concentrations was agitated with the known amount of adsorbent till the equilibrium was achieved. The effect of temperature on the sorption characteristics was investigated by determining the adsorption isotherms at different temperature and different initial concentration (C_0) of organic compounds. Blank experimental runs, with only the adsorbent in 50 ml of double-distilled water, were conducted simultaneously at similar conditions to account for any colour leached by the adsorbents and adsorbed by glass containers.

Two-parameter isotherm models Langmuir, Freundlich, Dubinin - Redushkevich (D-R) Tempkin and three-parameter isotherm Redlich – Peterson models were used to describe observed adsorption phenomena of various organic compounds on fly ash and fly ash supported adsorbents.

(i) **Langmuir isotherm**

The Langmuir isotherm applies to adsorption on completely homogenous surfaces of the adsorbent with negligible interaction between adsorbed molecules [27, 33]. The linearized form of Langmuir isotherm model can be written in equation 2.15

$$\frac{C_e}{q_e} = \frac{1}{q_{max}K_L} + \frac{C_e}{q_{max}} \quad (2.15)$$

Where C_e (mg/L) is the equilibrium concentration of organic compound in solution. q_e (mg/g) is the adsorption capacity of fly ash and fly ash supported adsorbents at equilibrium. q_{max} (mg/g) is the maximum monolayer adsorption capacity of fly ash and fly ash supported adsorbents for organic pollutants. K_L (L/mg) is the Langmuir isotherm constant related to the free energy of adsorption. The values of q_{max} and K_L can be calculated from the intercept and the slope of the straight line of the linearized form of Langmuir isotherm. The essential characteristics of the Langmuir isotherm can be expressed in terms of a dimensionless constant separation factor, R_L , which is defined in equation 2.16

$$R_L = \frac{1}{1 + K_L C_0} \quad (2.16)$$

Where C_0 (mg/L) is the initial concentration of organic compound in solution. The adsorption is considered favorable when $0 < R_L < 1$ [33].

(ii) Freundlich isotherm

The Freundlich isotherm model is the well-known earliest relationship describing the adsorption process. This model applies to adsorption on heterogeneous surfaces with the interaction between adsorbed molecules and the application of the Freundlich equation also suggests that sorption energy exponentially decreases on completion of the sorption centers of an adsorbent [25, 34]. It is an empirical model used to describe adsorption in aqueous systems, was also used to explain the observed phenomena of adsorption of organic compound on fly ash materials. The linearized form of Freundlich isotherm model can be written as [equation 2.17](#)

$$\ln(q_e) = \ln(K_F) + \frac{1}{n} \ln(C_e) \quad (2.17)$$

Where K_F ((mg/g)(L/mg)^{1/n}) and $1/n$ are the Freundlich constants which are related to the adsorption capacity and adsorption intensity, respectively. The values of K_F and $1/n$ can be calculated from the intercept and the slope of the straight line of the linearized form of the Freundlich isotherm.

(iii) Redlich-Peterson isotherm

The Redlich-Peterson isotherm model is used as compromise between Langmuir and Freundlich isotherm models [35]. The non-linearized form of Redlich-Peterson isotherm can be given as [equation 2.18](#)

$$q_e = \frac{K_R C_e}{1 + \alpha_R C_e^\beta} \quad (2.18)$$

Where K_R (L/g), α_R ((L/mg)) and β are Redlich-Peterson isotherm constant. β is the exponent which lies between 0 and 1 and can characterize the adsorption isotherm. If $\beta = 1$. [Eq. \(2.18\)](#) reduces to the Langmuir isotherm model, and if $\beta =$

0. Eq. (2.18) reduces to the linear isotherm model [35], the values of K_R , α_R and β can be obtained by nonlinear regression method.

(iv) **Dubinin–Radushkevich isotherm**

The DR isotherm is commonly used to describe the sorption isotherms of a single solute system. This isotherm, apart from being analogous to the Langmuir isotherm, is more general than the latter as it does not assume the homogeneity of the surface or constant adsorption potential [35, 36]. The linearized form of D-R isotherm model can be written as equation 2.19

$$\ln(q_e) = \ln(q_{\max}) - K_D \left[RT \ln \left(1 + \frac{1}{C_e} \right) \right]^2 \quad (2.19)$$

Where C_e (mg/L) is the equilibrium concentration of organic compounds solution. q_e (mg/g) is the adsorption capacity of fly ash and fly ash supported adsorbents at equilibrium. q_{\max} (mg/g) is the maximum adsorption capacity of fly ash and fly ash supported adsorbents. K_D (mg^2/kJ^2) is the D-R isotherm constant related to the free energy of adsorption. R (8.314J/mol K) is the gas constant. T (K) is the absolute temperature. The values of K_D and q_{\max} can be calculated from the intercept and the slope of the straight line of the linearized form of D-R isotherm.

(v) **Tempkin isotherm**

Tempkin isotherm equation assumes that the heat of adsorption of all the molecules in the layer decreases linearly with coverage due to adsorbent–adsorbate interactions and that the adsorption is characterized by a uniform distribution of the binding energies up to some maximum binding energy. It considers the effects of some indirect adsorbate/adsorbate interactions on adsorption isotherms and suggests that because of these interactions the heat of adsorption of all the molecules in the layer would decrease linearly with coverage [36].

The Temkin isotherm has generally been applied in the following form of equation 2.20

$$q_e = B_T \ln K_T + B_T \ln C_e \quad (2.20)$$

where $B_T = RT/bT$, T (K) is the absolute temperature, R (8.314 J/mol) is the universal gas constant, K_T (l/mg) is the equilibrium binding constant and b_T (J/mol) is related to the heat of adsorption. The isotherm constants K_T and b_T are calculated from the slope and intercept of the q_e versus $\ln C_e$. The different isotherm parameters are evaluated from the linear plots.

2.7.3 Error Analysis

The different isotherm parameters were evaluated by correlation coefficients root mean square error (RMSE) and chi-square (χ^2). The RMSE and χ^2 are used to measure the goodness of fit of an isotherm defined as [equation 2.21](#) and [2.22](#) respectively.

$$RMSE = \sqrt{\left(\frac{1}{m-2}\right) \sum_{i=1}^m (q_{i,exp} - q_{i,cal})^2} \quad (2.21)$$

$$\chi^2 = \sum_{i=1}^m \frac{(q_{i,exp} - q_{i,cal})^2}{q_{i,exp}} \quad (2.22)$$

Where m is the number of observation in the experimental isotherm $q_{i,exp}$ is the calculated capacity observed from the experiment's value and $q_{i,cal}$ is the calculated capacity observed from the isotherm for the corresponding $q_{i,exp}$ value. A better curve fitting is observed by smaller RMSE value. If the data obtained from the isotherm model are nearer to the experiment results the χ^2 values will be lesser digit [\[36, 37\]](#).

2.8 Thermodynamic Studies

To study the feasibility, spontaneity, heat of adsorption and type of adsorption like physical, chemical or other involved mechanism thermodynamics studies are required. The thermodynamic parameters of standard enthalpy (ΔH°) and entropy (ΔS°) for the adsorption process were estimated from the Van't - Haff equation represented as [equation 2.23](#) and [2.24](#)

$$\ln K_L = \frac{\Delta S^\circ}{R} - \frac{\Delta H_{ads}^\circ}{RT} \quad (2.23)$$

$$\Delta G^\circ = -RT \ln K_L \quad (2.24)$$

Where K_L (L/mol) is Langmuir constant. R (8.314 J/mol K) is the gas constant. T (K) is absolute temperature. The values of K_L for Langmuir isotherm at different temperatures were used to calculate thermodynamic parameters such as Gibbs free energy change (ΔG°). The values of ΔH° and ΔS° can be calculated from the intercept and the slope of the linear plot of $\ln K_L$ versus $1/T$.

The negative values of ΔG° suggest that feasibility of the adsorption of organic compounds onto fly ash and fly ash supported adsorbents, the spontaneous and a favourable process. In general, the value of ΔG° for physisorption is < 8.0 kJ/mol, and that chemisorption is between 20 and 40 kJ/mol [35].

The negative value of ΔH° indicates that the adsorption process is exothermic in nature and vice versa. The energy of adsorption from different forces [38] shown in Table 2.2. The positive value of ΔS° shows a increase in randomness at the solid/liquid interface during the adsorption process [39].

Table 2.2: Energy of adsorption for different type of forces

<i>Type of forces</i>	<i>Energy of adsorption (kJ/mol)</i>
Van der Wall	4 – 10
Hydrophobic bond	≈ 5
Hydrogen bond	2-40
Coordination exchange	≈ 40
Dipole bond	2-29
Chemical bond	>60

The details of experimental methods, characterization techniques, kinetics models, isotherms and thermodynamic parameters etc. described in this chapter are also referred in coming chapters.

2.9 References

- [1] V.S. Somerset, L.F. Petric, R.A. White, M.J. Klink, D. Key, E.I. Wuoha, *Talanta*, 64 (2004) 109-14.
- [2] J. Goldstein Springer (2003). ISBN 978-0-306-47292-3, Retrieved 26 May 2012.
- [3] W.H. Bragg, W.L. Bragg, *Proc. Roy. Soc. London*, 88 (1993) 428.
- [4] Basic of X-Ray Diffraction 10040 Bubb Road Cuperlins, U.S.A www.Scintag.com
- [5] C. Su, J. Li, He. Z. Chang, Q. Zhu. *Appl. Catal. A: Gen.*, 202 (2000) 81-89.
- [6] B.D. Cullity, S.R. Stock, *Elements of X-Ray Diffraction*, 3 (2001) 388-99.
- [7] J.M. Thomas, O. Terasaki, P.L. Gai, W.Z. Zhou, J.G. Calbet, *Acc. Chem. Res.*, 34 (2001) 583-94.
- [8] E.A. Stepanova, V.S. Komarov, M.F. Sinilo, L.P. Shrinskaya, *Zh. Prikl. Spektrosk.*, 51 (1989) 950.
- [9] M.A. Legodi, D.de Waal, J.H. Potgieter, S.S. Potgieter, *Mineral Engineering*, 14 (2001) 1107-11.
- [10] S.C. Mojumdar, L. Raki, *Nanocomposite Materials, J. Therm. Anal. Cal.*, 85 (2006) 99-105.
- [11] K.S.W. Sing, *Carbon*, 32 (1994) 1311.
- [12] S. Brunauer, *The Adsorption of Gases and Vapors*, Princeton University Press, Princeton, 1945.
- [13] Recommendations: Reporting Physisorption Data for Gas/Solid Systems with Special Reference to the Determination of Surface Area and Porosity, IUPAC Commission on Colloid and Surface Chemistry Including Catalysis, *Pure Appl. Chem.*, 57 (1985) 603; Recommendations for the Characterization of Porous Solids, IUPAC Commission on Colloid and Surface Chemistry, *Pure Appl. Chem.*, 66 (1994) 1311.

-
- [14] E. Flood, in: E.A. Flood (Ed.), *The Solid–Gas Interface*, Ch. 2, vol. 1, Marcel Dekker, New York, 1967.
- [15] A.W. Adamson, *Physical Chemistry of Surfaces*, Wiley, New York, 1976.
- [16] F. Rouquerol, J. Rouquerol, K. Sing, *Adsorption by Powders and Porous Solids Principles, Methodology and Applications*, Academic Press, San Diego, CA, 1999.
- [17] C. Khatri, A. Rani, *Fuel*, 87 (2008) 2886-98.
- [18] N. Uchida, M. Shinmei, *J. Non crystal solid*, 122 (1990) 221-325.
- [19] P. Roy, N.K. Mondal, S. Bhattacharya, B. Das, K. Das, *Appl. Water Sci.*, 3 (2013) 293-309.
- [20] J.X.H., G.L., G.J. *Euro. ceram. Sco.*, 22 (2002) 1307-11.
- [21] Y. Yukselen, A. Kaya, *Eng. Geol.*, 102 (2008) 38-45.
- [22] S.M. Mak, B.T. Tey, K.Y. Cheah, W.L. Siew, K.K. Tan, *J. Chem. Technol. Biotechnol.*, 84 (2009) 1405-11.
- [23] ISRIC, in: L.P. van Reeuwijk (Ed.), *Procedures for Soil analysis*, International Soil Reference and Information Centre, Wageningen, 1992, p. 91.
- [24] T. W. Weber, R. K. Chakravorthi, *J. AM. Ins. Chem. Eng.*, 2 (1974) 228-38.
- [25] A. Achmad, J. Kassim, T.K. Suan, R.C. Amat, T.L. Seey, *J. of Physi. Sct.*, 23(1) (2012) 1-13.
- [26] V. S. Mane, I. D. Mall, V. C. Srivastava, *J. of Environ. Manag.*, 84 (2007) 390-400.
- [27] C. Aharoni, S. Sideman, E. Hoffer, *J. of Chem. Tech. and Biotech.*, 29 (1979) 404-12.
- [28] Jr. W. J. Weber, J. C. Morris, *J. Sanit. Eng. Div. ASCE*, 18 (1963) 31-42.
- [29] D. Rameshraj, V.C. Srivastava, J.P. Kushwaha, I.D. Mall, *Chem. Eng. J.*, 181-182 (2012) 343-51.
- [30] X. Querol, N. Moreno, J.C. Umana, et al. *J. Chen. Technol. Biotechnol.*, 77 (2002) 292-98.

- [31] O. Altin, H. O. Ozbelege, T. Dogu, *J. Collid. Interface Sci.*, 198 (1998) 130-40.
- [32] K.Y. Foo, B.H. Hameed, *J. of Chem. Eng.*, 156 (2010) 2-10.
- [33] I. Langmuir, *J. Am. Chem. Soc.*, 40 (1918) 1361-1403.
- [34] H. M. F. Freundlich, *J. Phy. Chem.*, 57 (1906) 385-470.
- [35] J. Lin, Y. Zhan, Z. Zhu, Y. Xing, *J. Hazard. Mater.*, 193 (2011) 102-11.
- [36] B.A. Shah, C.B. Mistry, A.V. Shah, *Chem. Eng. J.*, 220 (2013) 172-84.
- [37] K. Vijayraghvan, T.V. Padmesh, K. Palanivelu, M. Velan, *J. of Hazard. Mater.*, B133 (2006) 304-8.
- [38] J.H. Huang, Y.F. Liu, X.G Wang, *J. of Hazard. Mater.*, 160 (2008) 382-87.
- [39] S.C.D.A. Fernada, F.S.V. Eunice, R.C. Antini, *J. of Colloid and Interface Sci.*, 253 (2002) 243-46.



Chapter-3

***Kinetics of Adsorptive Removal of Dyes
(Methylene Blue and Brilliant Green) from
Aqueous Solution over Various Types of Fly
Ash: Equilibrium, Kinetics, Thermodynamics
and Modeling***

ABSTRACT

In this study, eleven different types of fly ash collected from different industries were used as adsorbents for selection of the best fly ash to remove colour from textile waste. Ten fly ash samples are from coal based power plants and one is from lignite based thermal power plant. Out of eleven only six fly ash found to be best for adsorptive removal. Investigation revealed that the unburned carbon component and pH_{ZPC} of fly ash play an important role in its adsorption capacity. Adsorption experiments indicate that the extent of adsorption is strongly dependent on pH of the dyes solution. The adsorption for both Brilliant green (BG) and Methylene blue (MB) followed pseudo-second-order kinetics. The maximum adsorption capacities (q_m) calculated from the best fit Langmuir isotherm were 100.0 mg/g for BG and 3.184 mg/g for MB. Thermodynamic parameters (ΔG^0 , ΔH^0 and ΔS^0) confirm the adsorption process on fly ash feasible, exothermic and spontaneous in nature for both the dyes.

3.1 Introduction

Dyes may be defined as substances that, when applied to a substrate, provide color by a process. Such substances with considerable coloring capacity are widely employed in the textile, pharmaceutical, food, cosmetics, plastics, photographic and paper industries. Due to ever-growing demands in textiles, synthetic organic dyes are widely used for dyeing textile fibers such as cotton and polyester. Approximately 10,000 different dyes and pigments are used for industries and over 7×10^5 tons of these dyes are annually produced worldwide [1]. Dyes and pigments represent one of the problematic groups; they are emitted into wastewaters from various industrial branches, mainly from the dye manufacturing and textile finishing [2] and also from food colouring, cosmetics, paper and carpet industries. Synthetic dyes have complex aromatic structures which provide them physico-chemical, thermal and optical stability [3, 4]. Dyes in effluents, if not removed, cause disturbance to the ecological systems of the receiving waters. These materials also pose certain health hazards and environmental pollution while considered highly toxic to humans and animals causing permanent injury to the eyes, irritation to the gastrointestinal tract with symptoms like nausea, vomiting, and diarrhea if consumed orally, skin allergy, etc [5].

Dyes are broadly classified as anionic, cationic, non-ionic and zwitter ionic depending on the ionic charge on the molecules. Cationic dyes are more toxic than anionic dyes [1]. Brilliant green (BG) is one of the commonly known cationic dye used for various purposes, e.g. biological stain, dermatological agent, veterinary medicine, an additive to poultry feed to inhibit propagation of mold, intestinal parasites and fungus. It is also extensively used in textile dyeing, paper printing, antiseptic and as a selective bacteriostatic agent in culture media. Methylene blue has also wider applications, which include colouring paper, temporary hair colorant, dyeing cottons, wools, coating for paper stock, medical purpose, etc.

For removal of dyes from the industrial effluents and water sources a range of conventional removal technologies such as activated sludge, chemical coagulation, carbon adsorption, electrochemical treatment, reverse osmosis and

hydrogen peroxide catalysis have been extensively used so far,. However, most of the above methods suffer from one or more limitations and none of them were successful in completely removing the colour from wastewater in a cost effective manner suitable for large industrial sector. The removal of dyes and organics in an economic way still remains an important problem, although a number of low cost adsorption technologies have been developed superior to other techniques for water re-use in terms of initial cost, simplicity of design, ease of operation and insensitivity to toxic substances [6].

The activated carbon has been found to be superior to other techniques in water re-use methodology and simplicity of design. However, commercially available activated carbons are still considered expensive thus need to be substituted by an inexpensive adsorbent endowed with reasonable adsorptive capacity. On the basis of research output use of fly ash, bottom ash, bagasse fly ash, starch, cellulose-based waste, rice husk, etc. [7, 8, 9] is suggested for replacing activated carbon. Fly ash (FA), a waste produced during the combustion of coal in the electricity generation processes, enriched with SiO_2 and Al_2O_3 with a portion of unburnt carbon is being used in building materials, soil amendment and fillers, zeolite synthesis [10], also as an adsorbent in waste water treatment technologies having potential of a low-cost adsorbent to remove various hazardous materials from wastewater [11-14].

The aim of the present work remained to identify the properties of fly ash for selection of the best sample for fast removal of colour from textile waste through adsorption and compare the adsorption behaviour of acidic (BG) and basic (MB) dyes. To achieve this, the effects of factors such as initial pH, adsorbent dose (m), contact time (t), initial dye concentration (C_0) and temperature (T) were investigated for MB and BG removal on best selected sample FA₄₀. The kinetics of MB and BG adsorption onto FA₄₀ was analyzed by fitting various kinetic models, equilibrium data were fitted to the Freundlich, Langmuir and Tempkin isotherm equations to determine the best-fit isotherm equation. Thermodynamics of adsorption process is studied and the changes in Gibbs free energy, enthalpy and entropy of adsorption are determined.

3.2 Materials and methods

3.2.1 Adsorbent: FA

Fly ash (FA) samples were collected from Sriram Fertilisers and Chemical Ltd., Kota from Four different types of Boilers named according to their capacity 10MW, 30MW, 35MW and 40MW (FA₁₀, FA₃₀, FA₃₅, FA₄₀) and various thermal power plants situated at Kota (FA_{KT}), Barmer (FA_{BM}) and Suratgarh (FA_{SG}) in Rajasthan, Jamshedpur (FA_{JM}) in Jharkhand, Bhatinda (FA_{BT}) in Punjab Vindhyachal (FA_{VL}), Talchar (FA_{TR}), etc. All FA used after heating in a hot air oven at 105°C for 24h to remove moisture. The dried materials were then stored in desiccators for use.

3.2.2 Adsorbate: Brilliant Green (BG) and Methylene blue (MB)

The adsorbate, BG (MW: 462.65), MB ((MW: 373.91) and all the chemicals were of analytical grade and S.D. Fine India Make. The structure of BG and MB is illustrated in [Figure 3.1 \(a & b\)](#). An accurately weighed quantity of the dye was dissolved in double-distilled water to prepare stock solution (1000 mg/l). Experimental solutions of the desired concentrations were obtained by successive dilutions with distilled water.

3.2.3 Analytical Measurements

Concentration of dyes were determined by measuring the maximum absorbance (λ_{\max}) as determined from the plots were 625 nm and 660 nm for BG and MB respectively using a double beam UV/Visible spectrophotometer (model Spectrscan UV 2600/02).

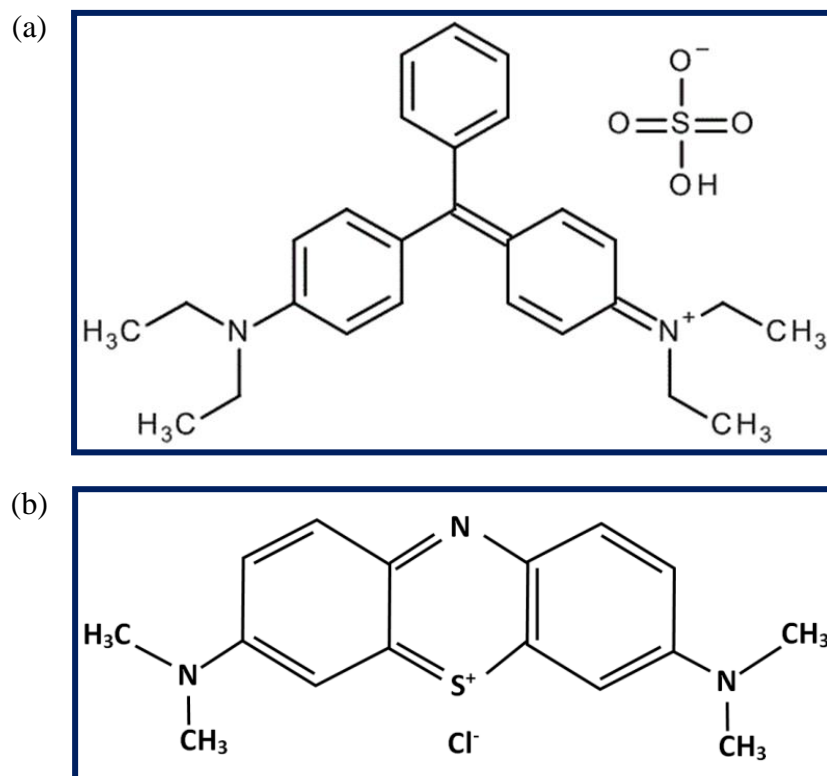


Figure 3.1: Chemical structure of (a) brilliant green (b) methylene blue dye

3.2.4 Batch experimental programme

To study the effect of important parameters like pH, m , C_0 and t on the adsorptive removal of MB and BG, batch experiments were conducted. For each experimental run, 50 ml of dye solution of known concentration and a known amount of the adsorbent, FA₄₀ were taken in a 250 ml stoppered conical flask. The effect of pH on dye removal was studied over a pH range of 3-11 which was adjusted by the addition of dilute aqueous solutions of HCl or NaOH (0.10 M). For the optimum amount of adsorbent per unit mass of adsorbate, a 50 ml dye solution was contacted with different amounts of FA₄₀ till equilibrium was attained. The effect of temperature on the sorption characteristics was investigated by determining the adsorption isotherms at 298, 308 and 318 K for MB and 303, 313 and 323K for BG,. C_0 was varied from 5 to 20 mg/l for MB and 40-200 mg/l for BG. Blank experimental runs, with only the adsorbent in 50 ml of double-distilled water, were conducted simultaneously at similar conditions to account for any colour leached by the adsorbents and adsorbed by glass containers.

3.3 Result and discussion

3.3.1 Characterization of Adsorbent

(i) XRF studies

The primary mineralogical constituents of all eleven different FA are shown in the [Table 3.1](#) and XRF spectrum of FA₄₀ is shown in [Figure 3.2](#). According to the American Society for Testing Materials (ASTM C618) [\[16\]](#), the ash containing more than 70 wt% SiO₂ + Al₂O₃ + Fe₂O₃ and being low in lime is defined as class F, while those with a SiO₂ + Al₂O₃ + Fe₂O₃ content between 50 and 70 wt% and high in lime are defined as class C [\[10\]](#). All fly ash samples as mentioned in [Table 3.1](#), except FA_{BM} (C-type) are considered as F-Type. There was not much difference in wt% of SiO₂, Al₂O₃ and other metal oxide contents in all samples but significant difference was noticed in carbon content. The carbon content in the fly ash mainly depends upon the handling and processing of coal to feed into boilers [\[10\]](#). The condition and the type of coal crusher can affect the particle size of the coal itself. Coarser ground coal may leave a higher percentage of unburnt carbon in fly ash [\[17\]](#).

Table 3.1: Chemical composition and properties of various fly ash

Type of fly ash	Chemical components (Wt % by XRF)									pH _{ZPC}	Carbon Content (%)	Moisture (%)
	SiO ₂ (%)	Al ₂ O ₃ (%)	Fe ₂ O ₃ (%)	CaO (%)	K ₂ O (%)	MgO (%)	TiO ₂ (%)	Na ₂ O (%)	Trace Elements (%)			
FA _{KT}	56.47	24.13	3.99	3.64	4.05	0.68	0.54	1.25	5.25	8.5	6.0	1.24
FA _{BT}	60.9	28.7	4.36	0.88	1.63	0.59	1.83	0.14	0.97	9.1	6.5	1.1
FA _{JM}	61.9	31.7	2.67	0.45	0.79	0.31	1.43	0.68	0.682	7.5	3.0	0.4
FA _{ST}	58.23	29.11	5.72	1.3	1.55	0.73	0.63	2.54	0.19	8.3	6.0	0.6
FA _{TR}	57.00	29.48	6.20	1.00	0.41	0.35	1.90	0.15	3.51	7.9	7.0	1.52
FA _{VL}	60.0	25.01	5.99	1.0	0.75	0.5	0.85	0.5	5.4	7.4	5.5	1.1
FA ₁₀	59.99	24.02	4.01	1.23	2.0	1.2	1.32	0.23	6.0	8.4	11.0	1.3
FA ₃₀	60.1	21.36	3.96	1.63	1.99	1.45	1.52	0.32	7.67	9.8	14.0	1.2
FA ₃₅	58.99	22.06	4.36	1.55	1.82	1.35	1.43	0.20	8.24	10.1	16.0	1.1
FA ₄₀	60.46	21.50	4.30	7.63	1.25	0.82	1.53	0.19	2.32	10.8	18.0	1.46
FA _{BM}	42.01	15.91	8.08	20.1	2.2	5.24	0.92	4.1	1.44	11.2	7.0	1.24

FA_{KT} - Kota Super Thermal Power Station, Kota, Rajasthan

FA_{BT} - Lehra Mohabbat Thermal Power Plant, Bhatinda, Punjab

FA_{JM} - Tata Thermal Power Plant, Jamshedpur, Jharkhand.

FA_{ST} - Suratgarh Thermal Power Station, Ganganagar, Rajasthan

FA_{TR} - Talchar Super Thermal Power Station, Angul, Orissa

FA_{VL} - Vindhyachal Super Thermal Power Station, Singrauli, Madhya Pradesh

FA₁₀, FA₃₀, FA₃₅, FA₄₀ - Shri Ram Fertilizers & Chemicals Ltd., Kota, Rajasthan

FA_{BM} - Giral Lignite Thermal Power Station, Barmer, Rajasthan

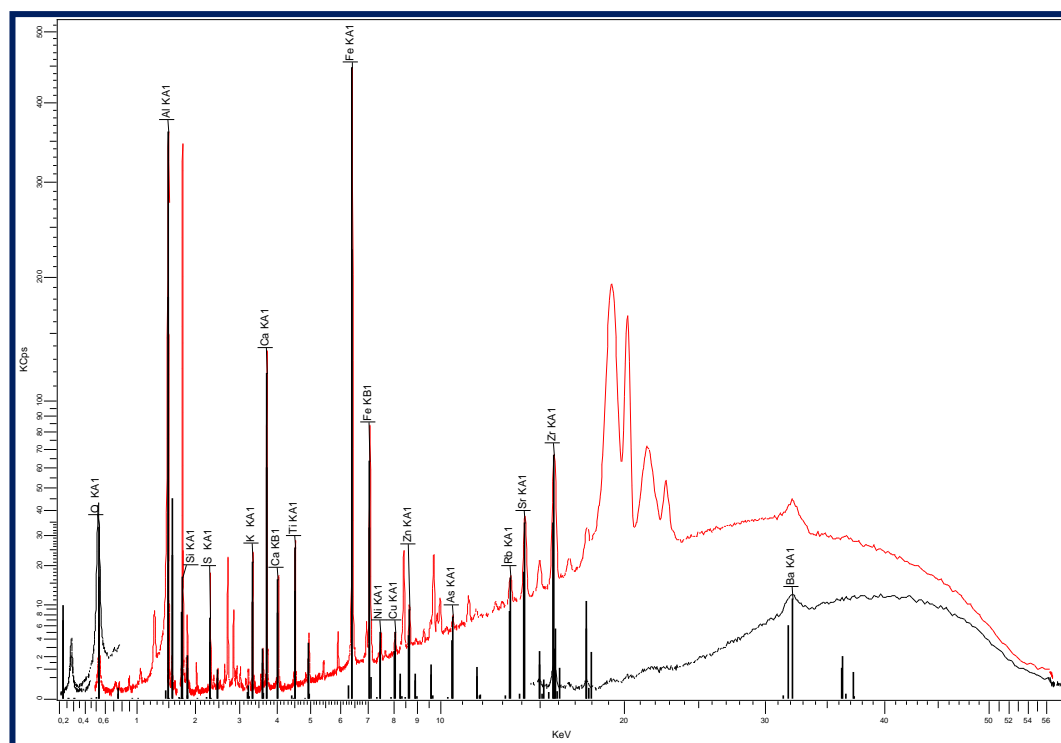


Figure 3.2: XRF spectrum of FA₄₀

(ii) **Field Emission Scanning Electron Microscopic (FE-SEM) study**

The Field emission scanning electron microscopy (FE-SEM) of FA₄₀, BG dye adsorbed FA₄₀ and MB dye adsorbed FA₄₀ are shown in Figure 3.3 (a, b & c). The FA particles typically show compact or hollowed spherical shapes and different sizes, with a slight rough surface made up of an aluminosilicate glass phase. The unburned carbonaceous portion of FA with porous structure of the particle is clearly seen (Figure 3.3a), with macropores and embedded micro-sized glassy spheres (cenospheres), indicating that the unburned coal may be a good candidate for adsorbent. Figure 3.3 (b & c) shows that the surface of the FA become smooth due to adsorption of dye. Maximum hollow spheres are covered with dye molecule forming a smooth layer.

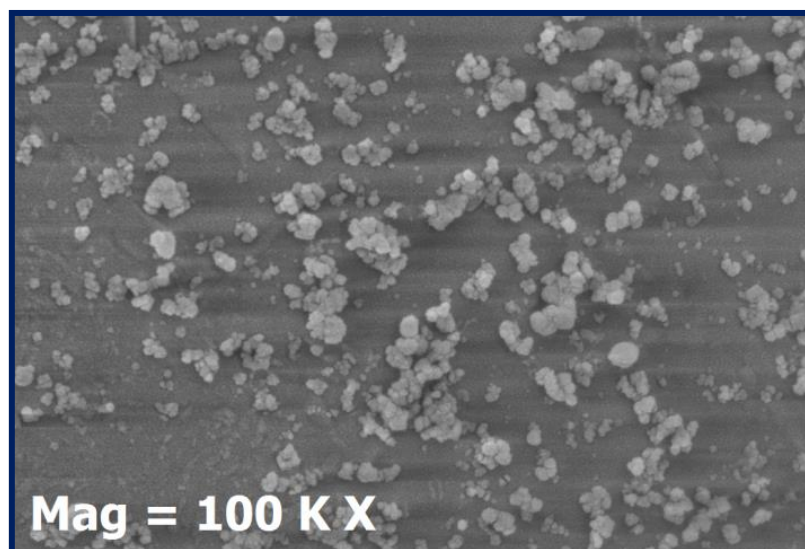
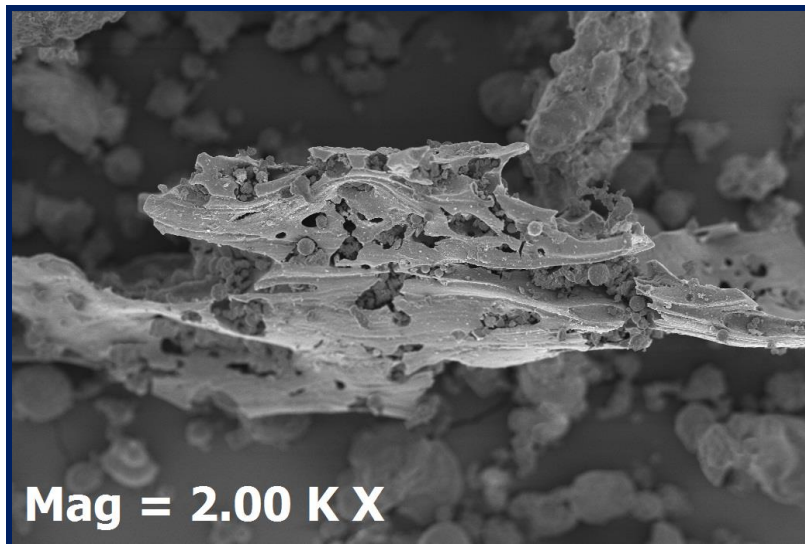
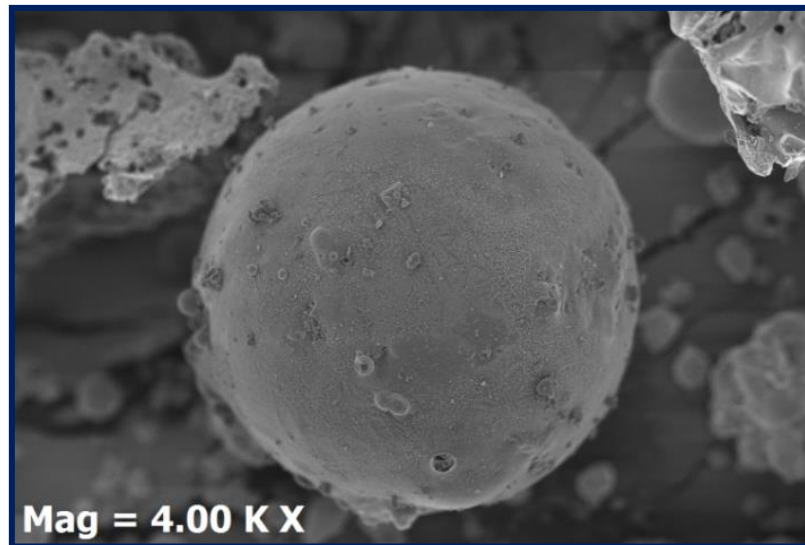


Figure 3.3(a): Scanning electron micrographs (FE-SEM) of FA₄₀

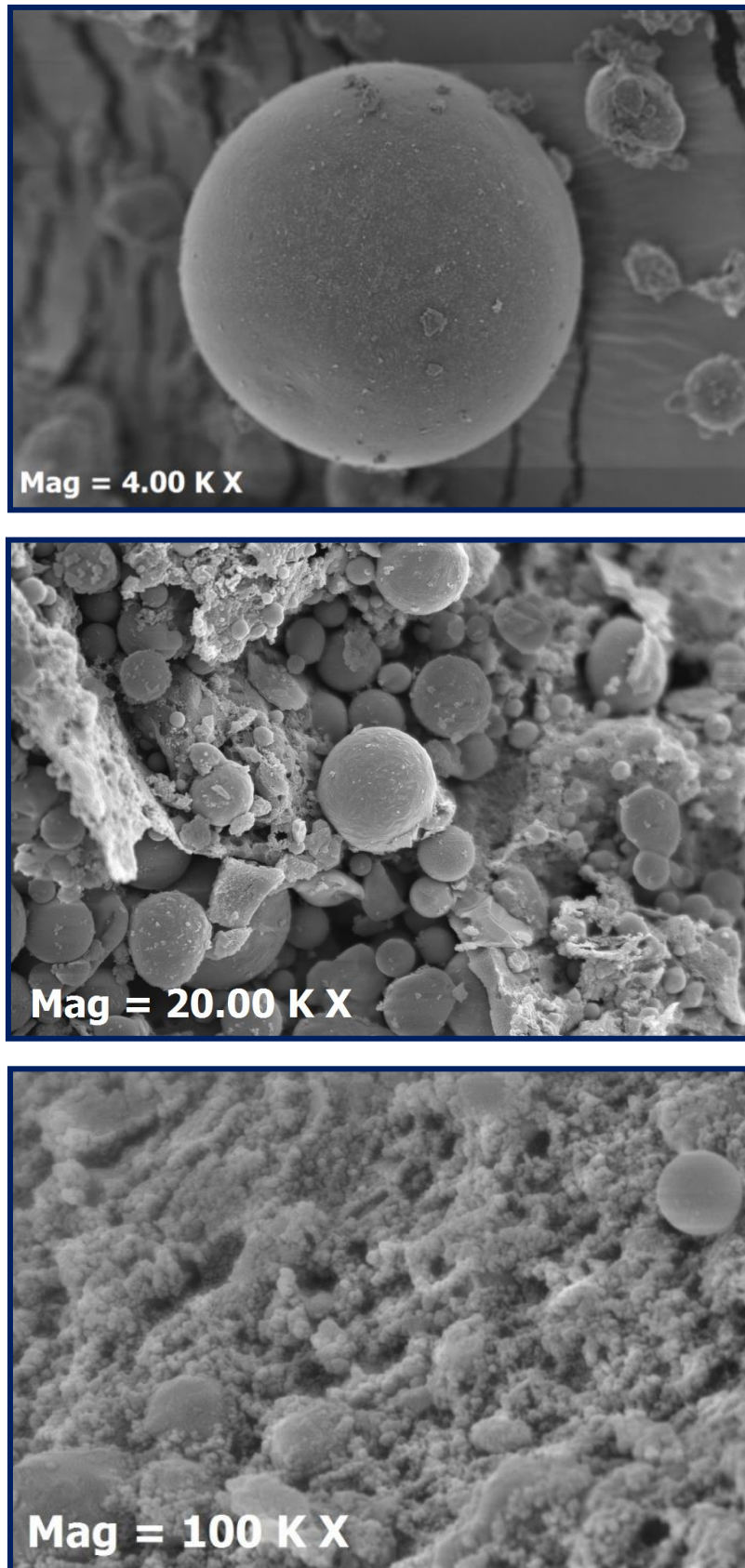


Figure 3.3(b): Scanning electron micrographs (FE-SEM) of FA₄₀ after BG adsorption

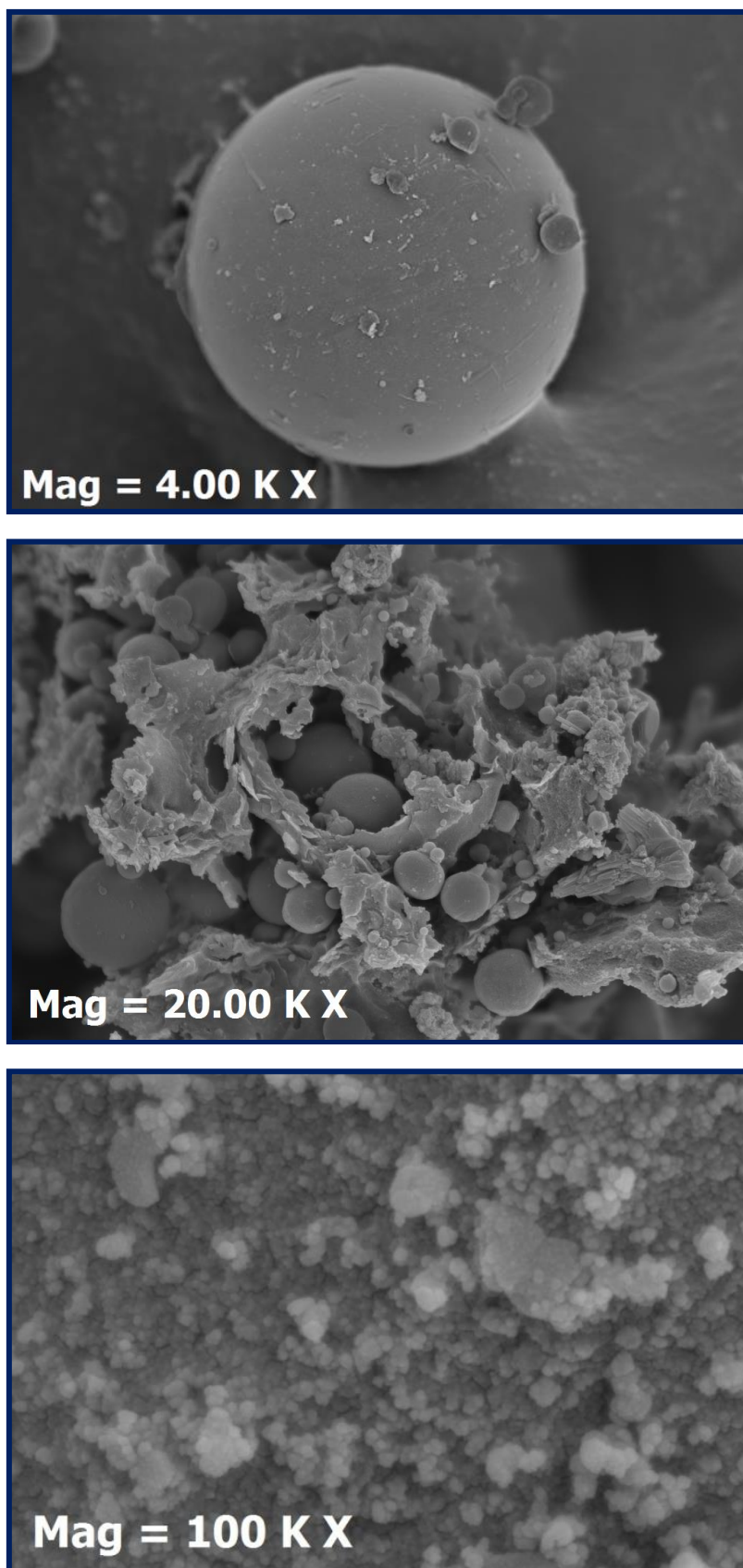


Figure 3.3(c): Scanning electron micrographs (FE-SEM) of FA₄₀ after MB adsorption

(iii) X-Ray Diffraction (XRD) study

The XRD patterns of the FA₄₀, BG adsorbed FA₄₀ and MB adsorbed FA₄₀ are shown in Figure 3.4 (a, b & c) and XRD details are given in Table 3.2 (a, b & c). The very wide reflection at low 2θ values (3-16°) on XRD pattern of FA₄₀ gives the evidence of the presence of amorphous material [18] with a major peak around 26° and minor peaks around 16°, 32° and 34°, corresponding to quartz (SiO₂) and mullite (3Al₂O₃·2SiO₂), respectively, Figure 3.4 (a) shows that FA₄₀ have well defined peaks with high intensity than the BG and MB adsorbed FA₄₀ (Figure 3.4 b & c). When the FA₄₀ get covered by the dye molecules (Figure 3.4 b & c) the crystalline nature of FA₄₀ slightly decreased. It has been concluded that the dye molecule diffused into the micro and macropores of the FA molecules. An XRD study reveals that the peak height of FA₄₀ decrease after adsorption of dyes due to increase in carbon content but there was no significant changes in the patterns of BG adsorbed FA₄₀ and MB adsorbed FA₄₀.

(iv) Fourier Transformed Infrared Spectra (FTIR) study

Fourier transformed infrared (FTIR) spectra of FA₄₀, BG adsorbed FA₄₀ and MB adsorbed FA₄₀ are shown in Figure 3.5 (a, b & c). For aromatic compounds, the most characteristic C=C stretching bands are at 1612, 1580, 1520 and 1343 cm⁻¹ shown in FTIR spectra of BG adsorbed FA₄₀ (Figure 3.5 b) and at 1638 and 1474 cm⁻¹ shown in FTIR spectra of MB adsorbed FA₄₀ (Figure 3.5 c), but absent in FA₄₀ (Figure 3.5 a). Band at 2975 and 2883 cm⁻¹ shown in FTIR spectra of BG adsorbed FA₄₀ and at 2926 and 2856 cm⁻¹ shown in FTIR spectra of MB adsorbed FA₄₀ represent the C-H symmetric and asymmetric stretching vibration in -CH₂ and -CH₃. These all peaks gives an evidence of adsorption of BG and MB dye on FA₄₀. The peak in the low frequency region (<1000 cm⁻¹) which are present in the FTIR of dye alone but are not observed in the FTIR of dye adsorbed FA₄₀ due to low concentration of dye on the fly ash surface. Table 3.3 gives a comparison and information of shifting of different vibrational bands of fly ash after dye adsorption.

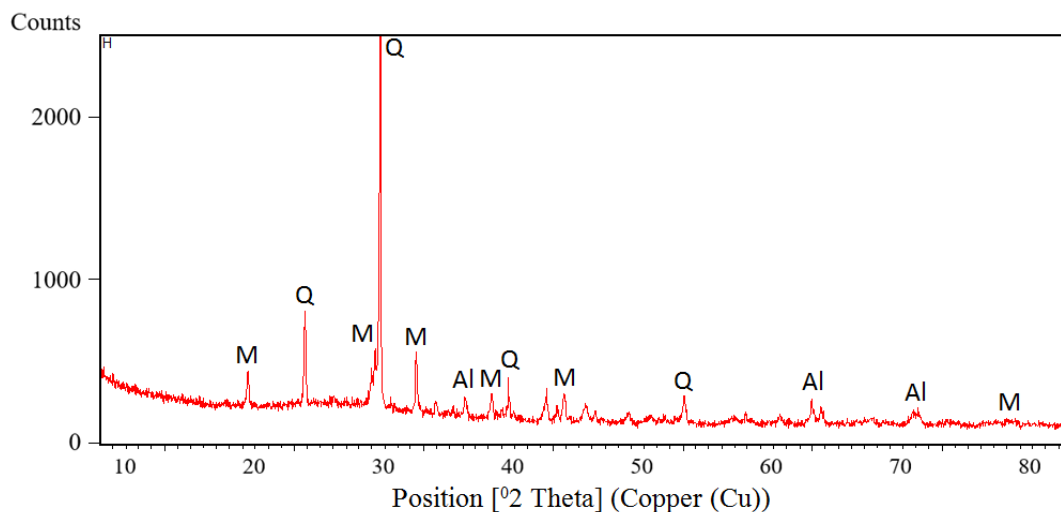


Figure 3.4(a): The XRD patterns for FA₄₀ in which the abbreviation was as follows: Q, quartz; M, mullite; Al, aluminium

Table 3.2(a): XRD details of FA₄₀

Pos. [°2Th.]	FWHM [°2Th.]	d-spacing [Å]	Rel. Int. [%]	Area [cts*°2Th.]
16.4235	0.1338	5.39750	8.85	26.78
20.8344	0.1171	4.26370	24.74	65.50
25.9722	0.1004	3.43074	9.59	21.76
26.2494	0.1004	3.39514	15.66	35.53
26.6279	0.1338	3.34773	100.00	302.55
29.4400	0.1171	3.03405	14.61	38.67
30.9406	0.2007	2.89024	3.18	14.43
33.1995	0.1673	2.69856	5.06	19.15
35.2309	0.1338	2.54748	6.22	18.83
36.5410	0.0502	2.45910	11.38	12.91
39.4524	0.1338	2.28409	7.00	21.17
40.3111	0.1338	2.23739	3.85	11.66
40.8346	0.1506	2.20991	7.33	24.95
42.4587	0.2676	2.12906	4.60	27.85
43.2398	0.2007	2.09239	2.64	11.97
45.8231	0.2676	1.98027	2.56	15.48
47.4670	0.4015	1.91545	1.55	14.11
50.1036	0.2676	1.82066	6.74	40.78
54.8521	0.2007	1.67376	2.24	10.15
57.5048	0.2676	1.60270	2.44	14.74
59.9393	0.1004	1.54329	5.96	13.52
60.6526	0.1338	1.52684	4.17	12.61
64.5772	0.4015	1.44320	1.37	12.46
68.2014	0.2676	1.37508	3.39	20.49
75.3785	0.9792	1.25994	0.83	24.98

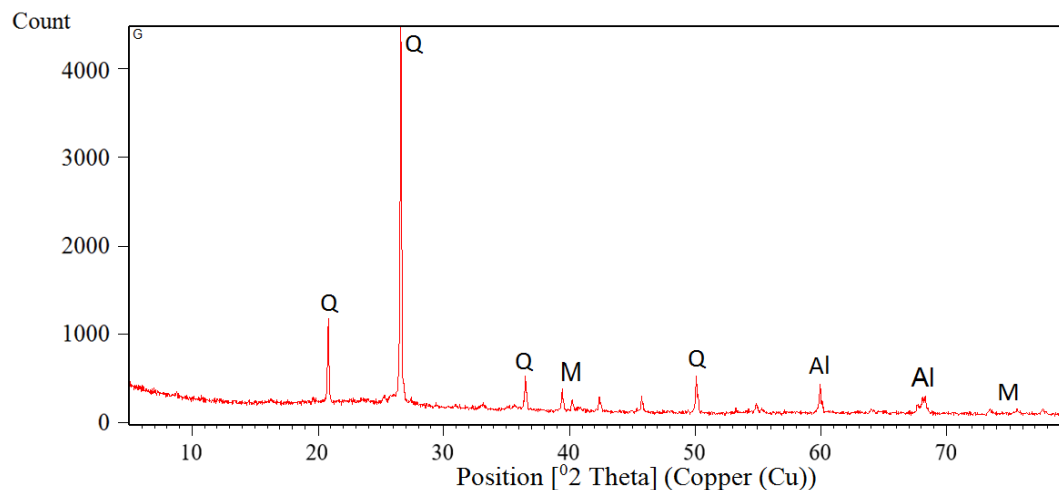


Figure 3.4(b): The XRD patterns FA₄₀ after BG adsorption, in which the abbreviation was as follows: Q, quartz; M, mullite; Al, aluminium

Table 3.2 (b): XRD details of BG Dye adsorbed FA40

Pos. [°2Th.]	FWHM [°2Th.]	d-spacing [Å]	Rel. Int. [%]	Area [cts*°2Th.]
16.3299	0.8029	5.42376	0.61	20.33
20.8018	0.1004	4.26677	20.33	84.98
25.2340	0.2676	3.52648	1.47	16.35
26.5769	0.1004	3.35126	100.00	418.05
27.3666	0.2007	3.25632	1.55	12.93
33.0931	0.2676	2.70475	1.18	13.12
36.4616	0.0669	2.46223	8.74	24.35
39.3972	0.0669	2.28526	5.92	16.49
40.2062	0.1004	2.24113	2.73	11.43
42.3590	0.1673	2.13207	3.70	25.81
45.7242	0.1004	1.98268	4.63	19.36
50.1070	0.1224	1.81904	9.74	67.13
54.8561	0.2448	1.67226	2.01	27.64
59.9259	0.0612	1.54233	8.06	27.76
64.0128	0.3264	1.45336	0.87	15.91
67.6697	0.2040	1.38344	2.25	25.85
68.1915	0.4080	1.37412	3.27	75.21
73.3858	0.3264	1.28915	1.25	22.99
75.6386	0.9792	1.25625	0.77	42.24
77.6115	0.2448	1.22917	1.40	19.29

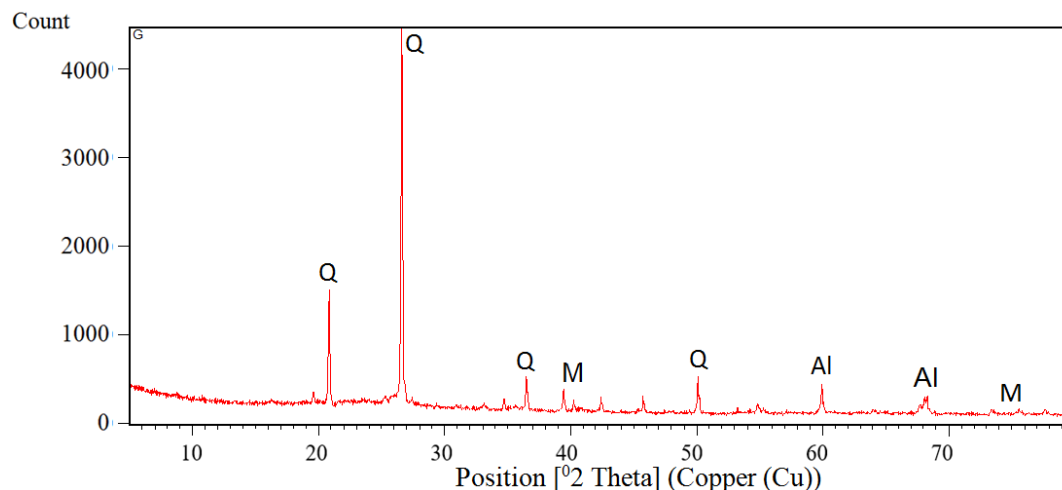


Figure 3.4(c): The XRD patterns for FA₄₀ after MB adsorption, in which the abbreviation was as follows: Q, quartz; M, mullite; Al, aluminium

Table 3.2 (c): XRD details of MB Dye adsorbed FA₄₀

Pos. [°2Th.]	FWHM [°2Th.]	d-spacing [Å]	Rel. Int. [%]	Area [cts*°2Th.]
16.3278	0.8030	5.42376	0.63	21.33
20.8020	0.1002	4.26677	21.33	85.98
25.1538	0.2673	3.52648	1.49	15.35
26.6269	0.1004	3.35126	100.00	417.05
27.3666	0.2017	3.25632	1.45	13.93
33.0931	0.2676	2.70475	1.18	12.12
36.4616	0.0669	2.46223	8.74	24.35
39.3972	0.0669	2.28526	5.92	16.49
40.2062	0.1004	2.24113	2.73	11.43
42.3590	0.1673	2.13207	3.70	25.81
45.7242	0.1004	1.98268	4.63	19.36
50.1070	0.1224	1.81904	9.74	67.13
54.8561	0.2448	1.67226	2.01	27.64
59.9259	0.0612	1.54233	8.06	27.76
64.0128	0.3264	1.45336	0.87	15.91
67.6697	0.2040	1.38344	2.25	25.85
68.1915	0.4080	1.37412	3.27	75.21
73.3858	0.3264	1.28915	1.25	22.99
75.6386	0.9792	1.25625	0.77	42.24
77.6115	0.2448	1.22917	1.40	19.29

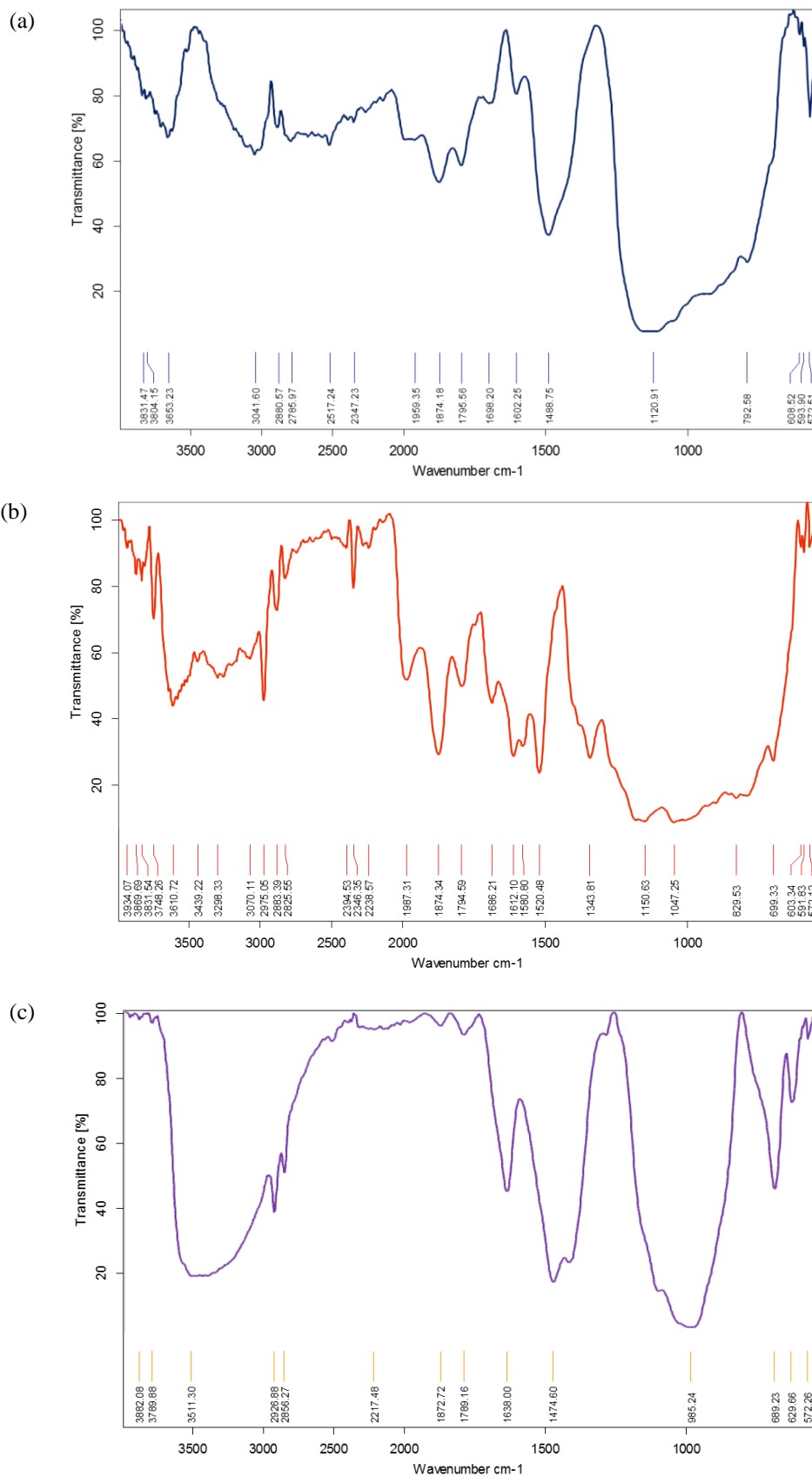


Figure 3.5: The FTIR pattern for (a) FA₄₀ (b) FA₄₀ after BG adsorption and (c) FA₄₀ after MB adsorption

Table 3.3: Comparison and shifting of bands data for FA₄₀, BG adsorbed FA₄₀ and MB adsorbed FA₄₀ in FTIR spectroscopy

Possible Assignments	Characteristic absorption range, Vibrational Bands (cm ⁻¹)			Ref.
	FA ₄₀	BG adsorbed FA ₄₀	MB adsorbed FA ₄₀	
Surface -OH of SiOH/Al ₂ O ₃	3831.47 3804.15 3653.23	3610 3439	3882.08 3789.88 3511.30	[19]
O-H Stretch (Alcoholic & Water)	-		-	[20]
CH ₂ Stretching	2880.57 2785.97	2975 2883	2926.88 2856.27	[19]
v _{OH} -group	2517.24 2347.23			[21]
H-SiO ₃			2217.48	[22]
≡Si-H (monohydride)	1959.35			[23]
C-H bending	1874.18		1872.72	[24]
C=O Stretching	1795.56		1789.16	[25]
bending mode of O-H(water molecule), aromatic ring and CO ₃ ⁻² group Symmetric stretch	1698.20 1602.25	1612 1580	1638.00	[26]
vibration of interstitial water, amide and N-H group	1488.75	1520 1343	-1474.60	
Si-O-Si Stretching	1120.91	1150	-	[27]
Inner surface Al-OH deformation		1047	985.24	
Si-O planar stretching	925.59		-	
Si-O/Kaolin	792.58	829	-	[28]
Si-O-Al bending			689.23 629.66 572.26	

(v) Surface area and porosity measurements

The N₂-adsorption/desorption isotherm at 77 K for FA₄₀ with both adsorption and desorption branches measured (Figure 3.6 (a)). The hysteresis seen between the adsorption (lower) and desorption (upper) curves indicates the existence of mesoporosity (pores in the range of 20-500 Å) and provides information regarding the connectivity of the porous network. Isotherm data can be derived either from the desorption branch or from the adsorption branch of the isotherm to calculate the mesopore-size distribution. The pore-size distribution of the FA₄₀ is shown in Figure 3.6 (d) have been calculated from the adsorption branch of the isotherm by the BJH method. An adsorption is the source of information about properties, such as the porous structure of the adsorbent, heat of adsorption and physical and chemical characteristics. The BET surface area, pore diameter and pore volume of FA₄₀ are 1.7950 m²/g, 149.6238 Å and 0.006714 cm³/g respectively as shown in Table 3.4. The combination of type II and type IV adsorption isotherm for FA₄₀ implies the mesoporous structure of materials according to the IUPAC and Brunauer, Deming, Deming and Teller (BDDT) classification [29] as described in chapter 2. The pore size distribution confirms that the pore size of FA₄₀ ranged from 20Å (1Å = 0.1 nm) to 500 Å.

Table 3.4: Surface area and Pore Structure of FA₄₀

Parameter		Value
Surface area of pores (m ² /g)	BET	1.7950
	BJH	
	a. Adsorption cumulative	1.1465
	b. Desorption cumulative	1.7148
BJH Cumulative Pore Volume (cm ³ /g)	Single Point Total	0.006714 ^a
	BJH Adsorption	0.006264 ^b
	BJH desorption	0.006732 ^b
Average pore diameter (Å)	Single Point Total	149.6238
	BJH Adsorption	218.5352
	BJH desorption	157.0288

^aPores less than 900.1879 Å diameter^bPores between 17.00 Å and 3000.00 Å diameter

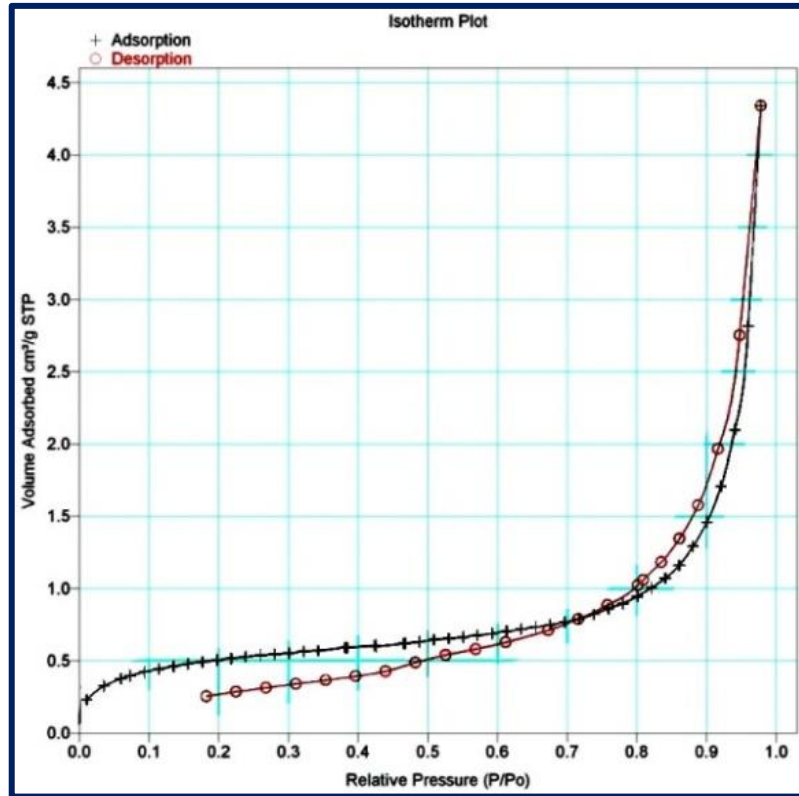


Figure 3.6(a): Adsorption isotherms of nitrogen at 77 K for FA₄₀

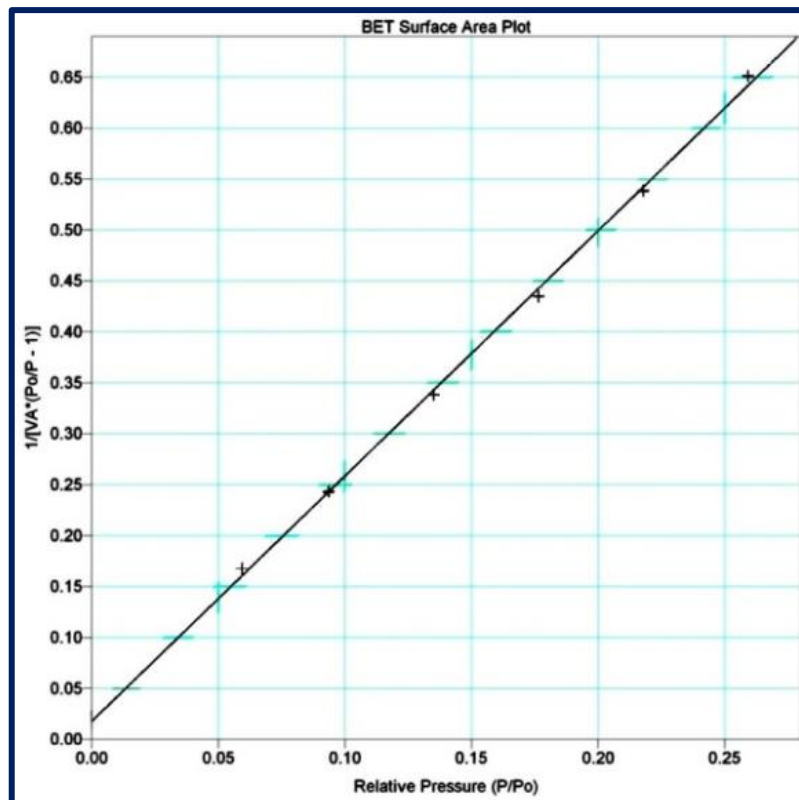


Figure 3.6(b): Surface area plot for FA₄₀

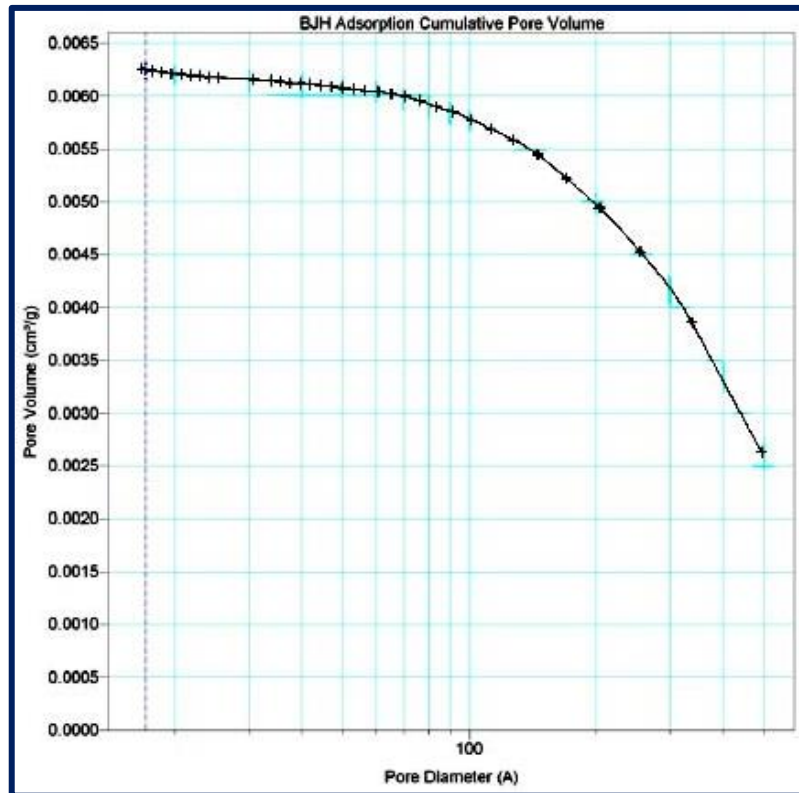


Figure 3.6(c): Pore-size distribution (BJH Adsorption Cumulative Pore Volume) for FA₄₀

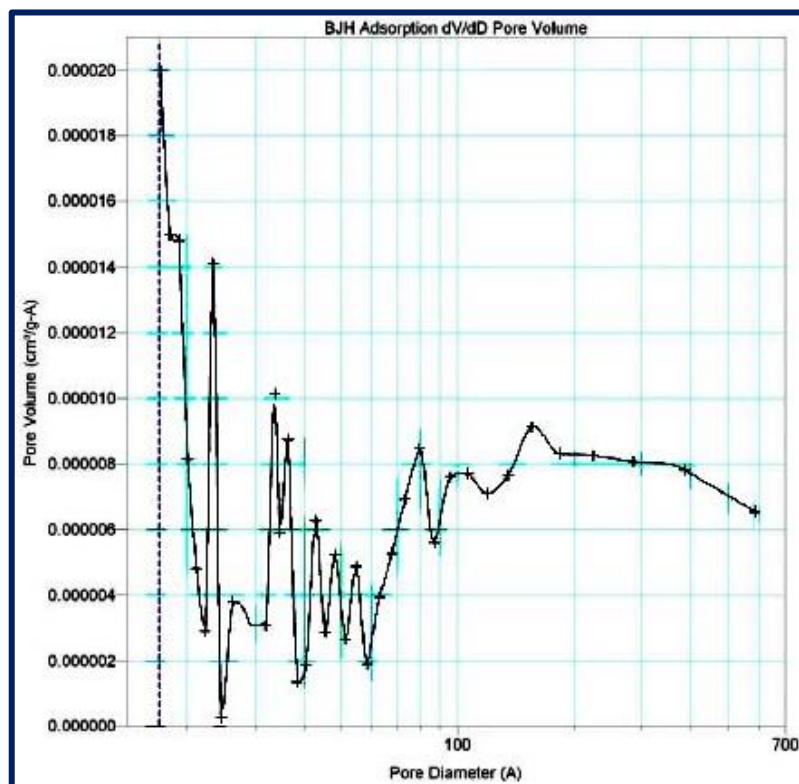


Figure 3.6(d): Pore-size distribution (BJH Adsorption dV/dD Pore Volume) for FA₄₀

(vi) pH_{zpc} of various Fly ash

The Point of zero charge (pH_{ZPC}) (as described in chapter 2) value of all fly ash FA_{KT} , FA_{BT} , FA_{JM} , FA_{ST} , FA_{TR} , FA_{VL} , FA_{10} , FA_{30} , FA_{35} , FA_{40} and FA_{BM} are 8.5, 9.1, 7.5, 8.3, 7.9, 7.4, 8.4, 9.8, 10.1, 10.8 and 11.2 respectively (Table 3.1) which are used in experiment, pH_i versus ΔpH plots of various fly ash samples are shown in Figure 3.7.

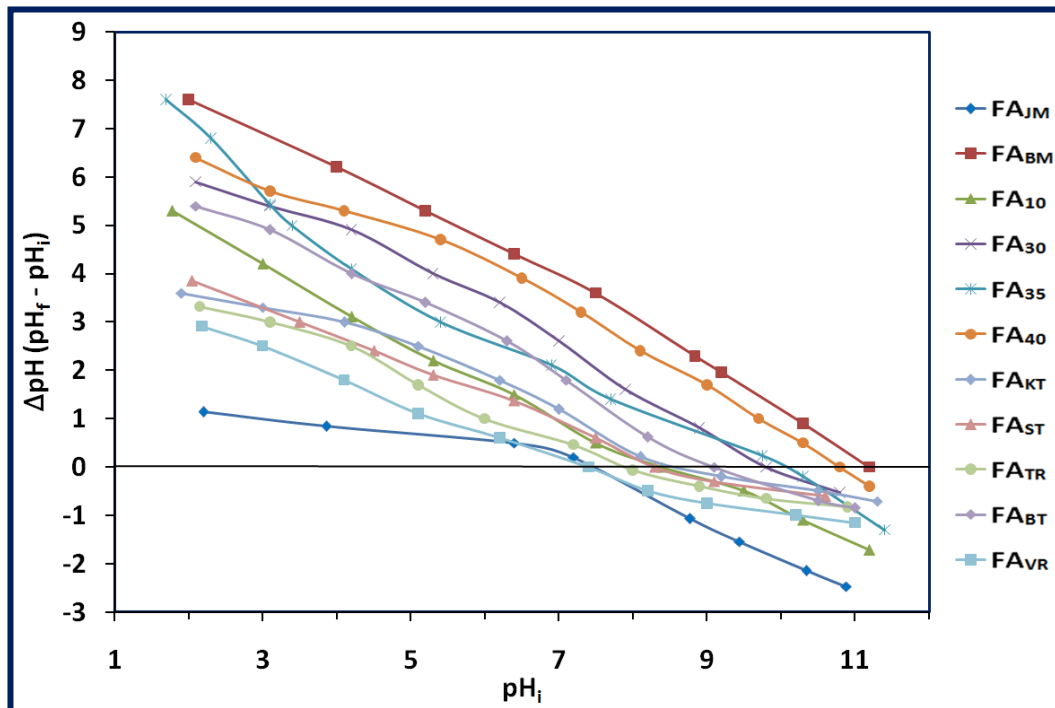


Figure 3.7: Point Zero Charge of various fly ash

3.3.2 Optimization of Adsorption parameters

(i) Preliminary experiments with various fly ash samples

The preliminary adsorption experiments were carried out using eleven different FA (FA₁₀, FA₃₀, FA₃₅, FA₄₀, FA_{KT}, FA_{JM}, FA_{BT}, FA_{VL}, FA_{SG}, FA_{TR}, FA_{BM}) for removal of two different dyes (acidic dye Brilliant green and basic dye Methylene blue) from aqueous solution. The % removal of BG and MB on all FA samples are shown in Table 3.5 and Figure 3.18 (a & b) respectively. It was observed that out of 11 fly ash samples only 6 samples (FA₁₀, FA₃₀, FA₃₅, FA₄₀, FA_{SG}, FA_{BM}) are good for adsorptive removal of dyes from effluents of textiles and dye manufacturing industries due to high carbon content and pH_{ZPC} in the range from 7.4 to 11.2. Fly ash with high carbon content is not useful for cementation but very effective for adsorption of dyes. Figure 3.18 clearly show that (FA₁₀, FA₃₀, FA₃₅, FA₄₀, FA_{BM}) show maximum adsorption within 30 minutes, with fast dye removal but FA_{ST} took more time to achieve maximum adsorption. The detailed explanation on the effect of pH and carbon content for governing the removal of dye on fly ash is discussed elsewhere in the chapter.

The maximum % removal of BG dye was with FA_{BM} whereas maximum % removal of MB dye was with FA₄₀. In the % removal of both dyes on various fly ash, two factors pH_{ZPC} and carbon content of fly ash mainly contribute. MB is a basic dye its % removal increases with decrease in pH_{ZPC} and with increase in carbon content. It shows maximum adsorption on FA₄₀ which has maximum carbon content. pH_{ZPC} of fly ash show little effect than carbon content on % adsorption. Both the dyes show good adsorption with FA₄₀ due to high carbon content. Therefore, further experiments were carried out using FA₄₀ for removal of BG (acidic dye) and MB (basic dye) to optimize adsorption parameters and for comparison.

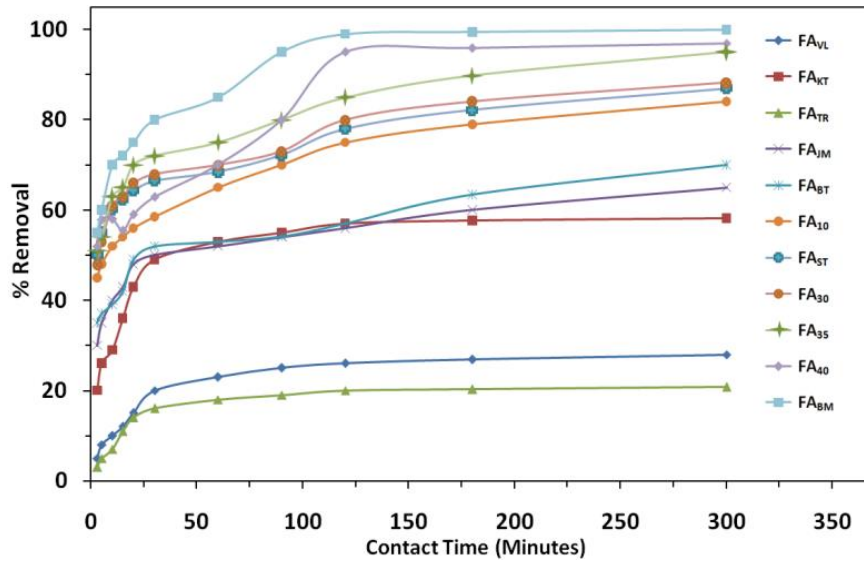


Figure 3.18(a): Percentage Removal of Brilliant Green on various fly ash samples
($C_0 = 100$ ppm, $m = 4$ g/l, $T = 303$ K, $\text{pH} = 5.6$)

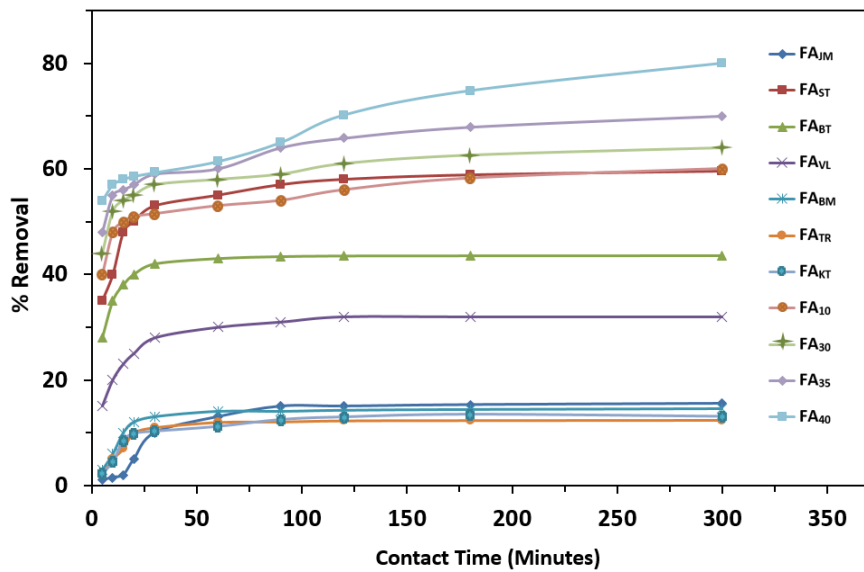


Figure 3.18(b): Percentage Removal of Methylene Blue on various fly ash samples
($C_0 = 20$ ppm, $m = 4$ g/l, $T = 303$ K, $\text{pH} = 7.4$)

Table 3.5: Percentage Removal of BG and MB on various fly ash

	t (min)	5	10	15	20	30	60	90	120	180	300
% Removal of BG ^a	FA _{MP}	8	10	12	15	20	23	25	26	26.9	27.96
	FA _{KT}	26	29	36	43	49	53	55	57	57.7	58.19
	FA _{OR}	5	7	11	14	16	18	19	20	20.3	20.78
	FA _{JM}	35	40	43	48	50	52	54	56	60	65
	FA _{BT}	37	39	42	49	52	53	54.2	57.02	63.4	70
	FA ₁₀	48	52	54	56	58.5	65	70	75	79	84
	FA _{ST}	55	60.1	62.3	64.3	66.5	68.5	72.2	78	82.2	86.97
	FA ₃₀	53	61	63	66	68	70	73	80	84.1	88.28
	FA ₃₅	54	63	65	70	72	75	80	85	89.8	95
	FA ₄₀	57.84	58	55.5	59	62.92	70	80	95	95.94	96.96
	FA _{BR}	60	70	72	75	80	85	95	99	99.48	100
% Removal of MB ^b	FA _{JM}	1	1.5	2	5	10	13	15	15.01	15.28	15.52
	FA _{ST}	35	40	48	50	53	55	57	58	58.85	59.56
	FA _{BT}	28	35	38	40	42	43.01	43.38	43.5	43.53	43.56
	FA _M	15	20	23	25	28	30	31	32	32	32
	FA _{BM}	3	6	10	12	13	14	14	14.2	14.35	14.5
	FA _{OR}	2	5	7	10	11	12	12.1	12.3	12.35	12.4
	FA _{KT}	2.3	4.6	8.5	9.9	10.3	11.2	12.5	13	13.5	13.1
	FA ₁₀	40	48	50	51	51.5	53	54	56	58.2	60
	FA ₃₀	44	52	54	55	57	58	59	61	62.6	64
	FA ₃₅	48	55	56	57	59	60	64	65.8	67.9	70
	FA ₄₀	54	57	58	58.6	59.3	61.4	65	70.2	74.8	80

^a C₀ = 100 ppm, m = 4 g/l, T = 303 K, pH = 5.6^b C₀ = 20 ppm, m = 4 g/l, T = 303 K, pH = 7.4

(ii) *Effect of pH*

The initial pH of the dye solution has been identified as the most important variable governing adsorption process particularly the adsorption capacity. pH of the solution may change: (1) the surface charge of the adsorbent, (2) the degree of ionization of the adsorbate molecule and (3) extent of dissociation of functional groups on the active sites of the adsorbent. To observe the effect of pH on the extent of dye adsorption, dye solution pH is varied from 2.8 to 11.2. The adsorption capacity of MB and BG dye at different pH is shown in [Table 3.6](#) and [Figure 3.19 \(a & b\)](#). From this study, it is observed that maximum adsorption takes place at pH value of 11.2 for BG and 7.4 for MB. [Figure 3.19 \(a\)](#) also shows that the removal of MB dye slightly increases with the increase of pH up to 7.4 and thereafter remains constant. The variation in the dye uptake with respect to the initial solution pH can be explained on the basis of the structure of dye molecule and point of zero charge (pH_{ZPC}) of FA₄₀. For FA₄₀, the point of zero charge is estimated to be 10.8. Above this pH, FA₄₀ particle acquires a negative surface charge. MB dye is basic (pH 7.4) in nature so it shows ionization below pH 7.4. At pH lower than pH_{ZPC} , the FA₄₀ surface acquires positive charge and dye molecules also become positively charged due to ionization below pH 7.4. Due to this there is an electrostatic repulsion between dye molecules and FA₄₀ that causes decrease in MB dye uptake $\text{pH} < 7.4$. Above that pH adsorption is constant because of no ionization for MB.

For BG, a sharp increase in adsorption observed with an increase in pH from 2.8 to 11.2 as shown in [Figure 3.19 \(b\)](#). The pH trends observed clearly indicate that the protonation of BG takes place in a highly acidic medium, while on the other hand with decrease in acidity of the solution, the BG dye becomes deprotonated. Another possibility that can be taken into account is that development of positive charge on the FA₄₀ takes place in solution $\text{pH} < 10.8$ ($\text{pH}_{\text{ZPC}} = 10.8$), which inhibits the adsorption of dye over it, resulting in low adsorption. However, on increasing the basicity, the uptake of dye increases due to electrostatic attraction between positively charged dye molecule and negatively charged surface of FA₄₀ (above pH 10.8) leading to the formation of an electrical

double layer around the adsorbent [30]. All further experiments were done on the natural pH due to change in stability of dye with change in pH.

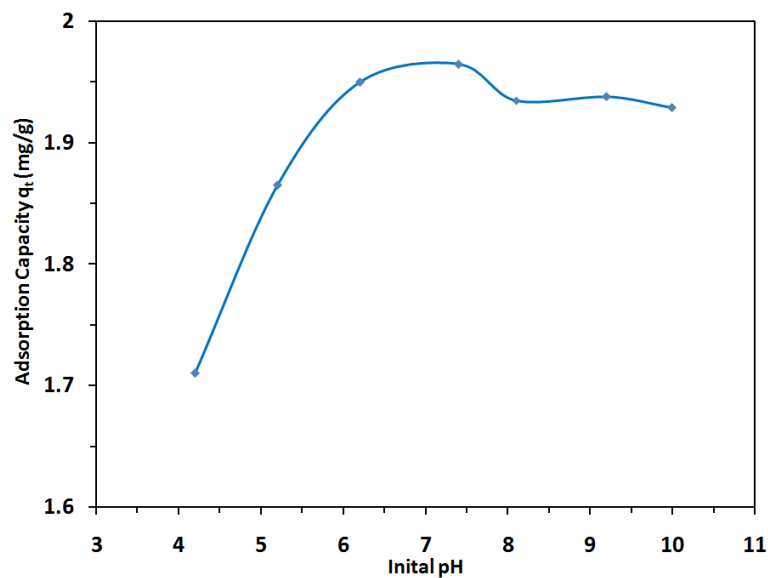


Figure 3.19(a): Effect of pH on adsorption capacity of FA₄₀ for MB adsorption
($m = 8.0$ gm/l, $t = 5$ hr, $T = 298$ K, $C_0 = 20$ ppm)

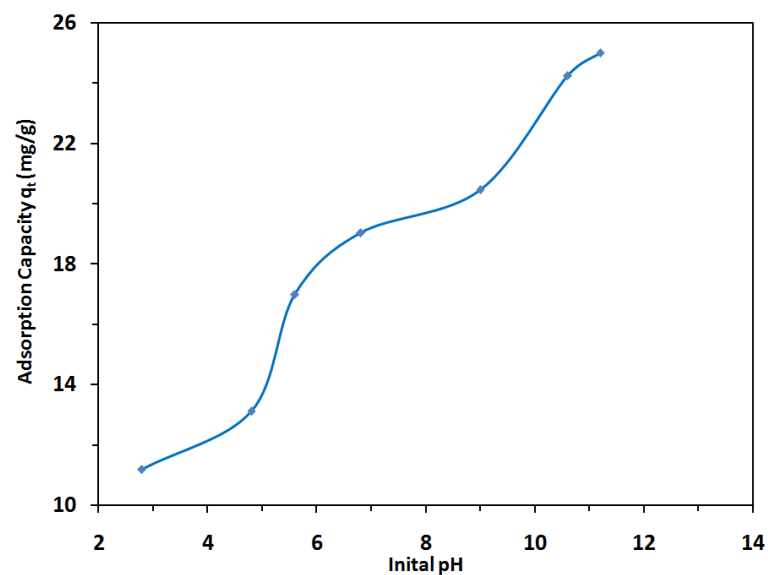


Figure 3.19(b): Effect of pH on adsorption capacity of FA₄₀ for BG adsorption
($m = 4.0$ gm/l, $t = 30$ min, $T = 303$ K, $C_0 = 100$ ppm)

Table 3.6: Effect of pH on adsorption capacity of FA₄₀ for MB and BG adsorption

MB ^a		BG ^b	
Initial pH	Adsorption Capacity (mg/g)	Initial pH	Adsorption Capacity (mg/g)
4.2	1.71	2.8	11.2
5.2	1.865	4.8	13.13
6.2	1.95	5.6	17
7.4	1.965	6.8	19.05
8.1	1.935	9	20.46
9.2	1.938	10.6	24.25
10	1.929	11.2	25

^a m = 8.0 gm/l, t = 5 hr, T = 298 K, C₀ = 20 ppm

^b m = 4.0 gm/l, t = 30 min, T = 303 K, C₀ = 100 ppm

(iii) *Effect of initial dye concentration (C₀)*

The effect of C₀ on the removal of MB and BG by FA₄₀ is shown in [Table 3.7](#) & [Figures 3.20 \(a & b\)](#) respectively. It is evident from the figures that the amounts of MB and BG adsorbed per unit mass at equilibrium (q_e) of FA₄₀ increase with the increase in C₀, although percentage removal is decreased with increase in C₀. The C₀ provides the necessary driving force to overcome the resistances to the mass transfer of MB and BG between the aqueous and the solid phases [31]. The increase in C₀ also enhances the interaction between dye and FA₄₀. Therefore, an increase in C₀ of MB and BG enhances the adsorption uptake of MB and BG.

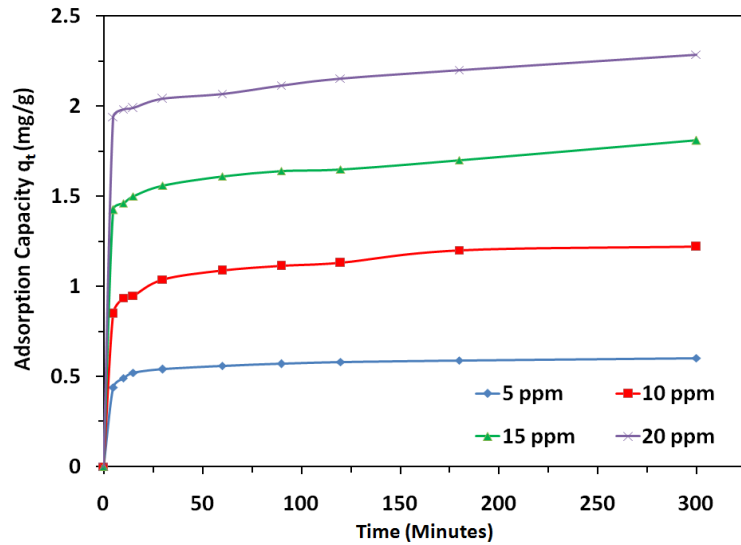


Figure 3.20(a): Effect of Initial Concentration of MB on adsorption capacity of FA₄₀ ($m = 8.0 \text{ gm/l}$, $\text{pH} = 7.4$, $T = 298 \text{ K}$)

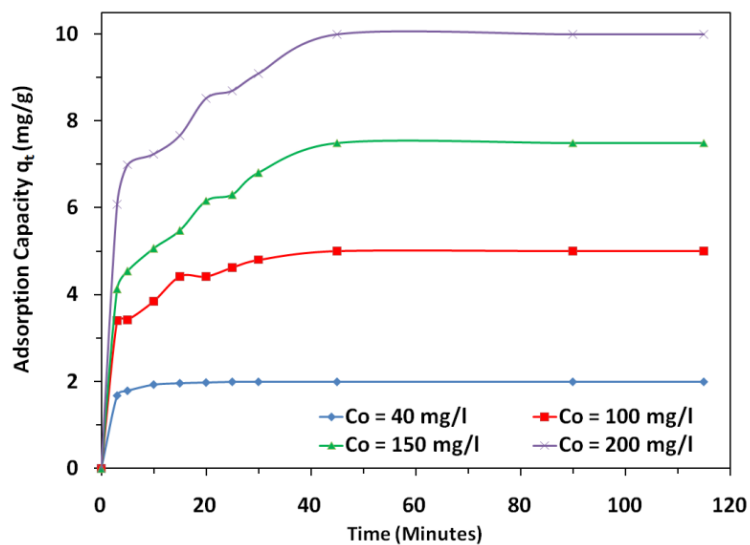


Figure 3.20(b): Effect of Initial Concentration of BG on adsorption capacity of FA₄₀ ($m = 20.0 \text{ gm/l}$, $\text{pH} = 5.6$, $T = 303 \text{ K}$)

Table 3.7: Effect of Initial Concentration of BG and MB on adsorption capacity of FA₄₀

	t (min)	C ₀ =40 ppm		C ₀ =100 ppm		C ₀ =150 ppm		C ₀ =200 ppm	
		q _t (mg/g)	% removal	q _t (mg/g)	% removal	q _t (mg/g)	% removal	q _t (mg/g)	% removal
BG^a	0	0	83.8	0	68.14	0	55.2	0	60.8
	3	1.676	89.1	3.407	68.5	4.14	60.69	6.08	69.94
	5	1.782	96.3	3.425	77.08	4.55	67.66	6.994	72.42
	10	1.926	98.45	3.854	84.92	5.07	73.12	7.242	76.68
	15	1.969	99.175	4.426	88.3	5.484	82.27	7.668	85.18
	20	1.983	99.475	4.415	92.4	6.17	84.13	8.518	86.96
	25	1.989	99.75	4.625	96.15	6.31	90.8	8.696	90.09
	30	1.995	99.9	4.807	98.2	6.81	96.8	9.09	94.21
	45	2	100	5	100	7.5	100	10	100
	90	2	100	5	100	7.5	100	10	100
	115	2	100	5	100	7.5	100	10	100
	MB^b		C ₀ =5 ppm		C ₀ =10 ppm		C ₀ =15 ppm		C ₀ =20 ppm
t (min)		q _t (mg/g)	% removal	q _t (mg/g)	% removal	q _t (mg/g)	% removal	q _t (mg/g)	% removal
5		0.44	70	0.848	67.86	1.425	76	1.94	77.6
10		0.49	78.2	0.9345	74.76	1.462	78	1.982	79.3
15		0.52	83.6	0.9482	75.86	1.5	79.87	1.99	79.65
30		0.54	87	1.039	83.1	1.56	83.33	2.04	81.55
60		0.56	89.8	1.087	86.97	1.61	85.87	2.069	82.8
90		0.57	91.4	1.112	88.97	1.64	87.33	2.116	84.65
120		0.58	93.4	1.13	90.5	1.65	88	2.154	86.15
180		0.59	94.9	1.2	96.8	1.7	92.3	2.2	89.8
300	0.602	96.28	1.22	97.59	1.81	96.4	2.286	91.45	

^a m = 8.0 gm/l, pH = 7.4, T = 298 K^b m = 20.0 gm/l, pH = 5.6, T = 303 K

(iv) Effect of adsorbent dosage (m)

The effect of m on the removal of MB by FA₄₀ at C_0 10 mg/l and for BG at C_0 100 mg/l are shown in Table 3.8 & Figures 3.21 (a & b) respectively. Different initial concentrations were selected for both the dyes according to their adsorption capacity on fly ash on the basis of preliminary experiments. It can be seen that for both the dyes, removal increases up to a certain limit at all 'm' values and then remains almost constant. An increase in the adsorption with the increase in adsorbent dosage can be attributed to greater surface area and the availability of more adsorption sites. With increase in the m , the dye removal increases due to increased dye uptake by the increased amount of adsorbent.

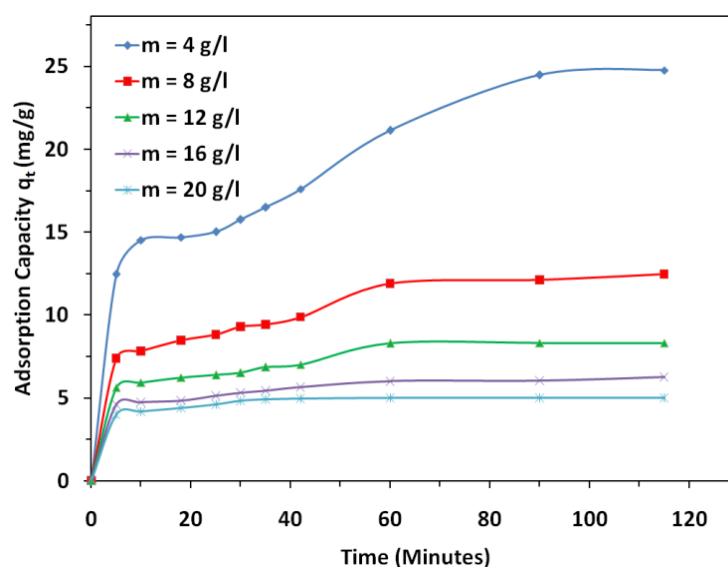


Figure 3.21(a): Effect of adsorbent dose on adsorption capacity of FA₄₀ for BG adsorption ($T = 303$ K, $\text{pH} = 5.6$, $C_0 = 100$ ppm)

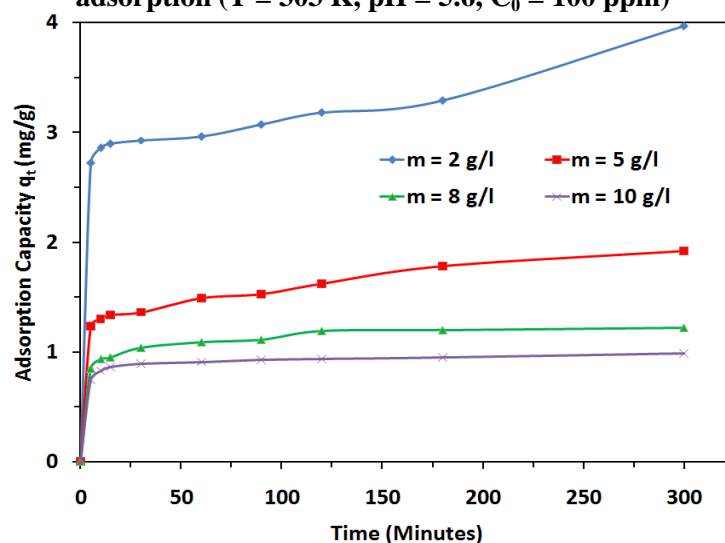


Figure 3.21(b): Effect of adsorbent dose on adsorption capacity of FA₄₀ for MB adsorption ($T = 298$ K, $\text{pH} = 7.4$, $C_0 = 10$ ppm)

Table 3.8(a): Effect of adsorbent dose on adsorption capacity of FA₄₀ for BG adsorption

t (min)	Adsorption Capacity (mg/g)				
	m=4 g/l	m=8 g/l	m=12 g/l	m=16 g/l	m=20 g/l
0	0	0	0	0	0
5	12.46	7.385	5.613	4.595	3.99
10	14.52	7.82	5.92	4.72	4.18
18	14.69	8.46	6.23	4.832	4.38
25	15.01	8.82	6.38	5.12	4.6
30	15.74	9.275	6.513	5.31	4.81
35	16.5	9.42	6.85	5.43	4.89
42	17.6	9.865	7.006	5.645	4.94
60	21.12	11.88	8.29	6	4.98
90	24.46	12.12	8.31	6.02	5
115	24.76	12.46	8.312	6.24	5

(T = 303 K, pH = 5.6, C₀ = 100 ppm)**Table 3.8(b):** Effect of adsorbent dose on adsorption capacity of FA₄₀ for MB adsorption

t (min)	Adsorption Capacity (mg/g)			
	at m = 2 g/l	at m = 5 g/l	at m = 8 g/l	at m = 10 g/l
0	0	0	0	0
5	2.72	1.236	0.848	0.7448
10	2.86	1.3	0.9345	0.8297
15	2.9	1.336	0.9482	0.8621
30	2.93	1.362	1.039	0.8897
60	2.965	1.488	1.087	0.91
90	3.07	1.524	1.112	0.925
120	3.18	1.62	1.19	0.938
180	3.29	1.78	1.2	0.95
300	3.97	1.92	1.2198	0.9897

(T = 298 K, pH = 7.4, C₀ = 10 ppm)

(v) *Effect of contact time (t)*

Effect of contact time for the removal of MB on to FA₄₀ at C₀ = 5, 10, 15 and 20 mg/l at m=8 g/l and for BG C₀=40, 100, 150 and 200 mg/l at m=20 g/l showed rapid adsorption of dyes in the first 15 min and, thereafter, decreases gradually and reaching at equilibrium in about 5 h as shown in [Table 3.7](#) and [Figure 3.20 \(a & b\)](#). Aggregation of dye molecules with increase in contact time makes it almost impossible to diffuse deeper into the adsorbent structure at highest energy sites. This aggregation negates the influence of contact time as the mesopores get filled up and start offering resistance to diffusion of aggregated dye molecules in the adsorbents. The adsorption curves were single, smooth and continuous leading to saturation and indicated the possible monolayer coverage on the surface of adsorbents by the dye molecules [\[30, 31\]](#). Predication of dyes adsorption by the combined effect of C₀, adsorption capacity (q_t) and time are described in three dimensional plots ([Figure 3.22](#)).

3.3.3 Adsorption Kinetics

Four widely used kinetic models, pseudo-first-order, pseudo-second-order, Bangham and intra-particle diffusion model as described in Chapter 2 were employed to interpret the kinetics. All kinetic results are shown in [Figures 3.23 and 3.24](#) and [Tables 3.9 and 3.10](#).

For pseudo-first -order kinetic model, although the R^2 value obtained was relatively high ($R^2 = 0.919$) for MB and ($R^2 = 0.981$) for BG, the calculated q_e value did not agree with the experimental one. This suggests that the pseudo-first-order kinetic model is not appropriate to represent the adsorption kinetics data of both BG and MB onto FA₄₀.

For pseudo-second-order kinetic model, the R^2 value obtained was very high ($R^2 > 0.999$) for both dyes, and the calculated q_e value was in good agreement with the experimental one, suggesting the applicability of the pseudo-second-order kinetic model to describe the adsorption kinetics data of BG and MB onto FA₄₀.

Linear plots of q_e and h against C_0 were regressed to obtain the value of q_e and h in terms of C_0 with high value of a coefficient of regression (> 0.9816).

Therefore, q_e and h can be express as a function of C_0 as follows:

For Methylene Blue

$$q_e = 1.1076 \ln C_0 - 1.2727 \quad (3.1)$$

$$h = 4.1 \times 10^{-3} C_0^2 - 0.007 C_0 + 0.175 \quad (3.2)$$

$$q_t = \frac{t}{1/(4.1 \times 10^{-3} C_0^2 - 0.007 C_0 + 0.175) + (1/1.1076 \ln C_0 - 1.2727) t} \quad (3.3)$$

For Brilliant Green

$$q_e = 4.507 \ln C_0 - 14.944 \quad (3.4)$$

$$h = 3 \times 10^{-4} C_0^2 - 0.0573 C_0 + 5.1098 \quad (3.5)$$

$$q_t = \frac{t}{1/(3 \times 10^{-4} C_0^2 - 0.0573 C_0 + 5.1098) + (1/4.507 \ln C_0 - 14.944) t} \quad (3.6)$$

A comparison of experimental data points and the surface predicted by the equations (3.3 & 3.6) is given in Figure 3.22 (a & b). It can be used to derive the sorption capacity, q_t at any given C_0 and t [32].

Bangham's equation show (Figure 3.23c & 3.24c) linear curves for both the dyes removal by the FA₄₀, signifying that the diffusion of adsorbate into the pores of the adsorbent was the only rate-controlling step [32, 33] that means pore diffusion was important in the removal process.

For the Intra-particle diffusion model, graphical plot of q_t versus $t^{0.5}$ (Figure 3.23d and 3.24d) are straight line passing through the origin, then the sorption process fits to the intraparticle diffusion kinetic model. Values of C (Table 3.10) give an idea about the thickness of the boundary layer, i.e. the larger the intercept the greater is the boundary layer effect [34].

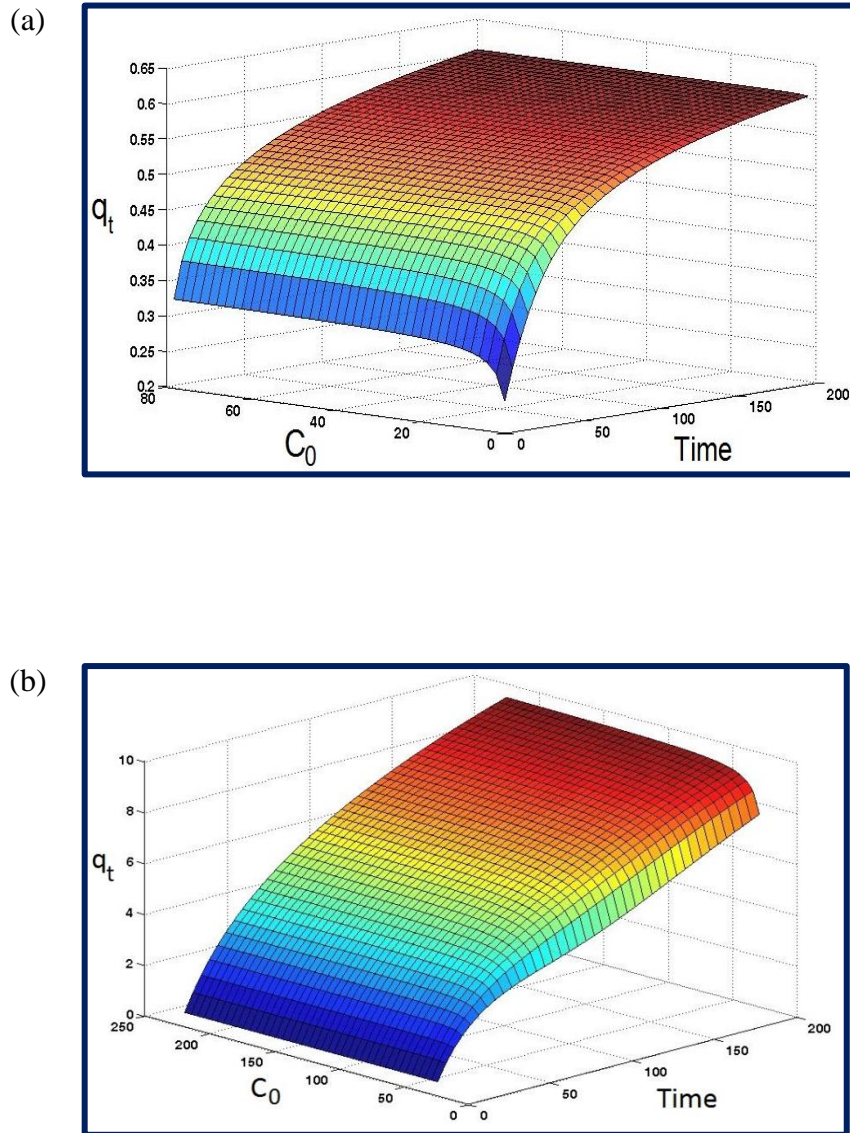


Figure 3.22: Three dimensional plot showing the interaction effect of Initial Concentration (C_0) and Time (t) of FA₄₀ on adsorption capacity (q_t) of (a) MB and (b) BG

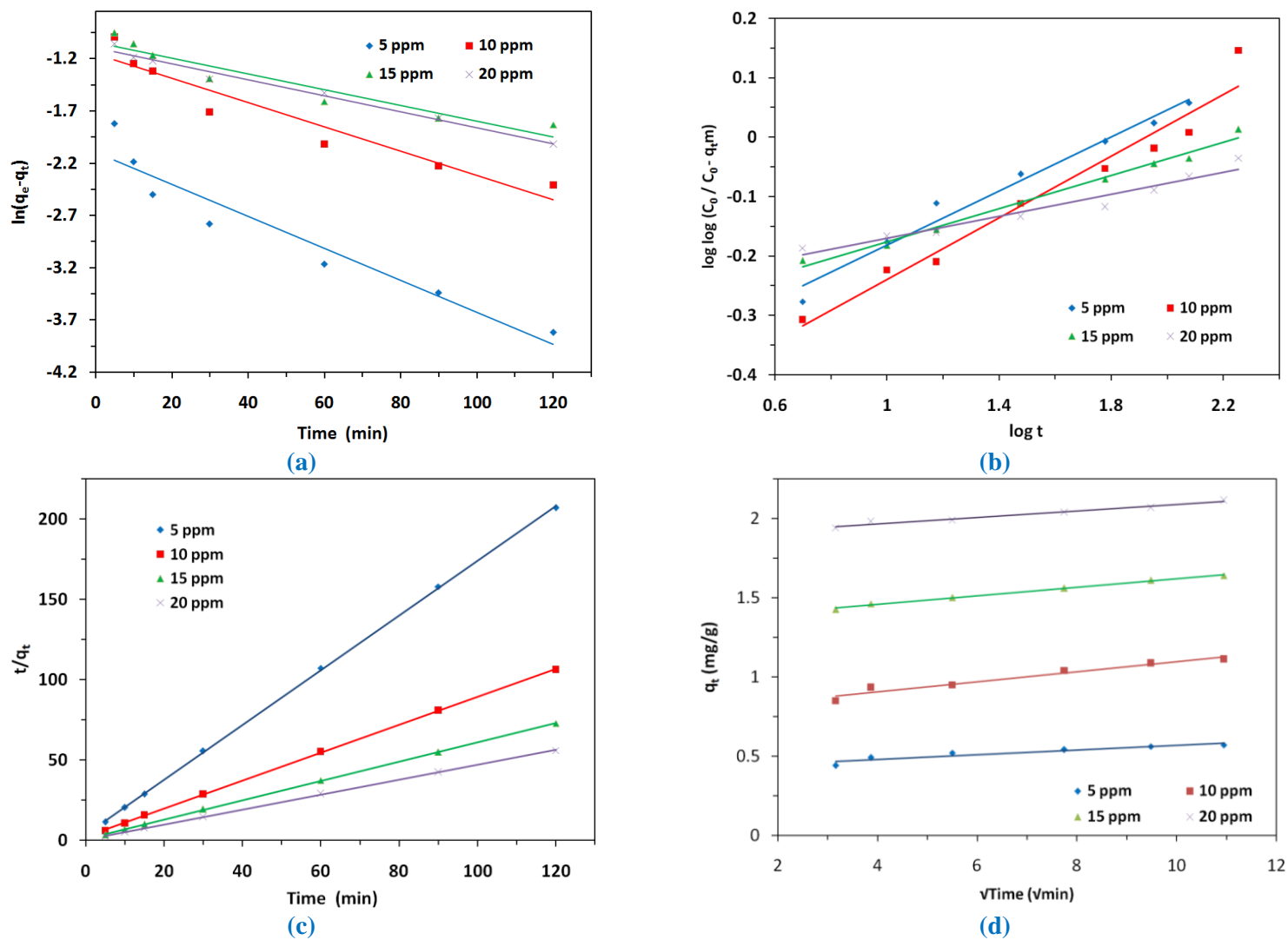
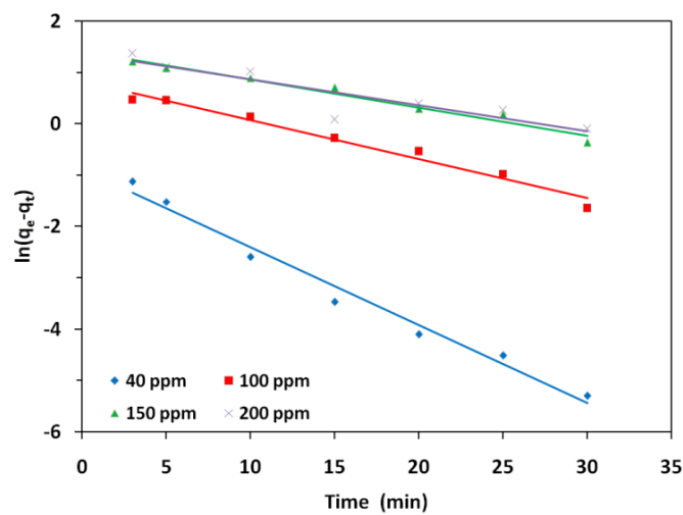
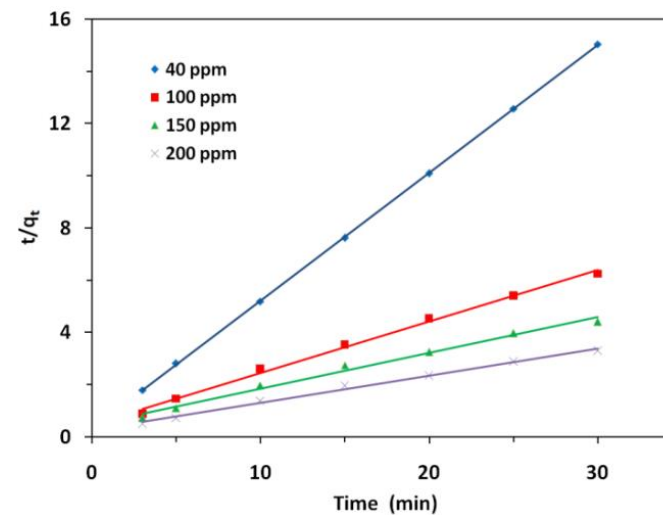


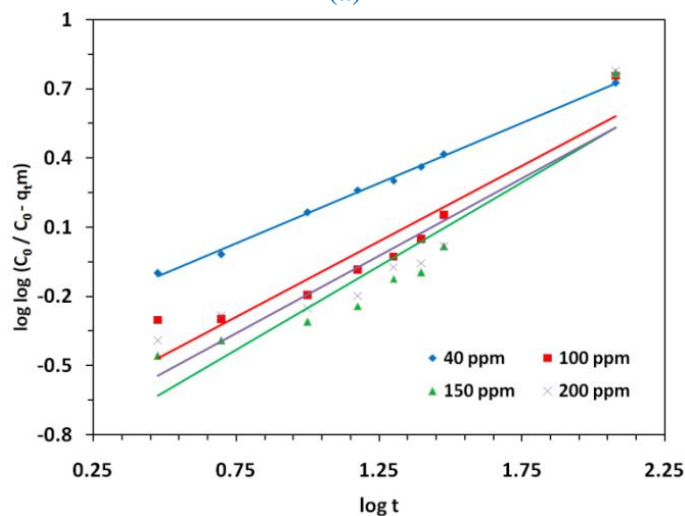
Figure 3.23: Kinetic Model (a) Pseudo Second Order, (b) Pseudo Second Order, (c) Bangham's equation and (d) intra-particle diffusion model of MB adsorption on FA₄₀



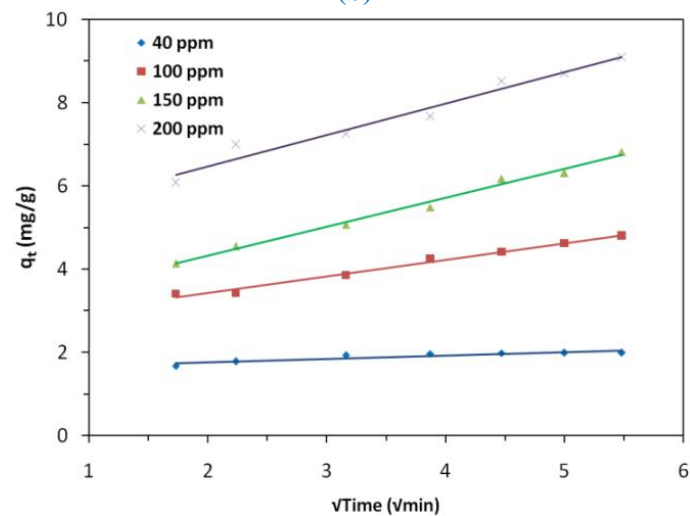
(a)



(b)



(c)



(d)

Figure 3.24: Kinetic Model (a) Pseudo Second Order, (b) Pseudo Second Order, (c) Bangham's equation and (d) intra-particle diffusion model of BG adsorption on FA₄₀

Table 3.9(a): Details of all kinetic parameters for MB adsorption on FA₄₀

BG C ₀	time (min.)	5	10	15	30	60	90	120
		$\sqrt{\text{time}}$	2.24	3.16	3.87	5.5	7.75	9.49
	$\log t$	0.69897	1	1.176091	1.477121	1.778151	1.954243	2.079181
5 ppm	$\ln(q_e - qt)$	-1.82	-2.189	-2.5	-2.78	-3.17	-3.44	-3.82
	t/qt	11.36	20.41	28.85	55.56	107.14	157.89	206.9
	qt	0.44	0.49	0.52	0.54	0.56	0.57	0.58
	$\log \log (C_0/C_0 - qt)$	-0.27678	-0.17682	-0.11087	-0.06225	-0.00746	0.023465	0.05792
10 ppm	$\ln(q_e - qt)$	-0.99	-1.25	-1.32	-1.71	-2.02	-2.23	-2.41
	t/qt	5.896	10.7	15.82	28.87	55.2	80.94	106.2
	qt	0.848	0.9345	0.9482	1.039	1.087	1.112	1.13
	$\log \log (C_0/C_0 - qt)$	-0.30743	-0.22386	-0.20978	-0.11203	-0.05319	-0.01907	0.007632
15 ppm	$\ln(q_e - qt)$	-0.954	-1.056	-1.17	-1.39	-1.61	-1.77	-1.832
	t/qt	3.51	6.84	10	19.23	37.27	54.88	72.73
	qt	1.425	1.462	1.5	1.56	1.61	1.64	1.65
	$\log \log (C_0/C_0 - qt)$	-0.20776	-0.1824	-0.15554	-0.11087	-0.07071	-0.04483	-0.03583
20 ppm	$\ln(q_e - qt)$	-1.06	-1.191	-1.22	-1.4	-1.53	-1.77	-2.02
	t/qt	2.58	5.045	7.54	14.71	29	42.53	55.71
	qt	1.94	1.982	1.99	2.04	2.069	2.116	2.154
	$\log \log (C_0/C_0 - qt)$	-0.18725	-0.16626	-0.16092	-0.13361	-0.11721	-0.08958	-0.06608

Table 3.9(b): Details of all kinetic parameters for BG adsorption on FA₄₀

MB C ₀	time (min.)	3	5	10	15	20	25	30
		$\sqrt{\text{time}}$	1.732	2.236	3.162	3.873	4.47	5
	log t	0.477121	0.69897	1	1.176091	1.30103	1.39794	1.477121
40 ppm	ln(qe - qt)	-1.13	-1.52	-2.6	-3.47	-4.1	-4.51	-5.3
	t/qt	1.79	2.81	5.19	7.62	10.08	12.57	15.04
	qt	1.676	1.782	1.926	1.969	1.984	1.989	1.995
	log log (C ₀ /C ₀ -q _t m)	-0.09915	-0.01836	0.163141	0.261003	0.30103	0.361922	0.415317
100 ppm	ln(qe - qt)	0.466	0.454	0.136	-0.282	-0.536	-0.981	-1.645
	t/qt	0.881	1.46	2.6	3.53	4.53	5.41	6.24
	qt	3.407	3.425	3.854	4.246	4.415	4.625	4.807
	log log (C ₀ /C ₀ -q _t m)	-0.30314	-0.29837	-0.19499	-0.08412	-0.02894	0.048902	0.152355
150 ppm	ln(qe - qt)	1.21	1.08	0.888	0.701	0.285	0.174	-0.371
	t/qt	0.725	1.099	1.972	2.74	3.24	3.96	4.41
	qt	4.14	4.55	5.07	5.484	6.17	6.31	6.81
	log log (C ₀ /C ₀ -q _t m)	-0.45752	-0.39229	-0.31029	-0.24271	-0.12424	-0.09717	0.015449
200 ppm	ln(qe - qt)	1.366	1.101	1.015	0.0847	0.393	0.265	-0.0943
	t/qt	0.493	0.715	1.38	1.96	2.35	2.88	3.3
	qt	6.08	6.994	7.242	7.668	8.518	8.696	9.09
	log log (C ₀ /C ₀ -q _t m)	-0.39071	-0.2828	-0.25252	-0.19884	-0.07487	-0.05742	0.017433

Table 3.10: Pseudo-first order, Pseudo-second order, Bangham and Intra-particle Diffusion Model rate constant for MB and BG adsorption on FA₄₀ at various concentration

MB ^a Dye	C ₀ (mg/L)		5	10	15	20
	q _{e, exp} (mg/g)		0.602	1.22	1.81	2.286
	Pseudo-first order model	K ₁ (1/min)	0.0153	0.0116	0.0076	0.0077
		q _{e, cal} (mg/g)	0.123	0.315	0.353	0.335
		R ²	0.9179	0.9187	0.9138	0.9826
	Pseudo-second order	K ₂ (g/mg min)	0.7945	0.3248	0.3924	0.3559
		q _{e, cal} (mg/g)	0.5866	1.1486	1.666	2.158
		R ²	0.9998	0.9998	0.9999	0.9997
	Bangham	K ₀ (g)	5.620	4.572	6.964	7.857
		α	0.2269	0.2587	0.1391	0.0923
		R ²	0.976	0.959	0.989	0.948
	Intra-particle Diffusion Model	K _{id} (mg/g(min ^{0.5}))	0.0146	0.0317	0.027	0.0203
		C	0.421	0.78	1.35	1.88
		R ²	0.882	0.951	0.994	0.969
BG ^b Dye	C ₀ (mg/L)		40	100	150	200
	q _{e, exp} (mg/g)		2.0	5.0	7.5	10.0
	Pseudo-first order model	K ₁ (1/min)	0.151	0.076	0.054	0.050
		q _{e, cal} (mg/g)	0.409	2.296	4.104	3.915
		R ²	0.981	0.974	0.971	0.816
	Pseudo-second order	K ₂ (g/mg min)	0.762	0.079	0.039	0.0421
		q _{e, cal} (mg/g)	2.045	5.11	7.299	9.615
		R ²	1.0	0.995	0.989	0.993
	Bhangham	K ₀ (g)	2.495	0.9526	0.6066	0.7880
		α	0.5218	0.6555	0.7264	0.6711
		R ²	0.998	0.894	0.864	0.835
	Intra-particle Diffusion Model	K _{id} (mg/g(min ^{0.5}))	0.081	0.398	0.695	0.751
		C	1.6	2.64	2.93	4.97
		R ²	0.838	0.987	0.989	0.964

^a (m = 8.0 g l⁻¹, agitation rate = 200 rpm, pH = 7.4, T = 25 °C)

^b (m = 20.0 g l⁻¹, agitation rate = 200 rpm, pH = 5.6, T = 30 °C)

3.3.4 Adsorption Isotherms

The adsorption isotherms of MB onto FA₄₀ at 25°C, 35°C and 45°C and for BG at 30°C, 40°C and 50°C are shown in Figure 3.25. Values of isotherms parameters are compiled in Tables 3.11 (a & b) for both the dyes. Results showed that adsorption capacity increased with increasing dyes concentration until equilibrium was reached. Three isotherm models Langmuir, Freundlich and Tempkin were used to fit the experimental data as already described in Chapter 2.

The different isotherm parameters were evaluated from the linear plots and presented in Table 3.12 along with constants and correlation coefficients, root mean square error (RMSE), sum of the squares of the errors (SSE) and chi-square (χ^2). The RMSE, SSE and χ^2 are used to measure the goodness of fit of an isotherm defined in chapter 2.

The value of RMSE and χ^2 for the Langmuir, Freundlich and Tempkin isotherm models were low for MB, indicating that the equilibrium data for the adsorption of MB onto FA₄₀ can be well represented by these isotherm models but adsorption of BG obeyed only Langmuir isotherm. From Langmuir isotherm model it is concluded that the adsorption of MB and BG onto FA₄₀ takes place as monolayer adsorption and the surface of FA₄₀ is homogenous in adsorption affinity. The predicted maximum monolayer MB and BG adsorption capacity for FA₄₀ derived from Langmuir isotherm was found to be 3.184 mg/g for MB and 100.0 mg/g for BG. The values of R_L obtained in this study were between 0.03 to 0.18 for MB and 0.0074 to 0.129 for BG indicating that the adsorption of both dyes onto FA₄₀ is favourable. The above experimental data was evaluated by Langmuir isotherm model.

Table 3.11(a): Isotherm parameters for adsorption of MB on FA₄₀

T (°C)	Parameter				
25 °C	C _e	0.186	0.366	0.538	1.71
	ln C _e	-1.68	-1.01	-0.62	0.54
	log C _e	-0.73	-0.44	-0.27	0.23
	q _e	0.602	1.2	1.81	2.286
	log q _e	-0.22	0.08	0.26	0.36
	C _e / q _e	0.309	0.305	0.297	0.748
35 °C	C _e	0.255	1	2.062	3.89
	ln C _e	-1.37	0	0.724	1.36
	log C _e	-0.593	0	0.314	0.59
	q _e	0.593	1.125	1.62	2
	log q _e	-0.227	0.051	0.21	0.3
	C _e / q _e	0.43	0.889	1.273	1.945
45 °C	C _e	0.312	1.103	3.4	4.5
	ln C _e	-1.165	0.098	1.224	1.504
	log C _e	-0.506	0.043	0.532	0.653
	q _e	0.586	1.11	1.45	1.94
	log q _e	-0.232	0.045	0.161	0.288
	C _e / q _e	0.532	0.994	2.35	2.32

Table 3.11(b): Isotherm parameters for adsorption of BG on FA₄₀

T (°C)	Parameter						
30 °C	C _e	0.1	0.79	1.69	4.41	32.6	151
	ln C _e	-2.3	-0.236	0.525	1.484	3.484	5.017
	log C _e	-1	-0.102	0.2279	0.6444	1.513	2.179
	q _e	12.48	24.8	49.6	73.89	91.85	87.25
	log q _e	1.096	1.394	1.695	1.868	1.9631	1.941
	C _e / q _e	0.008	0.032	0.034	0.06	0.355	1.73
40 °C	C _e	0.79	1.5	3.12	7.58	50.2	225.1
	ln C _e	0.236	0.405	1.138	2.026	3.916	5.417
	log C _e	-0.102	0.176	0.494	0.88	1.701	2.352
	q _e	12.3	24.63	49.22	73.105	87.45	68.72
	log q _e	1.09	1.391	1.692	1.864	1.942	1.837
	C _e / q _e	0.064	0.061	0.064	0.104	0.574	3.28
50 °C	C _e	1.58	2.98	5.89	15.1	91.3	302.3
	ln C _e	0.457	1.092	1.77	2.715	4.52	5.71
	log C _e	0.199	0.474	0.77	1.179	1.96	2.48
	q _e	12.1	24.25	48.52	71.225	77.18	49.42
	log q _e	1.083	1.385	1.686	1.853	1.89	1.694
	C _e / q _e	0.131	0.123	0.121	0.212	1.183	6.12

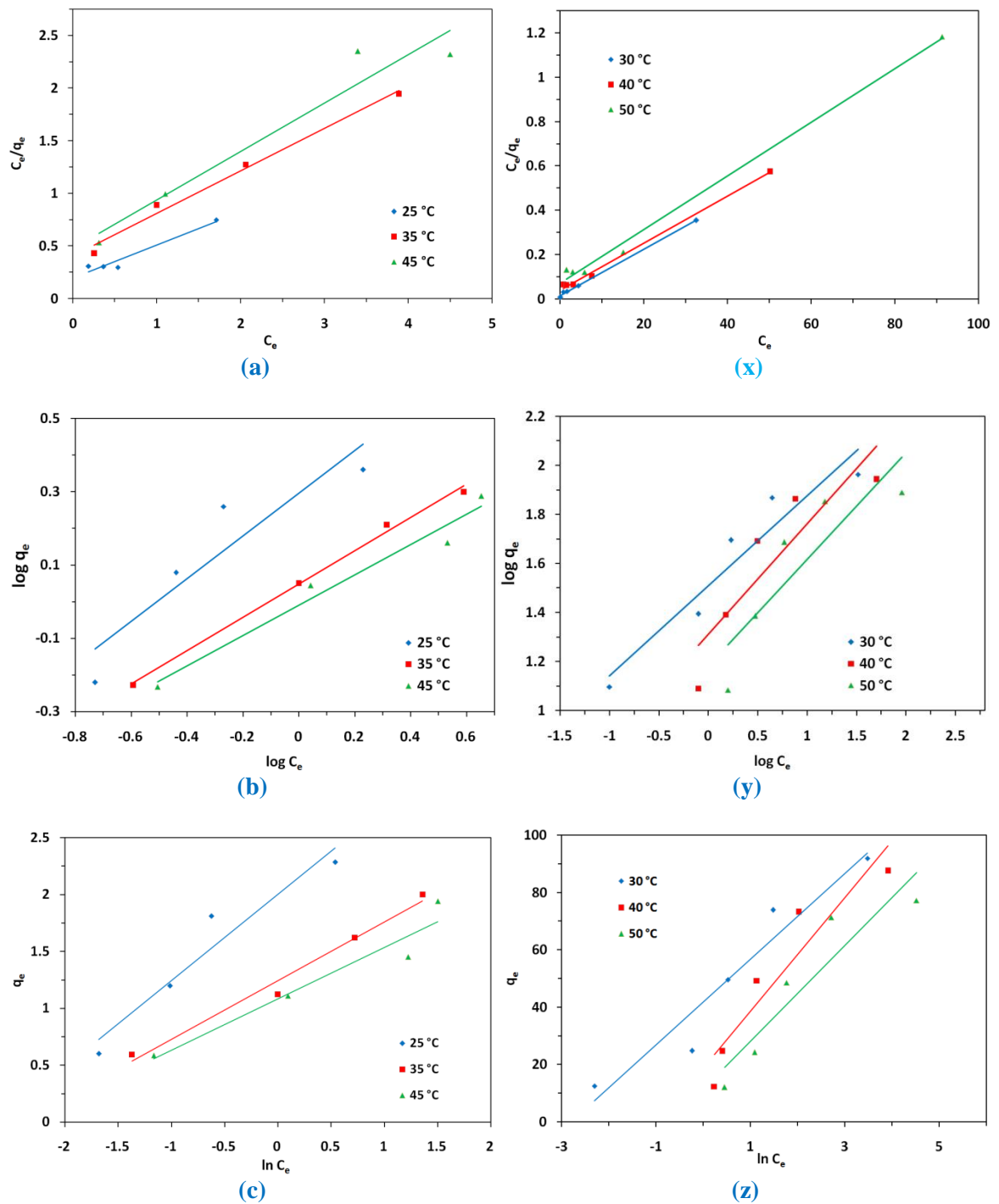


Figure 3.25: Adsorption Isotherm (a) Langmuir, (b) Freundlich and (c) Tempkin of MB adsorption and (x) Langmuir, (y) Freundlich and (z) Tempkin of BG adsorption on FA₄₀

Table 3.12: Isotherm parameters for MB and BG adsorption on FA₄₀ at various temperature

MB ^a Dye	Langmuir	Temperature	q_{\max} (mg/g)	K_L (L/mg)	R^2	SSE	RMSE	χ^2
		at 25°C	3.184	1.612	0.947	0.1298	0.2547	0.09
		at 35°C	2.48	0.994	0.988	0.0237	0.109	0.026
		at 45°C	2.172	0.966	0.939	0.0812	0.2015	0.057
	Freundlich	Temperature	K_F (mg/g)(L/mg) ^{1/n}	1/n	R^2	SSE	RMSE	χ^2
		at 25°C	1.98	0.582	0.848	0.3857	0.439	0.218
		at 35°C	1.12	0.454	0.996	0.0094	0.0686	0.005
		at 45°C	0.979	0.413	0.968	0.051	0.1598	0.040
	Tempkin	Temperature	K_T (mg/g)	B_T	R^2	SSE	RMSE	χ^2
		at 25°C	13.94	0.759	0.931	0.1097	0.2342	0.076
		at 35°C	11.11	0.516	0.982	0.0207	0.1017	0.020
		at 45°C	10.98	0.452	0.931	0.0672	0.1833	0.042
BG ^b Dye	Langmuir	Temperature	q_{\max} (mg/g)	K_L (L/mg)	R^2	SSE	RMSE	χ^2
		at 30°C	100	0.667	0.998	159.33	1.56	7.29
		at 40°C	100	0.256	0.996	132.32	6.64	3.54
		at 50°C	83.33	0.169	0.995	218.36	8.53	5.77
	Freundlich	Temperature	K_F (mg/g)(L/mg) ^{1/n}	1/n	R^2	SSE	RMSE	χ^2
		at 30°C	32.21	0.367	0.913	1041	18.63	14.04
		at 40°C	20.46	0.450	0.802	1764	24.25	25.89
		at 50°C	15.14	0.435	0.766	1711	23.88	30.58
	Tempkin	Temperature	K_T (mg/g)	B_T	R^2	SSE	RMSE	χ^2
		at 30°C	16.36	14.92	0.929	309.18	10.15	10.7
		at 40°C	2.59	19.76	0.882	472.14	12.54	15.28
		at 50°C	1.988	16.67	0.864	438.18	12.08	10.55

^a (m = 8.0 g l⁻¹, agitation rate = 200 rpm, pH = 7.4 and C₀ = 5 - 20 mg l⁻¹)

^b (m = 4.0 g l⁻¹, agitation rate = 200 rpm, pH = 5.6 and C₀ = 50 - 300 mg l⁻¹)

A comparison of the maximum adsorption capacity (q_m), for some dyes on various adsorbent is presented in Table 3.13. The q_m of acid dye BG obtained from this study is similar to that obtained in the other investigations, while the values of basic dyes MB are relatively low compared to other studies. Despite relatively low adsorption capacity of the studied fly ash, the use of this adsorbent for dye removal is of interest since it is low-cost and readily available waste.

Table 3.13: Comparison of the maximum monolayer adsorption of some dyes onto various adsorbents

Adsorbents	Adsorbate	Adsorption Capacity (mg/g)	References
Kaolin	Brilliant green	65.42	[35]
Bottom ash	Brilliant green	0.00034	[43]
Deoiled soya	Brilliant green	0.00074	[43]
Bagasse fly ash	Brilliant green	133.33	[36]
Fly ash (FA ₄₀)	Brilliant green	100.0	This work
Sepiolite	RB21	66.7	[37]
Chitosan	Acid red	53.5	[38]
Fly ash	RB21	106.7	[37]
Fly ash	Acid red 1	92.59	[39]
Fly ash - NaOH	Acid red 1	12.66	[39]
Fly ash	Acid red 91	1.46	[40]
Fly ash	Reactive blue 171	3.75	[41]
Fly ash (FA ₄₀)	Methylene blue	3.184	This work
Fly ash	Acid Black 1	18.94	[41]
Fly ash	Acid Black 193	22.08	[41]
Fly ash	Reactive red 23	5.04	[41]
Coal fly ash	Reactive Yellow 84	37.26	[42]

3.3.5 Effect of Temperature and Thermodynamic Studies

The amounts of both the dyes adsorbed on to FA₄₀ at different temperatures 298-318 K (MB) and 303-323 K (BG) has been estimated obtain thermodynamic parameters for adsorption system. Adsorption increased with decrease in temperature for both the dyes (Figure 3.26 a & b) can be explained on the basis of thermodynamic parameters of standard enthalpy (ΔH°) and entropy (ΔS°) for the adsorption process estimated from the Vant-Haff equation represented as discussed in chapter 2.

The values of K_L for Langmuir isotherms at different temperature are used to calculate thermodynamic parameters such as Gibbs free energy change (ΔG°). The values of ΔH° and ΔS° is calculated from the intercept and the slope of the linear plot of $\ln K_L$ versus $1/T$ as shown in Figures 3.27 (a & b) for MB and BG adsorption respectively.

The obtained values of the thermodynamic parameters of MB and BG adsorption onto FA₄₀ are given in Table 3.14. The negative values of ΔG° suggests that feasibility of the adsorption of both MB and BG onto FA₄₀ is spontaneous and favorable process. In general, the value of ΔG° for physiosorption is < 8.0 kJ/mol, and that chemisorption is between 20 and 40 kJ/mol [44]. The values of ΔG° obtained in this study are in the range of physiosorption for both, which is dependent on carbon content and pH_{zpc} of fly ash.

The negative values of ΔH° indicates that the adsorption process is exothermic in nature. The absolute value of ΔH° was 20.06 kJ/mol for MB and 56.23 kJ/mol for BG. The positive values of ΔS° for both the dyes show an increase in randomness at the solid/liquid interface during the adsorption process [45]

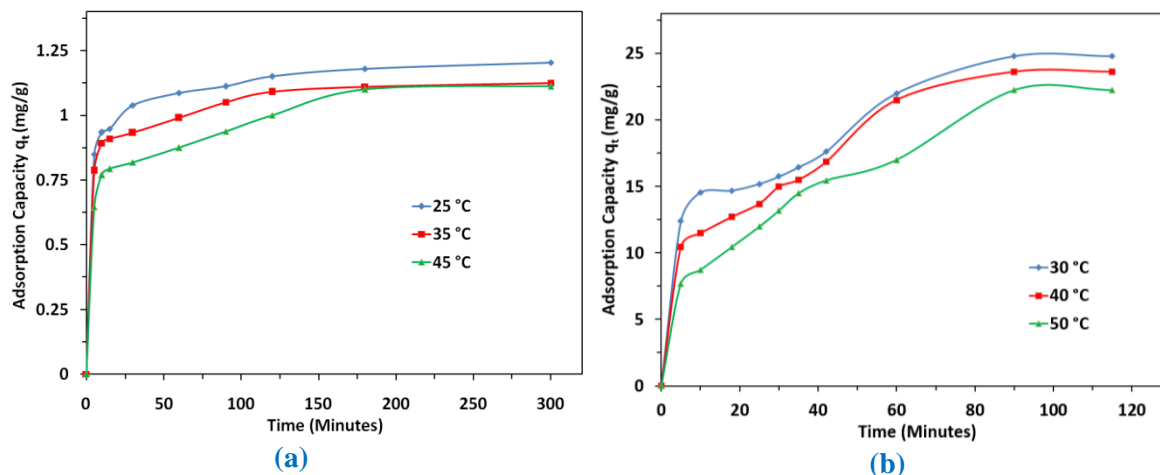


Figure 3.26: Effect of Temperature of solution on adsorption capacity of FA₄₀ on MB^a and BG^b adsorption
^a ($m = 1.0\text{gm/l}$, $\text{pH} = 7.4$, $C_0 = 10\text{ ppm}$) ^b ($m = 4.0\text{gm/l}$, $\text{pH} = 5.6$, $C_0 = 100\text{ ppm}$)

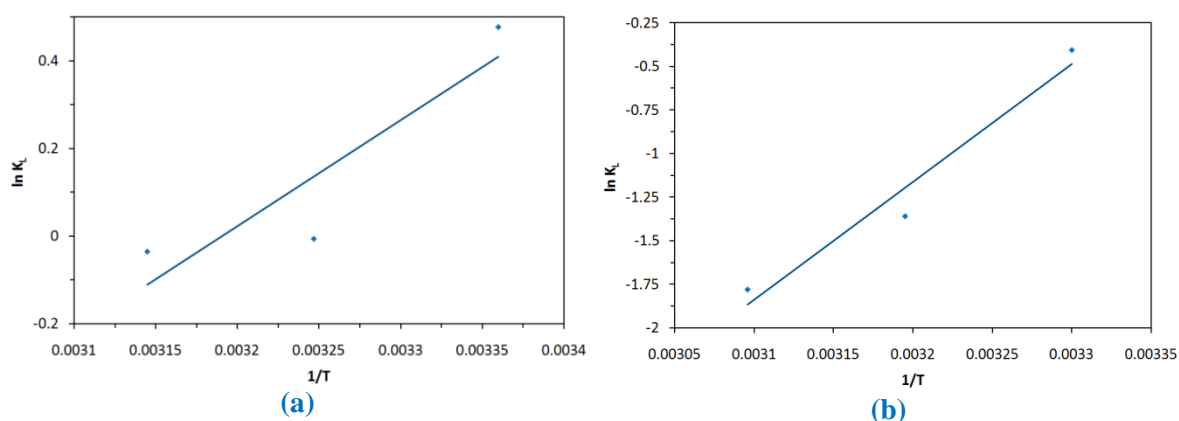


Figure 3.27(a): Van' t Hoff plot for the adsorption of (a) MB and (b) BG adsorption on FA₄₀

Table 3.14: Thermodynamic parameters for MB and BG adsorption on FA₄₀

MB Dye	ΔH° (KJ/mol)	ΔS° (J/mol)	$-\Delta G^\circ$ (KJ/mol)			R^2
			25 °C	35 °C	45 °C	
	-20.06	64.12	1.18	0.0154	0.0925	0.815
BG Dye	ΔH° (KJ/mol)	ΔS° (J/mol)	$-\Delta G^\circ$ (KJ/mol)			R^2
			30 °C	40 °C	50 °C	
	-56.23	189.56	1.02	3.54	4.78	0.959

3.3.6 Recyclability and reusability of FA₄₀ for BG and MB adsorption

To check the recyclability of fly ash for BG & MB adsorption, 1 mg fly ash (FA₄₀) sample was added into 50 ml of BG solution (100 mg/l) and 50 ml of MB solution (10 mg/l) separately and both stirred for 24 hour. Then, the supernatant was centrifugated at 2000 rpm for 4 min. and the concentrations of the residual dyes supernatant were detected by UV-visible spectroscopy. The same fly ash samples after the adsorption of particular dye was heated for regeneration at 380 °C for 6h in furnace. Following the above procedure, the recyclable fly ash was continuously reused for dye adsorption five to six times. Importantly, the adsorbed dyes can be easily removed from the fly ash by simple heating. Remarkably, the fly ash adsorbent is highly stable and can be reused for several cycles without losing adsorption activity. For instance, the adsorption capacity maintains upto 95% for BG and 93.8% for MB after 5 cycles of adsorption- desorption, as shown in [Figure 3.28 \(a & b\)](#), Furthermore, the FTIR spectra were used to examine the recovered ability of fly ash after BG & MB adsorption and desorption. Apparently, it can be seen that the absorption band of such as at 2975 cm⁻¹ and 2926 cm⁻¹ were present in BG and MB adsorbed fly ash respectively ([Figure 3.5 b & c](#)), but absent on BG & MB desorbed fly ash after heat treatment ([Figure 3.29 a & b](#)). The characteristic peaks of fly ash after BG and MB adsorption and after BG and MB desorption were almost the same as that of initial. Therefore, it was concluded that the fly ash could be a promising competitive candidate for wastewater treatment.

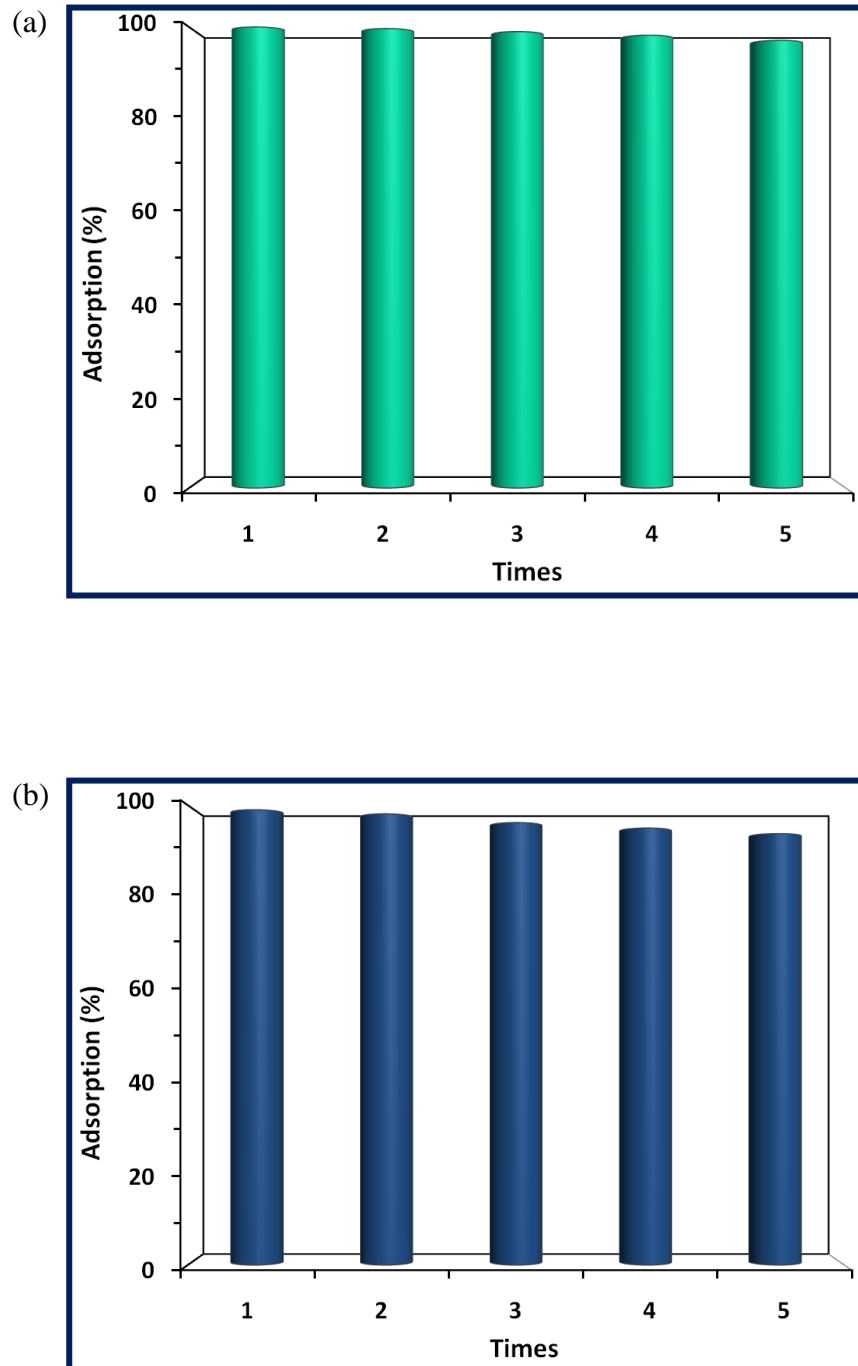


Figure 3.28: The percentage adsorption of (a) BG and (b) MB solution using recyclable FA₄₀ up to 5 times

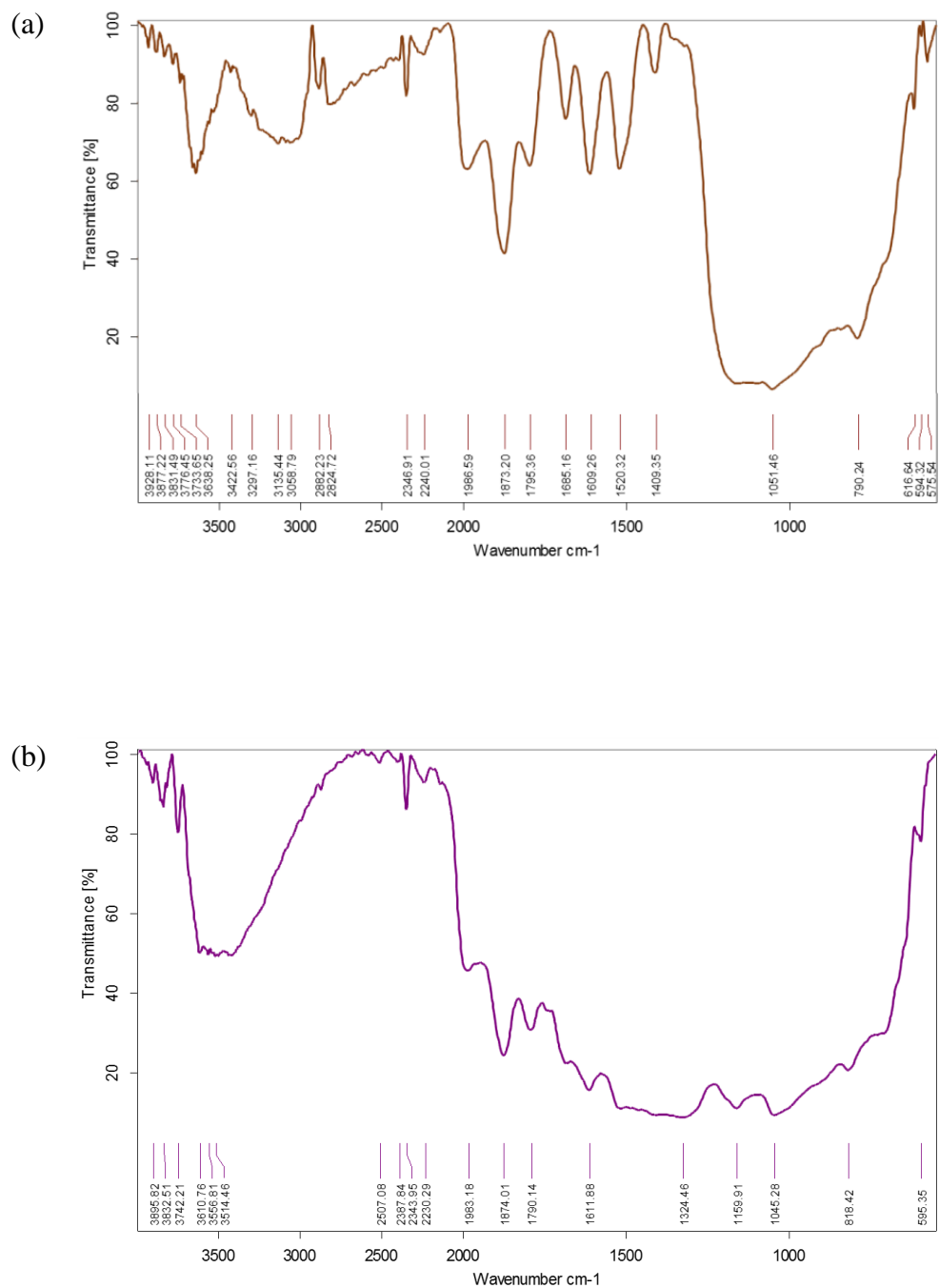


Figure 3.29: The FTIR pattern for regenerated FA₄₀ after (a) BG and (b) MB adsorption

3.4 Conclusion

Various Fly ash were investigated for the removal of acidic dye BG and basic dye MB from aqueous solutions. The following conclusions could be derived from the present study.

1. The present study shows that all fly ash (FA) can remove dyes from aqueous solution with some extent but the FA with high carbon content are the best adsorbent for the removal of both acidic and basic dyes. Adsorption of acidic (BG) and basic (MB) dyes on the FA₄₀ was found to be dependent on the initial pH of dye solution. The optimal pH of BG dye was 11.2, while the optimum pH value of MB dye was 7.4. Maximum adsorption occurred within 60 minute for both the dyes used in the study. The equilibrium between the adsorbate in the solution and on the adsorbent surface was practically achieved in 2 hour. An increase in the initial dye concentration enhanced the adsorption capacity, but decreased the dye removal efficiency.
2. Adsorption processes for both dyes were found to follow the pseudo-second-order kinetics rate expression. Langmuir, Freundlich and Tempkin isotherms described the equilibrium data of MB on FA, while Langmuir isotherm fitted better to the equilibrium data of BG dye. Maximum adsorption capacity of MB on FA₄₀ was 3.184 at 25°C and 100.0 mg/g for BG at 30°C. The Thermodynamic parameters were calculated and indicated that each of these adsorption processes were spontaneous and exothermic in nature. Low cost FA₄₀ showed large adsorptive characteristics, high separation selectivity and excellent recyclability. These findings indicate that suitably selected FA could be employed as an effective and inexpensive adsorbent for the removal of dyes and colour from water and industrial waste water.

3.5 References

- [1] H. Zollinger Color chemistry synthesis, (1987) 92-102.
- [2] P. Janos, H. Buchtova, M. Ryznarova, *Water Res.*, 37 (2003) 4938-44.
- [3] G. McKay, S.J. Allen, I.F. Meconney, M.S. Ottrburn, *J. of Colloid Inter. Sci.*, 80 (1981) 323-39.
- [4] S. Seshadri, P.L. Bishop, A.M. Agha, *Waste Manage.*, 15 (1994) 127-37.
- [5] <http://h2o.enr.state.nc.us/admin/sso/msds/60080.htm>; last accessed on 13 May 2007.
- [6] V. Meshko, L. Markovska, M. Mincheva, A.E. Rodrigues. *Water Res.*, 35 (2001) 3357-66.
- [7] S. Xu, J. Wang, R. Wu, H. Li, *Chem. Eng. J.*, 117 (2006) 161-67.
- [8] G. Annadurai, R.S. Juang, D.J. Lee. *J. Hazard Mater.*, 92 (2002) 263-74.
- [9] K. Mohanty, J.T. Naidu, B.C. Meikap, *Ind. Eng. Chem. Res.*, 45 (2006) 5165-71.
- [10] M. Ahmaruzzaman, *Prog Energy Combust. Sci.*, 36 (2010) 327-63.
- [11] D. Mohan, K.P. Singh, G. Singh, K.Kumar, *Ind. Eng. Chem. Res.*, 41 (2002) 3688-95.
- [12] N. Dizge, C. Aydinler, E. Demirbas, M. Kobya, S. Kara *J. Hazard. Mater.*, 150 (2008) 737-46.
- [13] S. Wang, Y. Boyjoo, A. Choueib, *Chemosphere*, 60 (2005) 1401-1407.
- [14] K.R. Ramakrishna, T. Viraraghavan, *Water Sci. Technol.*, 36 (1997) 189-96.
- [15] P. Roy, N.K. Mondal, S. Bhattacharya, B. Das, K. Das, *Appl. Water Sci.*, 3 (2013) 293-309.
- [16] ASTM standard specification for coal fly ash and raw or calcined natural pozzolan for use in concrete (C618-05). In: Annual book of ASTM standards, concrete and aggregates, vol. 04.02. American Society for Testing Materials; 2005.

- [17] B.W. Ramme, M. Tharaniyil Coal combustion product utilization handbook. 3rd ed. United State of America: Wisconsin Electric Power Company; 2013, p. 18.
- [18] S. Agarwal, A. Rani, *J. of Environ. Chem. Eng.*, 5 (2017) 526-38.
- [19] C. Paze, S. Bordiga, C. Lamberti, M. Salvalaggio, A. Zecchina, A FTIR Investigation. *J. of Phy. Chem. B*, 101(1997) 4740-51
- [20] T. C. Xiao, A.P. York, H.A. Megren, C.V. Williams, H.T.Wang, M.L. Green. *J. Catal.*, 202 (2001) 100-21.
- [21] T. Arnold, M.Rana singh, J.yout cheff, *Transporation Reaserch Record*, 1962 (2006) 113-20.
- [22] X. H. Sun, S. D. Wang, N. B. Wong, D. D. D. Ma, S. T. Lee, B. K. Teo, *Inorg. Chem.*, 42 (2003) 2398-402.
- [23] M. V. Wolkin, J. Jorne, P.M. Fauchet, G. Allan, C. Delerue, *Phys. Rev. Lett.*, (1999), 82, 197-200.
- [24] Jacox, E. Marilyn, *J. Physical and Chemical Reference Data*, 32 (1) (2003) 1.
- [25] P. R. China, *Environment Science*, Najing Normal University, Nanjing 210097.
- [26] C. Anna, L.Z. Akbulut Mustaafa, *J. of Royal Society of Chemistry*, 2011.
- [27] H. Zou, W.U. Shishan, Jainshen School of Chemistry and Chemical Engineering, Nanjing University, Nanjing 210093.
- [28] J.M. Grau, J.C. Yori, C.R. Vera, F.C. Lovey, A.M. Condo, J.M. Parera, *J. Applied Catalysts*, 265 (2004) 141-52.
- [29] S.J. Gregg, K.S.W. Sing. *Adsorption*, in: *Surface Area and Porosity*. London: Acadmic Press; 1982. 2nd ed.
- [30] Y. Wong, Y. J. Laccase, *Water Res.*, 33 (1999) 3512-20.
- [31] P.K. Malik, *Dyes Pigments*, 56 (2003) 239-49.
- [32] V. S. Mane, I. D. Mall, V. C. Srivastava, *J. of Environ. Manag.*, 84 (2007) 390-400.
- [33] E. Tutem, R. Apak, C.F. Unal, *Water Research*, 32 (1998) 2315-24.

- [34] D. Rameshraj, V.C. Srivastava, J.P. Kushwaha, I.D. Mall. Chem. Eng. J., 181-182 (2012) 343-51.
- [35] K. Nandi, A. Goswami, M.K. Purkait, J of Hazard Mater., 161 (2009) 387-95.
- [36] V.S. Mane, I.D. Mall, V.C. Srivastava, Dyes and Pigments, 73 (2007) 269-78.
- [37] E. Demirbas, M.Z. Nas, Desalination, 243 (2009) 8-21.
- [38] O. Ozdemir, B. Armagan, M. Turan, M.S. Celik, Dyes Pigments, 62 (2004) 49-60.
- [39] T.J. Hsu, Fuel, 87 (2008) 3040-45.
- [40] K.R. Ramakrishna, T. Viraraghavan, Water Sci. Technol., 36 (1997) 189-96.
- [41] D. Suna, Zhanga X, Wub Y, Liua X, J of Hazard. Mater., 181 (2010) 335-42.
- [42] N. Dizge, C. Aydiner, E. Demirbas, M. Kobya, S. Kara, J. Hazard. Mater., 150 (2008) 737-46.
- [43] A. Mittal, D. Kaur, J. Mittal, J. of Colloid and Interface Sci., 326 (2008) 8-17.
- [44] S.C.D.A. Fernada, F.S.V. Eunice, R.C. Antini, J. of Colloid and Interface, Sci., 253 (2002) 243-46.
- [45] S.M. Venkat, I.D. Mall, V.C. Srivastava, Dyes and Pigments, 73 (2007) 269-78.

Chapter-4

Adsorption of Resorcinol from Aqueous Solution onto Low Cost Fly Ash (FA) and NaOH Treated Fly Ash (NaFA): Equilibrium, Kinetics, Thermodynamics and Modeling

ABSTRACT

In the present study, the use of low cost adsorbent (NaFA) derived from coal fly ash (FA), has been investigated as a substitute of expensive methods for the sequestration of resorcinol. The FA and NaFA adsorbents were well characterized by XRF, FE-SEM with EDX, FTIR, XRD and surface area and porosity measurement which proves the chemical constituents, functional groups and morphology of the adsorbents. The resorcinol adsorption capacities of synthesized NaFA and native material were determined by batch studies. The batch adsorption studies were carried out by different operational parameters and optimize it to get maximum adsorption capacities. The adsorption was slightly increased with increase in pH value upto 5.1-7.0. The monolayer adsorption capacities of FA and NaFA for resorcinol calculated from Langmuir isotherm were 100 mg g⁻¹ and 333.33 mg g⁻¹ respectively. The equilibrium data were in a superior way fitted by Freundlich isotherm than that of Langmuir and Temkin isotherms found on the basis of error analysis (RMSE, SSE and χ^2). Different thermodynamic parameters (ΔG° , ΔS° and ΔH°) were evaluated to conclude adsorption to be spontaneous and exothermic in nature. Kinetic studies have been performed to understand the mechanism of adsorption and pseudo-second-order kinetic model better fitted the data for both FA and NaFA.

4.1 Introduction

Resorcinol chemically named 1,3 dihydroxybenzene is a white crystalline compound. It is soluble in water and has a low vapour pressure. The resorcinol moiety has been found in a wide variety of natural products, as it is a monomeric by-product of the reduction, oxidation, and microbial degradation of humic substances [1]. The largest user of resorcinol is the rubber industry (about 50%). Resorcinol is also used for high-quality wood bonding applications (about 25%) and is an important chemical intermediate in the manufacture of speciality chemicals [1]. Other uses include the manufacture of dyestuffs, pharmaceuticals, flame retardants, agricultural chemicals, fungicidal creams, lotions and hair dye formulations. Resorcinol is released into the environment from a number of anthropogenic sources, including production, processing, and consumer uses, especially from hair dyes, pharmaceuticals, textile, paper and pulp, steel, petrochemical, petroleum refinery, plastics, cosmetics, oil shale mining etc., and in synthetic coal fuel conversion process wastewater [2]. Phenolic compounds are toxic to several biochemical functions and to fish life. It acts as a substrate inhibitor in the biotransformation process [3]. In studies, the toxicological effects reported to be caused by administration of resorcinol include thyroid dysfunction, skin irritation, Central Nervous System effects, decreases in body weight and altered relative adrenal gland weights. Resorcinol is irritating to eyes and skin and may cause sensitization on skin contact [2].

Due to their toxicity, polynuclear aromatic hydrocarbons and phenolic compounds are the two classes of compounds widely prevalent and classified by the US Environmental Protection Agency as priority pollutants [4, 5]. A suitable method, in terms of cost and techno feasibility, is needed for the complete removal or at least minimization of loads of such pollutants from water. The treatment technology, depending on the load of phenol in wastewater, may be either physico-chemical or biological. While the biological method is applicable for low levels of phenol in the wastewater, a physico-chemical method is applied for a moderate to high concentration range. Biological processes, moreover, may not always be possible in wastewater treatment due to long-term biodegradation.

The common chemical techniques for effective minimisation of phenol and its derivatives include destructive oxidation [6], catalytic and photocatalytic degradation [7], electrochemical conversion [8], or biodegradation [9], together with adsorption.

Adsorption technique is quite popular due to availability of a wide range of adsorbents. Edip Bayram [10] et al. studied removal of catechol and resorcinol from aqueous solutions by adsorption and electrosorption onto high area activated carbon cloth (ACC). Adsorption behaviour of resorcinol and catechol from aqueous solution onto the aminated hypercrosslinked polymers and the hypercrosslinked polymeric adsorbent NDA-100 without amino groups was compared by Yue Sun, [11] et al. It was found that the aminated hypercrosslinked polymers had higher adsorption capacities than NDA-100 due to the Lewis acid–base interaction between the phenolic compounds and the tertiary amino groups on the polymer matrix. Adsorption of resorcinol from aqueous solutions onto activated carbon was studied by Omer El-Amin [12] et al. The Langmuir isotherm model appears to have better regression coefficients, with a maximum adsorption capacity range (208.33 - 223.21 mg/g). Eva Rodríguez et al. [13] studied about activated carbon adsorption and chemical oxidation followed by activated carbon adsorption of resorcinol in water has been studied. Three chemical oxidants used were hypochlorite, permanganate and Fenton's reagent.

Preparation of Polymeric resins and polymeric adsorbents are the tedious and difficult process and the high cost leads to the search for other adsorbents. Several workers use a variety of adsorbents viz. zeolite [14], graphite [15], clay [16], hydrous metal surface [17], humic matter [18], as well as some waste materials [19]. For removal of phenols from water, solid phase extraction using different polymeric sorbents is also reported [20]. Yet development of effective and low cost adsorbents remain in need of the industries for better waste water treatment options. Fly ash is widely used as an additive in the cement and concrete building industry, and is largely still disposed in landfills [21]. There is an active field of research directed towards developing alternate uses for FA, such as adsorption of water pollutants and preparation of zeolitic materials. Different

varieties of fly ash have different sorption propensities for inorganic and organic pollutants such as cesium [22, 23], strontium [23], organic-basic [24-34], organic-acid [24-26] and organic-reactive dyes [35,36]. Because the adsorption capabilities of fly ash for cationic species are relatively low, heat and acid treatment [27,28] and zeolitization under alkaline hydrothermal conditions [37,38] are explored more. As a measure to recycle FA, zeolites synthesized from FA (ZFAs) have been extensively investigated in recent years. A number of zeolites have been produced from FA, including Na-P1, philipsite, chabazite, F linde, herchelite, faujasite, analcime, zeolite A, zeolite X, zeolite Y, and hydroxysodalite. Fly ash become now an ideal precursor for the production of zeolites, due to its compositional similarity to volcanic materials with high SiO₂ and Al₂O₃ content. Volcanic ash is converted into zeolites in the environment by the action of alkaline/saline surface and/or groundwater in a slow process that takes hundreds to thousands of years [37].

Some zeolitic materials have also been successfully synthesized from FA by relatively inexpensive and quick hydrothermal conversion processes. The fly ash-based zeolites are capable of absorbing both volatile compounds and water pollutants. They can selectively adsorb molecules that are smaller than their pore sizes, and their large surface areas make them versatile materials for targeting a wide range of pollutants. It has been found that the zeolitized fly ash (ZFA) has promising potential as a molecular sieve in purification treatments of CO₂, SO₂ and NH₃ [37, 38]. ZFA has been extensively used for reducing the dyes [26,31] heavy metal content of acidic mine water [39] and for the removal of ammonium, phosphate [40] and arsenate ions [41] from urban and industrial waste water. Although the adsorption of phenolic compound onto zeolites has been extensively investigated [42, 43] only a few studies have been reported [44] about the adsorption of Phenolic compounds onto fly ash-based zeolites. The process of zeolite synthesis is time consuming and requires technical setups by the industries. The marketed costs of zeolites are quite high restricting its use by small scale industries for removal of phenolic compounds. The present research proposes a simple method of alkaline treatment of FA to produce an effective adsorbent for resorcinol removal from waste water.

In the present research a comparative study of the adsorption of resorcinol from aqueous solution by fly ash (FA) and NaOH treated fly ash (NaFA) is reported. The effects of several experimental parameters such as contact time (t), initial adsorbate concentration (C_0), initial adsorbent dosage (m), temperature (T) and solution pH on resorcinol adsorption onto FA and NaFA were investigated. The experimental results were analyzed by kinetic and isotherm models. Thermodynamic parameters such as Gibbs free energy change (ΔG°), enthalpy change (ΔH°) and entropy change (ΔS°) were calculated.

4.2 Materials and Methods

4.2.1 Adsorbents and Adsorbate

Fly ash (FA) sample was collected from Shriram Fertilisers and chemical Ltd., Kota. FA used after heat in a hot air oven at 105°C for 24h to remove moisture. The dried materials were then stored in desiccators for use. NaFA was hydrothermally synthesized from FA. For NaFA synthesis, 25g of FA was placed in flask and was refluxed with stirring in 150 ml of 2.0 mol L⁻¹ NaOH solution for 24h at 96 °C. The obtained slurry was centrifuge and washed with doubly distilled water three times with repeated centrifugation followed by drying in an oven at 100 °C and calcined at 380°C for 2 hours in muffle furnace and ball milled in high energy planetary ball mill with ball to powder ratio of 10:1 for 2 h at 250 rpm. Schematic presentation of NaFA synthesis is given in [Scheme 4.1](#) and for simple representation, FA₄₀ denoted as FA.

Resorcinol was selected as phenolic compound used as adsorbate. The structure of resorcinol is illustrated in [Figure 4.1](#). Resorcinol solution for further study was prepared as described in chapter 2.

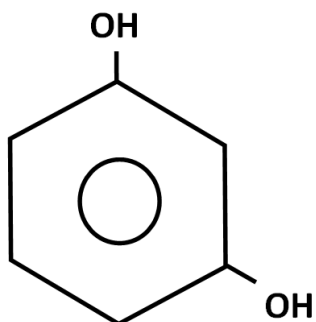
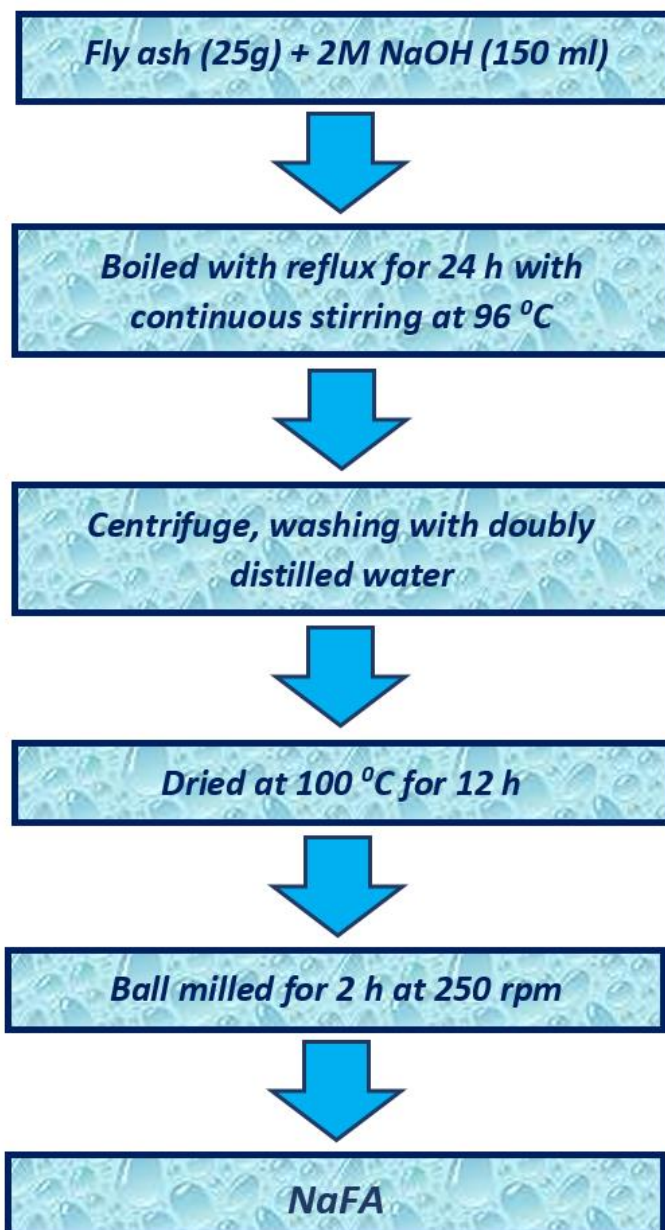


Figure 4.1: Chemical structure of Resorcinol

4.2.2 Adsorption experiments

The experimental parameter such as pH, temperature, initial concentration, contact time and adsorbent dose on the removal of resorcinol were studied in batch reactor. The concentrations were measured with Double Beam UV/Visible spectrophotometer (model Spectrscan UV 2600/02) at the wavelength of 313 nm for resorcinol. The characterization techniques and experimental setups is already described in Chapter 2.



Scheme 4.1: Procedure for synthesis of NaFA

4.3 Result and discussion

4.3.1 Characterization of Adsorbent

The primary mineralogical constituents of FA and NaFA like Silica, alumina and sodium contents are given in [Table 4.1](#). EDX spectrum of NaFA is shown in [Figure 4.2](#). The FA contains higher amount of SiO_2 which decreases in NaFA due to the dissolution of glass phase (aluminium – silicate) into the alkaline solution during the hydrothermal alkali treatment. The alumina-silicate gel is formed by dissolution of alumina and silicate ions, which is the primary material for the zeolitic material formation. The other oxide contents like CaO, MgO and Fe_2O_3 are found lower in NaFA than the native FA. Due to the production of zeolitic precursor gel, NaFA exhibited a greatly enhanced total cation exchange capacity (TCEC, 1.02 mmol g^{-1}) and Brunauer-Emmett-Teller (BET) area ($18.2875 \text{ m}^2 \text{ g}^{-1}$) when compared to FA ($<0.02 \text{ mmol g}^{-1}$ and $1.795 \text{ m}^2 \text{ g}^{-1}$, respectively) ([Table 4.1](#)). It is worthy of note that NaFA is not pure zeolite but contains some components as non zeolite fraction. The comparison of the TCEC value of a NaFA with that of a pure zeolite may provide a semiquantitative estimate of the zeolite content in the NaFA given that the NaFA contained only one kind of zeolite. External cation exchange capacity (ECEC) for FA and NaFA are < 0.02 & 0.068 respectively shown by [Figure 4.3\(a & b\)](#). The pH_{ZPC} values of adsorbents FA and NaFA were 10.8 and 10.1 respectively shown in [Figure 4.4 \(a & b\)](#) and [Table 4.1](#).

Table 4.1: Chemical composition and properties of coal FA & NaFA Study

Parameter	Coal Fly Ash (Wt%) (by XRF)	NaFA (Wt%) (by EDX)
SiO ₂ (%)	60.46	13.74
Al ₂ O ₃ (%)	21.50	5.99
Fe ₂ O ₃ (%)	4.30	2.79
CaO (%)	7.63	2.69
MgO (%)	0.82	0.23
Na ₂ O (%)	0.19	9.42
K ₂ O (%)	1.25	0.45
Moisture (%)	1.2	4.5
TiO ₂	1.53	0.69
TCEC (mmol g ⁻¹)	< 0.03	1.02
ECEC (mmol g ⁻¹)	< 0.02	0.068
pH _{ZPC}	10.8	10.1
Surface area of pores (m ² /g)		
(i) BET	1.7950	18.2875
(ii) BJH		
a. Adsorption cumulative	1.1465	15.6483
b. Desorption cumulative	1.7148	165528
BJH Cumulative Pore Volume (cm ³ /g)		
(i) Single Point Total	0.006714 ^a	0.102599 ^b
(ii) BJH Adsorption	0.006264 ^c	0.100457 ^c
(iii) BJH desorption	0.006732 ^c	0.102793 ^c
Average pore diameter (Å)		
(i) Single Point Total	149.6238	224.4138
(ii) BJH Adsorption	218.5352	256.7875
(iii) BJH desorption	157.0288	248.3996

^a Pores less than 900.1879 Å diameter

^b Pores less than 821.9909 Å diameter

^c Pores between 17.00 Å and 3000.00 Å diameter

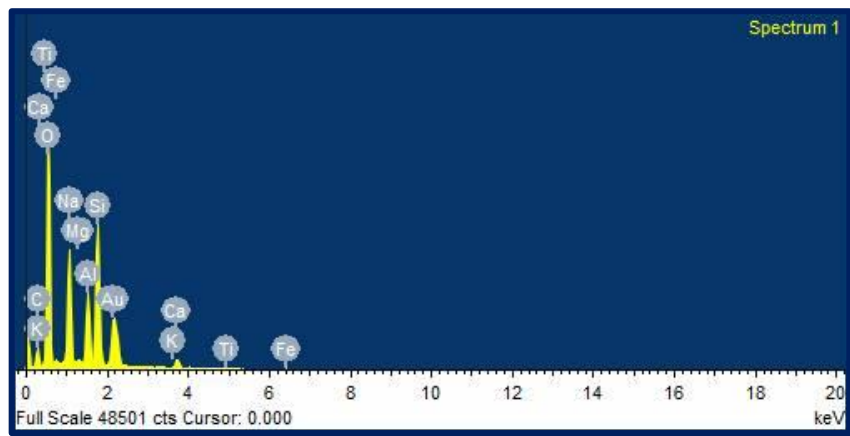


Figure 4.2: EDX Spectrum of NaFA

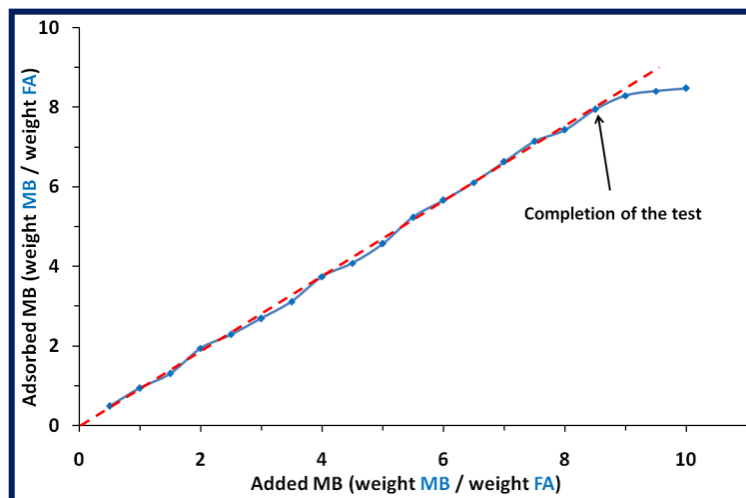


Figure 4.3(a): The determination of the point of complete replacement of cations from the titration curve of FA

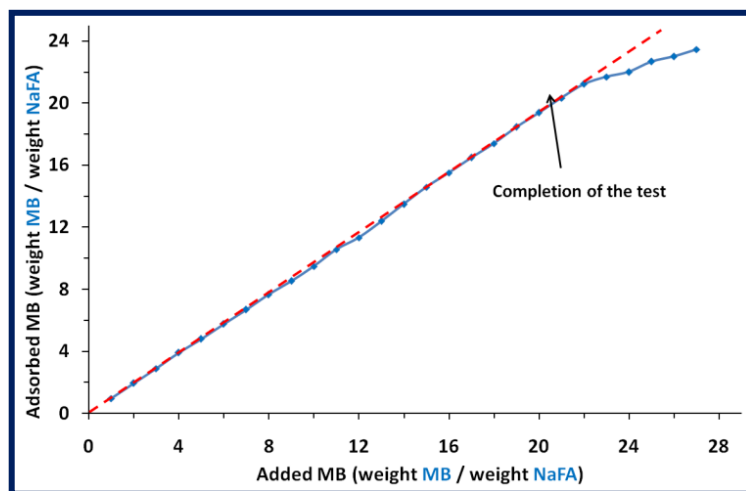


Figure 4.3(b): The determination of the point of complete replacement of cations from the titration curve of NaFA

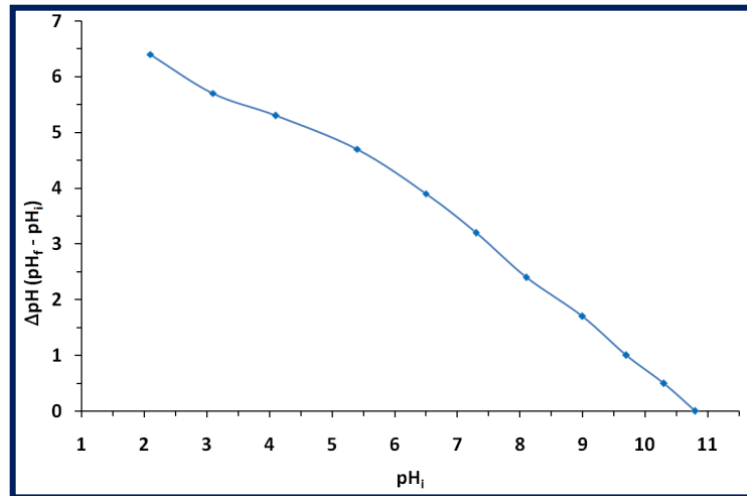


Figure 4.4(a): Point Zero Charge of FA

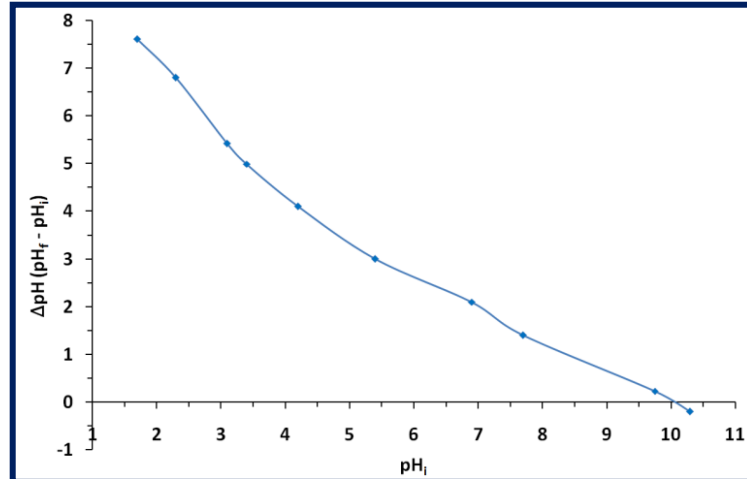


Figure 4.4(b): Point Zero Charge of NaFA

(i) *Scanning Electron Microscopic study*

In order to examine the surface morphology of the sorbents, SEM analysis was employed for this study. The SEM images of asorbents (FA and NaFA) were carried out at different magnifications and shown in [Figures 4.5 \(a & b\)](#). The original FA particles typically had spherical shapes and different sizes, with a smooth surface made of an aluminosilicate glass phase. Upon formation of NaFA, the surface became rough, indicating the deposition of clusters of zeolitic material and developed crystalline tubular habits. The morphological difference between FA and NaFA was observable. Some char and carbonaceous materials of FA are also removed by calcinations which are revealed from the SEM images of FA and NaFA.

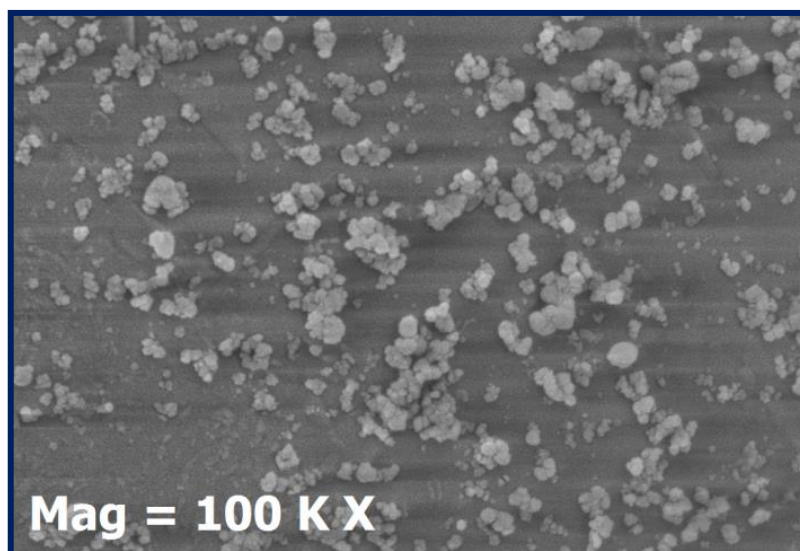


Figure 4.5(a) : Scanning electron micrographs (FE-SEM) of FA

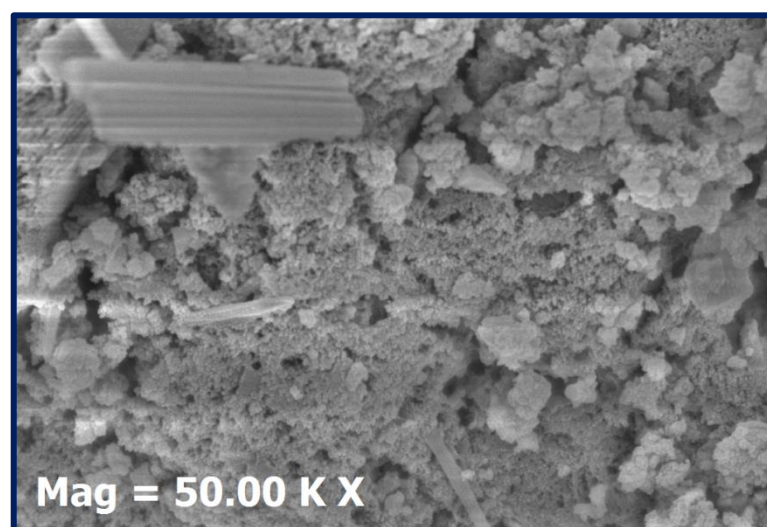
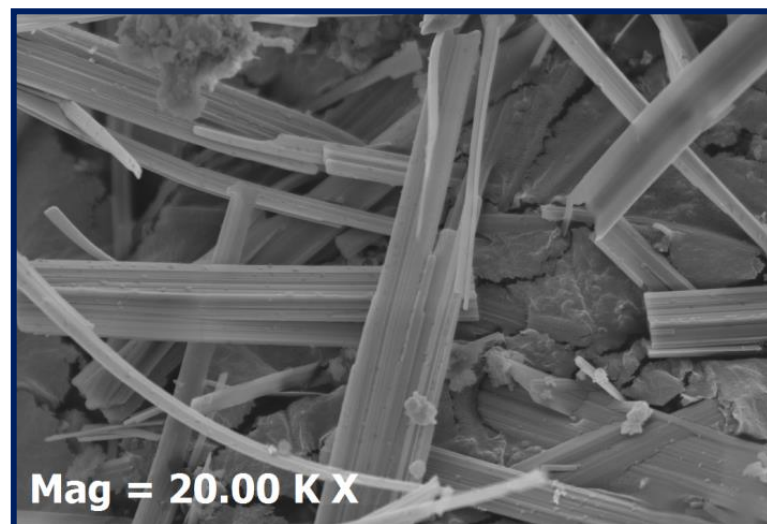
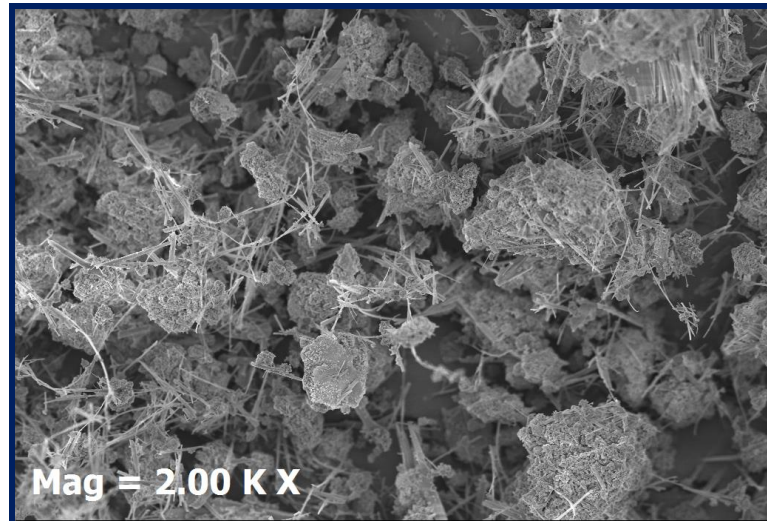


Figure 4.5(b): Scanning electron micrographs (FE-SEM) of NaFA at different magnifications

(ii) *Fourier Transform Infrared Spectroscopic study*

The functional groups and shifting of bands observed are described in [Table 4.2](#). The frequency band at 3525 cm⁻¹ for NaFA is assigned to H-O-H stretching and this is slightly less than that obtained for FA as 3653 cm⁻¹, the difference might be due to the amount of water vapour absorbed by the fly ash as a result of its exposure while crushing and treatment undergone before the spectral measurement. The stretching frequency observed at around 3400 cm⁻¹ arises from both the silanol groups (Si-OH) and adsorbed water. The asymmetric stretching vibrations of an internal tetrahedral band observed at 1250–850 cm⁻¹ indicates the TO₄ (T = Si, Al). Formation of zeolitic material in NaFA was confirmed by the shift of the band from 1120 cm⁻¹ for FA to 978 cm⁻¹ for NaFA on Fourier transformed infrared (FTIR) spectra ([Figure 4.6 b](#)), because tetrahedral Al is characteristic of the zeolite structure and an increase in tetrahedral Al (formation of zeolite) would induce a shift of the band within the range of 1180–950 cm⁻¹ (which is assigned to the asymmetric internal T-O stretching vibration mode of the TO₄ tetrahedra, where T = Si or Al) to a lower wave number [\[45\]](#). The four bands at 577, 612, 687 and 789 cm⁻¹ confirm the formation of zeolitic material on alkali and hydrothermal treatment of fly ash [\[46\]](#). [Figures 4.6 c & 4.6 d](#) show the FTIR spectra of resorcinol adsorbed FA and NaFA respectively in which two new bands at 1596 & 1325 cm⁻¹ are for resorcinol adsorbed FA and 1583 & 1327 cm⁻¹ are for resorcinol adsorbed NaFA confirming the adsorption of resorcinol by both FA and NaFA.

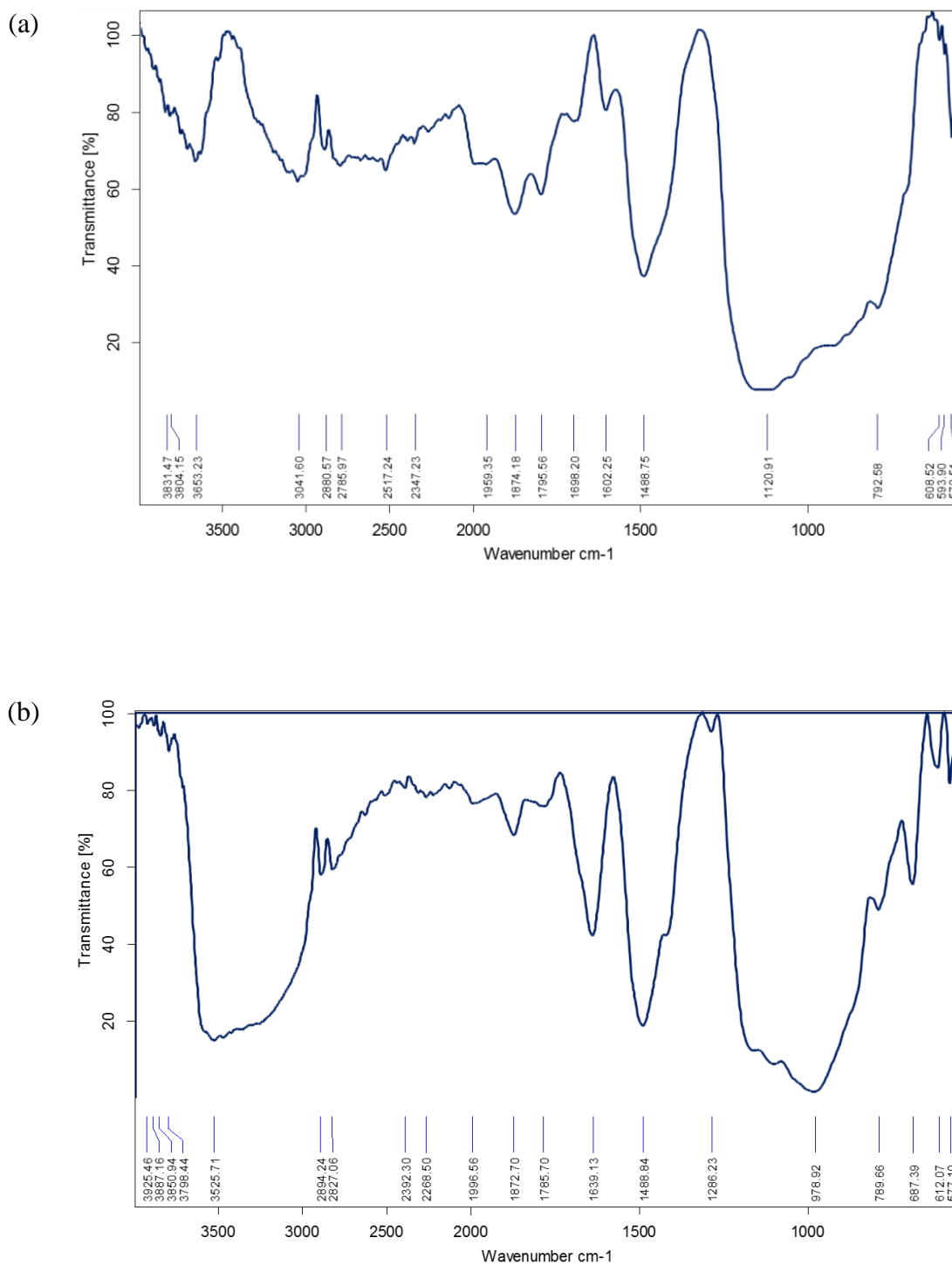


Figure 4.6: The FTIR patterns of (a) FA and (b) NaFA

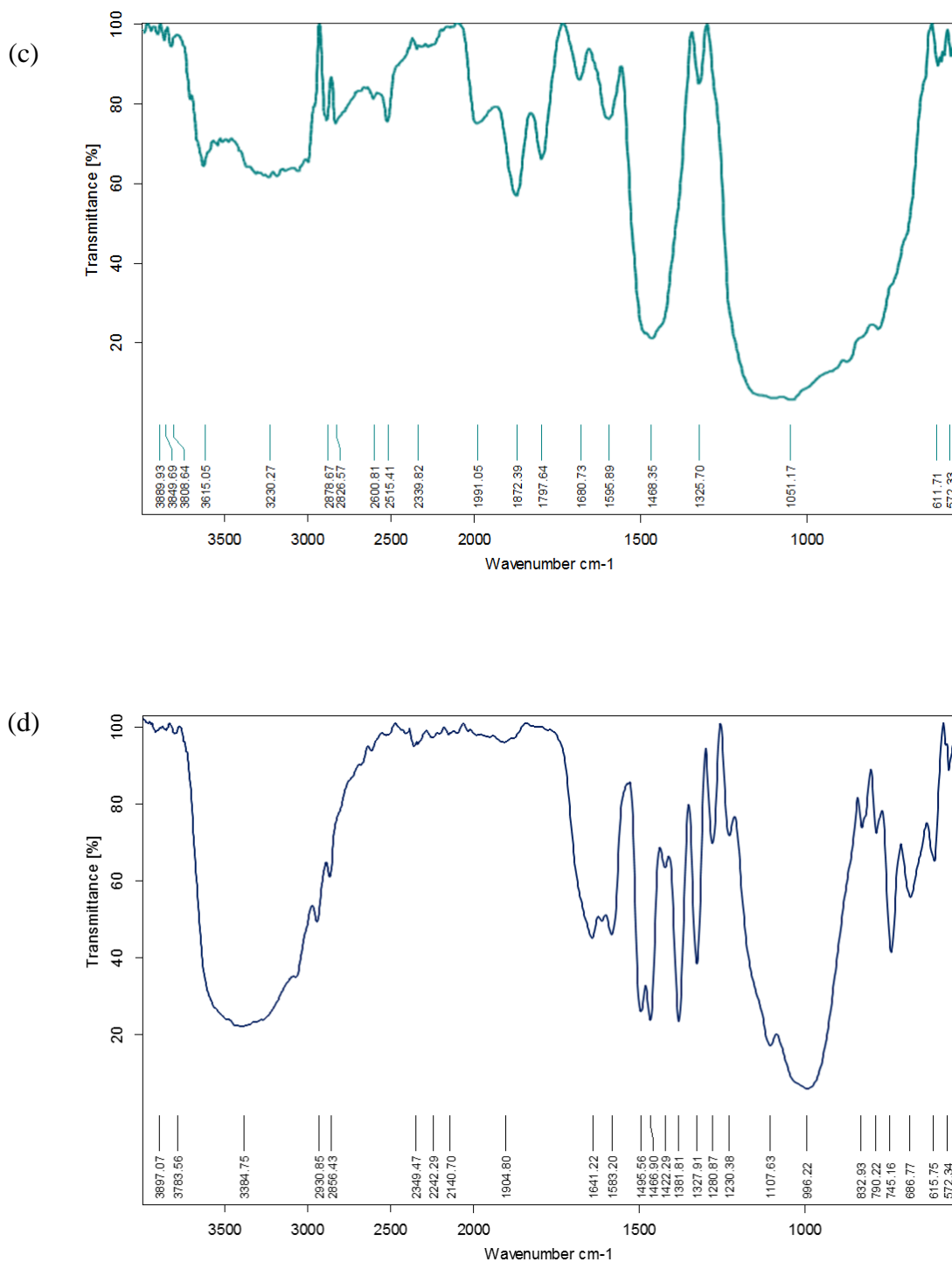


Figure 4.6: The FTIR patterns of (c) resorcinol adsorbed FA and (d) resorcinol adsorbed NaFA

Table 4.2: Comparison and shifting of bands data for FA, NaFA, resorcinol adsorbed FA and resorcinol adsorbed NaFA in FTIR spectroscopy

Wave number (cm ⁻¹)	Possible assignment	Observed Frequency (cm ⁻¹)			
		FA	NaFA	Resorcinol adsorbed FA	Resorcinol adsorbed NaFA
3600 - 3300	Stretching vibration of –OH group, Silanol (Si-OH)	3653	3525	3615 2878	3384
1700 - 1400	–OH deformation & bending vibration of interstitial water	1698 1602 1488	1639 1488	1680 1596 1488	1641 1583 1495 1466 1422
1250 - 850	Asymmetric stretching of internal tetrahedral TO ₄ , Si-O-Si (T=Si, Al)	1120	978	1051	1230 1107 996
720 - 650	Symmetric stretching of internal tetrahedral TO ₄ (T=Si, Al)	-	687	-	686

(iii) *X-ray diffraction study*

The XRD pattern of the FA and NaFA are shown in Figures 4.7(a & b) respectively and details are shown in Tables 4.3 and 4.4 provided different d-spacing values, which reflect the presence of minerals such as α -quartz (Q; JCPDS 5-490), mullite (M; JCPDS 15-0776). The broad hump is shown in FA at 2θ , 26.9° diffraction angle indicates the glass phase [47]. The glass phase intensity shown in FA at a lower diffraction angle was gradually decreased in NaFA. The reaction of quartz and mullite with sodium hydroxide in alkaline media creates the sodium aluminosilicate gel during hydrothermal treatment, which indicates the successful conversion of quartz and mullite peaks into zeolitic materials. It was observed that the XRD of NaFA exhibited some significant peaks of reflections at 2θ of about 13, 16, 22, 23.5, 27, 28 and 32 degrees, which were indicative of the probable formation of zeolite-P2 of Chemical formula $[(Ca_{0.6}Na_{2.6}K_{2.2})Al_6Si_{10}O_{32} \cdot 12H_2O]$ [48] with hydroxysodalite $[Na_{1.08}Al_2Si_{1.68}O_{7.44} \cdot 1.8H_2O]$ during the hydrothermal synthesis. The XRD peaks at about 27° and 28° 2θ suggest the presence of zeolite-P, which is topologically related to the natural zeolite called gobbinsite [49].

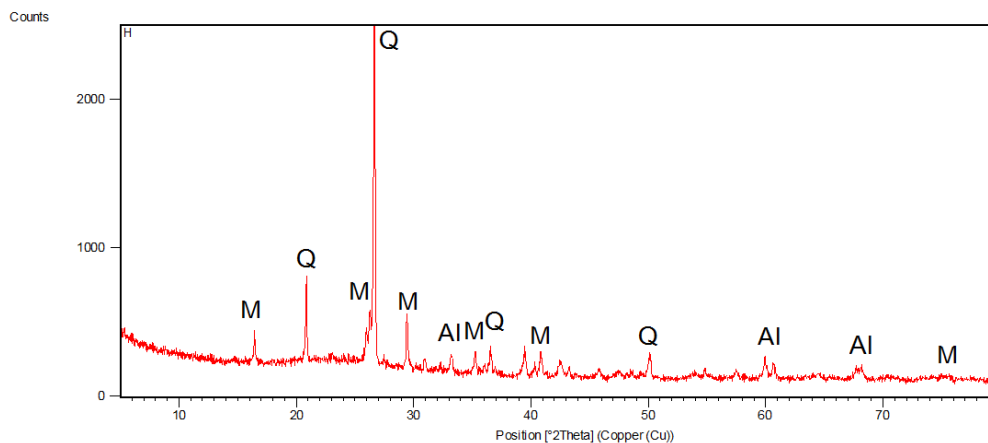


Figure 4.7(a): The XRD patterns for FA
(where Q, quartz; M, mullite; Al, aluminium)

Table 4.3: Results of XRD measurements of FA

Pos. [°2Th.]	FWHM [°2Th.]	d-spacing [Å]	Rel. Int. [%]	Area [cts*°2Th.]
16.4235	0.1338	5.39750	8.85	26.78
20.8344	0.1171	4.26370	24.74	65.50
25.9722	0.1004	3.43074	9.59	21.76
26.2494	0.1004	3.39514	15.66	35.53
26.6279	0.1338	3.34773	100.00	302.55
29.4400	0.1171	3.03405	14.61	38.67
30.9406	0.2007	2.89024	3.18	14.43
33.1995	0.1673	2.69856	5.06	19.15
35.2309	0.1338	2.54748	6.22	18.83
36.5410	0.0502	2.45910	11.38	12.91
39.4524	0.1338	2.28409	7.00	21.17
40.3111	0.1338	2.23739	3.85	11.66
40.8346	0.1506	2.20991	7.33	24.95
42.4587	0.2676	2.12906	4.60	27.85
43.2398	0.2007	2.09239	2.64	11.97
45.8231	0.2676	1.98027	2.56	15.48
47.4670	0.4015	1.91545	1.55	14.11
50.1036	0.2676	1.82066	6.74	40.78
54.8521	0.2007	1.67376	2.24	10.15
57.5048	0.2676	1.60270	2.44	14.74
59.9393	0.1004	1.54329	5.96	13.52
60.6526	0.1338	1.52684	4.17	12.61
64.5772	0.4015	1.44320	1.37	12.46
68.2014	0.2676	1.37508	3.39	20.49
75.3785	0.9792	1.25994	0.83	24.98

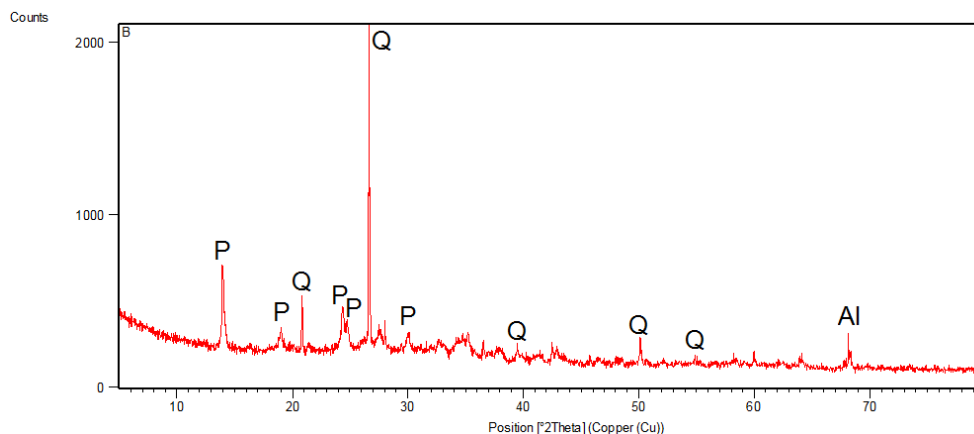


Figure 4.7(b): The XRD patterns for NaFA
(where Q, quartz; M, mullite; Al, aluminium)

Table 4.4: Results of XRD measurements of NaFA

Pos. [°2Th.]	FWHM [°2Th.]	d-spacing [Å]	Rel. Int. [%]	Area [cts*°2Th.]
13.9761	0.0836	6.33671	24.54	37.93
18.9646	0.2007	4.67964	5.36	19.88
20.8596	0.0669	4.25861	16.85	20.84
24.3819	0.1673	3.65078	13.88	42.93
26.6468	0.0669	3.34540	100.00	123.69
27.5567	0.3346	3.23697	7.07	43.75
28.0213	0.0502	3.18435	10.14	9.40
30.0734	0.2007	2.97157	6.41	23.79
32.7927	0.5353	2.73110	4.39	43.41
35.2309	0.2007	2.54748	7.47	27.73
37.9514	0.4015	2.37090	3.24	24.04
39.4740	0.2007	2.28289	3.11	11.54
41.4473	0.6691	2.17864	1.87	23.09
42.4247	0.1338	2.13069	4.61	11.41
42.8296	0.8029	2.11148	2.93	43.47
46.5028	0.4015	1.95289	1.57	11.68
48.3451	0.6691	1.88269	1.20	14.80
50.1264	0.0669	1.81989	8.67	10.73
54.9636	0.8029	1.67062	1.04	15.45
58.0943	0.8029	1.58783	0.79	11.67
59.9566	0.1004	1.54289	3.82	7.10
64.0112	0.4684	1.45459	1.60	13.87
68.1671	0.0612	1.37455	11.01	16.84

(iii) *Surface area and porosity measurement study*

The N₂-adsorption/desorption isotherm, surface area plot and the pore-size distribution of the NaFA are shown in Figure 4.8 & 4.9. The hysteresis (Figure 4.8a) seen between the adsorption (lower) and desorption (upper) curves indicates the existence of mesoporosity (pores in the range of 20-500 Å) and provides information regarding the connectivity of the porous network. The combination of type II and type IV adsorption isotherm is encountered for NaFA with a typical adsorbate uptake starting at 0.8 p/p₀ and this isotherm implies the mesoporous and micropores (with additional external surface area) structure of materials according to the IUPAC and Brunauer, Deming, Deming & Teller (BDDT) classification [50]. Description about FA has already described in Chapter 3. The specific surface area of the adsorbents by BET methods shows the following order NaFA (18.2875 m²g⁻¹) > FA (1.7950 m²g⁻¹), which indicates that the specific surface area is increased drastically due to the hydrothermal treatment. BET average pore diameters were 15.70 nm and 24.84 nm of FA and NaFA respectively. The analysis of BJH average adsorption/desorption pore diameter values of adsorbents (Table 4.1) lies between 2 nm to 50 nm. Thus, it can be concluded that the FA and NaFA are predominantly mesoporous adsorbents. As the pore diameter increases the pore volume (NaFA: 0.102793 cm³g⁻¹ > FA: 0.006732 cm³g⁻¹) also increases due to that the capacity of NaFA increases than that of FA.

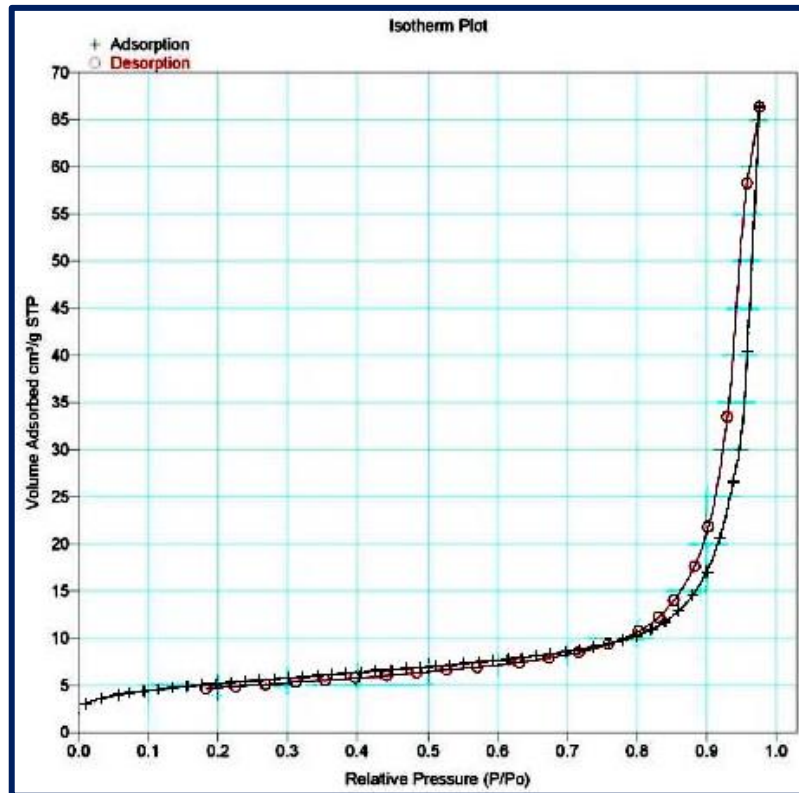


Figure 4.8(a): Adsorption isotherms of nitrogen at 77 K for NaFA

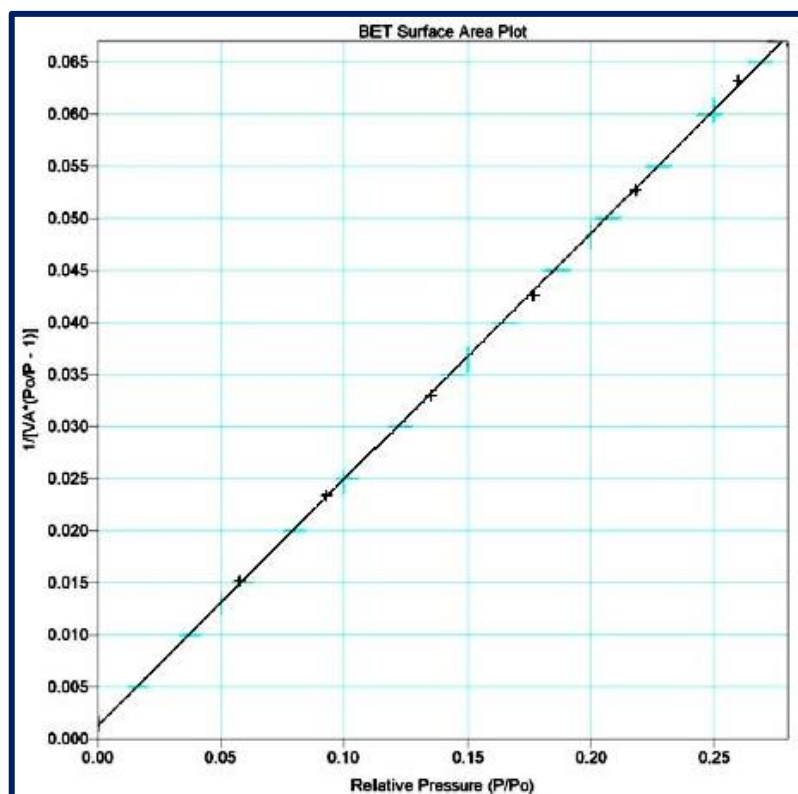


Figure 4.8(b): Surface area plot for NaFA

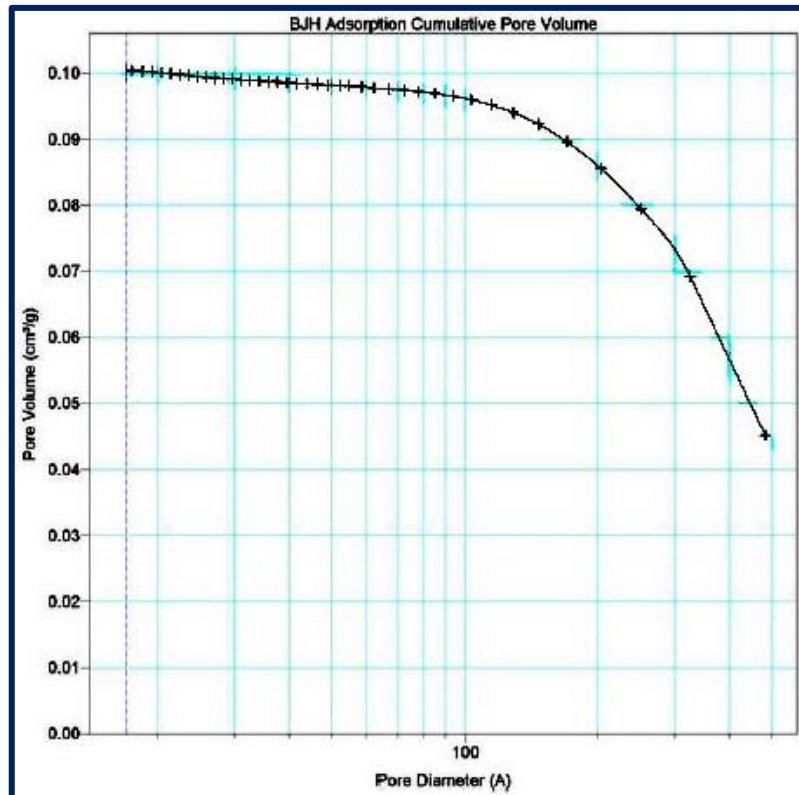


Figure 4.9(a): Pore-size distribution (BJH Adsorption Cumulative Pore Volume) for NaFA

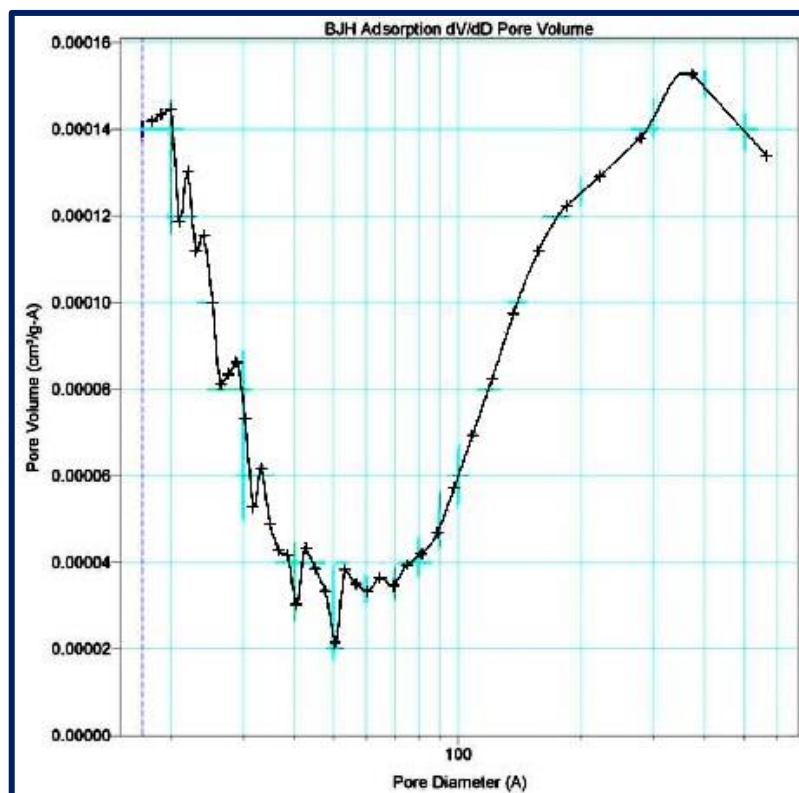


Figure 4.9(b): Pore-size distribution (BJH Adsorption dV/dD Pore Volume) for NaFA

4.3.2 Effect of pH

The initial pH of the resorcinol solution has been identified as the most important variable governing adsorption process particularly the adsorption capacity. To observe the effect of pH on the extent of resorcinol adsorption, resorcinol solution pH is varied from 3.0 to 11.0. The adsorption capacity of resorcinol at different pH is shown in [Table 4.5](#) and [Figures 4.10 \(a & b\) respectively](#). From this study, it is observed that adsorption of resorcinol slightly affected with pH value and maximum adsorption takes place at pH 10.2 for FA and pH 9.1 for NaFA. The variation in the resorcinol uptake with respect to the initial solution pH can be explained on the basis of the structure of resorcinol molecule and point of zero charge (pH_{ZPC}) of FA and NaFA. For FA, the point of zero charge is estimated to be 10.8. Above this pH, the FA particle acquires a negative surface charge. Resorcinol is acidic in nature so it shows ionization above pH 7.0. At pH lower than pH_{ZPC} , the FA surface acquires positive charge and resorcinol molecules are almost neutral below pH 7.0. Due to this there is less electrostatic attraction between neutral resorcinol molecules and positively charged FA that causes slight increase in resorcinol uptake $pH < 7.0$. After that it was increased because of ionization of resorcinol. After pH 7.0 deprotonation of resorcinol takes place in a basic medium and it become negatively charged but FA has positive charge on the surface at solution $pH < 10.8$. So on increasing the basicity, the uptake of resorcinol increases due to electrostatic attraction between positively charged surface of FA and negatively charged resorcinol molecule (pH from 7.0 - 10.2). Thereafter adsorption capacity decrease due to FA surface become negatively charged after pH 10.8, electrostatic repulsion between negatively charged surface of FA and negatively charged resorcinol molecule become effective. Results were attained for resorcinol adsorption on NaFA have same explanation (pH_{ZPC} of NaFA is 10.1). All further experiments were done on their natural pH due to change in stability of resorcinol with change in pH.

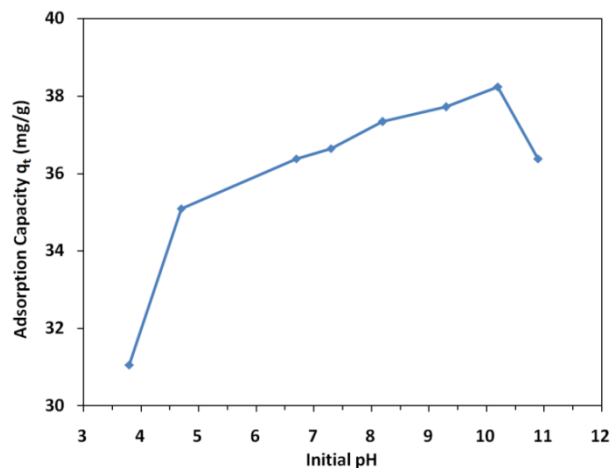


Figure 4.10(a): Effect of pH on adsorption capacity of FA for resorcinol adsorption ($m = 2.0$ gm/l, $t = 5$ hr, $T = 303$ K, $C_0 = 100$ ppm)

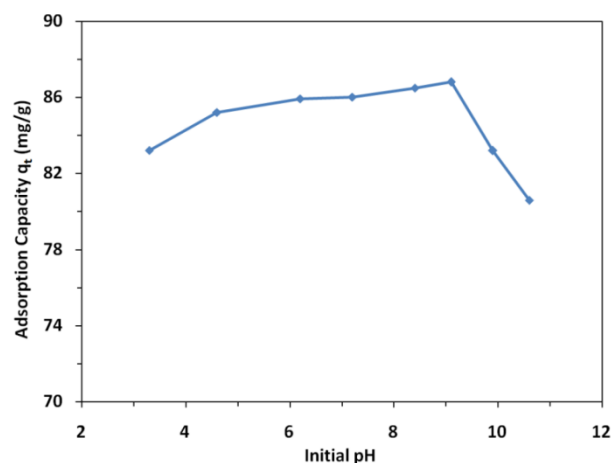


Figure 4.10(b): Effect of pH on adsorption capacity of NaFA for resorcinol adsorption ($m = 1.0$ gm/l, $t = 5$ hr, $T = 303$ K, $C_0 = 100$ ppm)

Table 4.5: Effect of pH on adsorption capacity of FA and NaFA for resorcinol adsorption

FA ^a		NaFA ^b	
Initial pH	q_t (mg/g)	Initial pH	q_t (mg/g)
3.8	31.055	3.3	83.22
4.7	35.09	4.6	85.21
6.7	36.38	6.2	85.92
7.3	36.64	7.2	86.01
8.2	37.34	8.4	86.5
9.3	37.72	9.1	86.81
10.2	38.24	9.9	83.2
10.9	36.38	10.6	80.6

^a $m = 2.0$ gm/l, $t = 5$ hr, $T = 303$ K, $C_0 = 100$ ppm

^b $m = 1.0$ gm/l, $t = 5$ hr, $T = 303$ K, $C_0 = 100$ ppm

4.3.3 Effect of initial resorcinol concentration (C_0)

The effect of C_0 on the removal of resorcinol by FA and NaFA is shown in Table 4.6 and Figures 4.11(a & b). It is evident from the figure that the amount of resorcinol adsorbed per unit mass (q_e) of FA and NaFA increased with the increase in C_0 , although percentage removal decreased with the increase in C_0 . The C_0 provides the necessary driving force to overcome the resistances to the mass transfer of resorcinol between the aqueous and the solid phases [51]. The increase in C_0 also enhances the interaction between resorcinol and FA and NaFA. Therefore, an increase in C_0 of resorcinol enhances the adsorption uptake.

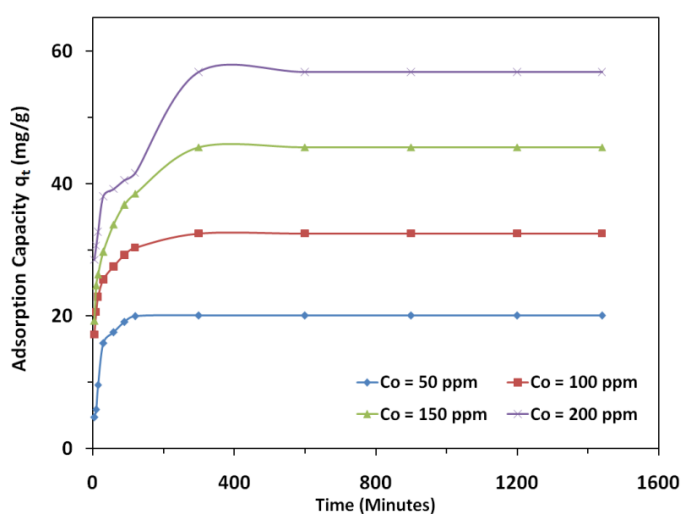


Figure 4.11(a): Effect of Initial Concentration of resorcinol on adsorption capacity of FA
($m = 2.0$ gm/l, $\text{pH} = 6.8$, $T = 303$ K)

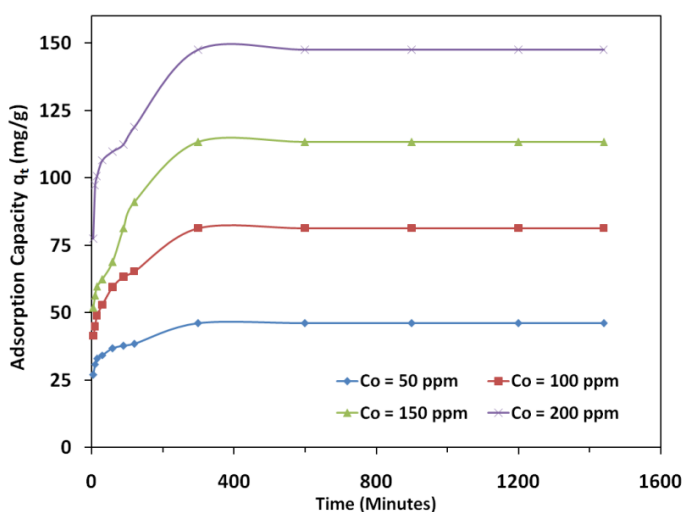


Figure 4.11 (b): Effect of Initial Concentration of resorcinol on adsorption capacity of NaFA
($m = 1.0$ gm/l, $\text{pH} = 6.8$, $T = 303$ K)

Table 4.6: Effect of Initial Concentration of resorcinol on adsorption capacity of FA and NaFA

	t (min)	C ₀ =50 ppm		C ₀ =100 ppm		C ₀ =150 ppm		C ₀ =200 ppm	
		q _t (mg/g)	% removal	q _t (mg/g)	% removal	q _t (mg/g)	% removal	q _t (mg/g)	% removal
FA^a	5	4.76	19.06	17.22	34.44	19.3	25.74	28.5	28.5
	10	5.94	23.74	20.64	41.29	24.65	32.87	30.64	30.64
	15	9.59	38.36	22.92	45.85	26.34	35.13	32.75	32.75
	30	15.94	63.74	25.5	51	29.68	39.57	38.07	38.07
	60	17.54	70.18	27.48	54.97	33.83	45.11	39.18	39.18
	90	19.12	76.5	29.21	58.42	36.82	49.09	40.5	40.5
	120	20	80	30.35	60.7	38.5	51.33	41.6	41.6
	300	20.12	80.47	32.46	64.92	45.5	60.67	56.82	56.82
NaFA^b	5	26.96	53.92	41.46	41.46	51.87	34.58	77.43	38.72
	10	30.92	61.84	44.97	44.97	56.46	37.66	97.31	48.66
	15	32.92	65.84	49	51.93	59.77	39.85	100.58	50.29
	30	34.27	68.54	52.92	52.92	62.34	41.56	106.49	53.24
	60	36.78	73.56	59.42	59.42	68.89	45.93	109.77	54.89
	90	37.66	75.32	63.39	63.39	81.4	64.27	112.34	56.17
	120	38.42	76.84	65.38	65.38	91	60.67	118.89	59.44
	300	46.08	92.16	81.34	81.34	113.22	75.48	147.48	73.74

^a m = 2.0 gm/l, pH = 6.8, T = 303 K^b m = 1.0 gm/l, pH = 6.8, T = 303 K

4.3.4 Effect of adsorbent dosage (m)

The effect of m on the removal of resorcinol by FA and NaFA at C_0 100 mg/l are shown in Table 4.7 & Figures 4.12 (a & b) respectively. It can be seen that resorcinol removal increases up to a certain limit and then it remains almost constant. An increase in the adsorption with the adsorbent dosage can be attributed to greater surface area and the availability of more adsorption sites. With increase in the m , the resorcinol removal increases due to increased resorcinol uptake by the increased amount of adsorbent.

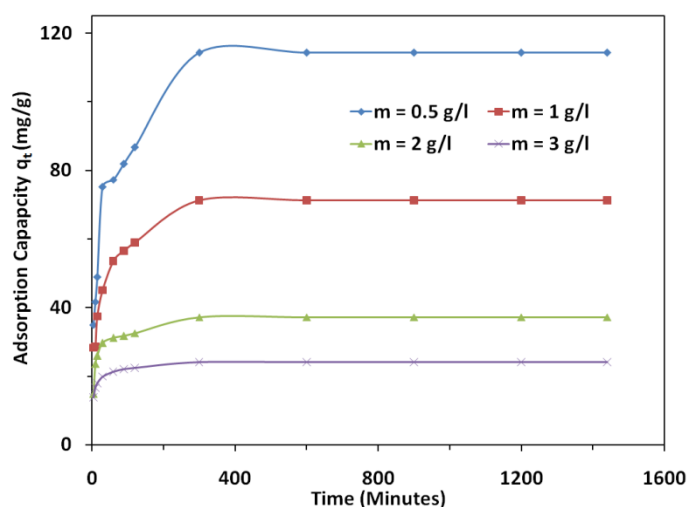


Figure 4.12 (a): Effect of adsorbent dose on adsorption capacity of FA for resorcinol adsorption
($T = 303$ K, $\text{pH} = 6.8$, $C_0 = 100$ ppm)

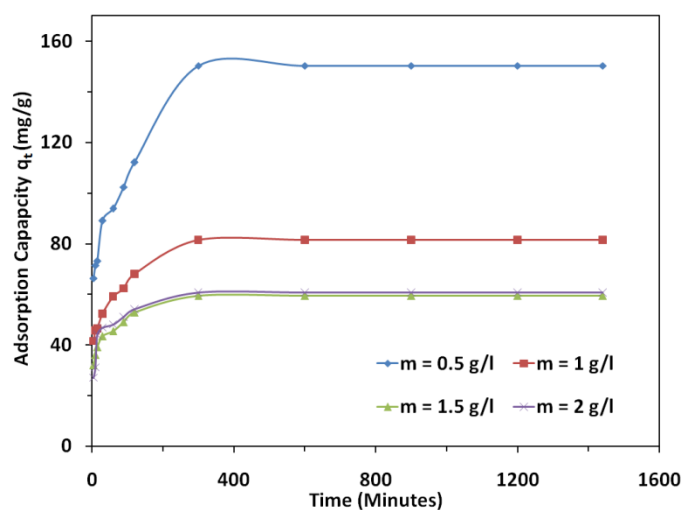


Figure 4.12 (b): Effect of adsorbent dose on adsorption capacity of NaFA for resorcinol adsorption
($T = 303$ K, $\text{pH} = 6.8$, $C_0 = 100$ ppm)

Table 4.7: Effect of adsorbent dose on adsorption capacity of FA and NaFA for resorcinol adsorption

	t (min)	Adsorption Capacity (mg/g)			
		m=0.5 g/l	m=1 g/l	m=2 g/l	m=3 g/l
FA ^a	5	34.96	28.25	14.79	13.76
	10	41.64	28.6	23.56	16.63
	15	48.88	37.37	25.94	17.89
	30	75.2	45.03	29.68	19.84
	60	77.3	53.51	31.06	21.27
	90	81.88	56.43	31.7	21.99
	120	86.66	58.89	32.49	22.36
	300	114.26	71.23	37.2	23.98
	5	34.96	28.25	14.79	13.76
	10	41.64	28.6	23.56	16.63
NaFA ^b	t (min)	m=0.5 g/l	m=1 g/l	m=1.5 g/l	m=2 g/l
	5	66.32	41.46	31.97	26.96
	10	71.34	45.55	35.91	31.06
	15	73.1	46.37	39.03	43.82
	30	89	52.22	43.33	46.75
	60	93.8	59.06	45.38	48.07
	90	102.34	62.28	48.93	51.03
	120	112	68	52.66	54.01
	300	150.3	81.34	59.3	60.58

^a T = 303 K, pH = 6.8, C₀ = 100 ppm ^b T = 303 K, pH = 6.8, C₀ = 100 ppm

4.3.5 Effect of contact time (t)

Effect of contact time for the removal of resorcinol by FA and NaFA at C₀ = 50, 100, 150 and 200 mg/l showed rapid adsorption of resorcinol in the first 30 min and, thereafter, the adsorption rate decreases gradually and the adsorption reached equilibrium in about 5 h as shown in Table 4.6 & Figures 4.12(a & b) respectively. Aggregation of resorcinol molecules with the increase in contact time makes it almost impossible to diffuse deeper into the adsorbent structure at highest energy sites. This aggregation negates the influence of contact time as the mesopores get filled up and start offering resistance to diffusion of aggregated dye molecules in the adsorbents. The adsorption curves were single, smooth and continuous leading to saturation and indicated the possible monolayer coverage on the surface of adsorbents by the resorcinol molecules [51]. Prediction of adsorption capacity (q_t) of resorcinol on FA and NaFA by the combined effect of C₀ and time are described in three dimensional plot (Figure 4.13).

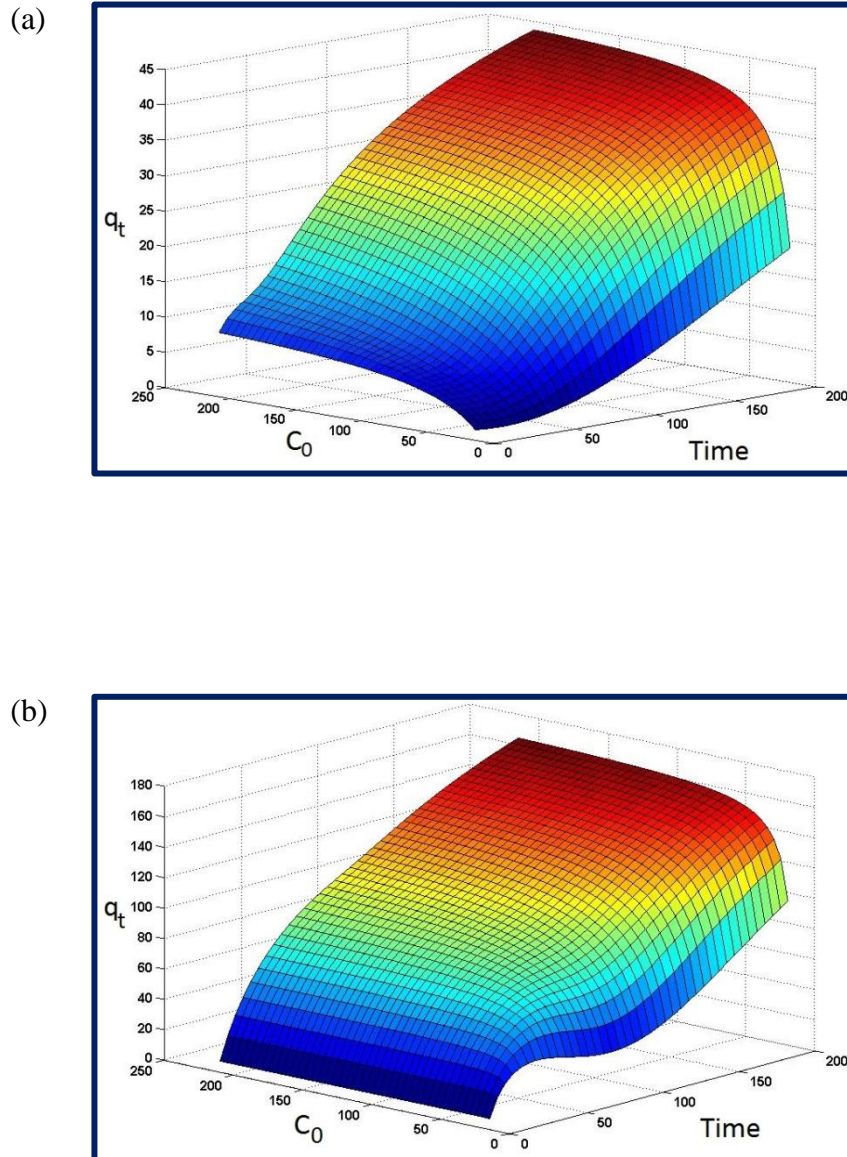


Figure 4.13: Three dimensional plot showing the interaction effect of Initial Concentration (C_0) and Time (t) on (a) FA and (b) NaFA for adsorption capacity of resorcinol

4.3.6 Adsorption Kinetics

Four widely used kinetic models, pseudo-first-order, pseudo-second-order, Bangham and intra-particle diffusion model were employed to interpret the kinetic as discussed in chapter 2 and the results were given in Table 4.8 & 4.9 and Figures 4.14 & 4.15.

For pseudo-second-order kinetic model, although the R^2 value obtained was relatively high ($R^2 = 0.961$) for FA and ($R^2 = 0.799$ to 0.966) for NaFA, the calculated q_e value did not agree with the experimental one. This suggests that the pseudo-first-order kinetic model is not appropriate to represent the adsorption kinetics data of both resorcinol onto FA and NaFA.

For pseudo-second-order kinetic model, the R^2 value obtained was very high ($R^2 > 0.999$) on both FA & NaFA, and the calculated q_e value was in good agreement with the experimental one, suggesting the applicability of the pseudo-second-order kinetic model to describe the adsorption kinetics data of resorcinol onto FA and NaFA.

Linear plots of q_e and h against C_0 were regressed to obtain the value of q_e and h in terms of C_0 with high a coefficient of regression (>0.9816). Therefore, q_e and h can be express as a function of C_0 as follows:

For FA

$$q_e = 14.53 \ln C_0 - 32.93 \quad (4.1)$$

$$h = 2 \times 10^{-4} C_0^2 - 0.0147 C_0 + 0.4553 \quad (4.2)$$

$$q_t = \frac{t}{1/(2 \times 10^{-4} C_0^2 - 0.0147 C_0 + 0.4553) + (1/14.53 \ln C_0 - 32.93) t} \quad (4.3)$$

For NaFA

$$q_e = 60.28 \ln C_0 - 199.6 \quad (4.4)$$

$$h = 28 \times 10^{-4} C_0^2 - 0.5652 C_0 + 35.5575 \quad (4.5)$$

$$q_t = \frac{t}{1/(28 \times 10^{-4} C_0^2 - 0.5652 C_0 + 35.56) + (1/68.28 \ln C_0 - 199.6) t} \quad (4.6)$$

A comparison of experimental data points and the surface predicted by the equations (4.3 & 4.6) is given in Figure 4.13. It can be used to derive the sorption capacity, q_t at any given C_0 and t [52].

Bangham's equation show (Figure 4.14c & 4.15c) linear curves for the resorcinol removal by the FA and NaFA, signifying that the diffusion of adsorbate into the pores of the adsorbent was the only rate-controlling step [52, 53]. It may be that pore diffusion was important in the removal process.

The Intra-particle diffusion model (Figure 4.14d and 4.15d) is giving straight line passing through the origin, then the sorption process fits to the intraparticle diffusion kinetic model. Values of C (Table 4.9) give an idea about the thickness of the boundary layer, i.e. the larger the intercept the greater is the boundary layer effect [54].

Table 4.8(a): Details of all kinetic parameters for resorcinol adsorption on FA

Resorcinol C_0	time (min.)	5	10	15	30	60	90	120
		$\sqrt{\text{time}}$	2.24	3.16	3.88	5.48	7.75	9.49
	$\log t$	0.699	1.000	1.176	1.477	1.778	1.954	2.079
50 ppm	$\ln(q_e - qt)$	2.73	2.65	2.35	1.43	0.948	0	-2.12
	t/qt	1.05	1.685	1.564	1.88	3.42	4.71	6
	qt	4.765	5.935	9.59	15.94	17.54	19.12	20
	$\log \log (C_0/C_0 - q_t m)$	-1.037	-0.929	-0.677	-0.356	-0.280	-0.202	-0.156
100 ppm	$\ln(q_e - qt)$	2.72	2.47	2.26	1.94	1.6	1.18	0.747
	t/qt	0.29	0.484	0.654	1.176	2.18	3.08	3.95
	qt	17.22	20.64	22.92	25.5	27.48	29.21	30.35
	$\log \log (C_0/C_0 - q_t m)$	-0.737	-0.636	-0.575	-0.509	-0.460	-0.419	-0.392
150 ppm	$\ln(q_e - qt)$	3.27	3.04	2.95	2.76	2.46	2.16	1.95
	t/qt	0.26	0.406	0.569	1.011	1.77	2.44	3.12
	qt	19.3	24.65	26.34	29.68	33.83	36.82	38.5
	$\log \log (C_0/C_0 - q_t m)$	-0.889	-0.762	-0.726	-0.660	-0.584	-0.533	-0.505
200 ppm	$\ln(q_e - qt)$	3.34	3.26	3.18	2.93	2.87	2.79	2.72
	t/qt	0.175	0.326	0.458	0.788	1.53	2.22	2.89
	qt	28.5	30.64	32.75	38.07	39.18	40.5	41.6
	$\log \log (C_0/C_0 - q_t m)$	-0.837	-0.799	-0.764	-0.682	-0.666	-0.647	-0.632

Table 4.8(b): Details of all kinetic parameters for resorcinol adsorption on NaFA

Resorcinol C_0	time (min.)	5	10	15	30	60	90	120
		$\sqrt{\text{time}}$	2.24	3.16	3.88	5.48	7.75	9.49
	$\log t$	0.699	1.000	1.176	1.477	1.778	1.954	2.079
50 ppm	$\ln(q_e - qt)$	2.95	2.72	2.58	2.47	2.23	2.13	2.04
	t/qt	0.185	0.323	0.456	0.875	1.63	2.39	3.12
	qt	26.96	30.92	32.92	34.27	36.78	37.66	38.42
	$\log \log (C_0/C_0 - qt)$	-0.473	-0.378	-0.331	-0.299	-0.238	-0.216	-0.197
100 ppm	$\ln(q_e - qt)$	3.69	3.59	3.48	3.35	3.09	2.89	2.77
	t/qt	0.121	0.222	0.306	0.567	1.01	1.42	1.84
	qt	41.460	44.970	49.000	52.920	59.420	63.390	65.380
	$\log \log (C_0/C_0 - qt)$	-0.633	-0.586	-0.534	-0.485	-0.407	-0.360	-0.337
150 ppm	$\ln(q_e - qt)$	4.12	4.04	3.98	3.93	3.79	3.46	3.1
	t/qt	0.096	0.177	0.251	0.481	0.871	1.11	1.32
	qt	51.870	56.490	59.770	62.340	68.890	81.400	91.000
	$\log \log (C_0/C_0 - qt)$	-0.734	-0.688	-0.656	-0.632	-0.573	-0.469	-0.392
200 ppm	$\ln(q_e - qt)$	4.25	3.92	3.85	3.71	3.63	3.56	3.35
	t/qt	0.065	0.103	0.149	0.282	0.547	0.801	1.009
	qt	77.430	97.310	100.580	106.490	109.770	112.340	118.890
	$\log \log (C_0/C_0 - qt)$	-0.672	-0.538	-0.518	-0.481	-0.461	-0.446	-0.407

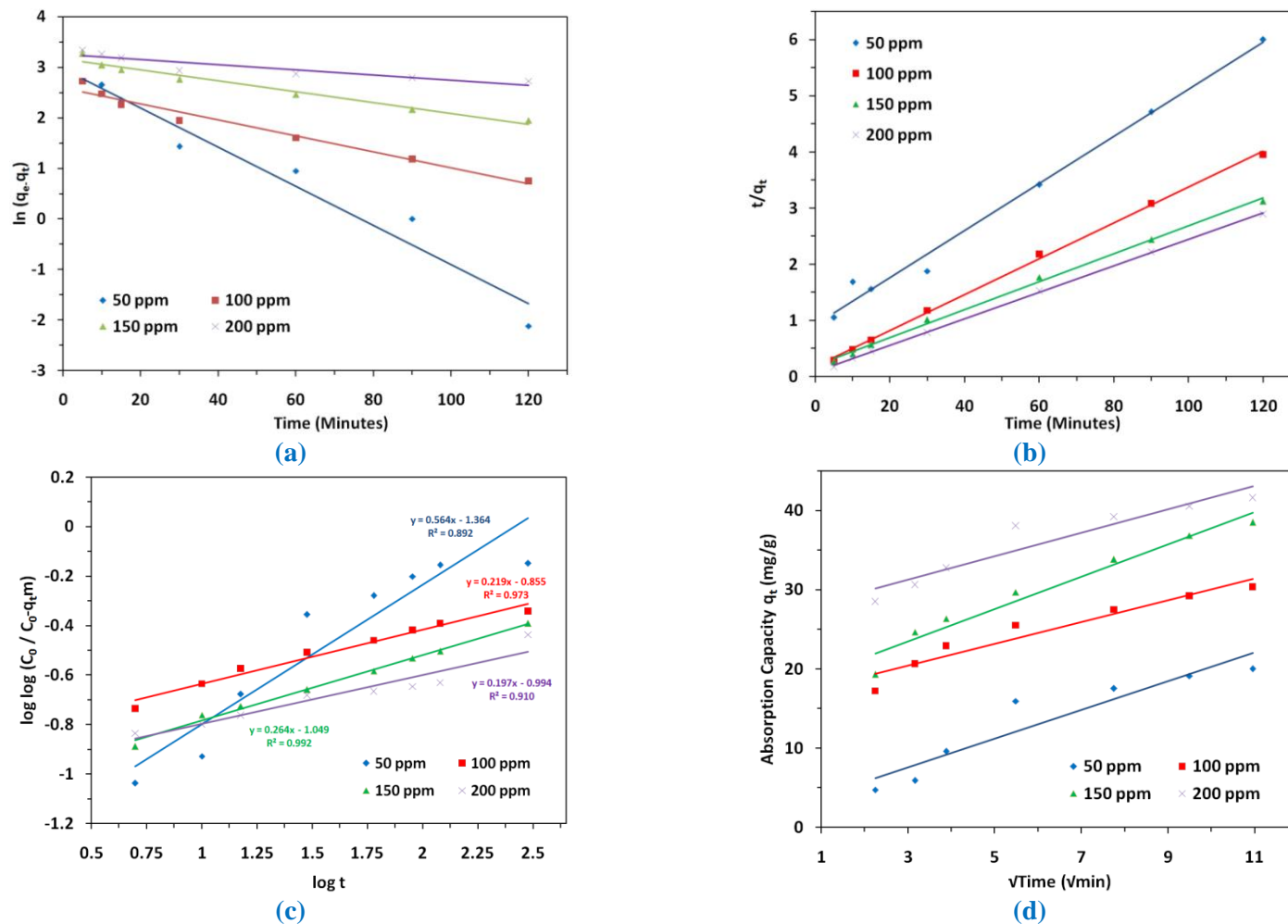


Figure 4.14: Kinetic Model (a) Pseudo Second Order, (b) Pseudo Second Order, (c) Bangham's equation and (d) intra-particle diffusion model of resorcinol adsorption on FA

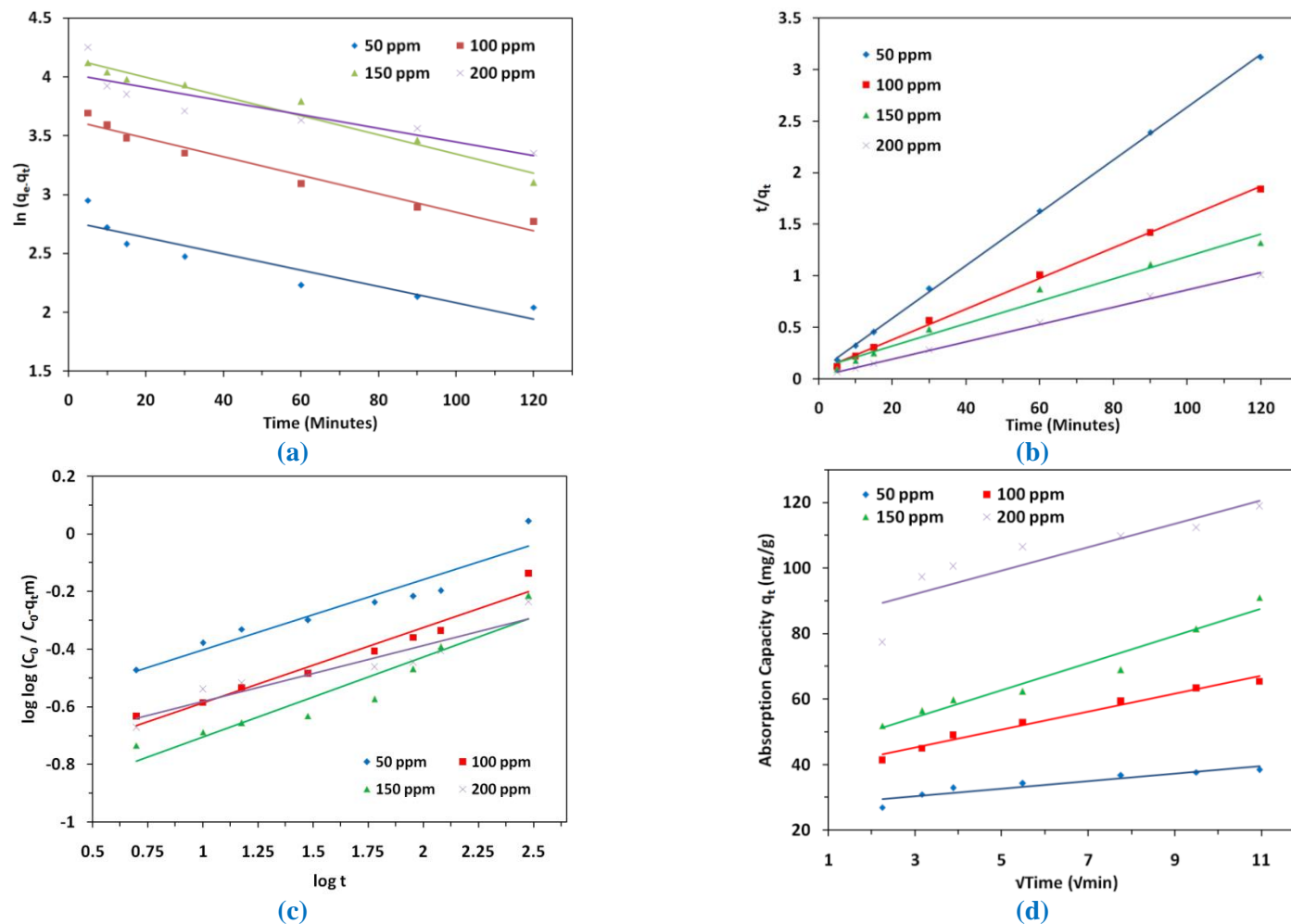


Figure 4.15: Kinetic Model (a) Pseudo Second Order, (b) Pseudo Second Order, (c) Bangham's equation and (d) intra-particle diffusion model of resorcinol adsorption on NaFA

Table 4.9: Pseudo-first order, Pseudo-second order and Intra-particle Diffusion Model rate constant for resorcinol adsorption on FA and NaFA at various concentration

	$C_0(\text{mg/L})$		50	100	150	200	
		$q_{e, \text{exp}}(\text{mg/g})$		20.12	32.46	45.50	56.81
FA ^a	Pseudo-first order model	$K_1 (1/\text{min})$	0.038	0.015	0.010	0.005	
		$q_{e, \text{cal}}(\text{mg/g})$	19.36	13.34	23.59	25.82	
		R^2	0.961	0.970	0.961	0.840	
	Pseudo-second order	$K_2(\text{g/mg min})$	1.81×10^{-3}	5.28×10^{-3}	2.94×10^{-3}	6.01×10^{-3}	
		$q_{e, \text{cal}}(\text{mg/g})$	24.39	32.26	41.67	43.48	
		h	1.079	5.49	5.10	11.36	
		R^2	0.989	0.998	0.997	0.999	
	Bangham	$K_0(\text{g})$	2.487	8.039	5.132	5.826	
		α	0.564	0.2192	0.2649	0.1974	
		R^2	0.892	0.9737	0.9925	0.9109	
	Intra-particle Diffusion Model	$K_{id}(\text{mg/g}(\text{min}^{0.5}))$	1.808	1.374	2.043	1.476	
		C	2.172	16.32	17.33	26.83	
		R^2	0.890	0.923	0.958	0.899	
	NaFA ^b	$q_{e, \text{exp}}(\text{mg/g})$		46.08	81.34	113.22	148
		Pseudo-first order model	$K_1 (1/\text{min})$	0.007	0.007	0.008	0.005
$q_{e, \text{cal}}(\text{mg/g})$			16.01	37.94	63.94	56.09	
R^2			0.866	0.964	0.966	0.799	
Pseudo-second order		$K_2(\text{g/mg min})$	8.01×10^{-3}	2.33×10^{-3}	0.970×10^{-3}	2.37×10^{-3}	
		$q_{e, \text{cal}}(\text{mg/g})$	40	71.43	100	125	
		h	12.82	11.90	9.708	37.03	
		R^2	0.999	0.998	0.979	0.998	
Bhangham		$K_0(\text{g})$	26.0174	16.36681	11.95815	19.21604	
		α	0.2435	0.2609	0.2776	0.1947	
		R^2	0.9083	0.9569	0.9008	0.8892	
Intra-particle Diffusion Model		$K_{id}(\text{mg/g}(\text{min}^{0.5}))$	1.154	2.744	4.152	3.581	
		C	26.90	36.95	41.91	81.28	
		R^2	0.879	0.980	0.957	0.784	

^a ($m = 2.0 \text{ g l}^{-1}$, agitation rate = 200 rpm, pH 6.8, T = 30 °C)

^b ($m = 1.0 \text{ g l}^{-1}$, agitation rate = 200 rpm, pH 6.8, T = 30 °C)

4.3.7 Adsorption isotherm

The adsorption isotherm of resorcinol onto FA and NaFA at 30°C, 40°C and 50°C are shown in Tables 4.10(a & b) and Figure 4.16. Results showed that resorcinol removal increased with increasing the resorcinol concentration until

equilibrium was reached. Three isotherm models Langmuir, Freundlich and Tempkin were used to fit the experimental data.

The different isotherm parameters were evaluated from the linear plots and presented in [Table 4.11](#) along with constants and correlation coefficients root mean square error (RMSE), sum of the squares of the errors (SSE) and chi-square (χ^2). A better curve fitting is observed by smaller RMSE value. If the data obtained from the isotherm model are nearer to the experiment results the χ^2 values will be lesser digit [55].

The value of RMSE and χ^2 for the Langmuir, Freundlich and Tempkin isotherm model were low on FA at low temperature but at high temperature only Freundlich and Tempkin isotherm model have low value, indicating that the equilibrium data for the adsorption of resorcinol onto FA can be well represented by all these isotherm models at low temperature but at high temperature followed by only Freundlich and Tempkin isotherms. Adsorption of resorcinol on to NaFA obeyed only Freundlich isotherm. Freundlich isotherm concluding that the adsorption of resorcinol on both FA and NaFA takes place as multilayer adsorption and the surface of FA and NaFA is homogenous in adsorption affinity. The predicted maximum monolayer resorcinol adsorption capacity for FA and NaFA derived from Langmuir isotherm was found to be 100 mg/g on FA and 333.33 mg/g on NaFA. The values of R_L obtained in this study were between 0.015 to 0.052 on FA and 0.103 to 0.476 on NaFA indicating that the adsorption of resorcinol onto both FA and NaFA is favourable. The above experimental data was evaluated by Langmuir isotherm model.

A comparison of the maximum adsorption capacity, q_m , for resorcinol on various adsorbents was presented in [Table 4.12](#). The q_m of resorcinol obtained from this study was lesser for FA to that obtained in the other investigations. Despite relatively low adsorption capacity of the studied for FA, the use of this adsorbent for resorcinol removal is of interest since it is low-cost and readily available waste and NaFA is good adsorbent for resorcinol because it shows higher adsorption than other.

Table 4.10(a): Isotherm parameters for adsorption of resorcinol on FA

T (°C)	Parameters					
30 °C	C _e	9.77	35.09	59.01	86.38	114.52
	ln C _e	2.28	3.56	4.08	4.46	4.74
	log C _e	0.99	1.545	1.77	1.94	2.06
	q _e	20.12	32.46	45.5	56.81	67.74
	log q _e	1.304	1.511	1.66	1.75	1.831
	C _e / q _e	0.486	1.08	1.3	1.52	1.69
40 °C	C _e	12.54	38.12	71.06	102.81	135
	ln C _e	2.53	3.64	4.26	4.63	4.9
	log C _e	1.1	1.58	1.85	2.01	2.13
	q _e	18.73	30.94	39.47	48.6	57.5
	log q _e	1.27	1.49	1.6	1.69	1.76
	C _e / q _e	0.67	1.23	1.8	2.12	2.35
50 °C	C _e	15.01	41.05	80.01	108.3	140
	ln C _e	2.71	3.72	4.38	4.68	4.94
	log C _e	1.18	1.61	1.9	2.03	2.15
	q _e	17.5	29.5	38.28	44.385	49.296
	log q _e	1.24	1.47	1.583	1.647	1.693
	C _e / q _e	0.858	1.39	2.09	2.44	2.84

Table 4.10(b): Isotherm parameters for adsorption of resorcinol on NaFA

T (°C)	Parameters						
30 °C	C _e	3.918	18.66	36.78	52	70.18	93.68
	ln C _e	1.36	2.93	3.6	3.95	4.25	4.54
	log C _e	0.593	1.271	1.566	1.72	1.85	1.972
	q _e	46.08	81.34	113.22	148	179.82	206.32
	log q _e	1.66	1.91	2.05	2.17	2.26	2.32
	C _e / q _e	0.085	0.229	0.325	0.351	0.39	0.453
40 °C	C _e	3.62	16.43	34	50	65	85
	ln C _e	1.286	2.8	3.53	3.9	4.17	4.44
	log C _e	0.559	1.22	1.53	1.7	1.81	1.93
	q _e	46.38	83.57	116	150	185	215
	log q _e	1.67	1.92	2.07	2.18	2.27	2.33
	C _e / q _e	0.078	0.197	0.293	0.333	0.351	0.395
50 °C	C _e	2.92	14.68	32	48.88	62	80
	ln C _e	1.07	2.69	3.47	3.89	4.13	4.38
	log C _e	0.465	1.17	1.5	1.69	1.79	1.9
	q _e	47.08	85.35	118	151.12	188	220
	log q _e	1.67	1.93	2.07	2.179	2.27	2.34
	C _e / q _e	0.062	0.172	0.271	0.323	0.329	0.363

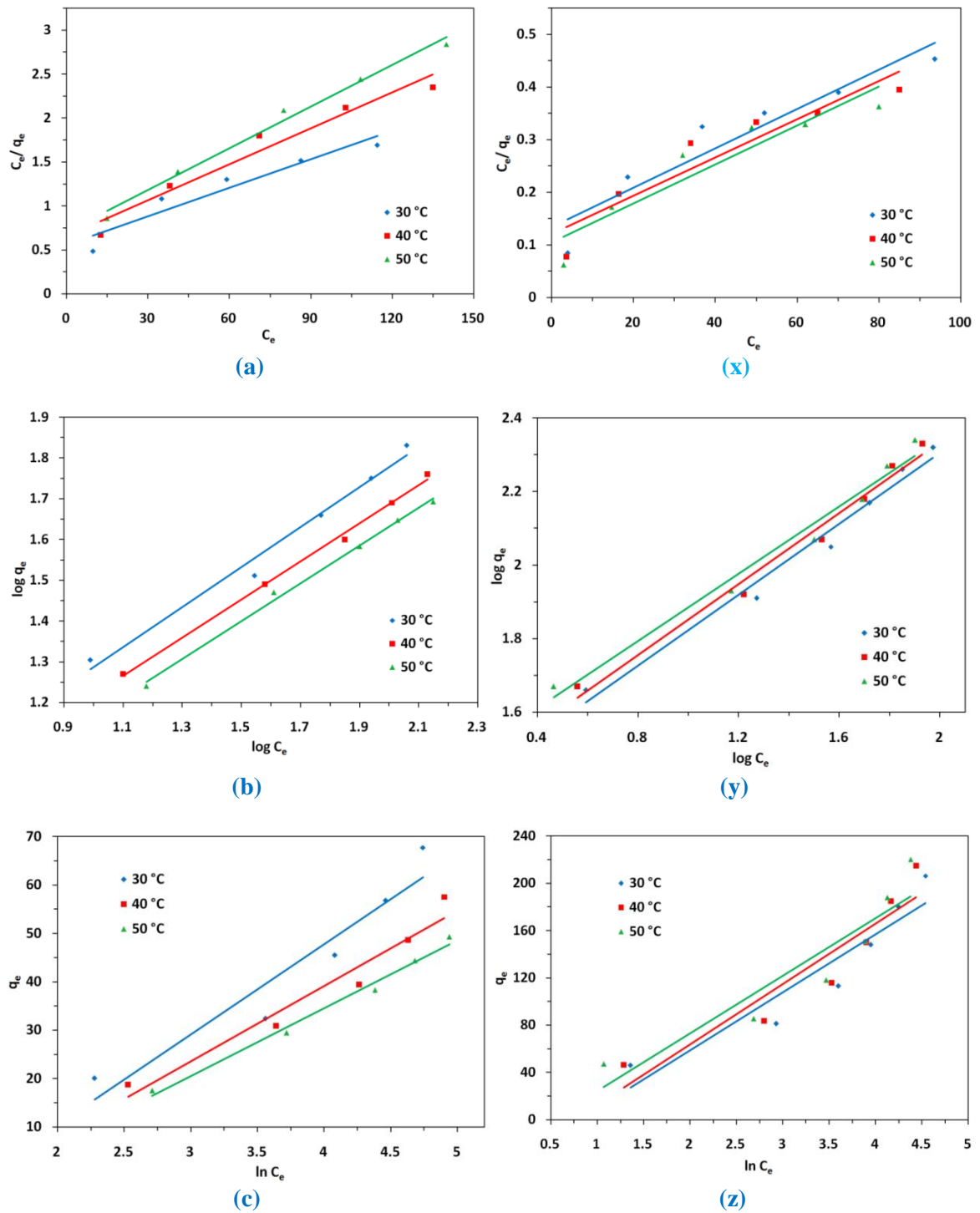


Figure 4.16: Adsorption Isotherm (a) Langmuir, (b) Freundlich and (c) Tempkin of resorcinol adsorption on FA and (x) Langmuir, (y) Freundlich and (z) Tempkin of resorcinol adsorption on NaFA

Table 4.11: Isotherm parameters for resorcinol adsorption on FA and NaFA at various temperature

FA ^a	Langmuir	T (°C)	q _{max} (mg/g)	K _L (L/mg)	R ²	RMSE	SSE	χ ²
		at 30	100	0.018	0.914	6.80	138.92	3.93
		at 40	76.92	0.020	0.955	40.94	5027	119.63
		at 50	66.67	0.0212	0.949	22.87	1569	37.78
	Freundlich	T (°C)	K _F (mg/g) (L/mg) ^{1/n}	1/n	R ²	RMSE	SSE	χ ²
		at 30	6.25	0.490	0.983	3.05	27.98	0.633
		at 40	5.64	0.467	0.997	1.51	6.83	0.151
		at 50	5.04	0.494	0.995	7.22	156.6	3.63
	Tempkin	T (°C)	K _T (mg/g)	B _T	R ²	RMSE	SSE	χ ²
		at 30	0.237	18.65	0.914	5.39	87.36	2.89
		at 40	0.228	15.57	0.949	3.90	45.64	1.23
		at 50	0.216	14.03	0.988	1.56	7.33	0.218
NaFA ^b	Langmuir	T (°C)	q _{max} (mg/g)	K _L (L/mg)	R ²	RMSE	SSE	χ ²
		at 30	333.33	0.022	0.894	30.17	3642	33
		at 40	333.33	0.025	0.884	137	75084	494
		at 50	333.33	0.029	0.876	18.90	1429	16.67
	Freundlich	T (°C)	K _F (mg/g)(L/mg) ^{1/n}	1/n	R ²	RMSE	SSE	χ ²
		at 30	21.93	0.481	0.978	10.57	446	3.48
		at 40	23.44	0.482	0.981	11.82	558	3.78
		at 50	26.73	0.457	0.977	14.88	885	5.35
	Tempkin	T (°C)	K _T (mg/g)	B _T	R ²	RMSE	SSE	χ ²
		at 30	0.448	48.99	0.883	23.09	2134	22.42
		at 40	0.472	50.94	0.879	24.49	2400	23.37
		at 50	0.606	48.69	0.864	26.59	2828	25.61

^a (m = 2.0 g l⁻¹, agitation rate = 200 rpm, pH = 6.8, C₀ = 50– 300 m g l⁻¹)

^b (m = 1.0 g l⁻¹, agitation rate = 200 rpm, pH = 6.8 C₀ = 50– 300 m g l⁻¹)

Table 4.12: Comparison of the maximum monolayer adsorption of resorcinol onto various adsorbents

Adsorbents	Adsorption Capacity (mg g ⁻¹)	References
Activated carbon	142.82	[3]
Granular activated carbon	209	[56]
Carbonaceous material	< 1.5 82% from activated carbon (AC), 72% from wood charcoal (WC), 79% from rice husk (RHA)	[57]
High area activated carbon cloth	232.1 (2.11 X 10 ⁻³ mol/g)	[58]
FA	100	This work
NaFA	333.33	This work

4.3.8 Effect of Temperature and Thermodynamic Studies

The amount of resorcinol at different temperatures (303-323 K) for FA and NaFA has been examined to obtain thermodynamic parameters for the adsorption system. Adsorption decreased with increase in temperature for both adsorbents shown in Table 4.13 and Figure 4.17 (a & b) can be explained on the basis of thermodynamic parameters of standard enthalpy (ΔH°) and entropy (ΔS°) for the adsorption process estimated from the Van-Haff equation. The values of K_L for Langmuir isotherm at different temperatures were used to calculate thermodynamic parameters such as Gibbs free energy change (ΔG°). The values of ΔH° and ΔS° can be calculated from the intercept and the slope of the linear plot of $\ln K_L$ versus $1/T$ as shown in Figure 4.18 (a & b).

The obtained values of the thermodynamic parameters of resorcinol adsorption onto FA and NaFA are given in Table 4.14. The negative values of ΔG° suggest that the feasibility of the adsorption of resorcinol onto both FA and NaFA is spontaneous and a favorable process. The values of ΔG° obtained in this study were in the range of physisorption for both.

The negative value of ΔH° indicates that the adsorption process is exothermic in nature. The absolute value of ΔH° was 7.026 kJ/mol for FA and

11.44 kJ/mol for NaFA, the positive value of ΔS° for both show an increase in randomness at the solid/liquid interface during the adsorption process.

Table 4.13: Effect of Temperature of solution on adsorption capacity of FA and NaFA for resorcinol adsorption

	Time (min)	Adsorption Capacity (mg/g)			
		25 °C	30 °C	40 °C	50 °C
FA ^a	5	20.73	17.22	13.28	12.04
	10	23.01	20.64	19.44	17.84
	15	27.55	22.92	20.56	19.39
	30	29.97	25	21.9	20.79
	60	32.34	27.48	25.91	23.8
	90	33.68	29.21	26.52	25.09
	120	35.52	30.35	29.15	26.67
	300	36.87	32.46	30.94	29.48
	NaFA ^b	5	40.82	41.46	44.33
10		44.6	44.97	47.02	46.02
15		47.6	51	48.83	49.65
30		49.18	52.92	54.97	56.49
60		50.58	59.42	64.8	69.71
90		55.38	63.39	69.71	74.91
120		62.28	65.38	72.69	76.67
300		76.61	81.34	83.57	85.38

^a (m= 2.0gm/l, pH = 6.8, C₀ = 100 ppm)

^b (m= 1.0gm/l, pH = 6.8, C₀ = 100 ppm)

Table 4.14: Thermodynamic parameters for resorcinol adsorption on FA and NaFA

Adsorbent	ΔH° (KJ/mol)	ΔS° (J/mol)	$-\Delta G^\circ$ (KJ/mol)			R ²
			30 °C	40 °C	50 °C	
FA	-7.026	10.19	8.313	10.18	10.34	0.988
NaFA	-11.44	5.98	9.615	9.60	9.51	0.989

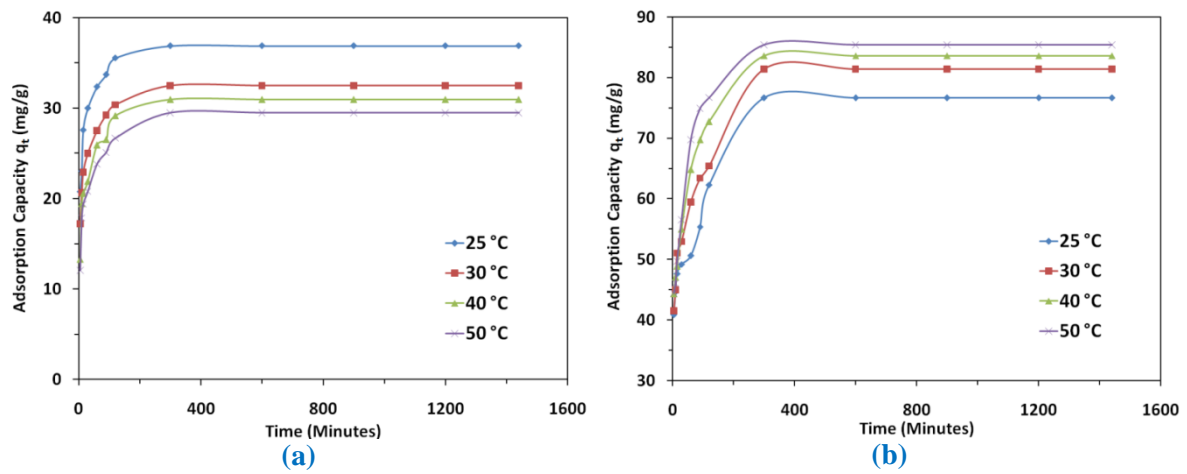


Figure 4.17: Effect of Temperature of solution on adsorption capacity of FA^a and NaFA^b for resorcinol adsorption

^a($m = 2.0 \text{ gm/l}$, $\text{pH} = 6.8$, $C_0 = 100 \text{ ppm}$) ^b($m = 1.0 \text{ gm/l}$, $\text{pH} = 6.8$, $C_0 = 100 \text{ ppm}$)

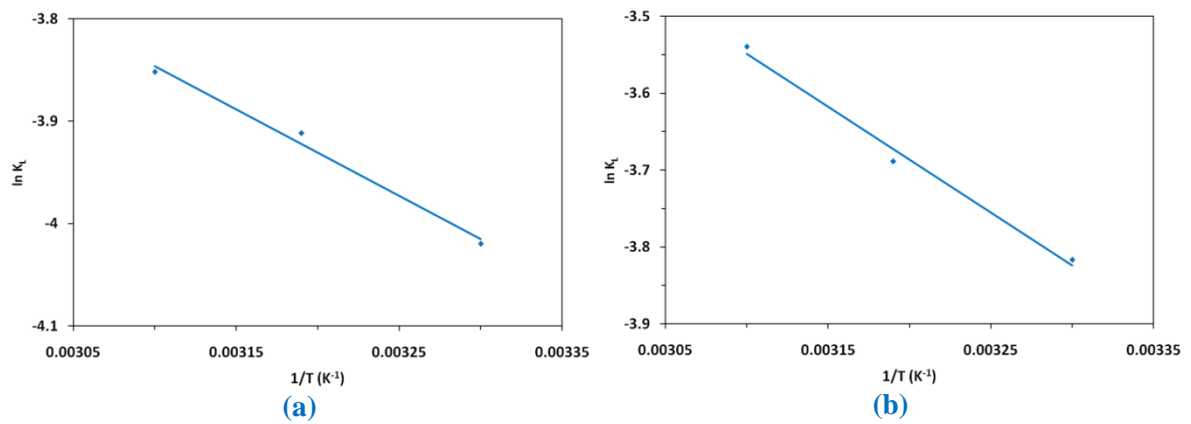


Figure 4.18: Van't Hoff plot for the adsorption of resorcinol on (a) FA and (b) NaFA

4.3.9 Recyclability and reusability of FA and NaFA on resorcinol adsorption

To probe the recyclability of FA and NaFA for resorcinol adsorption, 0.1g of FA and 0.05g of NaFA was added into 50 ml of resorcinol solution (100 mg/l) separately and stirred for 24 hour. Then, the supernatant was centrifugated at 2000 rpm for 4 min. and the concentration of the residual resorcinol supernatant was detected by UV-Visible spectroscopy. The same FA and NaFA sample after resorcinol adsorption were left for 24h at normal temperature for desorption study. Then for desorption study these adsorbent taken into double distilled water in same proportion and stirred for 24h. Then, the supernatant was centrifugated at 2000 rpm for 4 min. and the concentration of the resorcinol in supernatant was detected by UV-visible spectroscopy. After that the same FA and NaFA sample after resorcinol desorption was heated for regeneration at 500°C for 24h in furnace. Following the above procedure, the recyclable FA and NaFA were continuously reused for resorcinol adsorption five times. Remarkably, the FA and NaFA adsorbent are highly stable and can be reused for several cycles with little losing adsorption activity. For instance, the adsorption capacity maintain upto 75% for NaFA and 30 % for FA after 5 cycles of adsorption- desorption, as shown in [Figure 4.19](#). It can be concluded that NaFA is more efficient adsorbent for the removal of resorcinol than FA.

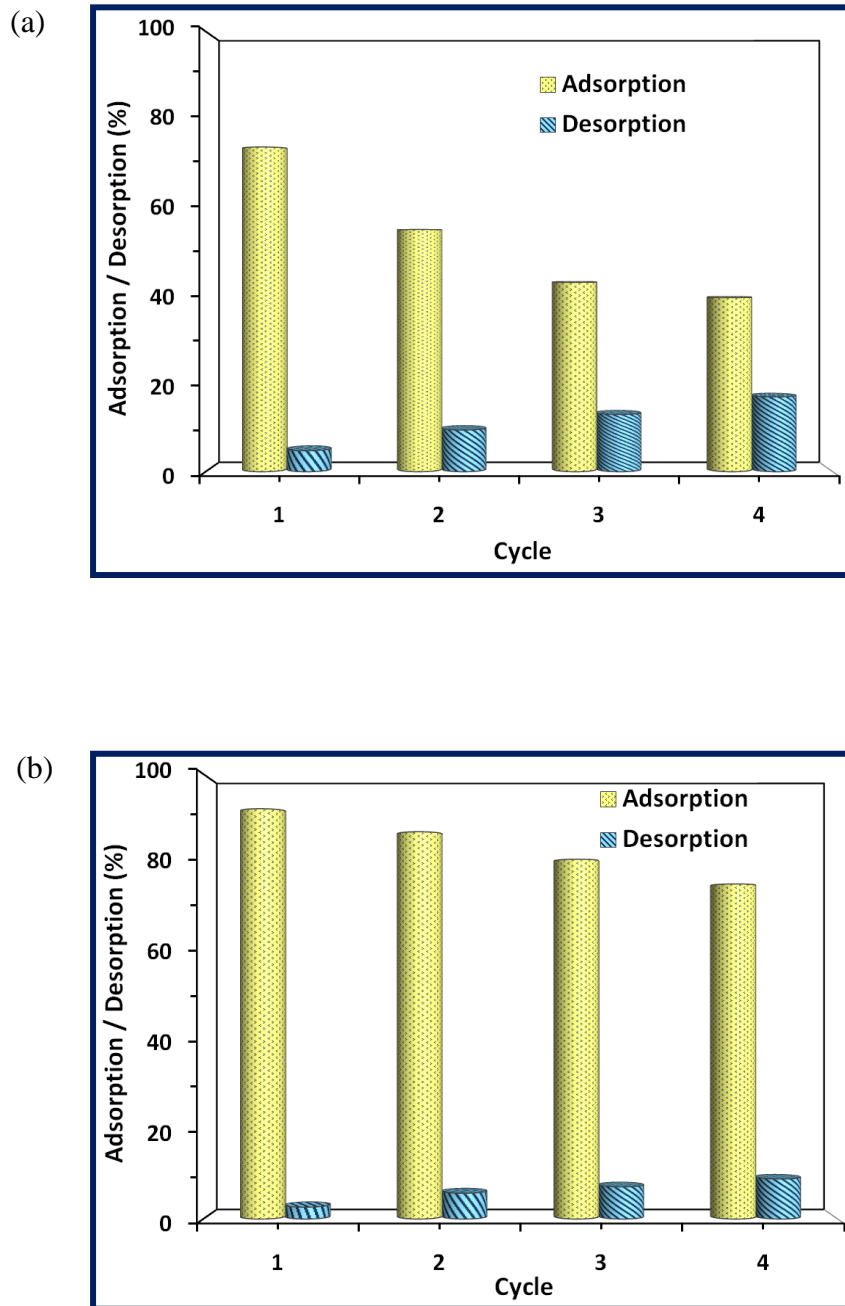


Figure 4.19: Adsorption / desorption of resorcinol for four reuse of (a) FA and (b) NaFA

4.4 Conclusion

Fly ash and its NaOH treated adsorbent were investigated for the removal of resorcinol from aqueous solutions. The following conclusions could be derived from the present study.

1. The present study shows that FA and NaFA both can remove resorcinol from aqueous solution but NaFA is the best adsorbent for the removal of resorcinol with great extent. Adsorption of resorcinol on the FA₄₀ and NaFA was found to be dependent on the initial pH of solution. The optimal pH of resorcinol on FA was in range of 10.2, while the optimum values for NaFA were in range of 9.1. Maximum adsorption occurs within 60 minute for both adsorbents used in this test. The equilibrium between the adsorbate in the solution and on the adsorbent surface was practically achieved in 3hour.
2. Adsorption processes for both adsorbents were found to follow the pseudo-second-order kinetics rate expression. Freundlich isotherm fitted better to the equilibrium data of resorcinol on both FA and NaFA. Maximum adsorption capacity of resorcinol on FA₄₀ was 100 mg/g at 30°C and 333.33 mg/g for NaFA at 30°C obtained. The Thermodynamic parameters were calculated and indicated that each of these adsorption processes was spontaneous and exothermic in nature. NaFA showed large adsorptive characteristics, high separation selectivity and excellent recyclability than FA. These finding indicate that NaFA could be employed as an effective and cost effective adsorbent for the removal of resorcinol from water and waste water.

4.5 References

- [1] I. Hahn, S. K. Concise International Chemical Assessment Document 71 on Resorcinol, II. World Health Organization. III. International Programme on Chemical Safety. IV. Series. ISBN 92 4 153071 5
- [2] A. Kumar, S. Kumar, S. Kumar, Carbon, 41 (2003) 3015-25.

-
- [3] Clayton, G.D., Clayton, F.A. (Eds.), 1981. Patty's Industrial Hygiene and Toxicology, vol. 2A. Wiley, NY, USA.
- [4] Environmental Protection Agency, 1977. Sampling and Analysis Procedure for Screening of Priority Pollutants. Environment Monitoring and Support Laboratory, Cincinnati, OH, USA.
- [5] Environmental Protection Agency, 1984. Methods 604, Phenols in Federal Register, October 26, Part VIII, 40, CFR, 58, USA.
- [6] A.A. Lea, Adesina, J. Chem. Technol. Biotechnol., 76(8) (2001) 803-10.
- [7] W. Katia, C. Assenhaimer, J. Chem. Technol. Biotechnol., 77 (7) (2002) 851-57.
- [8] B.K. Korbahti, B. Salih, A. Janyolac, J. Chem. Technol. Biotechnol., 7 (1) (2002) 70-76.
- [9] R.Y. Sheejan, T. Murugesan, J. Chem. Technol. Biotechnol., 77 (11) (2002) 1219-30.
- [10] E. Bayram, N. Hoda, E. Ayranci, J. of Hazard. Mater., 168 (2009) 1459-66
- [11] Y. Sun, J. Chen, A. L. F. Liu, Q. Zhang, Reactive and Functional Polymers, 64 (2) (2005) 63-73.
- [12] O. El-Amin, A. Adam, Ameri. Chem. Sci. J., 16(1) (2016) 1-13.
- [13] E. Rodríguez, A. Encinas, F. J. Masa, F. J. Beltrán Chemosphere, 70 (2008) 1366-74
- [14] R.I. Yousef, M.F. Tutunji, G.A.W. Derwish, S.M. Musleh, J. Colloid Interface Sci., 216 (1999) 348-59
- [15] C. Bertoncini, H. Odetli, E.J. Bottani, Langmuir, 16 (2000) 7457-63.
- [16] Y.H. Shen, Colloids Surf. A: Physicochem. Eng. Aspects, 232(2-3) (2004) 143-49.
- [17] J.C. Liu, C.P. Huang, J. Colloid Interface Sci., 153 (1992) 167-76.
- [18] J. Peuravuori, N. Paso, K. Pihlaja, Talanta, 56 (2002) 523-38.
- [19] M. Sarkar, M. Das, S. Manna, P. Acharya, Oxford and IBH Publishing Co. Pvt. Ltd., New Delhi, Calcutta, ISBN 81-204-1457-8 (2000) 191-94.
- [20] I. Rodriguez, M.P. Liompart, R. Cela, J. Chromatogr. A., 885 (2000) 291-304.

- [21] X. Querol, N. Moreno, J.C. Umana, et al., *Int. J. Coal Geol.*, 50 (2002) 413-23.
- [22] H. Mimura, K. Yokota, K. Akiba, Y. Onodera, *J. Nucl. Sci. Technol.*, 38 (2001) 872-78.
- [23] R. Apak, G. Atun, K. Guc, lu, E. Tutem, *J. Nucl. Sci. Technol.*, 33 (1996) 365-450.
- [24] P. Janos, H. Buchtova, M. Ryznarov, *Water Res.*, 37 (2003) 4938-44.
- [25] V.V.B. Rao, S. Rao, S.R.M. Rao, *Chem. Eng. J.*, 116 (2006) 77-84.
- [26] C.D. Woolard, J. Strong, C.R. Erasmus, *Appl. Geochem.*, 17 (2002) 1159-64.
- [27] S. Wang, Y. Boyjoo, A. Choueib, *Chemosphere*, 60 (2005) 1401-17.
- [28] S. Wang, Y. Boyjoo, A. Choueib, Z.H. Zhu, *Water Res.*, 39 (2005) 129-38.
- [29] S. Wang, M. Soudi, L. Li, Z.H. Zhub, *J. Hazard. Mater. B*, 133 (2006) 243-51.
- [30] K.V. Kumar, V. Ramamurthi, S. Sivanesan, *J. Colloid Interface Sci.*, 284 (2005) 14-21.
- [31] L. Li, S. Wang, Z. Zhu, *J. Colloid Interface Sci.*, 300 (2006) 52-59.
- [32] R.Y. Talman, G. Atun, *Colloid Surf. A*, 281 (2006) 15-22.
- [33] M. Matheswaran, T. Karunanithi, *J. Hazard. Mater.*, 145(25) (2007) 154-61.
- [34] S. Wang, H. Li, *J. Hazard. Mater.*, 126 (2005) 71-77.
- [35] K. Ravikumar, S. Krishnan, S. Ramalingam, K. Balu, *Dyes Pigments*, 72 (2007) 66-75.
- [36] Z. Eren, F.N. Acar, *Desalination*, 194 (2006) 1-10.
- [37] A. Srinivasan, W. Grutzeck, *Environ. Sci. Technol.*, 33 (1999) 1464-69.
- [38] X. Querol, N. Moreno, J.C. Umana, et al., *J. Chem. Technol. Biotechnol.*, 77 (2002) 292-98.
- [39] N. Moreno, X. Querol, C. Ayora, C. Fernandez-Pereira, M. Janssen-Jurcovicova, *Environ. Sci. Technol.*, 35 (2001) 3526-34.
- [40] W.U. Deyi, H.U. Zhanbo, X. Wang, H.E. Shengbing, H. Kong, *Front. Environ. Sci. Eng. China*, 1 (2) (2007) 213-20.

- [41] S.S. Rayalu, A.K. Bansiwala, S.U. Meshram, N. Labhsetwar, S. Devotta, *Catal. Surv. Asia*, 10 (2006) 74-88.
- [42] B. Koubaissy, G. Joly, P. Magnoux, *Ind. Eng. Chem. Res.*, 47 (2008) 9558-65.
- [43] B. Koubaissy, J. Toufaily, M. El-Murr et al., *Central European J. of Engin.*, 2(3) (2012) 435-44.
- [44] R. Tailor, B. Shah, A. Shah, *J. Chem. Eng. Data*, 57 (5) (2012) 1437-48.
- [45] J. Xie, W. Meng, D. Wu, Z. Zhang, H. Kong, *J. Hazard. Mater.*, 231-232 (2012) 57-63.
- [46] M. Sougazeh, J.C. Buhl, *J. of the Asso. of Arab Uni. For Basic and Applied Sci.*, 15 (2014) 35-42.
- [47] M. Inada, H. Tsujimoto, Y. Eguchi, N. Enomoto, J. Hojo, *Fuel*, 84 (2005) 1482-86.
- [48] C. Covarrubias, R. Garcia, R. Arriagada, J. Yanez, M.T. Garland, *Microp. Mesop. Mater.*, 88 (2006) 220-31.
- [49] L.B. Mc Cusker, Ch. Baerlocher, *Z. Kristallogr.*, 171 (1985) 281-89.
- [50] S.J. Gregg, K.S.W. Sing, *Adsorption*, in: *Surface Area and Porosity*, 2nd ed., Academic Press, London, 1982.
- [51] P.K. Malik, *Dyes Pigments*, 56 (2003) 239-49.
- [52] V. S. Mane, I. D. Mall, V. C. Srivastava, *J. of Environ. Manag.*, 84 (2007) 390-400.
- [53] E. Tutem, R. Apak, C.F. Unal, *Water Research*, 32 (1998) 2315-24.
- [54] D. Rameshraj, V.C. Srivastava, J.P. Kushwaha, I.D. Mall *Chem. Eng. J.*, 181-182 (2012) 343-51.
- [55] K.Vijayraghvan, T.V. Padmesh, *J. of Hazard. Mater.*, 133 (2006) 304-8.
- [56] S. Kumar, M. Zafar, J.K. Prajapati, S. Kumar, S. Kannepalli, *J. Hazard. Mater.*, 185 (2011) 287-94.
- [57] R.M. Aghav, S. Kumar, S.N. Mukherjee, *J. Hazard. Mater.*, 188 (2011) 67-77.
- [58] E. Bayram, N. Hoda, E. Ayranci, *J. of Hazard. Mater.*, 168 (2009) 1459-66.



Chapter-5

Adsorption of Resorcinol from Aqueous Solution onto CTAB / NaOH / Fly Ash Composites: Equilibrium, Kinetics, Thermodynamics and Modeling

ABSTRACT

NaOH treated coal fly ash (NaFA) was modified with cetyltrimethylammonium bromide (CTAB) and was examined for the adsorption of resorcinol from aqueous solutions. The resorcinol adsorption efficiencies for fly ash (FA), NaOH treated fly ash (NaFA) and surfactant modified NaOH treated fly ash (CTAB / NaOH / fly ash composite) were compared. CTAB / NaOH / fly ash composite presented higher resorcinol adsorption efficiency than FA and NaFA. This may be attributed to the hydrophobicity imparted by surfactant molecules on the surface of NaFA, consequently leading to organic partitioning. The adsorption of resorcinol onto CTAB / NaOH / fly ash composite as a function of initial resorcinol concentration, contact time, initial adsorbent dosage, temperature, ionic strength and solution pH were investigated for their optimization. The rate of adsorption of resorcinol was found to be maximum at 6.8. The adsorbents were characterized by x-ray diffraction (XRD), field emission scanning electron microscope (FE-SEM), surface area and porosity measurement, Fourier transform infrared (FT-IR) etc. The adsorption kinetics of resorcinol onto CTAB / NaOH / fly ash composite followed a pseudo-second order model. The equilibrium adsorption data were best fitted by Redlich-Peterson isotherm. The resorcinol adsorption capacity for CTAB / NaOH / fly ash composite slightly decreased with increasing ionic strength adjusted by NaCl. The adsorption was relatively high at solution pH 5.0-6.8 and decreased with an increase in solution pH from 7.0-11.0. The value of ΔG° , ΔS° and ΔH° indicated spontaneous and endothermic adsorption process.

5.1 Introduction

Water pollution by organic chemicals is a major problem over decades. Owing to this, there is growing public concern over the contamination of groundwater by organic compounds. The removal of organic contaminants from groundwater or separation of contaminants present in polluted water has become a major focus of research and policy debate. The presence of these compounds even at low concentrations can be an obstacle for reuse of water [1, 3]. These organic compounds constitute a very large group of pollutants in the wastewater. Amongst them aromatic compounds especially phenol and its derivatives such as resorcinol, catechol and cresols are widely found in the effluent of many industries [2, 3]. As described previously resorcinol is found in the effluents of many industries such as textile, paper and pulp, steel, petrochemical, petroleum refinery, rubber, dyes, plastics, pharmaceutical, cosmetics etc., and in synthetic coal fuel conversion process wastewater [5].

Phenolic compounds are very harmful to organisms even at very low concentration due to their toxicity, foul odour and carcinogenic properties [6, 8]. The health effects following repeated exposure to low levels of phenol in water include liver damage, diarrhoea, mouth ulcers, dark urine and hemolytic anemia [7, 8]. Ministry of Environment and Forest (MOEF), Govt. of India, New Delhi and United States Environmental Protection Agency (USEPA) has listed phenol and phenolic compound under priority pollutants list. As per the Bureau of Indian Standards, New Delhi, India, the allowable limit of phenol in drinking water is 1mg/L while MOEF (Govt. of India) has set a maximum concentration level of 1 mg/L of phenol in the industry effluents for safe discharge into inland surface water and 5 mg/L for safe discharge into public sewers and marine coastal areas [8]. The World Health Organization (WHO) recommended 0.001 mg/L as the permissible phenolic concentration in portable water. It is therefore necessary to reduce or to eliminate phenols from water and wastewater before discharge or reuse.

Various treatment methods are available for removal of phenolic compounds which include adsorption, ion exchange, reverse osmosis, chemical

oxidation, precipitation, distillation, gas stripping, solvent extraction, complexation and even bioremediation [9]. Various adsorbents such as mesoporous MCM-41 [1], parthenium based activated carbon [2], granular activated carbon [3], synthetic resin [4], coconut shell [6], agricultural waste material [7], carbonaceous adsorbents [8] and bagasse ash and wood charcoal [9] have been reported for removing resorcinol and phenolic compounds by adsorption from water and wastewater.

Surface-modified zeolite materials have been developed from commercial zeolite, and fly ash-based zeolite, by treating it with surface modifiers, such as, hexadecyltrimethylammonium bromide and tetramethylammonium bromide [10]. The adsorbent was evaluated for removal of arsenic and chromate anions. High selectivity, faster kinetics and high adsorption capacity ensure cost effectiveness of these materials compared to other conventional materials for de-arsenification. Surface modified zeolite from fly ash is being used for adsorption of phenol and o-chlorophenol from wastewater [11]. The comparison of adsorption of phenol and o-chlorophenol on commercial zeolite-Y, fly ash based zeolite (FAZ-Y) and surface modified fly ash based zeolite (SMZ-Y) were studied. Adsorption of phenol on SMZ-Y was 4.05 and 3.24 times higher than the FAZ-Y and commercial zeolite-Y, respectively. For o-chlorophenol, the efficiency is higher by a factor of 2.29 and 1.8 for FAZ-Y and commercial zeolite-Y, respectively. This may attributed to hydrophobicity imparted by surfactant molecules on the surface of fly ash zeolite, consequently leading to organic partitioning. The presence of salts has a substantially detrimental effect on adsorption of phenol and o-chlorophenol.

zeolites have a net permanent negative charge resulting from isomeric substitution of Si^{4+} by Al^{3+} , cationic surfactants such as hexadecyltrimethylammonium bromide (HTAB) and cetylpyridinium bromide (CPB) are suitable for surface modification of zeolites [12-23]. The positive head groups of cationic surfactants readily exchange with the exchangeable cations on the external surface of zeolites, forming surfactant monolayers [18]. In properly chosen conditions, the loaded cationic surfactants on the external surface of

zeolite form bilayers, where the upper layer is bound to the lower layer by the hydrophobic interaction between the tail groups of surfactants in both layers [16]. Surfactant-modified zeolites (SMZs) have been investigated as adsorbents for removing various pollutants such as chromate [13], arsenate [14], phosphate [15], nitrate [16], phenol [17], 4-chlorophenol [17], volatile petroleum hydrocarbons [18], orange II [19], bisphenol A [20], fulvic acid (FA) [21], humic acid (HA) [22] and sodium.

In the present work a systematic study of the adsorption capacity of resorcinol from aqueous solution by CTAB / NaOH / fly ash composite is reported. The effects of several experimental parameters such as contact time, initial adsorbate dosage, initial adsorbent concentration, temperature, ionic strength and solution pH on resorcinol adsorption onto CTAB / NaOH / fly ash composite were investigated. The experimental results were analyzed by kinetic and isotherm models. Thermodynamic parameters such as Gibbs free energy change (ΔG°), enthalpy change (ΔH°) and entropy change (ΔS°) were calculated. The mechanism for resorcinol adsorption onto CTAB / NaOH / fly ash composite is also proposed.

5.2 Materials and methods

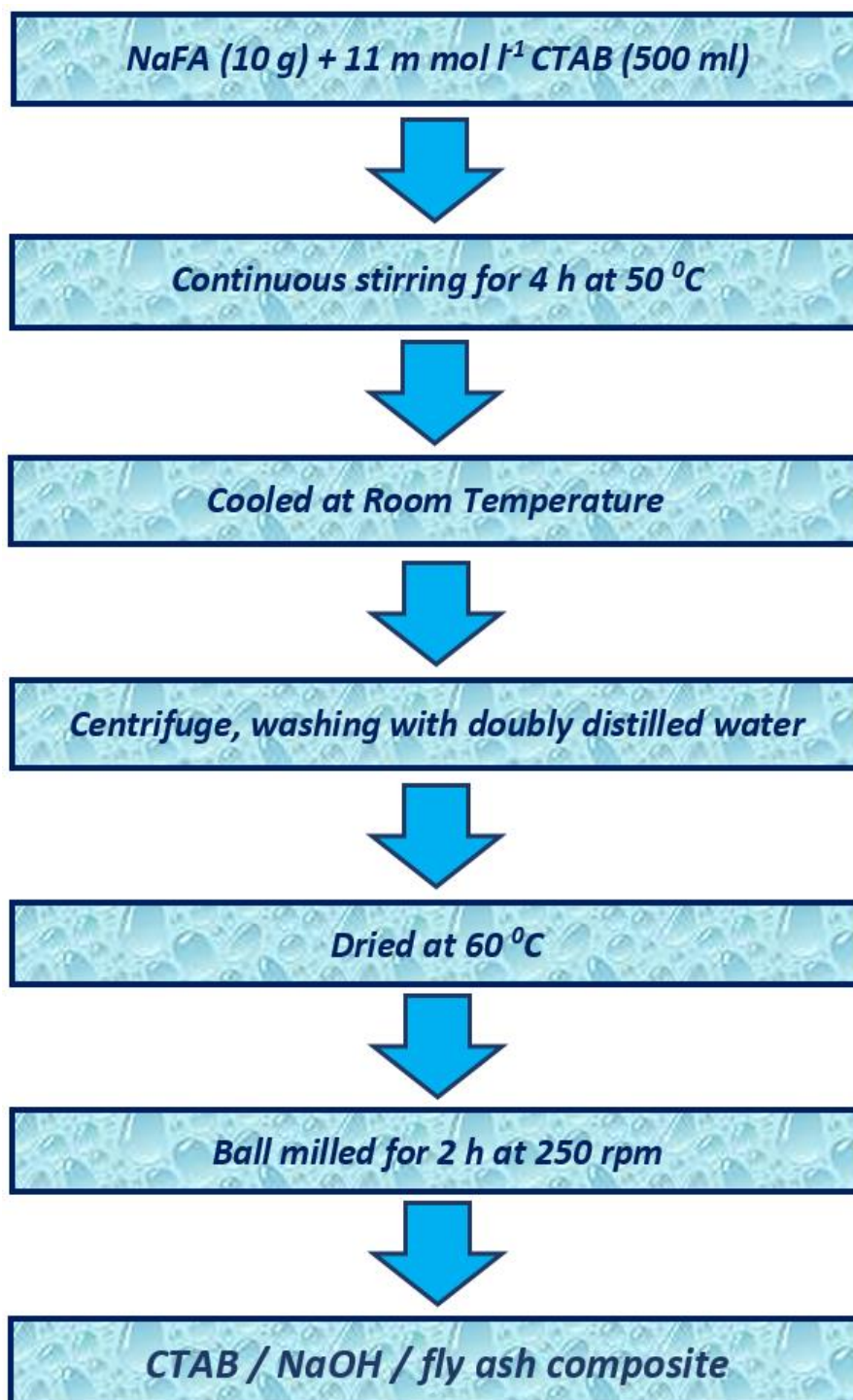
5.2.1 Materials

Fly ash (Class F Type with SiO_2 and $\text{Al}_2\text{O}_3 > 70\%$) was obtained locally from Sriram Fertilisers & Chemical Ltd. (Kota, Rajasthan, India). N-Cetyl-N, N, N-Trimethyl Ammonium Bromide (CTAB) of LOBA Chemi. was purchased as described in chapter 2.

5.2.2 Synthesis of CTAB / NaOH / fly ash composite

For synthesis of CTAB / NaOH / fly ash composite, 500 mL of the solution of the surfactant, Cetyltrimethylammonium bromide (CTAB), with a concentration of 11 mmol L^{-1} was vigorously mixed with 10 g of NaFA (synthesized the procedure described in chapter 4) at 50°C for 4 h. These reaction conditions were adopted to assure high loading of surfactant. After being cooled to room temperature, the product was centrifuged, washed with doubly

distilled water, dried in an oven at 60 °C and ball milled in high energy planetary ball mill with ball to powder ratio of 10:1 for 2 h at 250 rpm. Schematic presentation of synthesis of CTAB / NaOH / fly ash composite is shown in Scheme 5.1.



Scheme 5.1: Synthesis of CTAB / NaOH / fly ash composite

5.2.3 Adsorption experiments

Resorcinol was selected to assess the decontamination performance by CTAB / NaOH / fly ash composite. So that a clear out comparison can be observed on resorcinol removal after loading surfactant on NaOH / fly ash described in chapter 4.

5.3 Result and discussion

5.3.1 Characterization of Adsorbent

The primary mineralogical constituents of NaFA and CTAB / NaOH / fly ash composite like Silica, alumina and sodium contents are shown in the [Table 5.1](#). EDX spectrum of NaFA and CTAB / NaOH / fly ash composite shown in [Figure 4.2](#) (chapter 4) and [Figure 5.1](#) respectively. The amount of silica and alumina of CTAB / NaOH / fly ash composite were higher than NaFA.

(i) *Field emission scanning electron microscopy (FE-SEM)*

[Figure 5.2](#) shows the field emission scanning electron microscopy (FE-SEM) images of CTAB / NaOH / fly ash composite. Upon formation of NaFA, the surface of fly ash became rough, indicating the deposition of clusters of zeolitic material (as described in chapter 4) and developed crystalline tubular habits. The morphological difference between CTAB / NaOH / fly ash composite and NaFA was observable. After loading of CTAB on to NaFA, the surface of zeolitic crystal were covered with an organic layer and the crystalline depositions seen in [Figure 4.5 \(b\)](#), Chapter 4 were completely disappeared.

Table 5.1: Chemical composition and properties of NaFA and CTAB / NaOH / fly ash composite Study

Parameter	NaFA (Wt%) (by EDX)	CTAB / NaOH / fly ash composite (Wt%) (by EDX)
SiO ₂ (%)	36.39	40.25
Al ₂ O ₃ (%)	5.99	7.66
Fe ₂ O ₃ (%)	2.79	4.06
CaO (%)	4.35	5.97
MgO (%)	0.23	0.28
Na ₂ O (%)	9.42	7.89
K ₂ O (%)	0.45	0.24
Moisture (%)	4.5	5.1
TiO ₂	0.69	0.67
TCEC (mmol g ⁻¹)	1.02	0.815
pH _{ZPC}	10.1	7.3
ECEC (mmol g ⁻¹)	0.068	0.051
Surface area of pores (m ² /g)		
(i) BET	18.2875	51.1207
(ii) BJH		
a. Adsorption cumulative	15.6483	53.1196
b. Desorption cumulative	165528	63.6179
BJH Cumulative Pore Volume (cm ³ /g)		
(i) Single Point Total	0.102599 ^a	0.176996 ^b
(ii) BJH Adsorption	0.100457 ^c	0.169049 ^c
(iii) BJH desorption	0.102793 ^c	0.178586 ^c
Average pore diameter (Å)		
(i) Single Point Total	224.4138	138.4928
(ii) BJH Adsorption	256.7875	127.2969
(iii) BJH desorption	248.3996	112.2868

^aPores less than 821.9909 Å diameter^bPores less than 769.8010 Å diameter^cPores between 17.00 Å and 3000.00 Å diameter

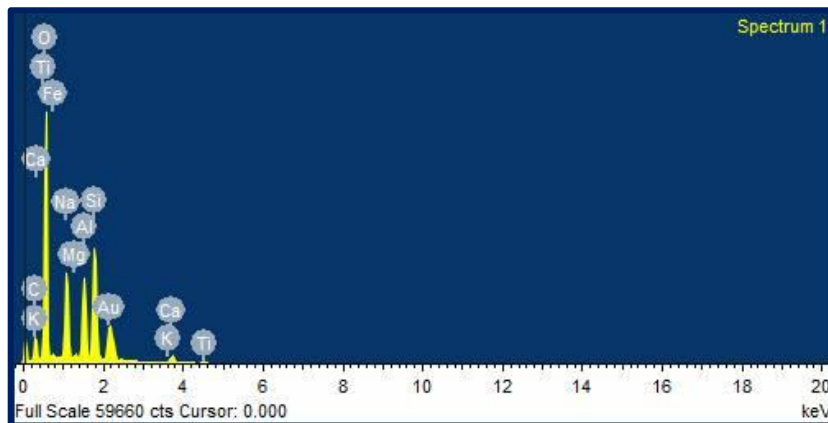
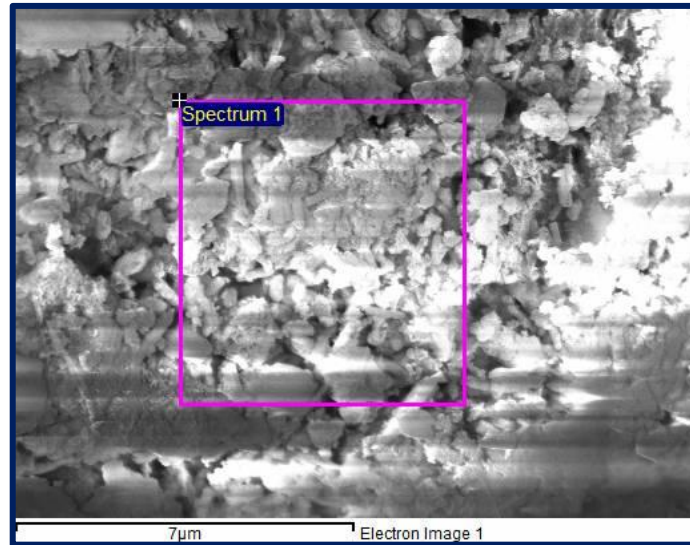


Figure 5.1: EDX Spectrum of CTAB / NaOH / fly ash composite

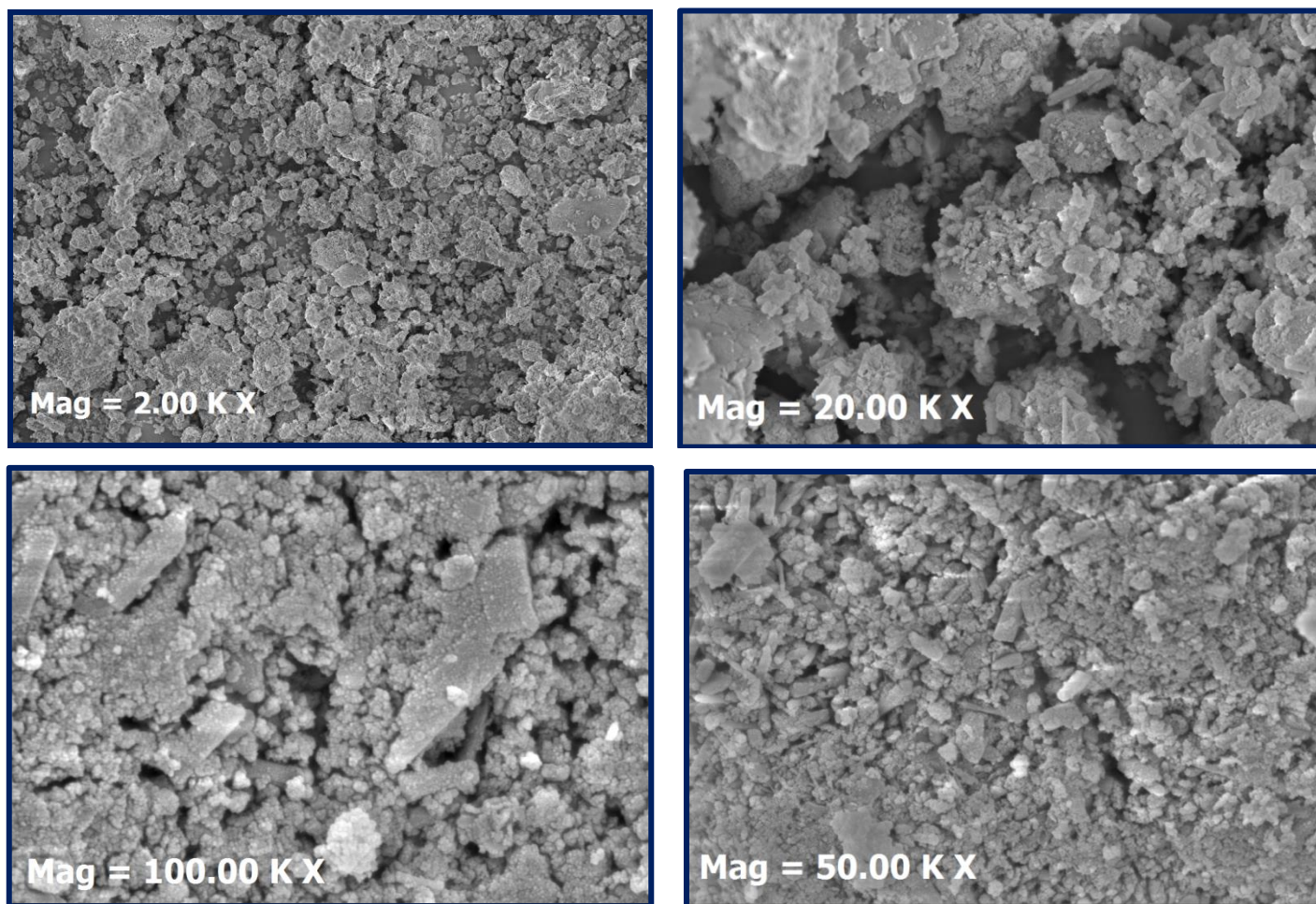


Figure 5.2: The FE-SEM images of CTAB / NaOH / fly ash composite at different magnitude

(ii) *Fourier Transformed Infrared (FTIR) Spectra*

Figures 5.3 (a & b), show a broad band between 3600-3300 cm^{-1} , which is attributed to surface -OH groups of -Si-OH and adsorbed water molecules on the surface of NaFA and and CTAB / NaOH / fly ash composite. The broadness of the band is due to the strong hydrogen bonding. The hydroxyl groups do not exist in isolation and a high degree of association is experienced as a result of extensive hydrogen bonding with other hydroxyl groups. A peak at 1639 cm^{-1} present in both is attributed to bending mode (δ O-H) of water molecule.

Formation of silicoaluminate crystalline material in NaFA and CTAB / NaOH / fly ash composite was confirmed by Fourier transformed infrared (FTIR) spectra (Figure 5.3a & b and Table 5.2), an increase in tetrahedral Al (formation of zeolitic phases) would induce a shift of the band within the range of 1180–950 cm^{-1} (which is assigned to the asymmetric internal T-O stretching vibration mode of the TO_4 tetrahedra, where T = Si or Al) to a lower wavenumber [24]. The FTIR absorption bands at 2856 and 2926 cm^{-1} (Figure 5.3b), which are attributed to the symmetric and asymmetric stretching vibrations of C-C in the alkyl chain of CTAB, indicate that CTAB formed a bilayer micelle, rather than monolayer coverage [25]. The frequency band at 1474 cm^{-1} is assigned to antisymmetric bending mode of the quaternary ammonium (alkyl) mode of the head methyl group ($(\text{CH}_3)_3\text{N}^{+-}$) as reported earlier [26]. However, the slight difference between this results and 2918-2849 cm^{-1} obtained by earlier study [27] might be due to the differences in the purity of the CTAB used in the analysis. The intense peaks is for CTAB / NaOH / fly ash composite at 2856 cm^{-1} observed as compared with 2864 cm^{-1} in the pure CTAB spectra and confirmed the presence of CTA⁺ in the modified fly ash. After the NaFA had been treated with CTA⁺ the absorption band at 3525 cm^{-1} for OH- groups became smaller and appeared at 3511 cm^{-1} . These observations can be interpreted as being the consequence of CTA⁺ exchanging the Na⁺ groups of the crystal structure of the NaFA. Also, the absorption band at 2894–2827 cm^{-1} of NaFA shifted to 2926-2856 for CTA⁺ loading can be considered as belonging to the C-H groups of CTA⁺ in free position in the NaFA (bonded in various ways to the NaFA).

Table 5.2: Comparison and shifting of bands data for NaFA and CTAB / NaOH / fly ash composite in FTIR spectroscopy

Wave number (cm ⁻¹)	Possible assignment	Observed Value (cm ⁻¹)	
		NaFA	CTAB / NaOH / fly ash composite
3600 - 3300	Stretching vibration of –OH group, Silanol (Si-OH)	3525.1	3511
3000-2800	symmetric and asymmetric stretching vibrations of C-C	2894 2827	2856 2926
1700 - 1400	–OH deformation & bending vibration of interstitial water	1639.13 1488.84	1638 1474.60
1250 - 850	Asymmetric stretching of internal tetrahedral TO ₄ , Si-O-Si (T=Si, Al)	978.92	985.24
720 - 650	Symmetric stretching of internal tetrahedral TO ₄ (T=Si, Al)	687.39	689.23

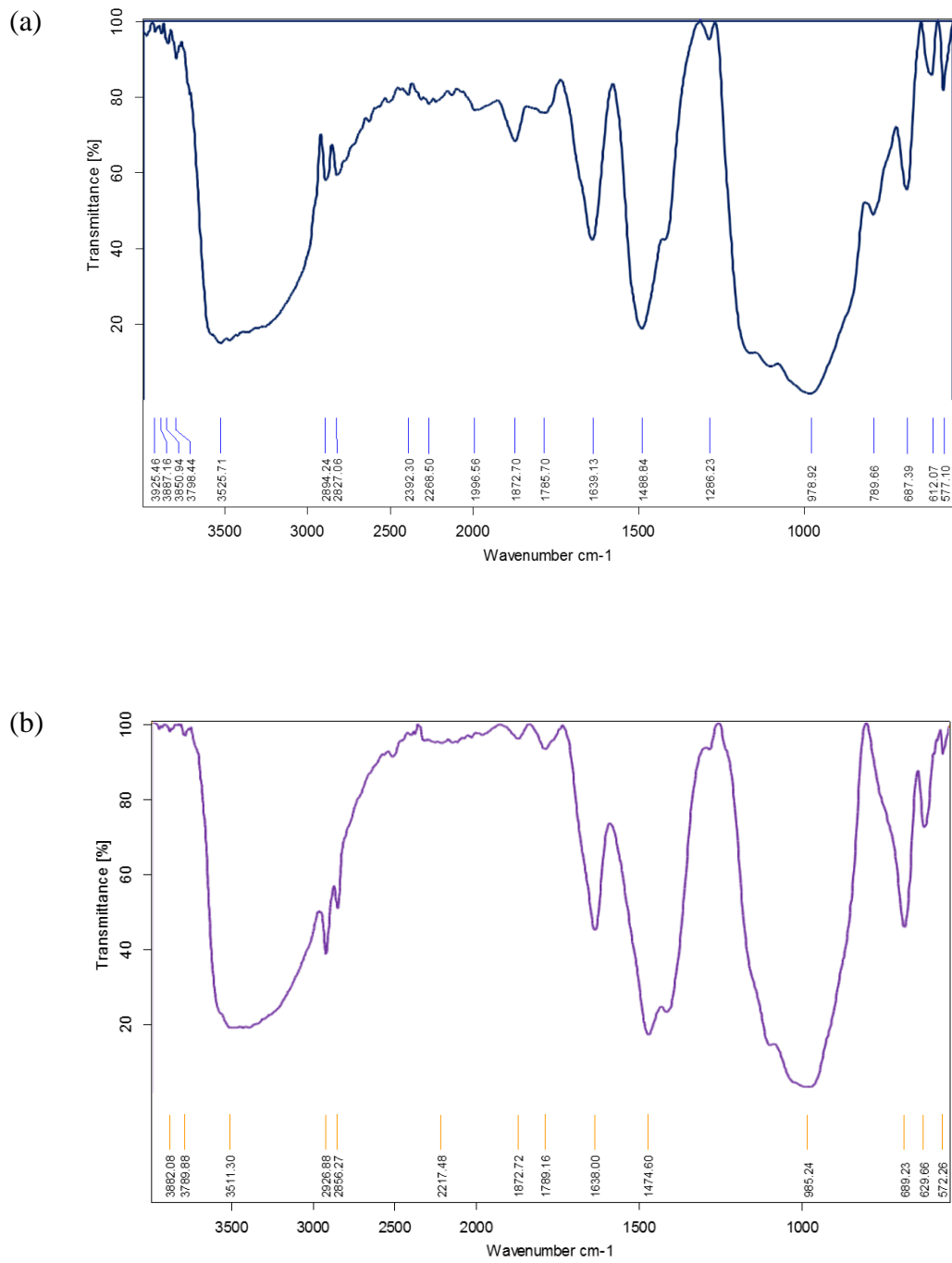


Figure 5.3: The FTIR patterns for (a) NaFA and (b) CTAB / NaOH / fly ash composite

(iii) X-ray diffraction (XRD) Study

The XRD patterns of NaFA and CTAB / NaOH / fly ash composite are shown in Figure 5.4 and XRD details of these adsorbents are shown in Table 4.4 (Chapter 4) and Table 5.3. XRD of NaFA show some zeolitic fraction confirmed by the XRD peaks at about 27° and 28° , 2θ . The Presence of CTA^+ ion on NaFA surface confirmed by first strong peak increased slightly the d-spacing of NaFA (Table 5.4). Mullite and quartz in NaFA and CTAB / NaOH / fly ash composite were also confirmed.

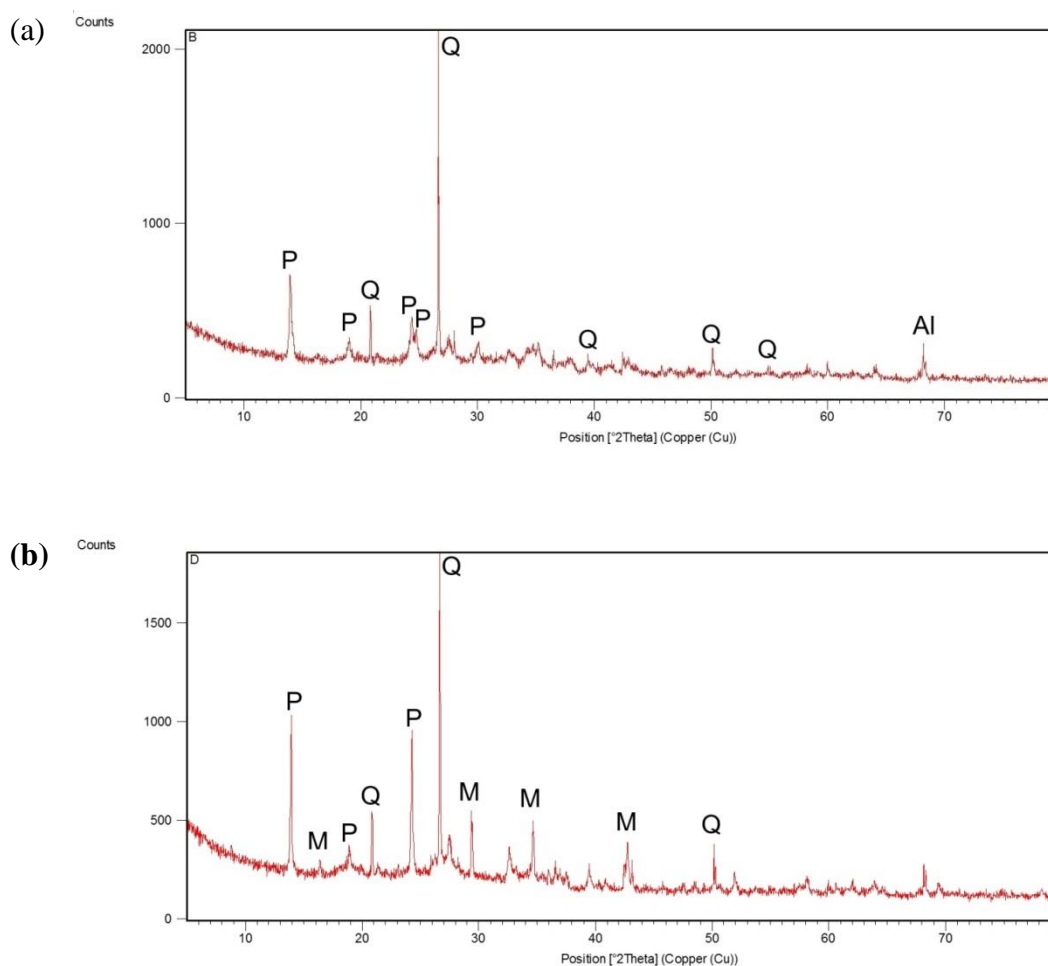


Figure 5.4: The XRD patterns for (a) NaFA and (b) CTAB / NaOH / fly ash composite, (where Q, quartz; M, mullite; Al, aluminium; P, zeolitic phase)

Table 5.3: XRD details of CTAB / NaOH / Fly ash composite

Pos. [°2Th.]	FWHM [°2Th.]	d-spacing [Å]	Rel. Int. [%]	Area [cts*°2Th.]
13.9271	0.0836	6.35364	52.97	65.53
16.3742	0.2007	5.40919	3.64	10.81
18.8661	0.1338	4.69995	8.62	17.07
20.8401	0.0836	4.25900	21.57	26.68
24.2574	0.1338	3.66620	49.09	97.17
26.6127	0.1004	3.34684	100.00	148.47
27.4632	0.2342	3.24509	12.94	44.83
29.3490	0.0669	3.04073	21.81	21.59
32.5581	0.1338	2.74797	11.31	22.39
34.6124	0.1171	2.58943	21.30	36.89
35.9753	0.2007	2.49439	4.96	14.73
37.4929	0.2007	2.39684	4.66	13.84
39.4021	0.1338	2.28499	6.75	13.35
42.6849	0.1171	2.11655	15.55	26.93
43.1168	0.0612	2.09634	9.84	12.04
48.4537	0.4015	1.87717	2.06	12.21
50.1542	0.0612	1.81744	15.75	19.27
51.9174	0.1224	1.75979	6.27	15.35
58.1721	0.2448	1.58458	4.10	20.08
62.0793	0.6528	1.49390	2.00	26.14
63.9044	0.4896	1.45556	2.78	27.19
68.1364	0.0612	1.37509	10.38	12.71
68.3181	0.0816	1.37188	8.52	13.90
69.3846	0.2856	1.35338	3.56	20.34
78.2715	0.4896	1.22045	2.16	21.14

Table 5.4: Comparison between XRD Peak and d-spacing of NaFA and CTAB / NaOH / fly ash composite

Adsorbent	d-spacing (Å)	2θ (degree)	Intensity (Counts)
NaFA	6.33671	13.9751	24.54
CTAB / NaOH / fly ash composite	6.35364	13.9271	52.97

(iv) Cation exchange capacity and pH_{ZPC}

The Total cation exchange capacity (TCEC) and external cation exchange capacity (ECEC) of NaFA are 1.02 & 0.068 respectively and for CTAB / NaOH / fly ash composite are 0.815 & 0.051 respectively as shown in Table 5.1. ECEC also shown by Figure 4.3(b) (Chapter 4) and Figure 5.5 respectively. The comparison of the TCEC value of a NaFA with that of a pure zeolite may provide a semiquantitative estimate of the zeolite content in the NaFA given that the NaFA contained only one kind of zeolite. The external surface was used to load CTAB because the pore size of NaFA is too small for the CTAB cation to enter. The amount of CTAB loaded was determined to be 0.141mmol g⁻¹ based on the difference in the carbon content between CTAB / NaOH / fly ash composite and NaFA. This was nearly twice as the amount of ECEC, indicating that CTAB formed a bilayer micelle on the external surface of NaFA. The pH_{ZPC} of NaFA and CTAB / NaOH / fly ash composite are 10.1 & 7.3 as shown in Figure 4.4(b) (Chapter 4) and Figure 5.6 respectively.

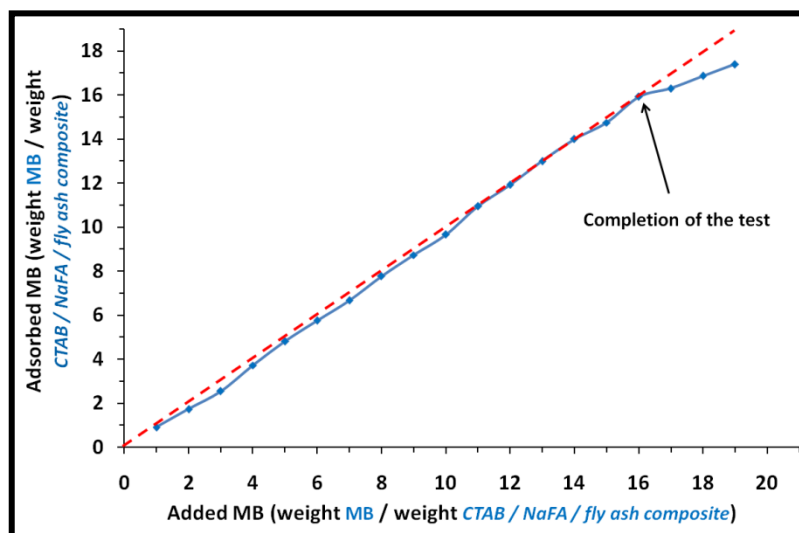


Figure 5.5: The determination of the point of complete replacement of cations from the titration curve (CTAB / NaFA / fly ash composite)

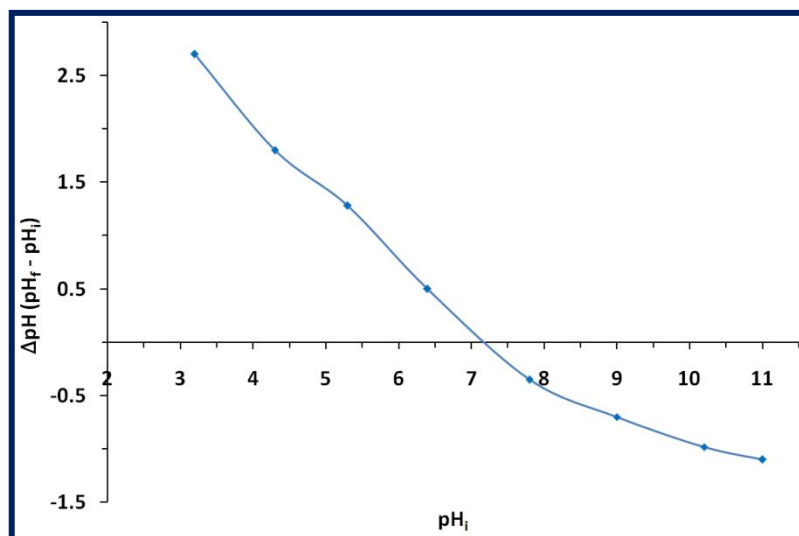


Figure 5.6: Point Zero Charge of CTAB / NaFA / fly ash composite

(v) *Surface area and porosity*

Figure 5.7 (a & b) show the N₂-adsorption/desorption isotherm and surface area plot of the CTAB / NaOH / fly ash composite respectively. The combination of type II and type IV adsorption isotherm (Figure 5.7a) are encountered for CTAB / NaOH / fly ash composite with a typical adsorbate uptake starting at 0.5 p/p₀ and this isotherm implies the mesoporous and micropores (with additional external surface area) structure of materials according to the IUPAC and Brunauer, Deming, Deming & Teller (BDDT) classification [28]. The pore-size distribution of the CTAB / NaOH / fly ash composite shown in Figure 5.7 (d) have been calculated from the adsorption branch of the isotherm by the BJH method. The mesoporous CTAB / NaOH / fly ash composite exhibits smaller mesopores (2±2.5 nm) associated with larger micropores (1±2 nm) according to the BJH method. The specific surface area of the adsorbents by BET methods shows the following order CTAB / NaOH / fly ash composite (51.1207 m²g⁻¹ > NaFA 18.2875 m²g⁻¹), which indicates that the specific surface area is increased drastically due to the surfactant loading on NaFA. BET average pore diameters were 22.44 nm and diameter 13.85 nm of NaFA and CTAB / NaOH / fly ash composite respectively. The analysis of BJH average adsorption/desorption pore diameter values of adsorbents (Table 5.1) lies between 2 nm to 50 nm. As the pore diameter increases the pore volume (NaFA: 0.102793 cm³g⁻¹ < : CTAB / NaOH /

fly ash composite $0.1769960 \text{ cm}^3 \text{ g}^{-1}$) also increases due to that the adsorption capacity of CTAB / NaOH / fly ash composite increases than that of NaFA.

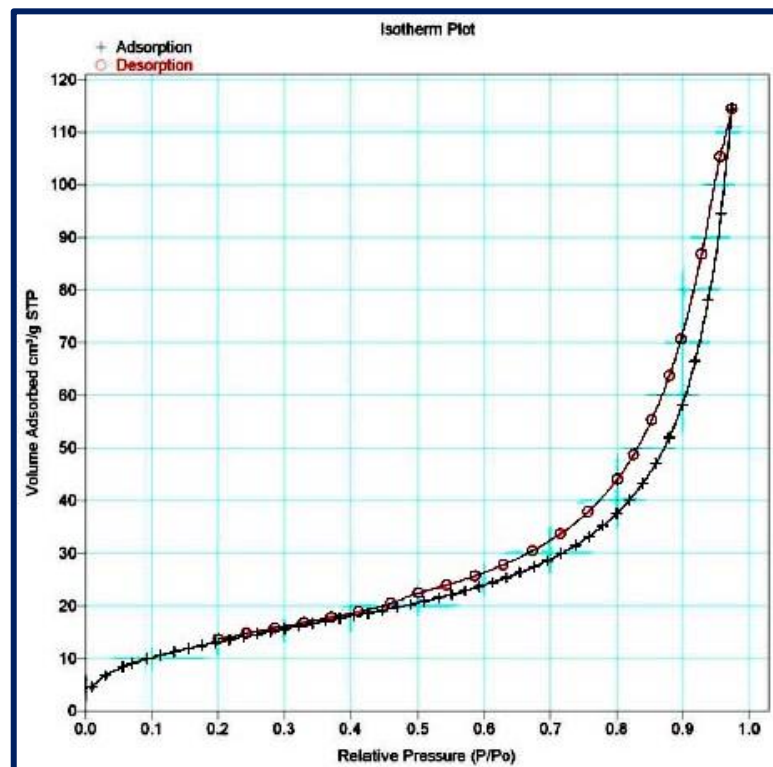


Figure 5.7(a): Adsorption isotherms of nitrogen at 77 K for CTAB / NaOH / fly ash composite

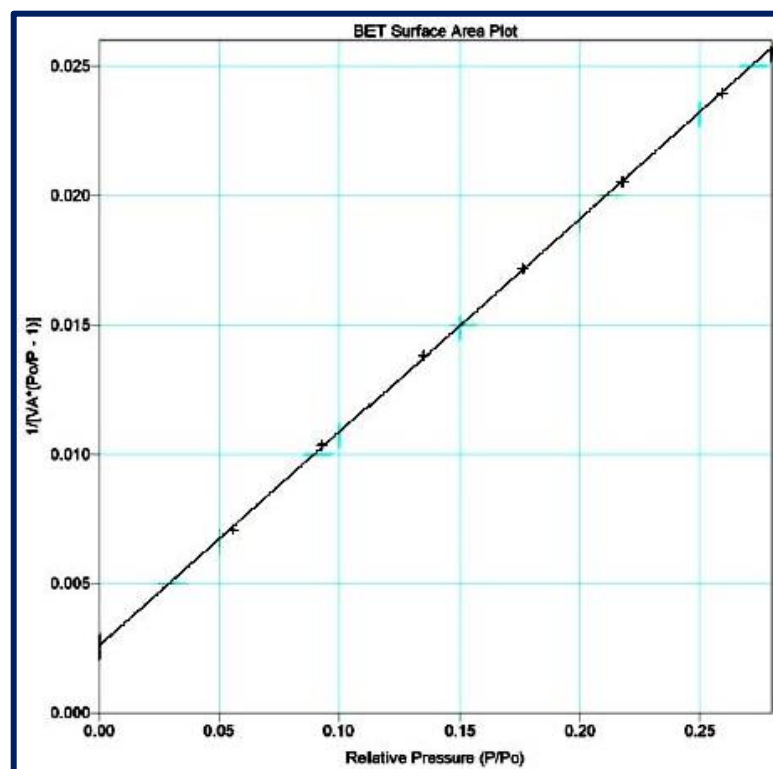


Figure 5.7(b): Surface area plot for CTAB / NaOH / fly ash composite

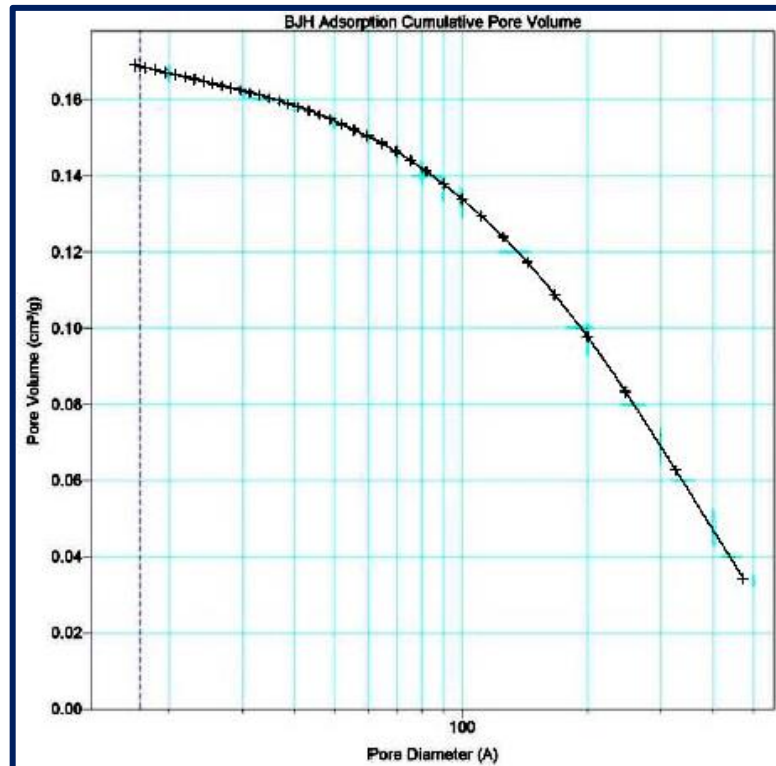


Figure 5.7(c): Pore-size distribution (BJH Adsorption Cumulative Pore Volume) for CTAB / NaOH / fly ash composite

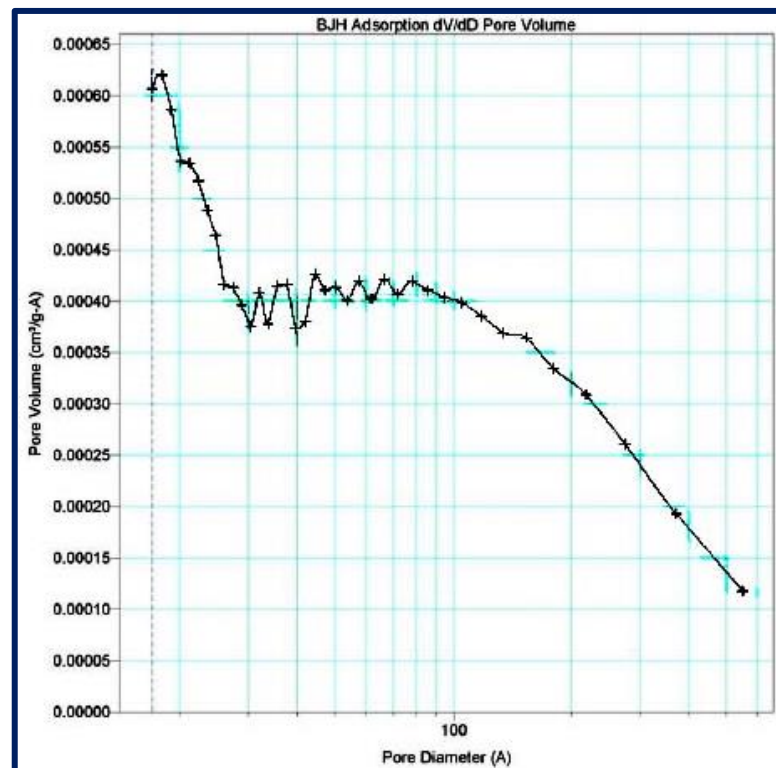


Figure 5.7(d): Pore-size distribution (BJH Adsorption dV/dD Pore Volume) for CTAB / NaOH / fly ash composite

5.3.2 Effect of surfactant loading on NaFA

When NaFA is mixed with the surfactant solution having concentration less than its critical micelle concentration ($9 \times 10^{-4} \text{mmoles l}^{-1}$)[29] then the surfactant molecule forms a monolayer on the external surface of NaFA via exchange. If the concentration of surfactant is increased then it forms micelle which attaches itself in a patchy layer and subsequently rear-ranges to form a second layer over the first layer via hydrophobic tail to tail interaction of surfactant due to weak Vander Walls cohesive forces. Due to this tail-to-tail interaction, an organic fraction is created over the NaFA surface, which is responsible for trapping organic hydrophobic pollutants like phenolics. Figure 5.8 reveals the schematic representation of mechanism of adsorption of resorcinol by CTAB / NaOH / fly ash composite. The effect of surfactant loading on removal of resorcinol was given in Table 5.5. It was found that the resorcinol adsorption efficiency was increase with increase loading amount of CTAB on NaFA. After surfactant loading with 11 mmol l^{-1} there was no more increase in adsorption efficiency due to excessive crowding of monomers of surfactant molecule on external surface of NaFA, which might have blocked the organic partitioning created by tails of long chain alkyl compound for adsorption of organics. Therefor CTAB / NaOH / fly ash composite with mmol l^{-1} loading amount of CTAB was the most efficient adsorbent for the removal of resorcinol from aqueous solution.

Table 5.5: Effect of surfactant loading on NaFA on adsorption capacity of resorcinol

NaFA dose (g)	CTAB concentration (mmol l^{-1})	Surfactant Loading (mmol l^{-1})	Adsorption capacity of resorcinol (mg/g)
10	2	0.032	70.1
10	4	0.045	82.2
10	6	0.062	90.05
10	8	0.096	95.2
10	11	0.141	102.25
10	15	0.201	102.85

($m = 0.4 \text{ g l}^{-1}$, agitation rate = 200 rpm, pH = 6.8, $C_0 = 50 \text{ ppm}$, $T = 303\text{K}$, $t = 24\text{hr}$)

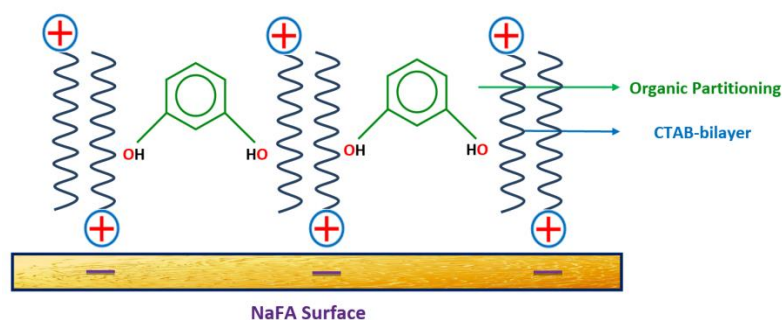



Figure 5.8: Schematic representation of adsorption of resorcinol on CTAB / NaOH / fly ash composite

(Interaction mechanisms of resorcinol, as an example of organic pollutants, with CTAB / NaOH / fly ash composite. In this figure, the meaning of the symbols are as follows: \oplus the head of CTAB; \sim The C-16 chain of CTAB;  NaFA in which $-$ represents the negative charge and show the interaction between the hydrophobic benzene ring of organic pollutants and the hydrophobic C-16 chain of CTAB as a function to contribute in adsorption.)

5.3.3 Effect of various parameters on adsorption of resorcinol

(i) Preliminary adsorption experiments

The preliminary adsorption experiments under identical set of experimental conditions were carried out using FA, NaFA and CTAB / NaOH / fly ash composite. The adsorption capacity of resorcinol by FA, NaFA and CTAB / NaOH / fly ash composite are shown in Figure 5.9. It was observed that the removal efficiency of FA and NaFA is significantly less as compared to CTAB / NaOH / fly ash composite. This may be attributed to the hydrophobicity imparted by surfactant leading to organic partitioning. In this chapter, CTAB / NaOH / fly ash composite was used for optimization of adsorption parameters.

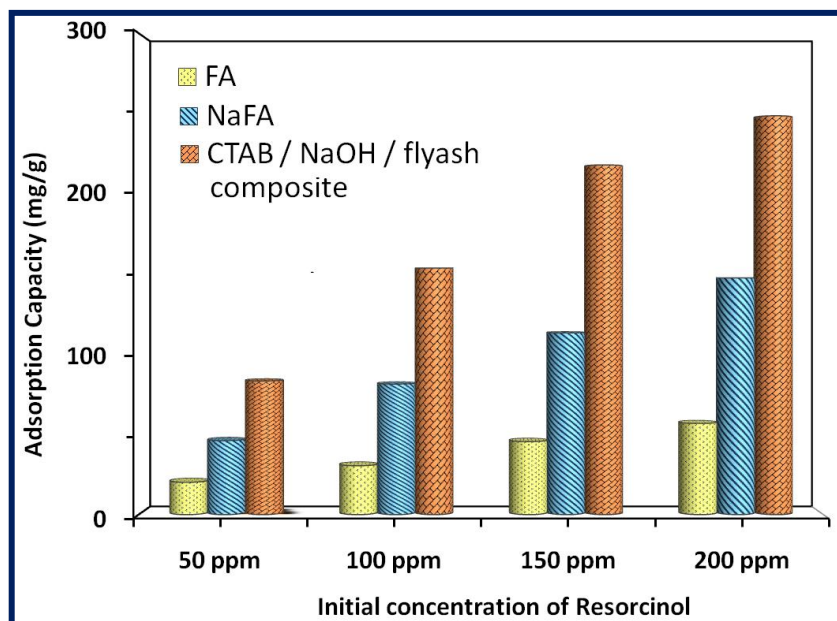


Figure 5.9: Comparison of removal of resorcinol using FA, NaFA & CTAB / NaOH / fly ash composite ($C_0 = 100 \text{ mg/l}$, $\text{pH} = 6.8$, $t = 24 \text{ h}$)

(ii) *Effect of adsorbent dosage*

The adsorption of resorcinol on CTAB / NaOH / fly ash composite was carried out at different adsorbent dosage by keeping other parameters constants. The relationship between adsorbent dose and contact time for resorcinol removal at same initial concentration is presented in Table 5.6 & Figure 5.10. It can be seen that the % removal of resorcinol increased with increase adsorbent dose due to greater surface area and availability of more adsorption site while adsorption capacity (amount of resorcinol loaded per unit weight of adsorbent) of resorcinol gradually decreased for same. This decrease in adsorption capacity is due to availability of lower number of solutes (resorcinol) per unit mass of adsorbent, i.e. lower solute/adsorbent ratio. These experiments were performed with initial concentration of 100 mg L^{-1} of solutes, temperature $30 \text{ }^\circ\text{C}$ and $\text{pH} 6.8$ of the solution. It can be concluded that the rate of resorcinol/ binding with adsorbent increases more rapidly in the initial stages and after some time the adsorption is marginal and becomes almost constant.

Table 5.6: Effect of adsorbent dose on adsorption capacity of CTAB / NaOH / fly ash composite for resorcinol adsorption

Time (min)	Adsorption Capacity (mg/g)			
	m = 0.5 g/l	m = 1 g/l	m = 1.5 g/l	m = 2 g/l
5	96.84	50.64	39.07	32.5
10	101.28	55.32	44.41	35
15	106.2	57.78	46.09	36.1
30	110.18	58.72	47.8	37
60	118.02	61.93	49.44	38.5
90	122.8	64.85	51.35	40
120	130.06	67.24	53.25	41
300	153.68	83.33	59.33	46.5
600	153.68	83.33	59.33	46.5

(T = 303 K, pH = 6.8, C₀ = 100 mg/l)

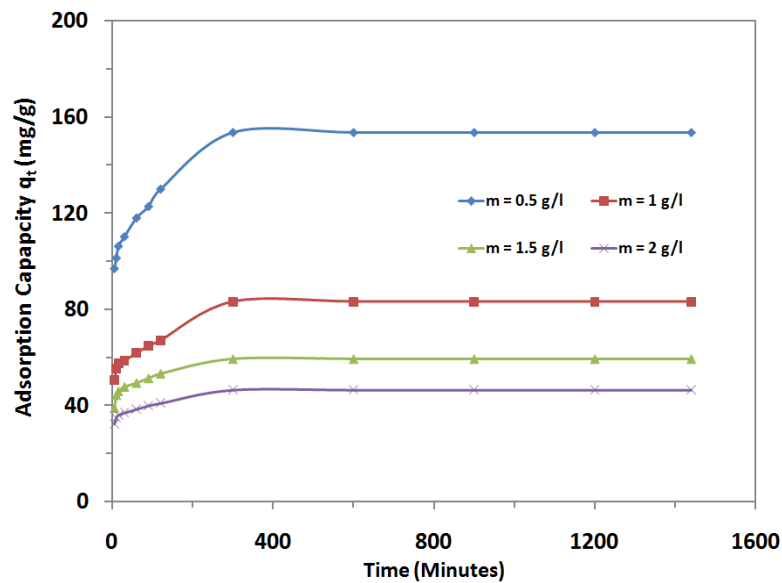


Figure 5.10: Effect of adsorbent dose on adsorption capacity of CTAB / NaOH / fly ash composite for resorcinol adsorption
(T = 303 K, pH = 6.8, C₀ = 100 mg/l)

(iii) *Effect of contact time and initial concentration*

The effect of contact time for removal of resorcinol Table 5.7 & (Figure 5.11) showed rapid adsorption in first 30 min. and thereafter the adsorption rate decreased gradually and the adsorption reached equilibrium in about 5 hours. A large number of vacant surface sites are available for adsorption during the initial stage, and after a lapse of time, the remaining vacant surface sites are difficult to be occupied due to repulsive forces between the solute molecules on the solid and bulk phases. Effect of initial concentrations on the adsorption capacity of resorcinol on CTAB / NaOH / fly ash composite was studied at different initial concentration from 50 to 200 mg L⁻¹ by keeping other parameters constant. From Figure 5.11, it was observed that with increase in initial concentration of resorcinol, the adsorption capacity increases. It was possible that the initial concentration of resorcinol provided the necessary driving force to overcome the resistances of mass transfer between the aqueous phases and the solid phase [30]. The increase in initial concentration also enhance the interaction between resorcinol and CTAB / NaOH / fly ash composite so increase in adsorption uptake.

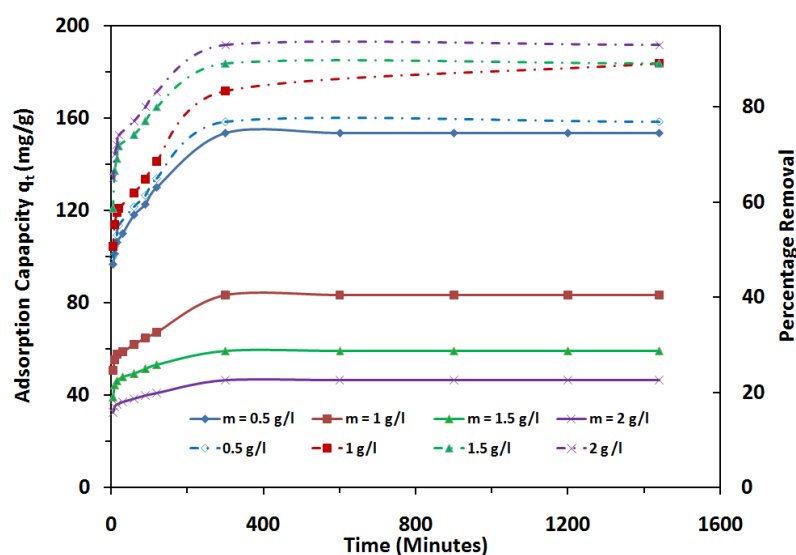


Figure 5.11: Effect of Initial Concentration of resorcinol on adsorption capacity and percentage removal by CTAB / NaOH / fly ash composite (m = 0.5 gm/l, pH = 6.8, T = 303 K)

Table 5.7: Effect of Initial Concentration of resorcinol on adsorption capacity and percentage removal by CTAB / NaOH / fly ash composite

t (min)	C ₀ =50 ppm		C ₀ =100 ppm		C ₀ =150 ppm		C ₀ =200 ppm	
	q _t (mg/g)	% removal	q _t (mg/g)	% removal	q _t (mg/g)	% removal	q _t (mg/g)	% removal
5	55.22	53.22	96.84	48.42	132	44	112	28
10	54.74	54.74	101.28	50.64	136.96	45.65	129.6	32.4
15	59.3	59.3	106.2	53.1	151.82	50.61	136.62	34.16
30	66.32	66.32	110.18	55.09	166.2	55.4	155.5	36.38
60	73.34	73.34	118.02	59.01	171.46	57.16	184.8	46.2
90	77.32	77.32	122.8	61.4	181.88	60.63	198.84	49.71
120	79.64	79.64	130.06	65.03	193.34	64.45	207.02	51.76
300	83.28	83.28	153.68	76.84	217.9	72.63	248.54	62.14
600	83.28	83.28	153.68	76.84	217.9	72.63	248.54	62.14

(m = 0.5 gm/l, pH = 6.8, T = 303 K)

(iv) *Effect of Temperature*

Effect of temperature on adsorption of resorcinol was studied at temperature 30°-50 °C as shown in Table 5.8 and Figure 5.12. It was observed that adsorption increased with increase in temperature. Higher temperature may provide more chance for phenolic compound molecule to pass the external boundary layer and produce the enlargement of pore volume and surface area enabling phenolic compound to penetrate.

Table 5.8: Effect of Temperature of solution on adsorption capacity of CTAB / NaOH / fly ash composite for resorcinol adsorption

Time (min)	Adsorption (mg/g)		
	30 °C	40 °C	50 °C
5	96.84	103.98	110.18
10	101.28	112.86	117.9
15	106.2	117.9	122.58
30	110.18	126.78	143.62
60	118.02	138.36	155.56
90	122.8	147.26	163.16
120	130.06	153.46	169.6
300	153.68	165.84	172.52
600	153.68	165.84	172.52

($m = 0.5\text{gm/l}$, $\text{pH} = 6.8$, $C_0 = 100\text{ ppm}$)

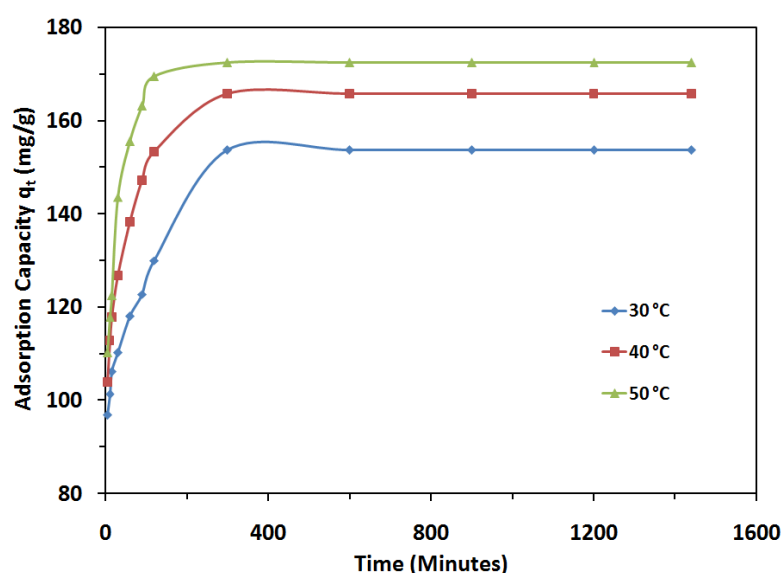


Figure 5.12 : Effect of Temperature of solution on adsorption capacity of CTAB / NaOH / fly ash composite for resorcinol adsorption
($m = 0.5\text{gm/l}$, $\text{pH} = 6.8$, $C_0 = 100\text{ ppm}$)

(v) *Effect of pH*

The initial pH of adsorption medium is one of the most important parameters affecting the adsorption process. Effect of initial pH on adsorption of resorcinol was studied with initial concentration of 100 mg l^{-1} , solution temperature $30 \text{ }^\circ\text{C}$ adsorbent dose of 0.5 g l^{-1} . The pH was adjusted by adding 0.1 mol l^{-1} or 0.01 mol l^{-1} HCl (or NaOH) to the solutions. Below pH 5.0 some zeolitic phases show dissolution so was not investigated. The adsorption of resorcinol onto CTAB / NaOH / fly ash composite as a function of solution pH is given in [Table 5.9](#) and [Figure 5.13](#). Results showed that the resorcinol adsorption capacity of CTAB / NaOH / fly ash composite was relatively high at solution pH 5.0-7.0, and decreased with increasing solution pH from 7.0 to 11.0. Resorcinol is a weak acid, and its ionization is strongly dependent on solution pH. The adsorption of unionized resorcinol onto the positively charged surface of CTAB / NaOH / fly ash composite is unlikely to be driven by the electrostatic attraction. Therefore, the hydrogen bonding and organic partitioning are responsible for the adsorption of resorcinol onto CTAB / NaOH / fly ash composite, at solution pH 5.0. Resorcinol molecules are ionized at solution pH above 5.0 and they are almost completely ionized at solution pH 7.0 [31]. Therefore, the electrostatic attraction together bonding with the hydrogen bonding and organic partition are responsible for the adsorption of resorcinol onto CTAB / NaOH / fly ash composite at solution pH 5.0-7.0. The increase of solution pH from 5.0 to 7.0 leads to decreased hydrogen bonding between resorcinol and CTAB / NaOH / fly ash composite but the increased electrostatic attraction between resorcinol and CTAB / NaOH / fly ash composite. The former is counteracted by the later, resulting in the adsorption of resorcinol on CTAB / NaOH / fly ash composite is slightly influenced by solution pH in the range 5.0-7.0. At solution pH above 7.0, completely ionized resorcinol molecules cannot provide hydroxyl hydrogen atom to nitrogen atom of CTAB bilayer to form hydrogen bonding. In this case, the electrostatic attraction plays an important role in the adsorption of resorcinol onto CTAB / NaOH / fly ash composite, the increase of solution pH from 7.0 to 11.0 leads to the increase in the competitions between the hydroxyl ion and the ionized resorcinol molecules

for the same positively charged adsorption sites, which causes a decrease in resorcinol adsorption.

Table 5.9: Effect of pH on adsorption capacity of CTAB / NaOH / fly ash composite for resorcinol adsorption

pH Initial	Adsorption Capacity (mg /g)
4.9	154.12
5.46	155.26
6.8	155.68
8.2	139.64
9.2	136.04
9.8	129.36
10.8	123.98

(m = 0.5 gm/l, t = 24hr, T = 303 K, C₀= 100 ppm)

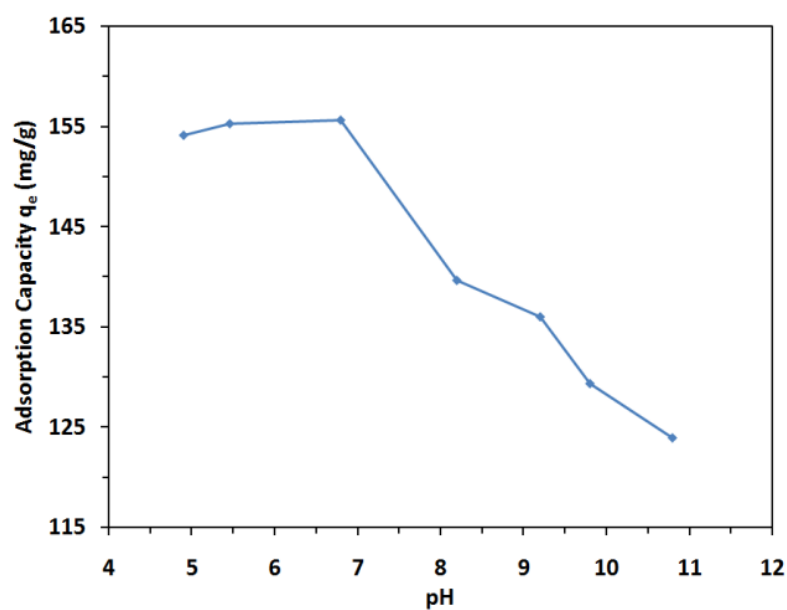


Figure 5.13: Effect of pH on adsorption capacity of CTAB / NaOH / fly ash composite for resorcinol adsorption
(m = 0.5 gm/l, t = 24 hr, T = 303 K, C₀ = 100 ppm)

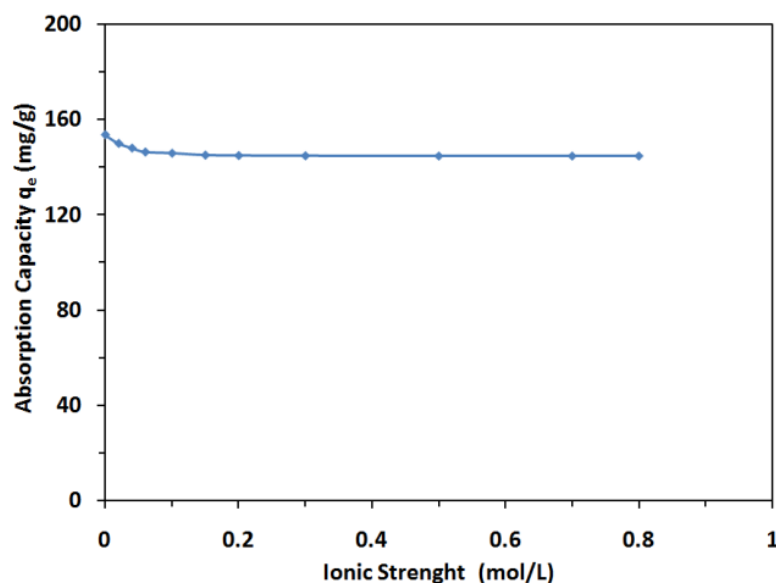
(vi) *Effect of ionic strength*

The adsorption of resorcinol onto CTAB / NaOH / fly ash composite as a function of ionic strength at solution pH 6.8 is shown in [Table 5.10](#) and [Figure 5.14](#). The presence of electrolytes such as NaCl in aqueous solution had a slight negative effect on resorcinol adsorption onto CTAB / NaOH / fly ash composite. When the ionic strength of the aqueous solution increased from 0 to 0.8 mol/L, the resorcinol adsorption capacity decreased from 153.68 to 144.6 mg/g. This result suggests that CTAB / NaOH / fly ash composite bilayer coverage is effective in removing resorcinol from water or wastewater containing salt. If electrostatic attraction is the main adsorption mechanism, the ionic strength should have a significant negative effect on the adsorption process [31, 32]. The slight negative effect of ionic strength on resorcinol adsorption onto CTAB / NaOH / fly ash composite at solution pH 6.8 confirms that the electrostatic attraction is not the only mechanism for the adsorption process and the electrostatic attraction together with the other mechanisms such as hydrogen bonding and organic partitioning control the adsorption process. There is only slight decrease of resorcinol adsorption after NaCl addition. On one hand, resorcinol adsorption onto CTAB / NaOH / fly ash composite may be reduced by chloride ions due to the competition between the chloride ions and the ionized resorcinol ions for the adsorption sites on the surface of the adsorbent. On the other hand, resorcinol adsorption onto CTAB / NaOH / fly ash composite may be enhanced by the sodium ions due to the weakening of the repulsive interaction between adsorbed resorcinol molecules on the surface of the adsorbent and resorcinol molecules in solution [31]. The decreased resorcinol adsorption caused by the chloride ions may be partially counteracted by the increased resorcinol adsorption caused by the sodium ion, resulting in that resorcinol adsorption caused by the sodium ion, resorcinol adsorption is slightly reduced by the ionic strength of the aqueous solution.

Table 5.10: Effect of Ionic Strength on adsorption capacity of CTAB / NaOH / fly ash composite for resorcinol adsorption

Ionic Strength (mol/L)	Adsorption Capacity (mg/g)
0	153.68
0.02	150
0.04	148
0.06	146.3
0.1	145.8
0.15	145
0.2	144.8
0.3	144.7
0.5	144.6
0.7	144.6
0.8	144.6

($m = 0.5$ gm/l, $t = 24$ hr, $T = 303$ K, $C_0 = 100$ ppm, $\text{pH} = 6.8$)

**Figure 5.14:** Effect of Ionic Strength on adsorption capacity of CTAB / NaOH / fly ash composite for resorcinol adsorption
($m = 0.5$ gm/l, $t = 24$ hr, $T = 303$ K, $C_0 = 100$ ppm, $\text{pH} = 6.8$)

5.3.4 Adsorption Kinetics

Four widely used kinetic models, pseudo-first-order, pseudo-second-order Bangham equation and intra-particle diffusion model were employed (as described in chapter 2) to interpret the kinetic. The results are given in [Tables 5.11](#) & [5.12](#) and [Figure 5.15](#).

Table 5.11: Details of all kinetic parameters for resorcinol adsorption on CTAB / NaOH / fly ash composite

Resorcinol C_0	time (min.)	5	10	15	30	60	90	120
		$\sqrt{\text{time}}$	2.240	3.160	3.880	5.480	7.750	9.490
	$\log t$	0.699	1.000	1.176	1.477	1.778	1.954	2.079
40 ppm	$\ln(q_e - qt)$	3.4	3.35	3.18	2.83	2.3	1.785	1.29
	t/qt	0.094	0.0183	0.253	0.452	0.818	1.164	1.51
	qt	53.22	54.74	59.3	66.32	73.34	77.32	79.64
	$\log \log (C_0/C_0 - q_t m)$	-0.482	-0.463	-0.408	-0.325	-0.241	-0.191	-0.160
100 ppm	$\ln(q_e - qt)$	4.04	3.96	3.86	3.77	3.57	3.43	3.16
	t/qt	0.052	0.099	0.141	0.272	0.508	0.733	0.923
	qt	96.840	101.280	106.200	110.180	118.020	122.800	130.060
	$\log \log (C_0/C_0 - q_t m)$	-0.541	-0.513	-0.483	-0.459	-0.412	-0.384	-0.341
150 ppm	$\ln(q_e - qt)$	4.45	4.39	4.191	3.95	3.84	3.58	3.2
	t/qt	0.038	0.073	0.099	0.18	0.35	0.495	0.621
	qt	132	136.96	151.82	166.2	171.46	181.88	193.34
	$\log \log (C_0/C_0 - q_t m)$	-0.599	-0.577	-0.514	-0.455	-0.434	-0.393	-0.348
200 ppm	$\ln(q_e - qt)$	4.92	4.78	4.72	4.64	4.16	3.91	3.73
	t/qt	0.045	0.078	0.11	0.206	0.325	0.453	0.58
	qt	112.000	129.600	136.620	145.500	184.800	198.840	207.020
	$\log \log (C_0/C_0 - q_t m)$	-0.846	-0.769	-0.741	-0.707	-0.570	-0.525	-0.500

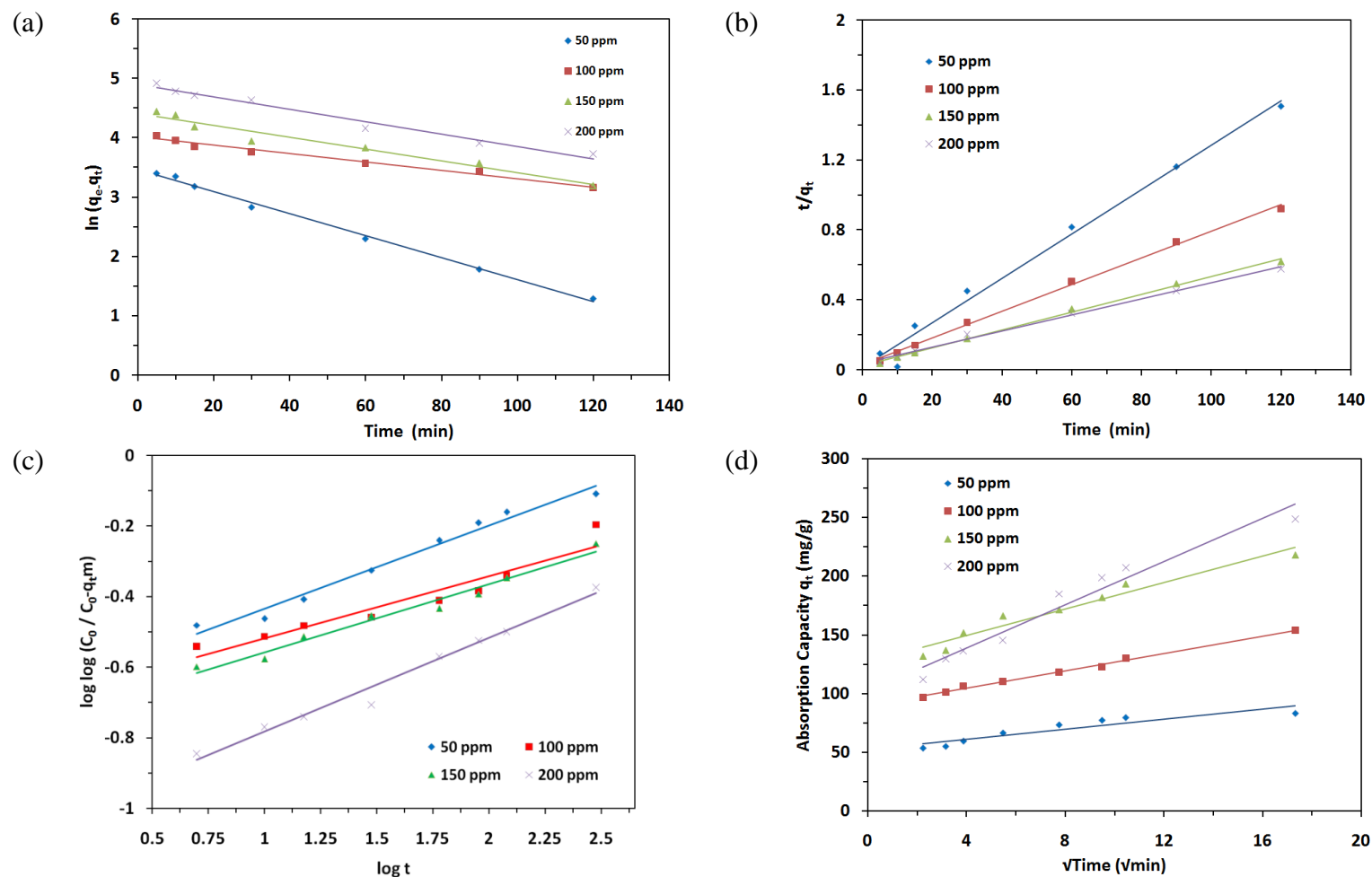


Figure 5.15: Kinetic Model of Resorcinol on CTAB / NaOH / fly ash composite (a) Pseudo First Order, (b) Pseudo Second Order, (c) Bangham equation and (d) intra-particle diffusion model

For pseudo-second-order kinetic model, although the R^2 value obtained was relatively high ($R^2 = 0.9825$), but the calculated q_e value did not agree with the experimental one. This suggests that the pseudo-first-order kinetic model is not appropriate to represent the adsorption kinetics data of resorcinol onto CTAB / NaOH / fly ash composite.

For pseudo-second-order kinetic model, the R^2 value obtained was very high ($R^2 > 0.9976$), and the calculated q_e value was in good agreement with the experimental one, suggesting the applicability of the pseudo-second-order kinetic model to describe the adsorption kinetics data of resorcinol onto CTAB / NaOH / fly ash composite.

Linear plots of q_e and h against C_0 were regressed to obtain the value of h and q_e in terms of C_0 with high a coefficient of regression. Therefore, q_e and h can be express as a function of C_0 as follows:

$$q_e = 103.6 \ln C_0 - 331.8 \quad (5.1)$$

$$h = 1 \times 10^{-3} C_0^2 - 0.445 C_0 + 79.16 \quad (5.2)$$

$$q_t = \frac{t}{1/(1 \times 10^{-3} C_0^2 - 0.445 C_0 + 79.16) + (1/103.6 \ln C_0 - 331.8) t} \quad (5.3)$$

A comparison of experimental data points and the surface predicted by the Eq. (5.3) is given in Figure 5.16. It can be used to derive the sorption capacity, q_t at any given C_0 and t .

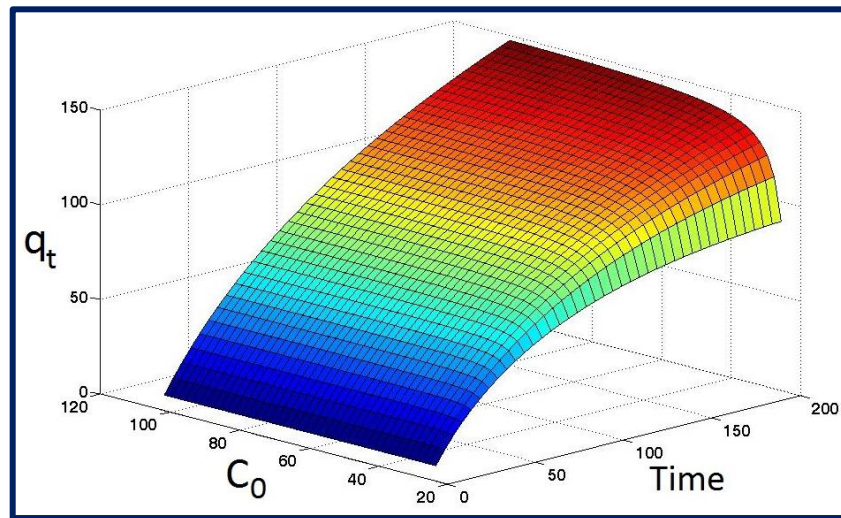


Figure 5.16: Comparison of experimental data points given by symbols and the surface predicated by the model given Equation (5.3)

Bangham's equation show (Figure 5.15 c) linear curves for the resorcinol removal by the CTAB / NaOH / fly ash composite , signifying that the diffusion of adsorbate into the pores of the adsorbent was the only rate-controlling step. It may be that pore diffusion was important to different extents in the removal process.

Intra-particle diffusion model gave straight line with a slope k_{diff} and intercept C . The term k_{diff} is indicative of an enhancement in the rate of adsorption. The value of C gives (Table 5.12) an idea about the boundary layer thickness.

Table 5.12: Pseudo-first order, Pseudo-second order, Bangham's equation and Intra-particle Diffusion Model rate constant for resorcinol adsorption onto CTAB / NaOH / fly ash composite at various concentration^a

$C_0(\text{mg/L})$		50	100	150	200
$q_{e, exp}(\text{mg/g})$		83.28	153.68	217.9	248.54
Pseudo-first order model	$K_1 (\text{1/min})$	0.0105	0.007	0.0099	0.0185
	$q_{e, cal}(\text{mg/g})$	134.5	55.46	82.35	31.93
	R^2	0.9764	0.9825	0.9583	0.9957
Pseudo-second order	$K_2(\text{g/mg min})$	9.83×10^{-4}	1.96×10^{-4}	1.09×10^{-4}	0.52×10^{-4}
	$q_{e, cal}(\text{mg/g})$	78.74	131.57	196.08	217.39
	h	62.5	34.48	43.48	25
	R^2	0.9878	0.9976	0.9971	0.9944
Bangham's equation	$K_0 (\text{g})$	49.24	46.43	40.83	20.60
	α	0.235	0.176	0.193	0.265
	R^2	0.979	0.913	0.974	0.981
Intra-particle Diffusion Model	$K_{id.}(\text{mg/g}(\text{min}^{0.5}))$	2.167	3.689	5.668	9.213
	C	52	89.81	126.5	101.5
	R^2	0.8491	0.9945	0.9487	0.9589

($m = 0.5 \text{ g l}^{-1}$, agitation rate = 200 rpm, pH 6.8, $T = 30 \text{ }^\circ\text{C}$)

5.3.5 Adsorption isotherms

The adsorption isotherm of resorcinol onto CTAB / NaOH / fly ash composite at 30°C , 40°C and 50°C and solution pH 6.8 is shown in Figure 5.16 and values of isotherm parameters are given in Table 5.13. Results showed that the resorcinol adsorption capacity increased with increasing the resorcinol concentration until equilibrium was reached. Two-parameter isotherm models Langmuir, Freundlich, Dubinin - Redushkevich (D-R), Tempkin and three-parameter isotherm model Redlich - Peterson were used to fit the experimental data.

Table 5.13: Isotherm parameters for adsorption of resorcinol on CTAB / NaOH / fly ash composite

T (°C)	Parameters						
30 °C	C_e	8.36	23.16	41.05	67	92	117.54
	$\ln C_e$	2.12	3.14	3.715	4.17	4.52	4.77
	$\log C_e$	0.922	1.365	1.613	1.812	1.96	2.07
	q_e	83.28	153.68	217.9	270.2	326	364.92
	$\log q_e$	1.92	2.19	2.34	2.43	2.5	2.56
	C_e / q_e	0.1	0.151	0.188	0.242	0.282	0.322
	$\ln(K_R C_e / q_e - 1)$	1.131	1.647	1.903	2.184	2.357	2.502
	$\ln q_e$	4.422	5.035	5.384	5.599	5.787	5.900
40 °C	ϵ^2	81014	11339	3676	1483	741	455
	C_e	6.37	17.07	35	58.42	79.77	112.63
	$\ln C_e$	1.85	2.837	3.56	4.07	4.38	4.72
	$\log C_e$	0.804	1.23	1.54	1.77	1.902	2.052
	q_e	87.26	165.86	230	283.16	340.46	374.74
	$\log q_e$	1.94	2.22	2.36	2.45	2.53	2.574
	C_e / q_e	0.073	0.103	0.152	0.206	0.234	0.301
	$\ln(K_R C_e / q_e - 1)$	1.128	1.562	2.017	2.355	2.494	2.764
50 °C	$\ln q_e$	4.469	5.111	5.438	5.646	5.830	5.926
	ϵ^2	134936	20568	5036	1828	984	495
	C_e	3.33	13.74	35.15	52	73.15	105.26
	$\ln C_e$	1.53	2.62	3.45	3.95	4.29	4.66
	$\log C_e$	0.663	1.14	1.55	1.72	1.86	2.02
	q_e	90.8	172.52	237	296	353.7	389.48
	$\log q_e$	1.96	2.24	2.36	2.47	2.55	2.59
	C_e / q_e	0.051	0.08	0.133	0.176	0.207	0.27
50 °C	$\ln(K_R C_e / q_e - 1)$	0.992	1.569	2.157	2.465	2.640	2.922
	$\ln q_e$	4.509	5.151	5.468	5.690	5.868	5.965
	ϵ^2	245561	31321	6198	2302	1169	567

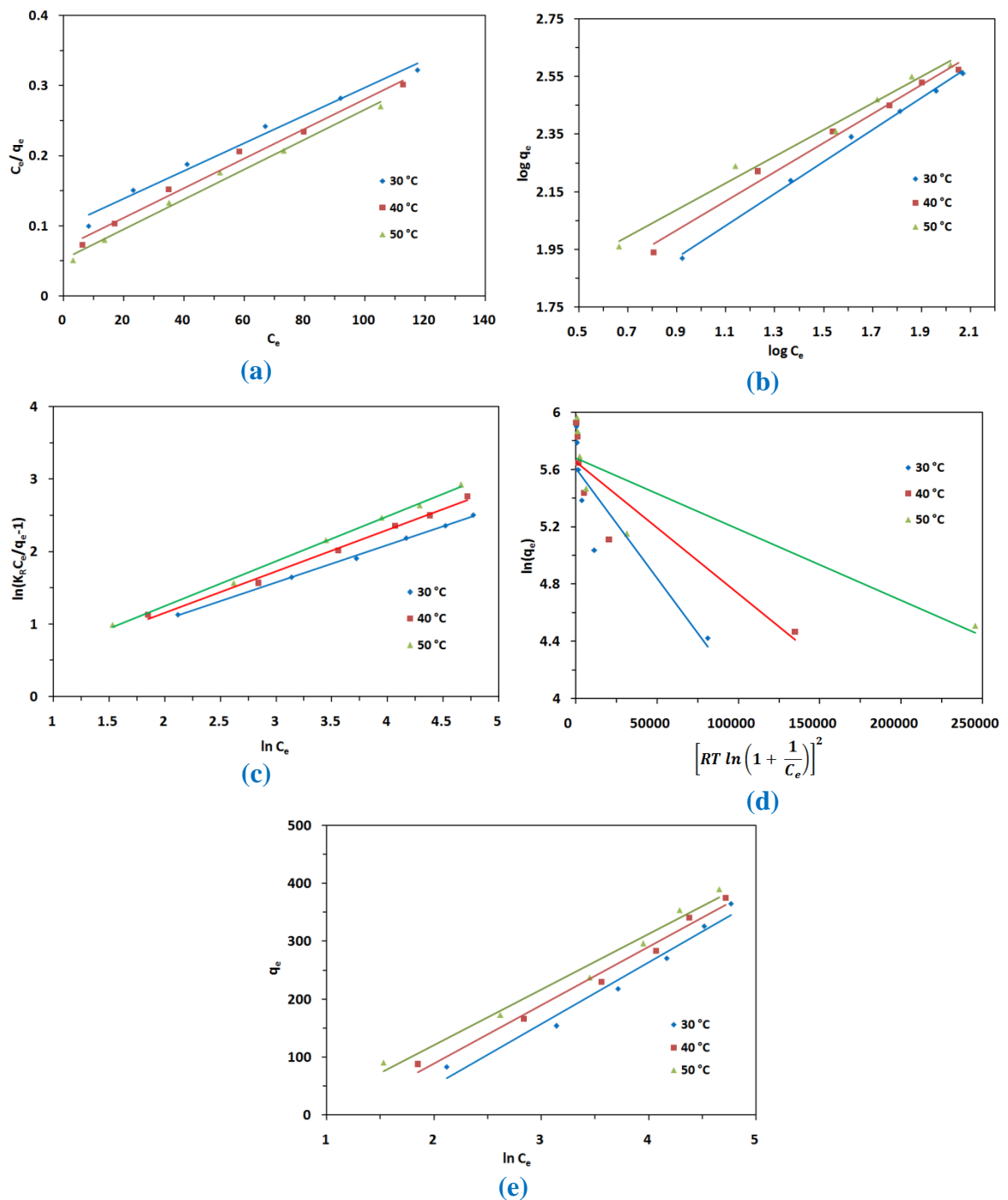


Figure 5.16: Adsorption Isotherm of resorcinol on CTAB / NaOH / flyash composite (a) Langmuir (b) Freundlich (c) Redlich-Peterson (d) D-R and (e) Tempkin

The different isotherm parameters were evaluated from the linear plots and presented in [Table 5.14](#) along with constants and correlation coefficients root mean square error (RMSE) and chi-square (χ^2). The RMSE and χ^2 are used to measure the goodness of fit of an isotherm defined as chapter 2.

The value of RMSE and χ^2 for the Tempkin and D-R isotherm model were high, indicating that the equilibrium adsorption of resorcinol onto CTAB / NaOH / fly ash composite cannot be represented appropriately by these isotherm models. The value of RMSE and χ^2 for the Redlich-Peterson, Langmuir and Freundlich isotherm models were low, indicating that the equilibrium data for the adsorption of resorcinol onto CTAB / NaOH / fly ash composite can be well represented by these three isotherm models but best fitted with Redlich-Peterson isotherm model. The predicted maximum monolayer resorcinol adsorption capacity for CTAB / NaOH / fly ash composite derived from Langmuir isotherm was found to be 500 mg/g. The values of R_L obtained in this study were between 0.07968 and 0.5 indicating that the adsorption of resorcinol onto CTAB / NaOH / fly ash composite is favorable.

The comparison of the maximum adsorption capacity of resorcinol onto various adsorbent has already given in [Table 4.12](#) (chapter 4). The CTAB / NaOH / fly ash composite prepared in this work has a relatively large adsorption capacity of 500 mg g⁻¹ compared to some other adsorbents reported in the literature. Therefore, the CTAB / NaOH / fly ash composite prepared in this work could be used as an effective adsorbent for removing resorcinol from solution.

Table 5.14: Isotherm parameters for resorcinol adsorption onto CTAB / NaOH / fly ash composite at various temperature

<i>Langmuir</i>	T (°C)	q_{max} (mg/g)	K_L (L/mg)	R²	RMSE	χ²	
	at 30	500	0.0202	0.984	12.98	3.5	
	at 40	500	0.02898	0.988	20.53	7.67	
	at 50	500	0.03846	0.999	28.95	3.22	
<i>Freundlich</i>	T (°C)	K_F (mg/g)(L/mg)^{1/n}	1/n	R²	RMSE	χ²	
	at 30	26.54	0.553	0.996	10.63	1.649	
	at 40	36.73	0.503	0.988	14.13	3.187	
	at 50	47.10	0.46	0.987	13.0	2.785	
<i>Tempkin</i>	T (°C)	K_T (mg/g)	B_T	R²	RMSE	χ²	
	at 30	1.52	106.4	0.973	251.88	1356	
	at 40	1.11	100.4	0.983	121.06	180.05	
	at 50	0.738	95.77	0.979	190.42	483	
<i>D-R</i>	T (°C)	q_{max} (mg/g)	K_D (mg²/KJ²)	R²	RMSE	χ²	
	at 30	272.33	-2 x 10 ⁻⁵	0.791	68.03	77.28	
	at 40	285.72	-9 x 10 ⁻⁶	0.818	67.86	70.42	
	at 50	292.66	-5 x 10 ⁻⁶	0.799	73.76	80.27	
<i>Redlich Peterson</i>	T (°C)	K_R (L/g)	α_R(L/mg)^β	β	R²	RMSE	χ²
	at 30	41	1.025	0.515	0.998	5.512	0.497
	at 40	56	1.008	0.572	0.993	11.61	1.95
	at 50	72.5	1.008	0.619	0.997	9.04	1.19

(m = 0.5 g l⁻¹, agitation rate = 200 rpm, pH = 6.8 and C₀ = 50 – 300 mg l⁻¹)

5.3.6 Thermodynamic Studies

The thermodynamic parameters of standard enthalpy (ΔH°) and entropy (ΔS°) for the adsorption process were estimated from the Van' t-Haff equation. The values of K_L for Langmuir isotherm at 30 °C, 40°C and 50 °C were used to calculate thermodynamic parameters such as Gibbs free energy change (ΔG°). The values of ΔH° and ΔS° can be calculated from the intercept and the slope of the linear plot of $\ln K_L$ versus $1/T$ as shown in [Figure 5.17](#).

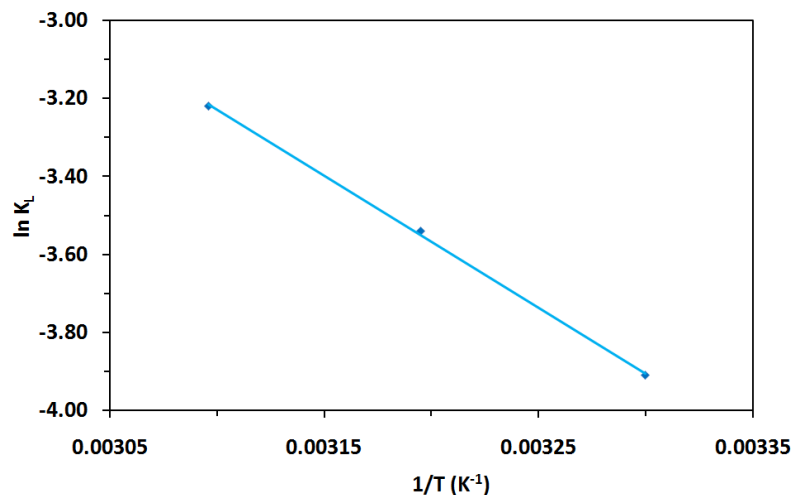


Figure 5.17: Van't Hoff plot for the adsorption of resorcinol onto CTAB / NaOH / fly ash composite

The obtained values of the thermodynamic parameters of resorcinol adsorption onto CTAB / NaOH / fly ash composite are given in Table 5.15. The negative values of ΔG° suggest that feasibility of the adsorption of resorcinol onto CTAB / NaOH / fly ash composite is a spontaneous and a favourable process. The values of ΔG° obtained in this study were in the range of neither physisorption nor chemisorption, indicating that the adsorption of resorcinol onto CTAB / NaOH / fly ash composite involves the other adsorption process such as interaction mechanism. This conclusion confirms that the mechanisms controlling the adsorption of resorcinol onto CTAB / NaOH / fly ash composite at solution of pH 6.8 include electrostatic attraction.

Table 5.15: Thermodynamic parameters for resorcinol adsorption on CTAB / NaOH / fly ash composite

ΔH° (KJ/mol)	ΔS° (J/mol)	ΔG° (KJ/mol)			R^2
		30 °C	40 °C	50 °C	
26.189	-54.332	-9.83	-9.22	-8.75	0.997

The positive value of ΔH° indicates that the adsorption process is endothermic in nature. The absolute value of ΔH° was 26.189 kJ/mol, also indicates that hydrogen bonding and organic partitioning are important to the adsorption process in addition to electrostatic attraction. The negative value of ΔS° shows a decrease in randomness at the solid/liquid interface during the adsorption process [33].

5.4 Conclusion

After Modification with the Surfactant (CTAB, Cetyltrimethylammonium bromide), hydrothermally treated fly ash exhibited greatly enhanced adsorptive capacity for resorcinol. CTAB / NaOH / fly ash composite has good physical as well as chemical stability; hence it can be used for various environmental applications. N₂ adsorption isotherms of CTAB / NaOH / fly ash composite is of combination of type II and type IV. The values of BET surface area, pore volume and pore diameter are 51.12 m²/gm, 0.176996 cm³/gm and 138.4928 Å respectively. The results show that CTAB / NaOH / fly ash composite includes mesopores. Redlich-Peterson equation is best fitted for the description of resorcinol adsorption isotherm. Adsorption of resorcinol onto CTAB / NaOH / fly ash composite increase with an increase in temperature indicating that the process is endothermic. The monolayer adsorption capacity for resorcinol is 500 mg/g. The adsorption kinetics of resorcinol onto CTAB / NaOH / fly ash composite was found to follow pseudo-second order model. The thermodynamic parameters such as ΔH° , ΔS° and ΔG° values of resorcinol adsorption onto CTAB / NaOH / fly ash composite show an endothermic heat of adsorption, the feasibility of the adsorption process and its spontaneity, respectively. The resorcinol adsorption capacity for CTAB / NaOH / fly ash composite slightly decreased with increasing ionic strength. The resorcinol adsorption capacity was relatively high at solution pH 5.0-7.0 and decreased with increasing solution pH from 7.0-11.0. The main mechanism controlling resorcinol adsorption onto CTAB / NaOH / fly ash composite at solution pH < 7.0 include electrostatic attraction, hydrogen bonding and organic partitioning.

5.5 References

- [1] P.A. Mangrulkar, S.P. Kamble, J. Meshram, S.S. Rayalu, *J. Hazard. Mater.*, 160 (2008) 414-21.
- [2] R.K. Singh, S. Kumar, S. Kumar, A. Kumar, *J. Hazard. Mater.*, 155 (2008) 523-35.
- [3] S. Kumar, M. Zafar, J.K. Prajapati, S. Kumar, S. Kannepalli, *J. Hazard. Mater.*, 185 (2011) 287-94.
- [4] S.H. Lin, R.S. Juang, *J. Environ. Manage.*, 90 (2009) 1336-49.
- [5] A. Kumar, S. Kumar, S. Kumar, *Carbon*, 41 (2003) 3015-25.
- [6] A.T.M. Din, B.H. Hameed, A.L. Ahmad, *J. Hazard. Mater.*, 161 (2009) 1522-29.
- [7] K.P. Singh, A. Malik, S. Sinha, P. Ojha, *J. Hazard. Mater.*, 150 (2008) 626-41.
- [8] R.M. Aghav, S. Kumar, S.N. Mukherjee, *J. Hazard. Mater.*, 188 (2011) 67-77.
- [9] S.N. Mukherjee, S. Kumar, A.K. Mishra, F. Maohong, *Chem. Eng. J.*, 129 (2007) 133-42.
- [10] P. Kumar, P.D. Jadhav, S.S. Rayalu, S. Devotta, *Curr. Sci.* 92 (2007) 512-7.
- [11] S. P. Kamble, P.A. Mangrulkar, A.K. Bansiwala, S.S. Rayalu, *Chem Eng J.* 138 (2008) 73-83.
- [12] S.B. Wang, Y.L. Peng, natural zeolites as effective adsorbents in water and waste water treatment, *Chem. Eng. J.* 156 (2010) 11-24.
- [13] Y. Zeng, H. Woo, G. Lee, J. Park, adsorption of Cr(VI) on hexadecylpyridinium bromide (HDPB) modified natural zeolites, *Microporous Mesoporous Mater.*, 130 (2010) 83-91.
- [14] P. Chutia, S. Kato, T. Kojima, S. Satokawa, Adsorption of AS(V) on of surfactant-modified natural zeolite, *J. Hazard. Mater.*, 162 (2009) 204-11.
- [15] J. Hrenovic, M. Rozic, L. Sekovanic, A. Anic-Vucinic, Interaction of surfactant-modified zeolite and phosphate accumulating bacteria, *J. Hazard. Mater.*, 156 (2008) 576-82.

- [16] H. Guan, E. Bestland, C.Y. Zhu, et al. *J. Hazard. Mater.*, 183 (2010) 616-21.
- [17] A. Kuleyin, *J. Hazard. Mater.*, 144 (2007) 307-15.
- [18] J.A. Simpson, R.S. Bowman, *J. Contam. Hydrol.*, 108 (2009) 1-11.
- [19] X.Y. Jin, M.Q. Jiang, X.Q. Shan, Z.G. Pei, Z.L. Chen, *J. Colloid Interface Sci.*, 328 (2008) 243-47.
- [20] Y. Dong, D.Y. Wu, X.C. Chen, Y. Lin, *J. Colloid Interface Sci.*, 348 (2010) 585-90.
- [21] S.G. Wang, W.X. Gong, X.W. Liu, B.Y. Gao, Q.Y. Yue, *Sep. Purif. Technol.*, 51 (2006) 367-73.
- [22] Y.H. Zhan, J.W. Lin, Y.L. Qiu, N.Y. Gao, Z.L. Zhu, *Front. Environ. Sci. Eng. China*, 5 (2011) 65-75.
- [23] S.R. Taffarel, J. Rubio, *Miner. Eng. Mater.*, 186 (2011) 771-79.
- [24] J. Xie, W. Meng, D. Wu, Z. Zhang, H. Kong, *J. Hazard. Mater.*, 231-232 (2012) 57-63.
- [25] K.H.S. Kung, K.F. Hayes, *Langmuir*, 9 (1993) 263-67.
- [26] T. C. Wong, B. N. Wong, P. A. Tanner, *J. of Colloid Inter. Sci.*, 186 (1997) 325-28
- [27] A. Macros, G. Laura, E. Carlos, *Surfactants and interfacial phenomena in waste water treatment*, 3rd edition, (2004) Pp.78-80, John Wiley and Sons, New York.
- [28] S.J. Gregg, K.S.W. Sing, *Adsorption*, in: *Surface Area and Porosity*, 2nd ed., Academic Press, London, 1982.
- [29] W. Li, M. Zhang, J. Zhang, Y. Han, *Front. Chem. China*, 1 (2006) 438-42.
- [30] W.T. Tsai, H.C. Hsu, T.Y. Su, K.Y. Yu Lin, C.M. Lin, T.H. Tai, *J. of Hazard. Mater.*, 147 (2007) 1056-62.
- [31] J. Lin, Y. Zhan, Z. Zhu, Y. Xing, *J. Hazard. Mater.*, 193 (2011) 102-11.
- [32] Z.H. Wang, B. Xiang, R.M. Cheng, Y.J. Li, *J. of Hazard. Mater.*, 183 (2010) 224-32.
- [33] S.C.D.A. Fernada, F.S.V. Eunice, R.C. Antini, *J. of Colloid and Interface Sci.*, 253 (2002) 243-46.



Chapter-6

Adsorption of Tannic Acid from Aqueous Solution onto Chitosan / NaOH / Fly Ash Composites: Equilibrium, Kinetics, Thermodynamics and Modeling

ABSTRACT

Chitosan, a natural biopolymeric cation, is a candidate to modify Chitosan / NaOH / fly ash composite for the adsorption of anions. As an anionic organic pollutant the adsorption of tannic acid was studied. Because of protonation / deprotonation reactions of both Chitosan / NaOH / fly ash composite and tannic acid, the adsorption process is strongly pH dependent. Chitosan / NaOH / fly ash composite presented higher tannic acid adsorption efficiency than FA and NaFA. It is thought that tannic acid is adsorbed also by van der Waals forces and H-bonding by Chitosan molecules on the surface of NaFA besides ionic forces. The adsorption of tannic acid onto Chitosan / NaOH / fly ash composite as a function of initial tannic acid concentration, contact time, adsorbent dosage, temperature, ionic strength and solution pH were investigated for their optimization. The adsorbents were characterized by XRD, FE-SEM, surface area - porosity measurement and FT-IR spectroscopy. The adsorption capacity for tannic acid was investigated with the batch technique at pH 5.5. The tannic acid adsorption slightly decreased with increasing ionic strength adjusted by NaCl. The maximal adsorption capacity for tannic acid is found 243.9 mg/g. The adsorption process fits in well with the Redlich-Peterson isotherm model and followed a pseudo-second order kinetic model. The value of thermodynamic parameters indicated spontaneous and exothermic process.

6.1 Introduction

Tannic acid (TA) is a component of natural organic matter (NOM) in surface and ground water, which is derived from the breakdown of plant biomass [1, 2]. TA is also found in wastewater discharged from coir and cork process, plant medicine, paper and leather industries [2, 3]. TA may cause a serious problem for drinking water production because TA can form carcinogenic disinfection by-products (DBTs) such as trihalomethanes (THMs) during chlorination process [1, 2], which currently are regulated by U.S. Environmental Protection Agency (EPA) under the stage 1 disinfectants and disinfection by-products (D/DBP) Rule [4]. In addition, as a water soluble polyphenolic compound, TA has toxicity for aquatic organisms such as algae, phytoplankton, fish and invertebrates [1]. Therefore, it is of great importance to remove TA from water and wastewater using techniques such as chemical oxidation, electrochemical process, coagulation, ultrafiltration, biological process and adsorption [1, 5]. Among these technologies, adsorption has been extensively developed to remove TA from water and wastewater [3]. Various adsorbents such as amino-functionalized magnetic mesoporous silica [1], bi-function resin [2], amino-functionalized magnetic nanoadsorbent [3], polymeric resin [6], cationic surfactant-modified bentonitealy [7], organically modified attapulgite clay [8], chitosan-montmorillonite [9], calcined and uncalcined hydrotalcites [10], activated carbon [11] and deacetylated konjac glucomannan [12] have been reported for removing TA from water and wastewater.

Activated carbon has vast surface area and affinity for many organic chemicals, but it is expensive and necessitates regeneration [13, 14]. Therefore, searching for alternative low-cost adsorbents that have comparable capacity to activated carbon is highly desired [15]. Recently, a variety of low-cost adsorbents have received more attention for these purposes. For example, clay and clay composites [16-18], soils and river sediments [19, 20], fly-ash and surface altered fly ash [21, 22] have been used as adsorbents for the adsorption of pollutants from water. Because there are many classes of pollutants with different properties in untreated water/wastewater, the merit of using other adsorbent developed with

naturally occurring materials to eliminate organic pollutants is essentially required.

Chitosan, a natural biopolymeric cation [31] and cheap material [32], was recently found to adsorb on montmorillonite up to 180 % of the cation exchange capacity (CEC). As a consequence of this high uptake, chitosanmontmorillonite is an adsorbent for anions with a relatively high capacity. Chitosan (poly N-acetyl-Dglucosamine) is the deacetylated product of chitin, which is obtained in the exoskeletons of crustaceans and insects. From the economical point of view, chitosan obtained from chitin is a relatively cheap material because chitin is the second most abundant polymer in nature, next to cellulose [32]. Chitosan has been widely used as an excellent adsorbent for heavy metal cations like Cu [33] and neutral or positively charged organic species like reactive dyes [34], because the amino (-NH₂) and hydroxyl (-OH) groups on the biopolymer chain can act as the coordination and reaction sites. The electrolytic nature and chelating ability of the biopolymer is mainly governed by the protonation degree of the -NH₃⁺ group (pK=6.3), which is dependent on pH [35]. Although chitosan shows excellent adsorption capacities, the unfavourable mechanical property (highly swollen in water) and the low specific gravity of chitosan make them rather inconvenient for the use as adsorbents in either batch or column modes. The physical nature of chitosan can be improved if it is adsorbed on fly ash. The present work reports improvement in physical nature of chitosan by loading onto NaOH activated fly ash as required for removal of organic waste also evidenced by characterization for structural, morphological and surficial properties.

The objective of this study was to synthesize and characterize Chitosan / NaOH / fly ash composite and examine its adsorptive capacity for removal of tannic acid from aqueous solution and suggest a suitable mechanism for adsorption. The effects of several experimental parameters such as contact time, adsorbent dosage, initial adsorbate concentration, temperature, ionic strength etc. were investigated for optimizing the process. The experimental results were analyzed by several kinetic and isotherm models. Thermodynamic parameters

such as Gibbs free energy change (ΔG°), enthalpy change (ΔH°) and entropy change (ΔS°) were calculated.

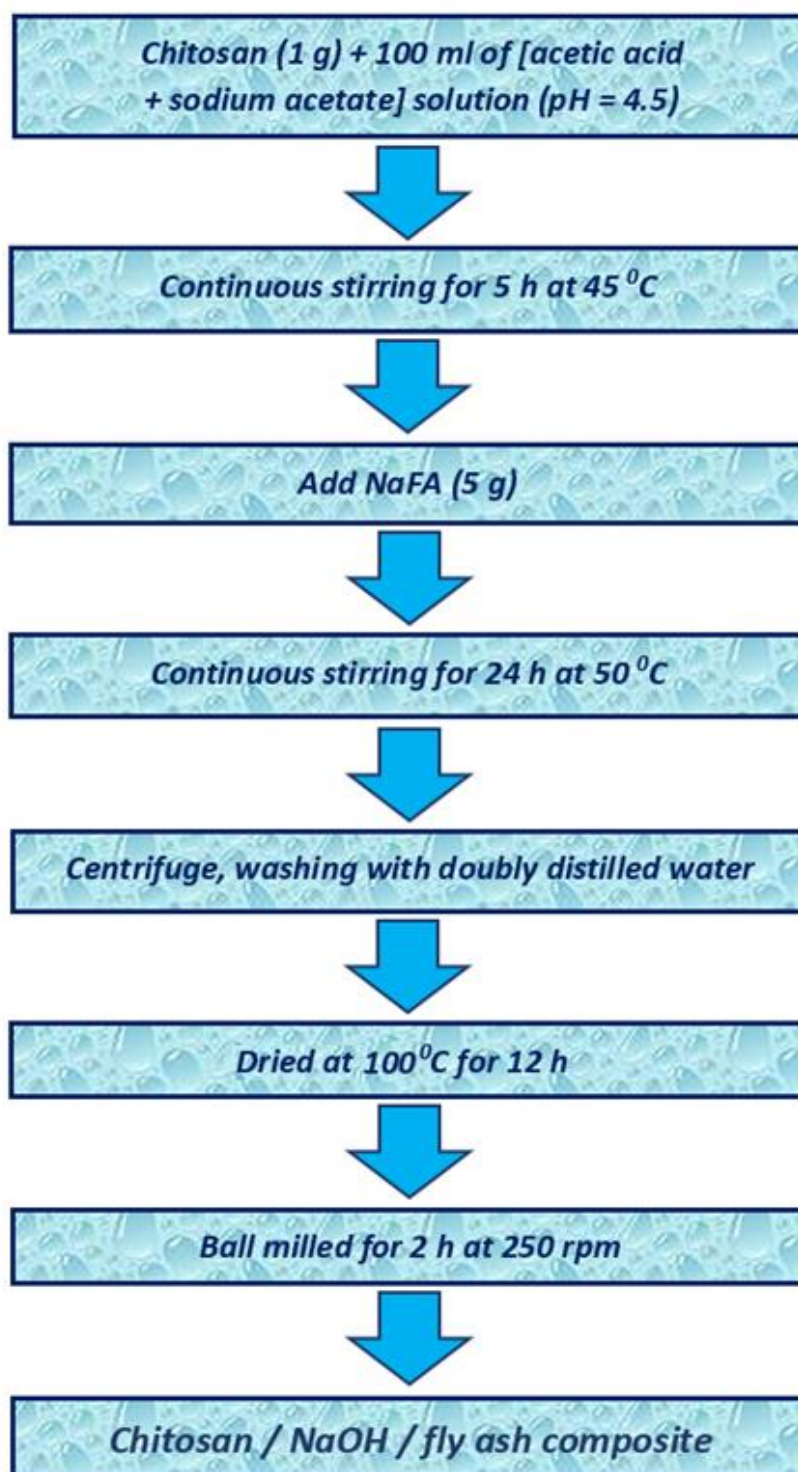
6.2 Materials and methods

6.2.1 Materials

Chitosan (75% deacetylated), tannic acid, acetic acid and sodium acetate were used with make described in chapter 2. FA was collected from Shri Ram Fertilizers & Chemical Ltd., Kota for simplicity FA₄₀ is used as FA in this chapter.

6.2.2 Synthesis of Chitosan / NaOH / fly ash composite

For synthesis of Chitosan / NaOH / fly ash composite, a chitosan solution (10 g/L) was first prepared by dissolving 1 g chitosan in 100 mL of acetic acid/sodium acetate solution (pH = 4.5). Complete dissolution was achieved by continuous agitation on an orbital shaker in a thermostatic chamber at 200 rpm for 5 h at 45 ± 0.1 °C. NaFA (5 g) (synthesis of NaFA has already described in chapter 4) was then added into chitosan solution (100 mL) and the mixture was agitated continuously in the thermostatic chamber at 200 rpm for 24 h at 50 ± 0.1 °C. After this procedure, the mixture was centrifuged and washed with double distilled water repeatedly four times to remove acetate. Finally, Chitosan / NaOH / fly ash composite was obtained after being cooled to room temperature, the product was centrifuged, washed with doubly distilled water, dried in an oven at 100 °C and ball milled in high energy planetary ball mill with ball to powder ratio of 10:1 for 2 h at 250 rpm. Schematic presentation of synthesis of Chitosan / NaOH / fly ash composite is given in [Scheme 6.1](#).



Scheme 6.1: Synthesis of Chitosan / NaOH / fly ash composite

6.2.3 Adsorption experiments

Polyphenolic compound tannic acid was selected to assess the decontamination performance by Chitosan / NaOH / fly ash composite. The concentrations were measured with Double Beam UV/Visible spectrophotometer (model Spectrscan UV 2600/02) at the wavelength of 212 nm for tannic acid.

6.3 Result and discussion

6.3.1 Characterization of Adsorbent

The primary mineralogical constituents of NaFA and Chitosan / NaOH / fly ash composite like silica, alumina and sodium contents are shown in the [Table 6.1](#) and EDX spectrum of NaFA and Chitosan / NaOH / fly ash composite are shown in [Figure 4.5 b](#) of Chapter 4 and [Figure 6.1](#) respectively. The amount of silica and alumina in Chitosan / NaOH / fly ash composite were higher than NaFA. The NaFA contains higher amount of Na₂O which decreases in Chitosan / NaOH / fly ash composite due to loading of chitosan ion on NaFA surface by sodium ion exchange. During the modification process, amino groups of Chitosan was cationized and electrostatically attracted by negative charge on the surface of NaFA ([Figure 6.8](#)).

Table 6.1: Chemical composition and properties of NaFA & Chitosan / NaOH / fly ash composite Study

Parameter	NaFA (Wt%) (by EDX)	Chitosan / NaOH / fly ash composite (Wt%) (by EDX)
SiO ₂ (%)	13.74	15.60
Al ₂ O ₃ (%)	5.99	9.03
Fe ₂ O ₃ (%)	2.79	1.62
CaO (%)	2.69	3.89
MgO (%)	0.23	0.33
Na ₂ O (%)	9.42	1.36
K ₂ O (%)	0.45	-
Moisture (%)	4.5	4.9
TiO ₂	0.69	1.19
CEC (mmol g ⁻¹)	1.02	0.704
ECEC (mmol g ⁻¹)	0.068	0.040
pH _{ZPC}	10.1	7.3
Surface area of pores (m ² /g)		
(i) BET	18.2875	23.7542
(ii) BJH		
a. Adsorption cumulative	15.6483	22.8151
b. Desorption cumulative	165528	26.6186
BJH Cumulative Pore Volume (cm ³ /g)		
(i) Single Point Total	0.102599 ^a	0.103612 ^b
(ii) BJH Adsorption	0.100457 ^c	0.100592 ^c
(iii) BJH desorption	0.102793 ^c	0.104079 ^c
Average pore diameter (Å)		
(i) Single Point Total	224.4138	174.4739
(ii) BJH Adsorption	256.7875	176.3611
(iii) BJH desorption	248.3996	156.4010

^a Pores less than 821.9909 Å diameter

^b Pores less than 841.3528 Å diameter

^c Pores between 17.00 Å and 3000.00 Å diameter

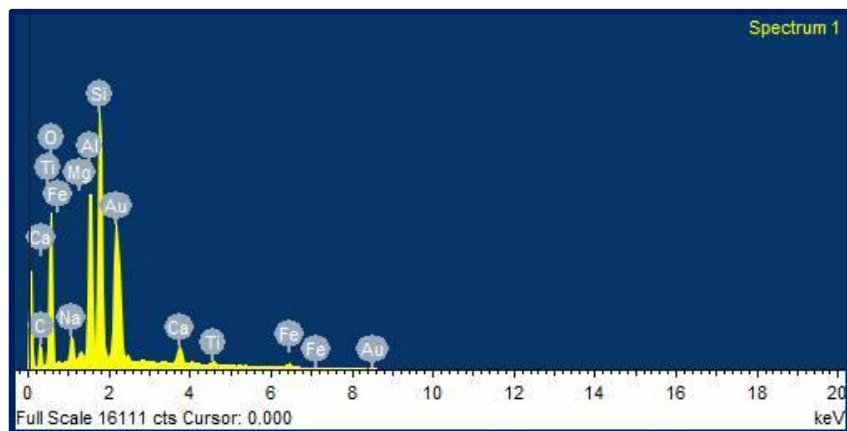
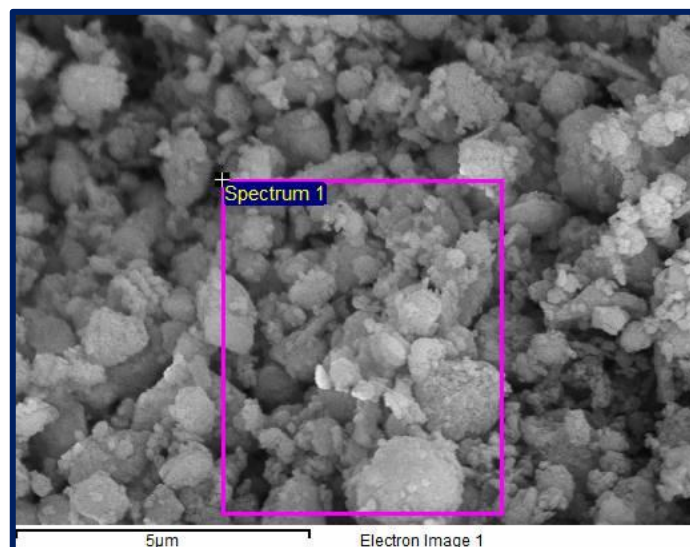


Figure 6.1: EDX Spectrum of Chitosan / NaOH / fly ash composite

(i) *Field Emission Scanning Electron Micrographs (FE-SEM)*

Figures 6.2 (a), (b) and (c) show the field emission scanning electron microscopy (FE-SEM) images of NaFA and Chitosan / NaOH / fly ash composite at different magnifications. Surface of NaFA was rough, indicating the deposition of clusters of zeolitic material on fly ash and developed crystalline tubular habits [36]. The morphological difference between Chitosan / NaOH / fly ash composite and NaFA was observable. After loading of Chitosan on to NaFA, the surface of zeolitic crystal were covered with an organic layer and the crystalline depositions seen in Figure 6.2 (b), (c) & (d) were completely disappeared.

(ii) *Fourier Transformed Infrared (FTIR) Spectra*

Formation of silicoaluminate crystalline material in NaFA was confirmed by the shift of the band from 1120 cm^{-1} for FA to 978.92 cm^{-1} for NaFA on Fourier transformed infrared (FTIR) spectra (Figure 6.3 and Table 6.2), because tetrahedral Al is characteristic of the zeolite structure and an increase in tetrahedral Al (formation of zeolite) would induce a shift of the band within the range of $1180\text{-}950\text{ cm}^{-1}$ (which is assigned to the asymmetric internal T-O stretching vibration mode of the TO_4 tetrahedra, where T = Si or Al) to a lower wave number [37]. After the NaFA had been treated with Chitosan the absorption band at 3525 cm^{-1} for OH- groups became smaller and appeared at 3324 cm^{-1} . These observations can be interpreted as being the consequence of chitosan exchanging the Na^+ groups of the crystal structure of the NaFA. Also, the absorption band at $2894\text{-}2827\text{ cm}^{-1}$ of NaFA shifted to $2894\text{-}2834$ for Chitosan loading can be considered as belonging to the C-H groups of Chitosan in free position in the NaFA (bonded in various ways to the NaFA). The FTIR absorption bands at 2894 and 2834 cm^{-1} (Figure 6.3), which are attributed to the symmetric and asymmetric stretching vibrations of C-C [38] in the alkyl chain of chitosan, the absorption peak at 1641.91 cm^{-1} & 1566.20 cm^{-1} were attributed to the bending vibration of amide and N-H indicate the chitosan layer.

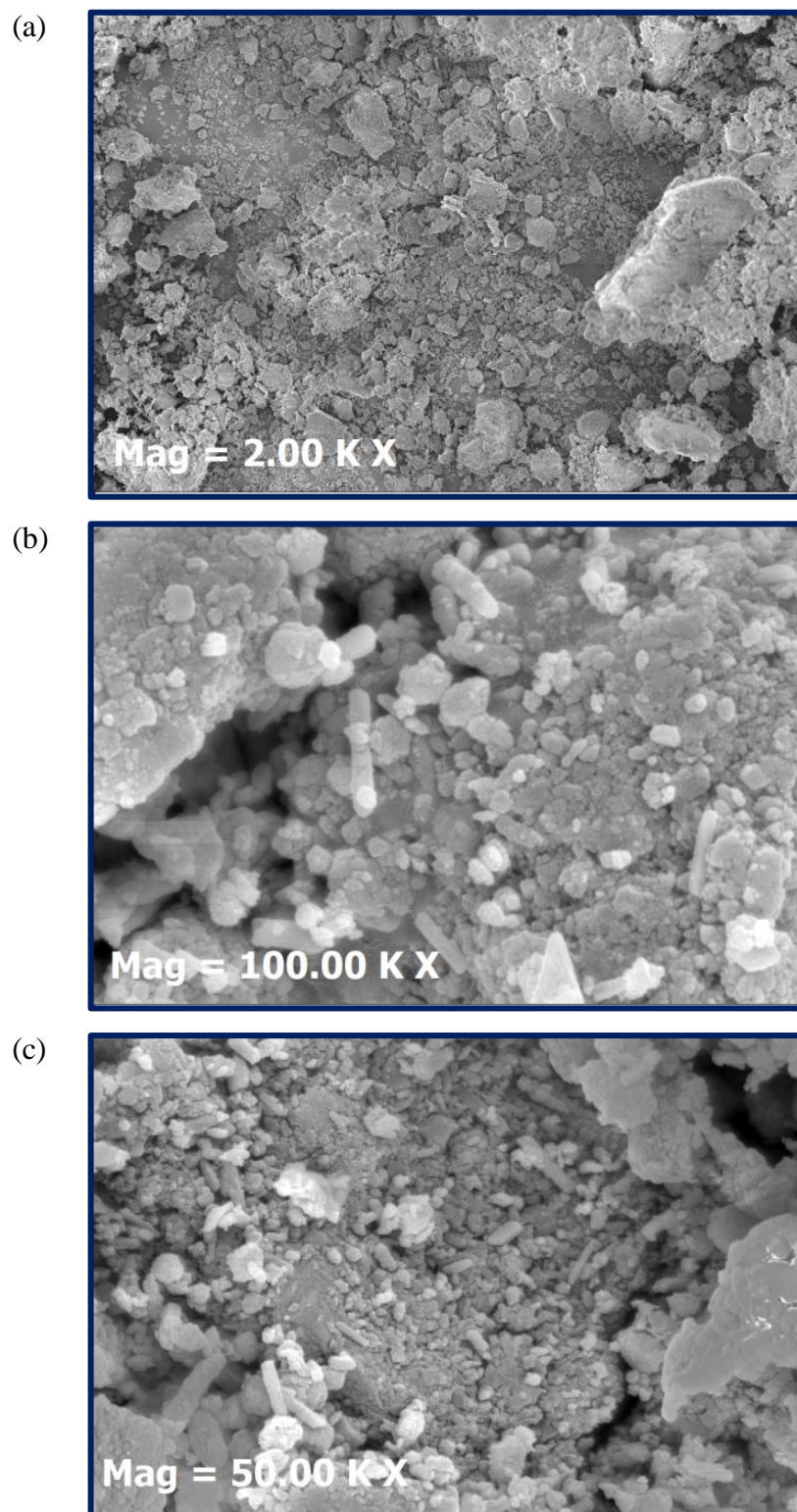


Figure 6.2: FE-SEM of Chitosan / NaOH / fly ash composite

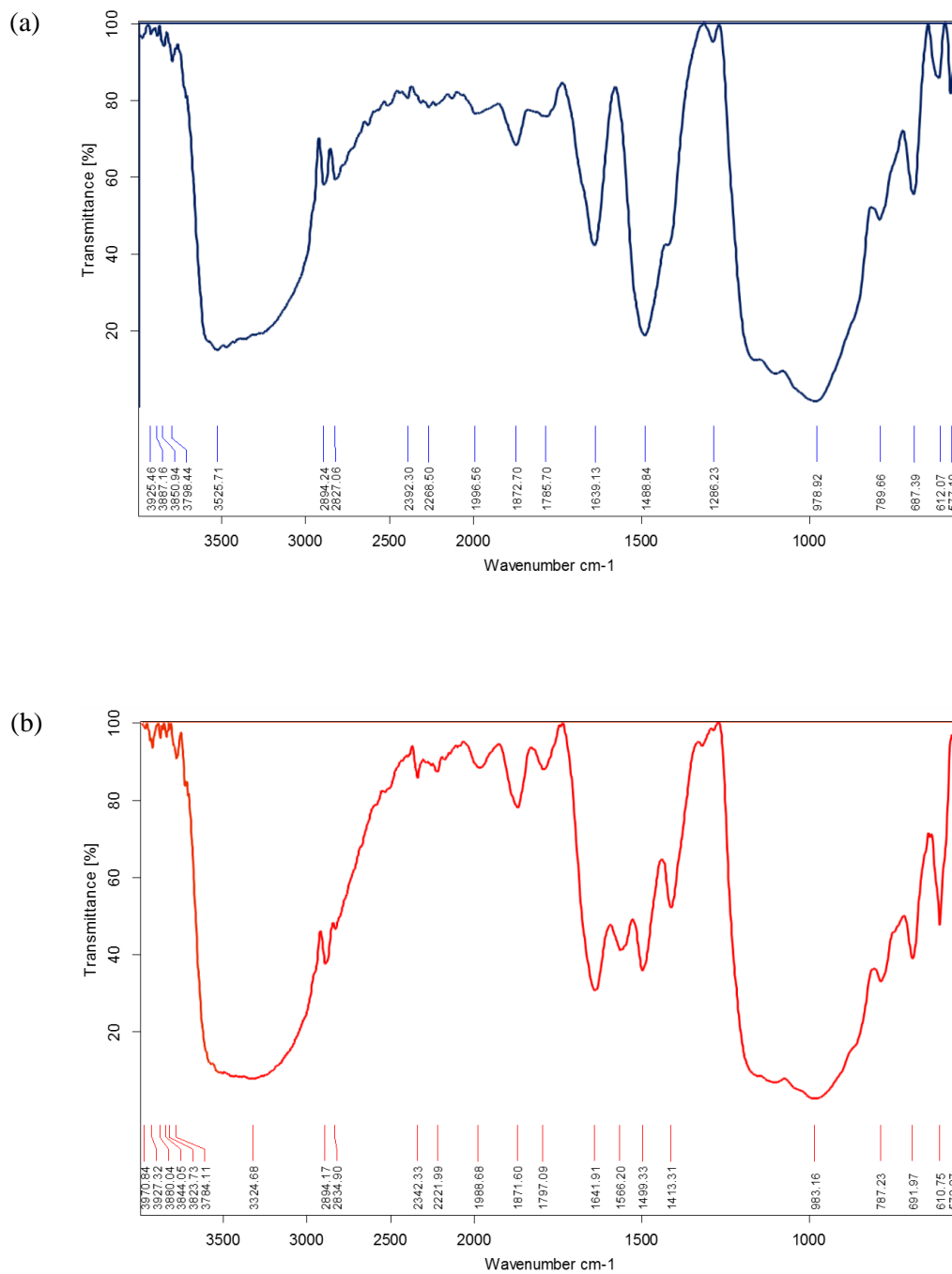


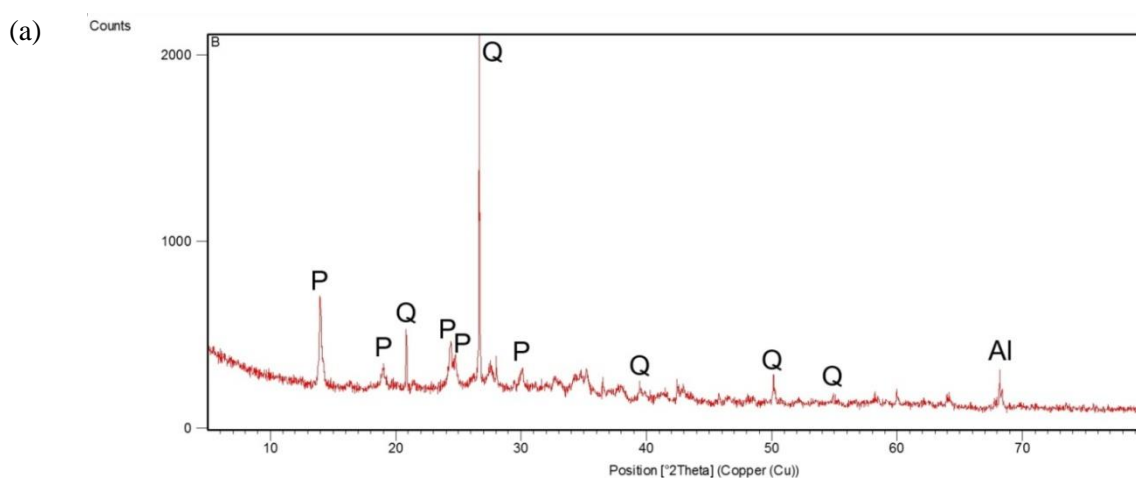
Figure 6.3: The FTIR patterns for (a) NaFA and (b) Chitosan / NaOH / fly ash composite

Table 6.2: Comparison and shifting of bands data for NaFA and Chitosan / NaOH / fly ash composite in FTIR spectroscopy

Wave number (cm ⁻¹)	Possible assignment	Observed value (cm ⁻¹)	
		NaFA	Chitosan / NaOH / fly ash composite
3600 - 3300	Stretching vibration of -OH group, Silanol (Si-OH) or N-H group	3525.1	3324.68
1700 - 1400	-OH deformation & bending vibration of interstitial water, amide and N-H group	1639.13	1641.91
		1488.84	1499.33
1250 - 850	Asymmetric stretching of internal tetrahedral TO ₄ , Si-O-Si (T=Si, Al)	978.92	983.16
720 - 650	Symmetric stretching of internal tetrahedral TO ₄ (T=Si, Al)	687.39	691.97

(iii) X-Ray Diffraction study

The XRD pattern of the NaFA and Chitosan / NaOH / fly ash composite are shown in [Figure 6.4](#) and XRD details of NaFA and Chitosan / NaOH / fly ash composite are shown in [Table 4.4](#) (chapter 4) & [Table 6.3](#) respectively. As described in chapter 4, NaFA has some zeolitic fraction observed from the XRD peaks at about 27° and 28° 2θ. The presence of chitosan on NaFA surface confirmed by first peak increased slightly the d-spacing of NaFA ([Table 6.4](#)) & a new peak at 2θ =67.74 has appeared ([Figure 6.4b](#)). Mullite and quartz in NaFA and Chitosan / NaOH / fly ash composite were also observed as crystalline peaks.



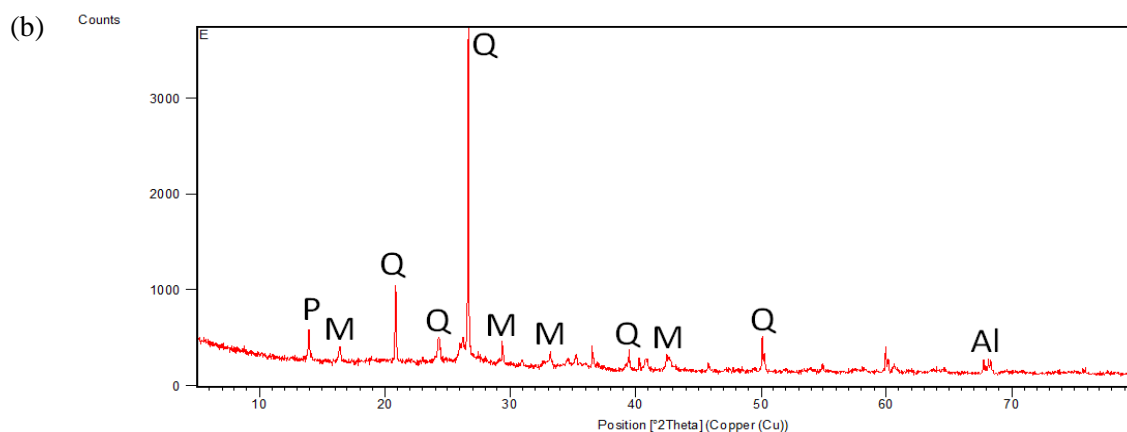


Figure 6.4: The XRD patterns for (a) NaFA and (b) Chitosan / NaOH / fly ash composite
(Where Q, quartz; M, mullite; Al, aluminium; P, zeolitic phase)

Table 6.3: XRD details of Chitosan / NaOH / fly ash composite

Pos. [$^{\circ}2\text{Th.}$]	FWHM [$^{\circ}2\text{Th.}$]	d-spacing [\AA]	Rel. Int. [%]	Area [cts* $^{\circ}2\text{Th.}$]
16.4105	0.1673	5.40177	10.01	23.04
20.8747	0.1506	4.25556	16.73	34.65
26.6313	0.1004	3.34730	100.00	138.07
31.0524	1.2918	2.88008	13.41	161.08
33.1768	0.4015	2.70036	4.64	25.65
35.2431	0.2007	2.54663	8.15	22.50
36.4955	0.2007	2.46206	5.93	16.37
39.3721	0.4015	2.28856	3.94	21.76
40.8247	0.1338	2.21042	8.86	16.31
42.4882	0.2676	2.12765	5.43	20.01
50.1372	0.2007	1.81952	6.35	17.55
60.7180	0.4015	1.52535	3.65	20.16
64.1814	0.8029	1.45115	1.99	22.02
68.1774	0.8160	1.37437	3.61	54.83

Table 6.4: Comparison between XRD Peak and d-spacing of NaFA and Chitosan / NaOH / fly ash composite

<i>Adsorbent</i>	<i>d-spacing (Å □)</i>	<i>2θ (degree)</i>	<i>Intensity (Counts)</i>
NaFA	6.33671	13.9751	24.54
Chitosan / NaOH / fly ash composite	6.33777	13.9621	9.23

(iv) *Cation exchange capacity and pH_{ZPC}*

External cation exchange capacity and pH_{ZPC} of Chitosan / NaOH / fly ash composite are 0.04 and 7.3 respectively shown by **Figure 6.5** and **6.6** and the values are shown are in **Table 6.1**. The external surface was used to load Chitosan because the pore size of NaFA is too small for the Chitosan to enter. The amount of Chitosan loaded was determined to be 0.143 mmol g⁻¹ based on the difference of the nitrogen content between Chitosan / NaOH / fly ash composite and NaFA.

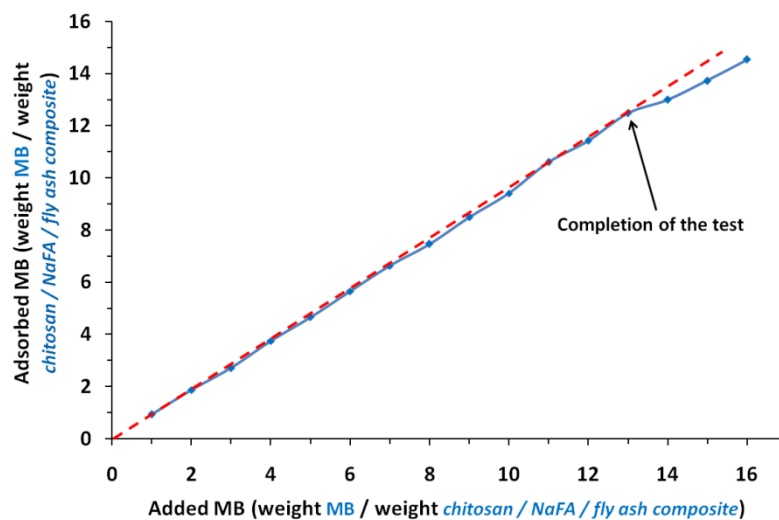


Figure 6.5: The determination of the point of complete replacement of cations from the titration curve (Chitosan / NaFA / fly ash composite)

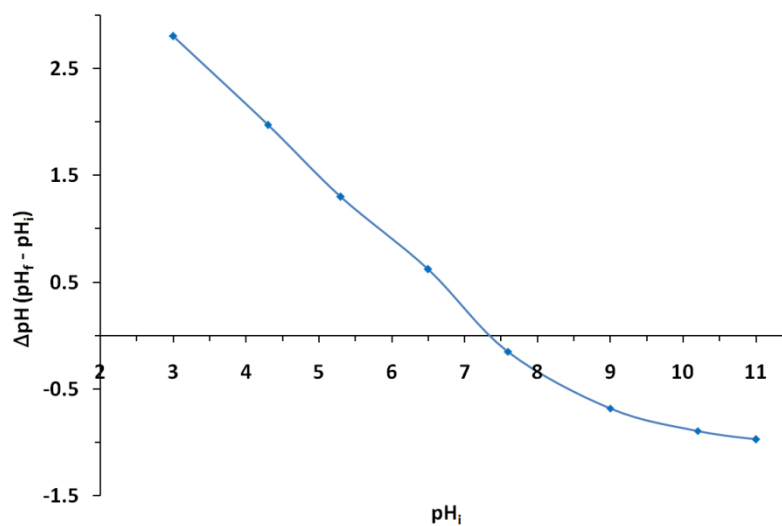


Figure 6.6: Point Zero Charge of Chitosan / NaFA / fly ash composite

(v) *Surface area and porosity*

Figure 6.7 (a & b) show the N₂-adsorption/desorption isotherm and surface area plot for the Chitosan / NaOH / fly ash composite respectively. The combination of type II and type IV adsorption isotherm (Figure 6.7a) are encountered for Chitosan / NaOH / fly ash composite with a typical adsorbate uptake starting at 0.6 p/p₀. The hysteresis seen between the adsorption (lower) and desorption (upper) curves indicates the existence of mesoporosity (pores in the range of 20-500 Å) according to the IUPAC and Brunauer, Deming, Deming & Teller (BDDT) classification [39] and provides information regarding the connectivity of the porous network. The pore-size distribution of the Chitosan / NaOH / fly ash composite shown in Figure 6.7 (c & d) have been calculated from the adsorption branch of the isotherm by the BJH method. A pore size maximum (Figure 6.7 d) for the Chitosan / NaOH / fly ash composite at about 10 nm has been found. The specific surface area of the adsorbents by BET methods shows (Table 6.1) the following order Chitosan / NaOH / fly ash composite (23.7542 m² g⁻¹) > NaFA (18.2875 m² g⁻¹), which indicates that the specific surface area is increased drastically due to loading of chitosan molecule on NaFA surface. The analysis of BJH average adsorption/desorption pore diameter values of adsorbent Chitosan / NaOH / fly ash composite lies between 2 nm to 50 nm. Thus, it can be concluded that the Chitosan / NaOH / fly ash composite is predominantly mesoporous adsorbents. BET average pore diameters were 17.48 nm and 24.84 nm of Chitosan / NaOH / fly ash composite and NaFA respectively. As the pore diameter decreases the pore volume (Chitosan / NaOH / fly ash composite: 0.103612 cm³ g⁻¹ > NaFA: 0.102793 cm³ g⁻¹) increases due to that the capacity of Chitosan / NaOH / fly ash composite increases than that of NaFA.

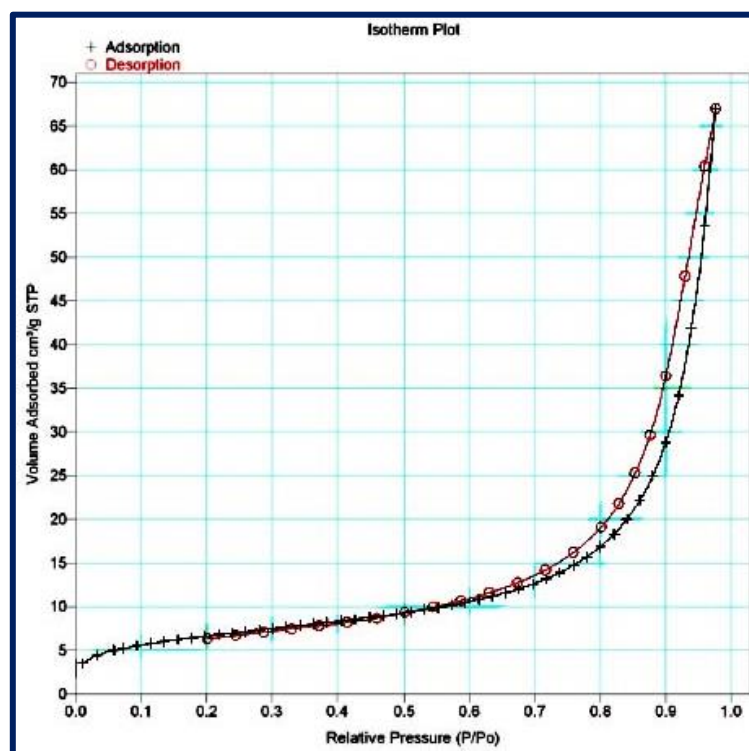


Figure 6.7(a): Adsorption isotherms of nitrogen at 77 K for Chitosan / NaOH / fly ash composite

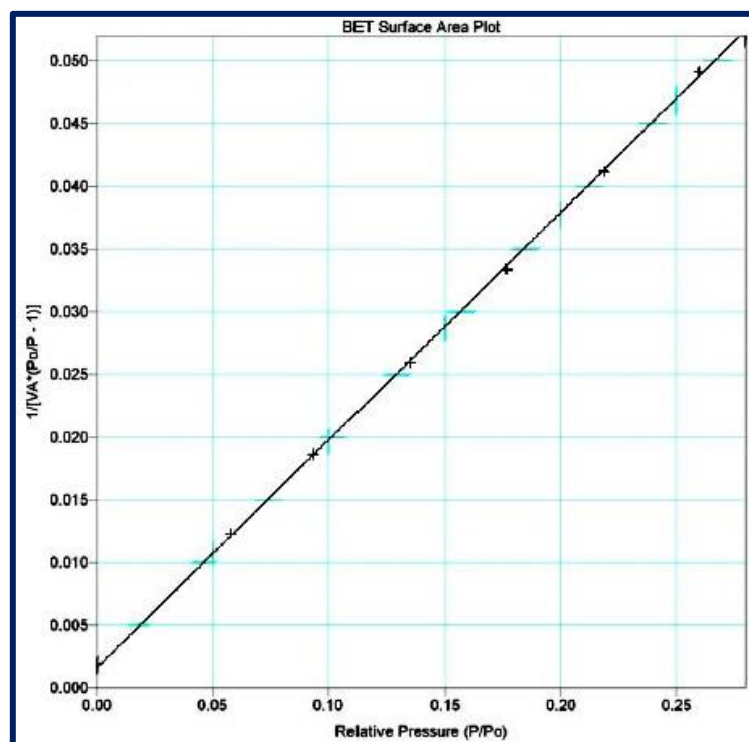


Figure 6.7(b): Surface area plot for Chitosan / NaOH / fly ash composite

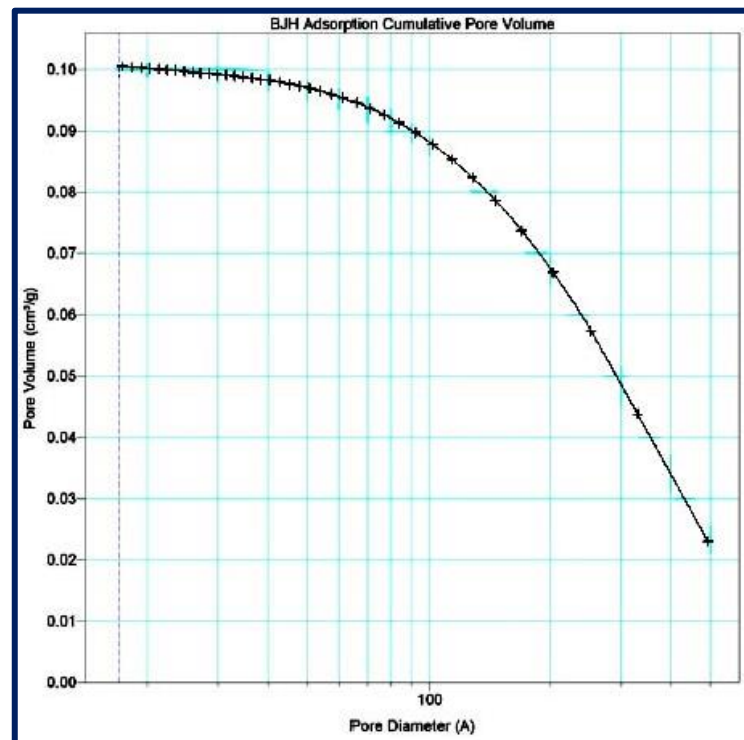


Figure 6.7(c): Pore-size distribution (BJH Adsorption Cumulative Pore Volume) for Chitosan / NaOH / fly ash composite

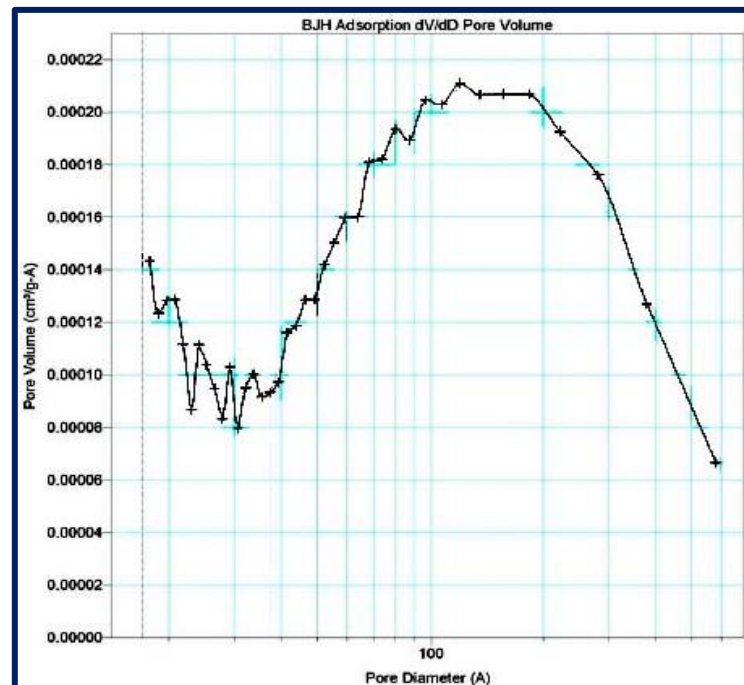


Figure 6.7(d): Pore-size distribution (BJH Adsorption dV/dD Pore Volume) for Chitosan / NaOH / fly ash composite

6.3.2 Effect of chitosan loading on NaFA

When NaFA is mixed with the chitosan solution then the chitosan molecule forms a monolayer on the external surface of NaFA via exchange. Chitosan does not form micelle on external surface. This is in contrast to many monovalent organic cation with a hydrophobic C-chain. Due to layer of chitosan, an organic fraction is created over the NaFA surface, which is responsible for trapping organic hydrophobic pollutants like tannic acid. The uptake of chitosan not only is ionic but also of the molecular form of glucosamine units with free amine groups. As these units act as anion exchange sites, the amount of the molecular form of chitosan adsorbed on NaFA surface is very important for the adsorption capacity for anion. Chitosan may show an extended structure that may facilitate the uptake in the interlayer space in contrast to analogous polysaccharides with coiled or helicoidally structures that can only be adsorbed on the external surface. [Figure 6.8](#) reveals the schematic representation of mechanism of adsorption of tannic acid by Chitosan / NaOH / fly ash composite. The effect of chitosan loading on removal of tannic acid was given in [Table 6.5](#). It was found that the tannic acid adsorption efficiency was increased with increase loading amount of chitosan on NaFA. After chitosan loading with 10g/100 ml there was no more increase in adsorption efficiency due to excessive crowding of monomers of chitosan molecule on external surface of NaFA, which might have blocked the organic partitioning created by the long chain alkyl compound for adsorption of organics. Therefore Chitosan / NaOH / fly ash composite with 10g/100 ml loading amount of chitosan was the most efficient adsorbent for the removal of tannic acid from aqueous solution.

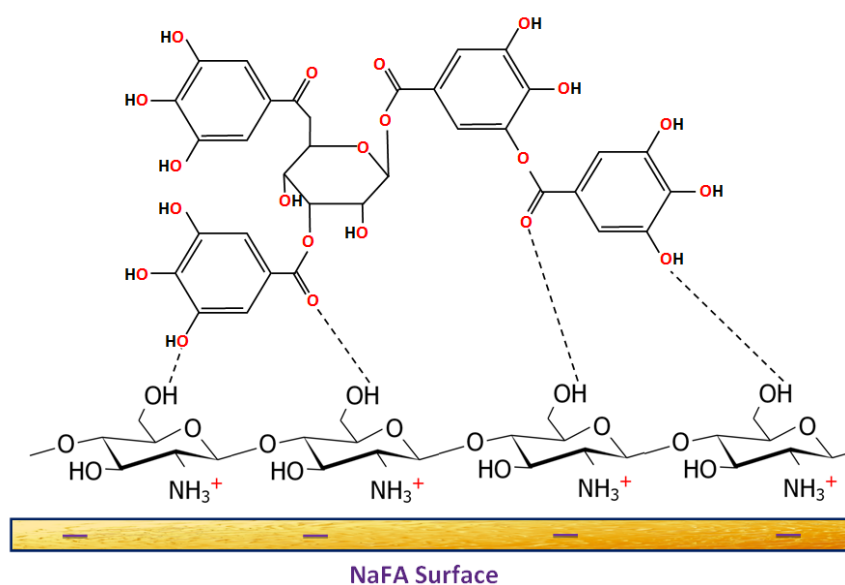


Figure 6.8: Schematic representation of chitosan modified NaFA surface with hydrogen bonded tannic acid

Table 6.5: Effect of chitosan loading on NaFA on adsorption of tannic acid

NaFA dose (g)	Chitosan concentration (g/100ml)	% loading of nitrogen	Chitosan Loading (mmol/g)	adsorption capacity of tannic acid (mg/g)
5	2.5	0.049	0.035	120
5	5.0	0.0728	0.052	143
5	7.5	0.116	0.083	168
5	9.0	0.185	0.132	195
5	10	0.197	0.143	202

(m = 1.0 g l⁻¹, agitation rate = 200 rpm, pH = 5.5, C₀ = 400 ppm, T = 298 K, t = 24 h)

6.3.3 Effect of various parameters on adsorption of tannic acid

(i) The preliminary adsorption experiments

The preliminary adsorption experiments under identical set of experimental conditions were carried out using FA, NaFA and Chitosan / NaOH / fly ash composite. The adsorption capacity of tannic acid by FA, NaFA and Chitosan / NaOH / fly ash composite are shown in Figure 6.9. It was observed that the removal efficiency of FA and NaFA is significantly less as compared to Chitosan / NaOH / fly ash composite. This may be attributed to the

hydrophobicity imparted by Chitosan leading to organic partitioning. Therefore, further experiments were carried out using Chitosan / NaOH / fly ash composite for optimization of adsorption parameters.

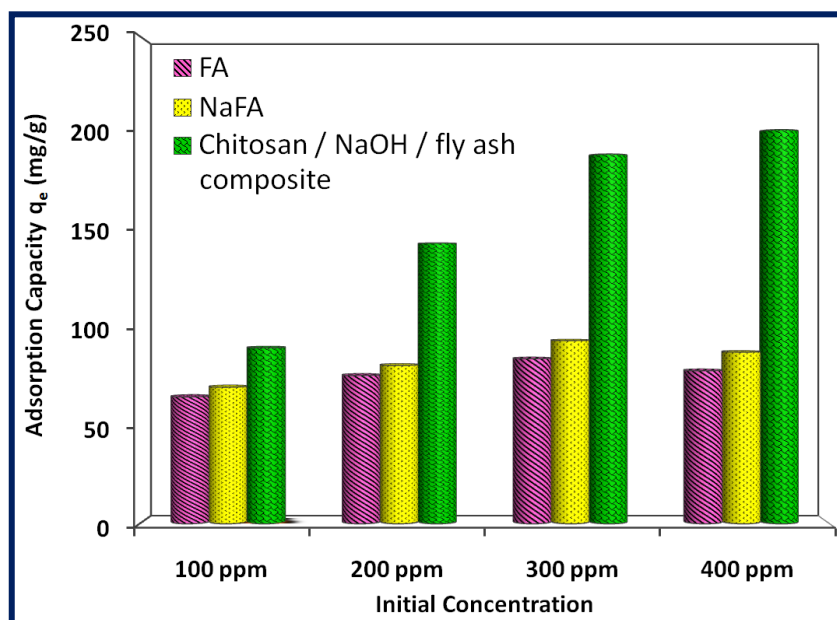


Figure 6.9 : Comparison of removal of tannic acid using FA, NaFA & Chitosan / NaOH / fly ash composite ($C_0 = 100$ mg/l, pH = 5.5, t = 24 h)

(ii) *Effect of adsorbent dose (m)*

The adsorption of tannic acid on Chitosan / NaOH / fly ash composite was carried out at different adsorbent dose with contact time by keeping other parameters constants. The relationship between adsorbent dose and contact time for tannic acid removal at same initial concentration is presented in [Table 6.6](#) & [Figure 6.10](#). It can be seen that adsorption capacity (amount of tannic acid loaded per unit weight of adsorbent) of tannic acid gradually decreased with increase in adsorbent dose. This decrease in adsorption capacity is due to availability of higher number of solutes (tannic acid) per unit mass of adsorbent, i.e. higher solute/adsorbent ratio. These experiments were performed with initial concentration of 100 mg L^{-1} of solutes, temperature $25 \text{ }^\circ\text{C}$ and pH 5.5 of the solution. It can be concluded that the rate of tannic acid/ binding with adsorbent increases more rapidly in the initial stages and after some time the adsorption is marginal and becomes almost constant.

Table 6.6: Effect of adsorbent dose on adsorption capacity of Chitosan / NaOH / fly ash composite for tannic acid adsorption

Time (min)	Adsorption Capacity (mg/g)			
	m = 0.5 g/l	m = 1 g/l	m = 1.5 g/l	m = 2 g/l
5	45.5	40.05	43.17	34.82
15	62.1	60.9	48.43	41.62
30	84.8	71.25	56.17	44.2
45	89.2	78.95	57.67	44.75
60	93	79.9	58.33	45.72
85	106.8	82.5	60.37	45.87
105	116.5	84.2	61.27	46.1
300	173	90.25	62.2	47
600	175.2	90.25	62.2	47

(T = 298 K, pH = 5.5, C₀ = 100 mg/l)

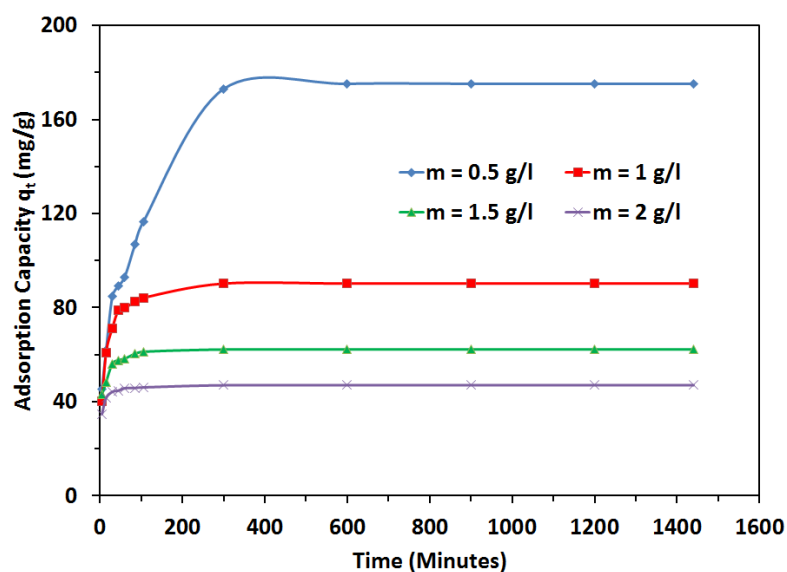


Figure 6.10: Effect of adsorbent dose on adsorption capacity of Chitosan / NaOH / fly ash composite for tannic acid adsorption
(T = 298 K, pH = 5.5, C₀ = 100 mg/l)

(iii) *Effect of initial concentration (C_0) with contact time*

Effect of initial concentrations on the adsorption capacity with contact time of tannic acid on Chitosan / NaOH / fly ash composite was studied at different initial concentration from 100 to 400 mg L⁻¹ by keeping other parameters constant. From Figure 6.11 and Table 6.7, it was observed that with increase in initial concentration of tannic acid, the adsorption increases. It was possible that the initial concentration of tannic acid provided the necessary driving force to overcome the resistances of mass transfer between the aqueous phases and the solid phase [40].

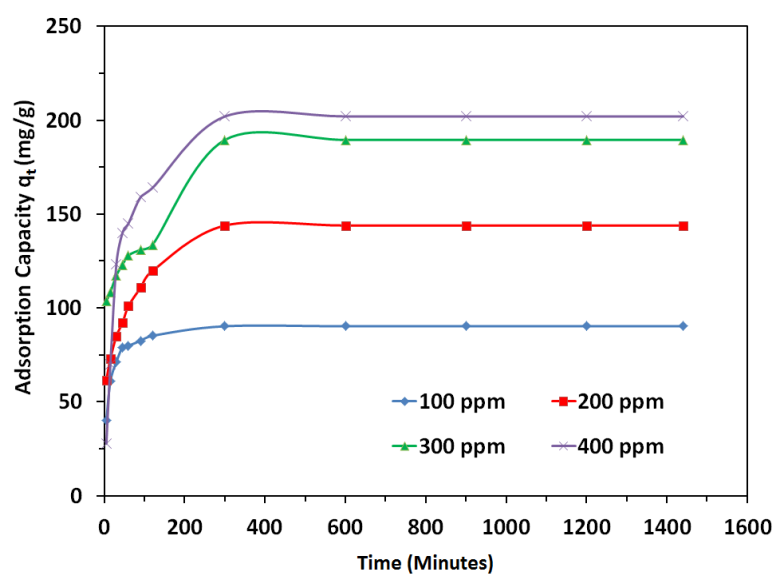


Figure 6.11: Effect of Initial Concentration of tannic acid on adsorption capacity of Chitosan / NaOH / fly ash composite ($m = 1.0$ gm/l, pH = 5.5, T = 298 K)

Table 6.7: Effect of Initial Concentration of tannic acid on adsorption capacity of Chitosan / NaOH / fly ash composite

t (min)	C ₀ =100 ppm		C ₀ =200 ppm		C ₀ =300 ppm		C ₀ =400 ppm	
	q _t (mg/g)	% removal	q _t (mg/g)	% removal	q _t (mg/g)	% removal	q _t (mg/g)	% removal
5	40.05	40.05	61.5	30.75	103.5	34.5	27.7	6.925
10	60.9	60.9	73	36.5	108.5	36.17	69.9	17.48
15	71.25	71.25	85	42.5	117.3	39.1	123.4	30.85
30	78.95	78.95	92	46	123	40	139.9	34.98
60	79.9	79.9	101	50.5	128	42.67	145	36.25
90	82.5	82.5	110.7	55.35	131	43.67	159	39.75
120	85.2	85.2	119.8	59.9	133.7	44.57	164	41.02
300	90.25	90.25	143.9	71.95	189.5	63.17	202	50.5
600	90.25	90.25	143.9	71.95	189.5	63.17	202	50.5

(m = 1.0 gm/l, pH = 5.5, T = 298 K)

(iv) *Effect of Temperature (T)*

Effect of temperature on adsorption of tannic acid was studied at temperature 25°C, 35°C and 45°C as shown in Table 6.8 & Figure 6.12. It is observed that adsorption increases with decrease in temperature. Lower temperature may provide more chance for phenolic compound molecule to pass the external boundary layer and produce the enlargement of pore volume and surface area enabling poly phenolic compound to penetrate.

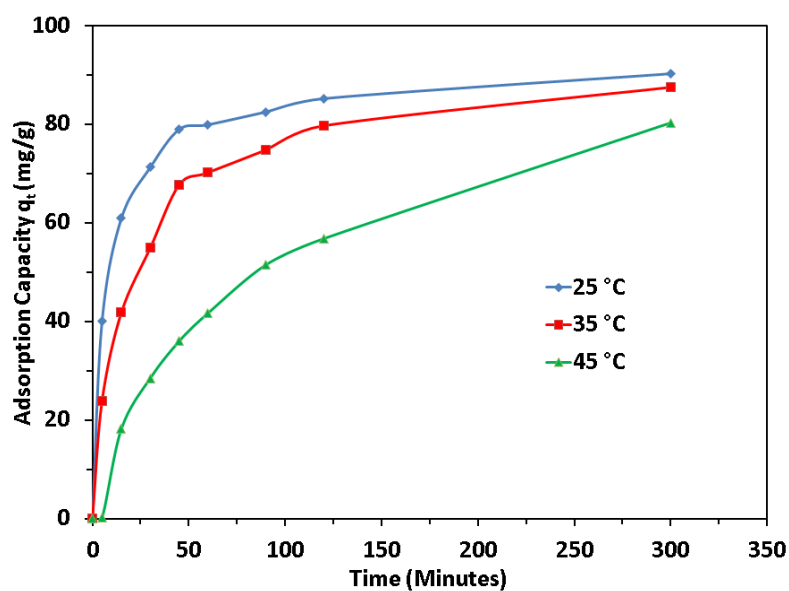


Figure 6.12 : Effect of Temperature of solution on adsorption capacity of Chitosan / NaOH / fly ash composite for tannic acid adsorption ($m = 1.0\text{gm/l}$, $\text{pH} = 5.5$, $c_0 = 100\text{ ppm}$)

Table 6.8: Effect of Temperature of solution on adsorption capacity of Chitosan / NaOH / fly ash composite for tannic acid adsorption

Time (min)	Adsorption Capacity (mg/g)		
	25 °C	35 °C	45 °C
5	40.05	23.92	0.2
15	60.9	41.8	18.2
30	71.25	54.9	28.5
45	78.95	67.7	36
60	79.9	70.2	41.7
90	82.5	74.8	51.5
120	85.2	79.7	56.8
300	90.25	87.5	80.3

(m= 1.0gm/l, pH = 5.5, $c_0 = 100$ ppm)

(v) *Effect of pH*

The initial pH of adsorption medium is one of the most important parameter affecting the adsorption process. Effect of initial pH on adsorption of tannic acid was studied with initial concentration of 100 mg l^{-1} , solution temperature $25 \text{ }^\circ\text{C}$ and adsorbent dose of 1.0 g l^{-1} . The pH was adjusted by adding 0.1 mol l^{-1} or 0.01 mol l^{-1} HCl (or NaOH) to the solutions. The effect of pH on the adsorption of tannic acid onto Chitosan / NaOH / fly ash composite and the relation of initial pH with final pH are shown in Table 6.9 & Figure 6.13. Results show that the tannic acid adsorption capacity for Chitosan / NaOH / fly ash composite is maximum at solution pH 5.5, decreases with increase in solution pH from 7.0 to 11.0 and final pH of solution change to 6.7 to 7.9. Thus pH 5.5 was selected for the following study. Tannic acid is a weak acid, and its ionization is strongly dependent on solution pH. The reduction of tannic acid adsorption below pH 5.5, is due to the low affinity between the uncharged almost undissociated tannic acid and the positively charged chitosan chain, where the left amine groups which are not used in surface attraction with NaFA are completely protonated [9] according to Eq. (6.1).



It is unlikely to be driven by the electrostatic attraction. Therefore, the hydrogen bonding and organic partitioning are responsible for the adsorption of tannic acid onto Chitosan / NaOH / fly ash composite, at solution pH 5.5. As a result, the adsorption capacity is highest at pH 5.5. Tannic acid molecules are ionized at solution pH above 5.5 and they are almost completely ionized at solution pH 7.0 [41]. Therefore, the electrostatic attraction together with the hydrogen bonding (Figure 6.8) and organic partition are responsible for the adsorption of tannic acid onto Chitosan / NaOH / fly ash composite at solution pH 5.5-7.0. The increase of solution pH from 5.5 to 7.0, despite the increasing ionization of tannic acid, the adsorption capacity decreased again, leads to decreased hydrogen bonding between tannic acid and Chitosan / NaOH / fly ash composite due to the increasing deprotonation of the OH and ammine groups of chitosan but the increased electrostatic attraction between tannic acid and Chitosan / NaOH / fly ash composite. Above pH 7.0, tannic acid is completely dissociated (equation 6.2), the OH group in chitosan chain is deprotonated (equation 6.3). Completely ionized tannic acid molecules cannot provide hydroxyl hydrogen atom to oxygen and nitrogen atom of Chitosan chain to form hydrogen bonding.



In this case, the electrostatic attraction plays an important role in the adsorption of tannic acid onto Chitosan / NaOH / fly ash composite, the increase of solution pH from 7.0 to 11.0 leads to the repulsion between the negatively charged hydroxyl group on the surface of Chitosan / NaOH / fly ash composite and the ionized tannic acid molecules, which causes a decrease in tannic acid adsorption capacity. So above this pH value it is thought that the adsorption of tannic acid mainly arises by vanderwaals interactions between tannic acid and Chitosan / NaOH / fly ash composite.

Table 6.9: Effect of pH on adsorption capacity of Chitosan / NaOH / fly ash composite for tannic acid adsorption

Initial pH	Adsorption Capacity (mg/g)	Final pH
3.6	77.5	6.7
4.1	88.8	7
5.4	91.6	7.2
6.6	90.2	7.3
7.5	83.9	7.4
8.6	80.8	7.5
9.6	77.5	7.9

($m = 1.0$ gm/l, $t = 24$ hr, $T = 298$ K, $C_0 = 100$ ppm)

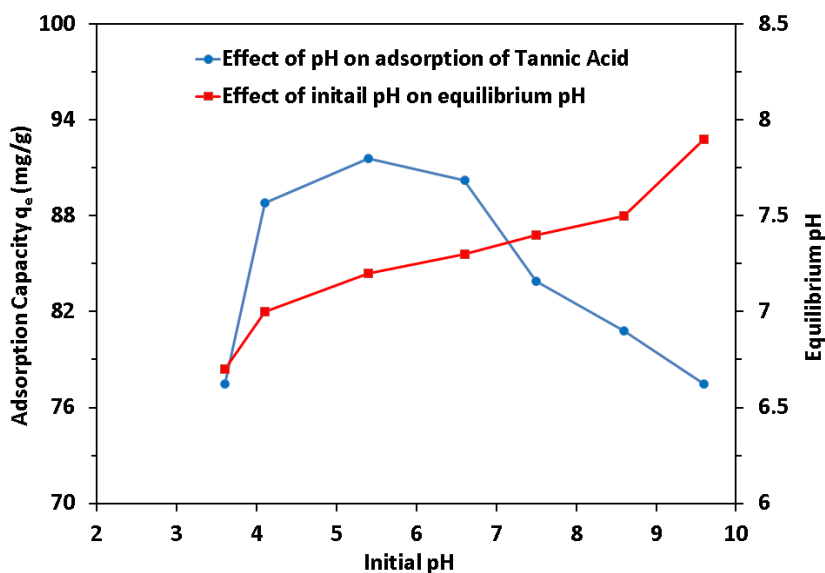


Figure 6.13: Effect of pH on adsorption capacity of Chitosan / NaOH / fly ash composite for tannic acid adsorption

($m = 1.0$ gm/l, $t = 24$ hr, $T = 298$ K, $C_0 = 100$ ppm)

(vi) *Effect of ionic strength*

The adsorption of tannic acid onto Chitosan / NaOH / fly ash composite as a function of ionic strength at solution pH 5.5 is shown in [Table 6.10](#) & [Figure 6.14](#). The presence of electrolytes such as NaCl in aqueous solution had a slight negative effect on tannic acid adsorption onto Chitosan / NaOH / fly ash composite. When the ionic strength of the aqueous solution increased from 0 to 0.05 mol/L, the tannic acid adsorption capacity decreases from 90.2 to 60 mg/g. This result suggests that Chitosan / NaOH / fly ash composite mono layer coverage is effective in removing tannic acid from water or wastewater containing salt. If electrostatic attraction is the main adsorption mechanism, the ionic strength should have a significant negative effect on the adsorption process [\[41, 42\]](#). The slight negative effect of ionic strength on tannic acid adsorption onto Chitosan / NaOH / fly ash composite at solution pH 5.5 confirms that the electrostatic attraction is not the only mechanism for the adsorption process and the electrostatic attraction together with the other mechanisms such as hydrogen bonding and organic partitioning control the adsorption process. The slight decrease of tannic acid adsorption capacity after NaCl addition may be explained below. On one hand, tannic acid adsorption onto Chitosan / NaOH / fly ash composite may be reduced by chloride ions due to the competition between the chloride ions and the ionized tannic acid ions for the adsorption sites on the surface of the adsorbent. On the other hand, tannic acid adsorption onto Chitosan / NaOH / fly ash composite may be enhanced by the sodium ions due to the weakening of the repulsive interaction between adsorbed tannic acid molecules on the surface of the adsorbent and tannic acid molecules in solution [\[36\]](#). The decreased tannic acid adsorption caused by the chloride ions may be partially counteracted by the increased tannic acid adsorption caused by the sodium ion, resulting in that tannic acid adsorption caused by the sodium ion, tannic acid adsorption is slightly reduced by the ionic strength of the aqueous solution.

Table 6.10: Effect of Ionic Strength on adsorption capacity of Chitosan / NaOH / fly ash composite for tannic acid adsorption

Ionic Strength	Adsorption Capacity (mg/g)
0	90.2
0.001	80.4
0.005	75.1
0.008	73.2
0.01	72
0.02	65
0.05	60

($m = 1.0$ gm/l, $t = 24$ hr, $T = 298$ K, $c_0 = 100$ ppm, $pH = 5.5$)

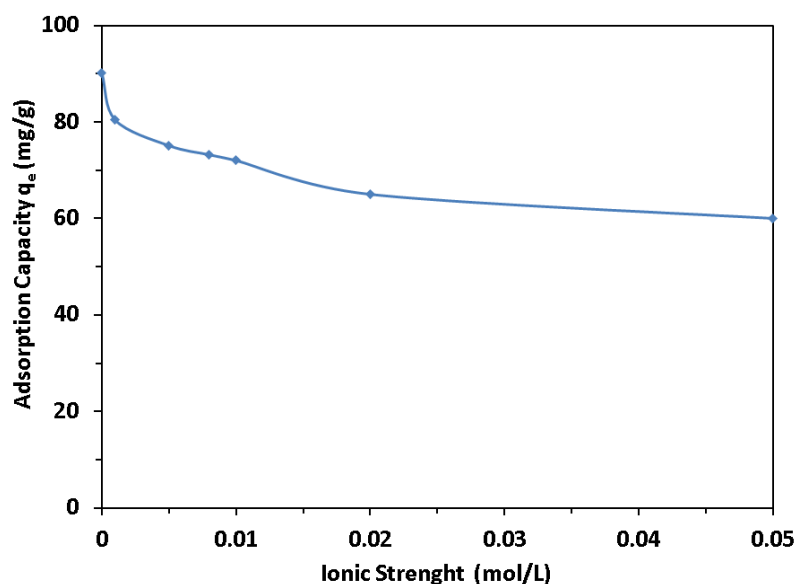


Figure 6.14: Effect of Ionic Strength on adsorption capacity of Chitosan / NaOH / fly ash composite for tannic acid adsorption

($m = 1.0$ gm/l, $t = 24$ h, $T = 298$ K, $C_0 = 100$ ppm, $pH = 5.5$)

6.3.4 Adsorption Kinetics

Four widely used kinetic models, pseudo-first-order, pseudo-second-order, Bangham's equation and intra-particle diffusion model were employed to interpret the kinetic results. All results are shown in Table 6.11 & 6.12 and in Figure 6.15.

Table 6.11: Details of all kinetic parameters for tannic acid adsorption on Chitosan / NaOH / fly ash composite

Tannic Acid C_0	time (min.)	5	15	30	45	60	90	120
		$\sqrt{\text{time}}$	2.240	3.880	5.480	6.708	7.750	9.490
	$\log t$	0.699	1.000	1.477	1.653	1.778	1.954	2.079
40 ppm	$\ln(q_e - qt)$	3.92	3.38	2.94	2.43	2.34	2.05	1.62
	t/qt	0.125	0.246	0.421	0.57	0.751	1.091	1.41
	qt	40.05	60.9	71.25	78.95	79.9	82.5	85.2
	$\log \log (C_0/C_0 - qt_m)$	-0.653	-0.399	-0.267	-0.170	-0.157	-0.121	-0.081
100 ppm	$\ln(q_e - qt)$	4.41	4.26	4.08	3.95	3.76	3.5	3.18
	t/qt	0.08	0.21	0.35	0.49	0.59	0.81	1
	qt	61.5	73	85	92	101	110.7	119.8
	$\log \log (C_0/C_0 - qt_m)$	-0.797	-0.705	-0.619	-0.573	-0.515	-0.456	-0.401
150 ppm	$\ln(q_e - qt)$	4.45	4.39	4.28	4.2	4.12	4.07	4.02
	t/qt	0.05	0.138	0.26	0.37	0.47	0.69	0.9
	qt	103.5	108.5	117.3	123	128	131	133.7
	$\log \log (C_0/C_0 - qt_m)$	-0.736	-0.71	-0.667	-0.64	-0.617	-0.603	-0.591
200 ppm	$\ln(q_e - qt)$	5.16	4.88	4.36	4.13	4.04	3.76	3.64
	t/qt	0.18	0.214	0.243	0.322	0.414	0.566	0.732
	qt	27.7	69.9	123.4	139.9	145	159	164
	$\log \log (C_0/C_0 - qt_m)$	-1.506	-1.079	-0.795	-0.728	-0.709	-0.657	-0.640

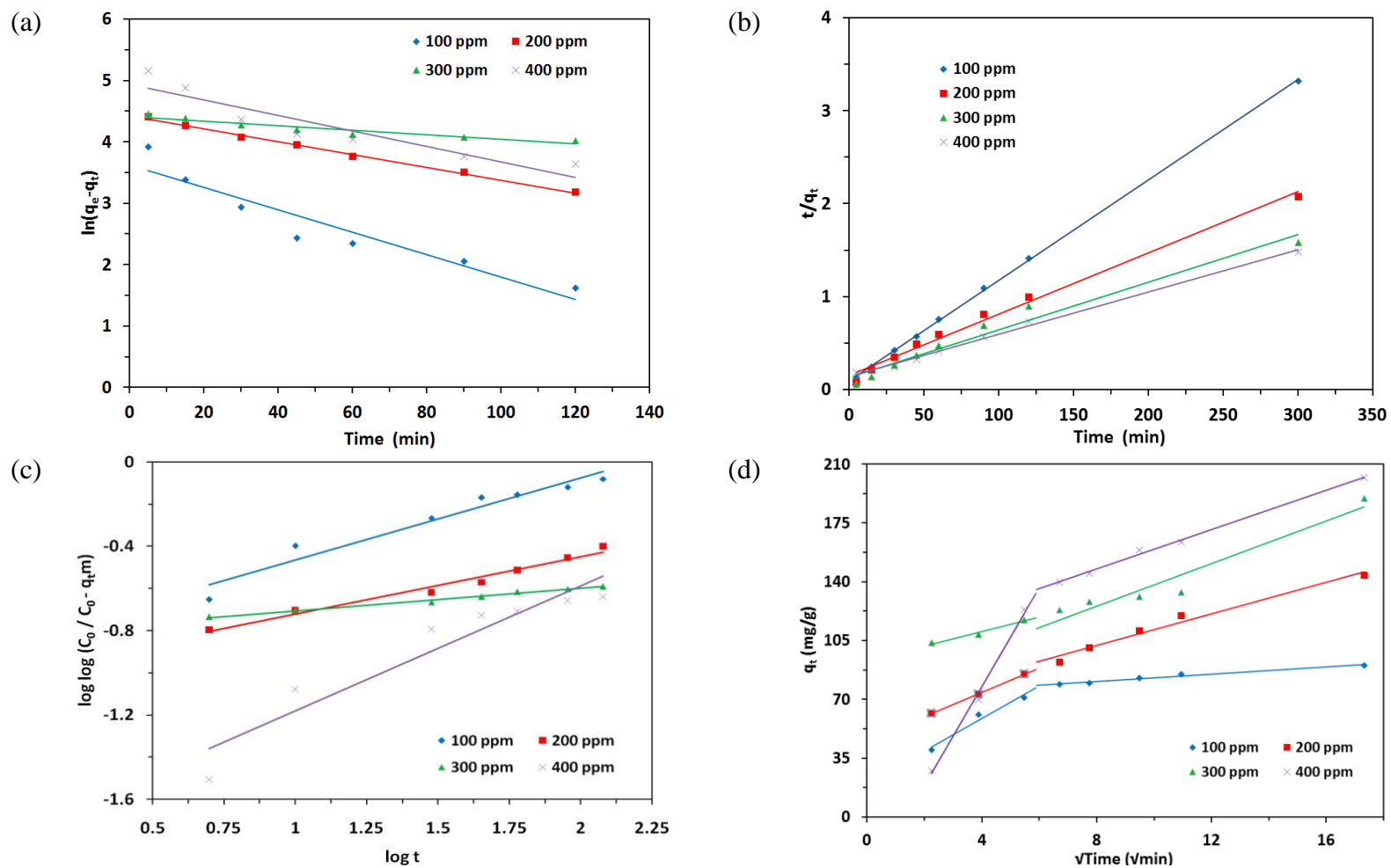


Figure 6.15: Kinetic Model (a) Pseudo Second Order, (b) Pseudo Second Order, (c) Bangham's equation and (d) intra-particle diffusion model of tannic acid adsorption on Chitosan / NaOH / fly ash composite

For pseudo-first-order kinetic model, although the R^2 value obtained was relatively high ($R^2 = 0.908$) but the calculated q_e value did not agree with the experimental one. This suggests that the pseudo-first-order kinetic model is not appropriate to represent the adsorption kinetics data of tannic acid onto Chitosan / NaOH / fly ash composite.

For pseudo-second-order kinetic model, the R^2 value obtained was very high ($R^2 > 0.999$), and the calculated q_e value was in good agreement with the experimental one, suggesting the applicability of the pseudo-second-order kinetic model to describe the adsorption kinetics data of tannic acid onto Chitosan / NaOH / fly ash composite.

Linear plots of q_e and h against C_0 were regressed to obtain these values in terms of C_0 with high a coefficient of regression (> 0.9816). Therefore, q_e and h can be express as a function of C_0 as follows:

$$q_e = 103.69 \ln C_0 - 380.71 \quad (6.4)$$

$$h = 9 \times 10^{-5} C_0^2 - 0.0541 C_0 + 14.916 \quad (6.5)$$

Substituting the value of q_e and h into Eq. (8), the relationship of q_t , C_0 and t can be represented as follows:

$$q_t = \frac{t}{1/(9 \times 10^{-5} C_0^2 - 0.0541 C_0 + 14.916) + (1/103.69 \ln C_0 - 380.71) t} \quad (6.6)$$

A comparison of experimental data points and the surface predicted by the Eq. (6.6) is given in Figure 6.16. It can be used to derive the sorption capacity, q_t at any given C_0 and t [43].

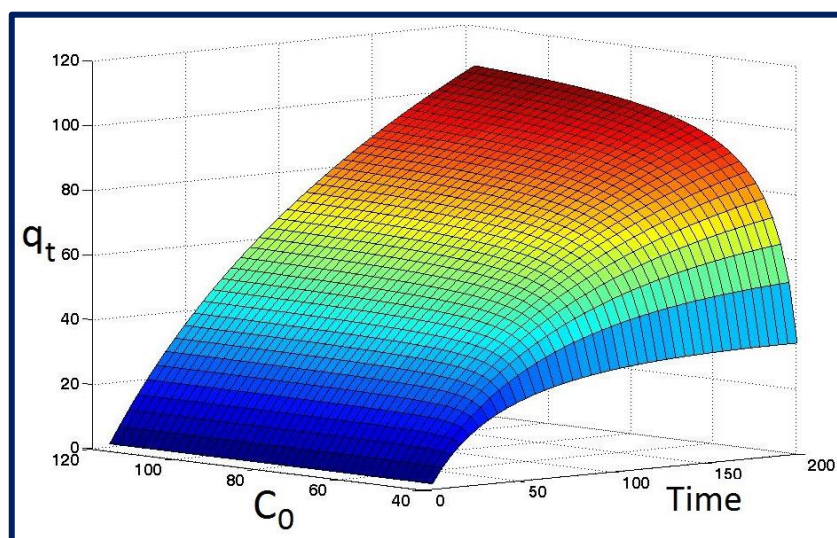


Figure 6.16: Comparison of experimental data points given by symbols and the surface predicted by the model given by Equation (6.6)

Bangham's equation [52,53] show (Figure 6.15 c) linear curves for the tannic acid removal by the Chitosan / NaOH / fly ash composite, signifying that the diffusion of adsorbate into the pores of the adsorbent was the only rate-controlling step [52,54]. It may be that pore diffusion was important to in the removal process.

For the intra-particle diffusion model, graphical plot of q_t versus $t^{0.5}$ (Figure 6.15 d) is giving straight line passing through the origin, then the sorption process fits to the intraparticle diffusion kinetic model. The intraparticle diffusion plot is found in two steps. It indicates that adsorption of tannic acid on Chitosan / NaOH / fly ash composite occur in two steps. In first step, the adsorption of adsorbates occurs on an external surface of adsorbents, while in second step, the adsorbates penetrate through the pores of the adsorbents indicating that intraparticle diffusion is the rate limiting step [27]. The $K_{id,1}$ and $K_{id,2}$ values (Table 6.12) are the rate parameter for first step and second step respectively. The values of rate parameters are lower indicating that tannic acid diffuses more into the interior pores of the sorbents. The values of intercepts 'C' which is in the range of 20.12-100.92 mg g^{-1} for tannic acid reveals the thickness of boundary layer having larger values. In intraparticle diffusion model, the coefficient values (R^2) are nearer to that of the pseudo-second-order kinetic model, which denote

that the intraparticle is not only the rate controlling step. It may be concluding that the film diffusion and intraparticle diffusion both function are parallel.

Table 6.12: Pseudo-first order, Pseudo-second order, Bangham's equation and Intra-particle Diffusion Model rate constants for tannic acid adsorption onto Chitosan / NaOH / fly ash composite at various concentrations

C_0 (mg/L)		100	200	300	400
$q_{e, exp}$ (mg/g)		90.25	143.9	189.5	202.0
Pseudo-first order model	K_1 (1/min)	0.018	0.010	0.003	0.012
	$q_{e, cal}$ (mg/g)	37.30	83.18	82.52	139.77
	R^2	0.898	0.996	0.908	0.860
Pseudo-second order	K_2 (g/mg min)	10.8×10^{-4}	2.4×10^{-4}	1.92×10^{-4}	1.12×10^{-4}
	$q_{e, cal}$ (mg/g)	100	166.67	200	250
	h	10.75	6.54	7.69	6.99
	R^2	0.999	0.990	0.966	0.996
Bangham's equation	K_0 (g)	16.14	11.67	17.59	1.930
	α	0.3881	0.2719	0.1079	0.5935
	R^2	0.9455	0.9771	0.9894	0.9022
Intra-particle Diffusion Model	$K_{id,1}$ (mg/g(min ^{0.5}))	9.643	7.252	4.254	29.25
	C_1	20.116	45.125	93.317	40.482
	R^2	0.9662	0.9996	0.9731	0.9941
	$K_{id,2}$ (mg/g(min ^{0.5}))	1.0756	4.7213	6.3393	5.85
	C_2	72.127	64.173	74.835	100.92
	R^2	0.9707	0.9765	0.9336	0.9961

($m = 0.5 \text{ g l}^{-1}$, agitation rate = 200 rpm, pH = 5.5, T = 25 °C)

6.3.5 Adsorption isotherm

The adsorption isotherms of tannic acid onto Chitosan / NaOH / fly ash composite at 25°C, 35°C and 45°C and solution pH 5.5 is shown in Figure 6.17 and values of isotherm parameters are given in Table 6.13. Results showed that the tannic acid adsorption capacity increased with increasing the tannic acid concentration until equilibrium was reached. Two-parameter isotherm models Langmuir, Freundlich, Dubinin - Redushkevich (D-R), Tempkin and three-parameter isotherm model Redlich - Peterson were used to fit the experimental data as described in chapter 2.

Table 6.13: Isotherm parameters for adsorption of tannic acid on Chitosan / NaOH / fly ash composite

T (°C)	Parameters						
25 °C	C_e	9.75	56.1	110.5	198	280.1	371
	$\ln C_e$	2.277	4.027	4.705	5.288	5.635	5.916
	$\log C_e$	0.989	1.749	2.043	2.297	2.447	2.569
	q_e	90.25	143.9	189.5	202	219.9	229
	$\log q_e$	1.96	2.16	2.28	2.3	2.34	2.36
	C_e / q_e	0.108	0.39	0.58	0.98	1.27	1.62
	$\ln(K_R C_e / q_e - 1)$	1.78	3.18	3.59	4.12	4.39	4.63
	$\ln q_e$	4.5	4.97	5.24	5.31	5.39	5.44
	ϵ^2	58518.6	1916.2	498.2	155.8	77.96	44.5
35 °C	C_e	12.5	68.8	134.7	220	312	408
	$\ln C_e$	2.53	4.23	4.9	5.39	5.74	6.01
	$\log C_e$	1.097	1.84	2.13	2.34	2.49	2.61
	q_e	87.5	131.2	165.3	180	188	192
	$\log q_e$	1.94	2.12	2.22	2.26	2.27	2.28
	C_e / q_e	0.143	0.524	0.815	1.22	1.66	2.12
	$\ln(K_R C_e / q_e - 1)$	2.03	3.42	3.87	4.28	4.59	4.84
	$\ln q_e$	4.47	4.88	5.12	5.19	5.24	5.26
	ϵ^2	38838.6	1365.4	858.7	134.9	67.1	39.3
45 °C	C_e	19.7	77	154.9	234.8	329.7	427.9
	$\ln C_e$	2.98	4.34	5.04	5.458	5.798	6.06
	$\log C_e$	1.29	1.89	2.19	2.37	2.52	2.63
	q_e	80.3	123	145.1	165.2	170.3	172.1
	$\log q_e$	1.9	2.09	2.16	2.22	2.23	2.24
	C_e / q_e	0.245	0.626	1.068	1.42	1.94	2.5
	$\ln(K_R C_e / q_e - 1)$	2.33	3.32	3.87	4.16	4.48	4.73
	$\ln q_e$	4.39	4.81	4.98	5.12	5.14	5.15
	ϵ^2	17137.6	1163.8	289.5	126.3	64.1	38.1

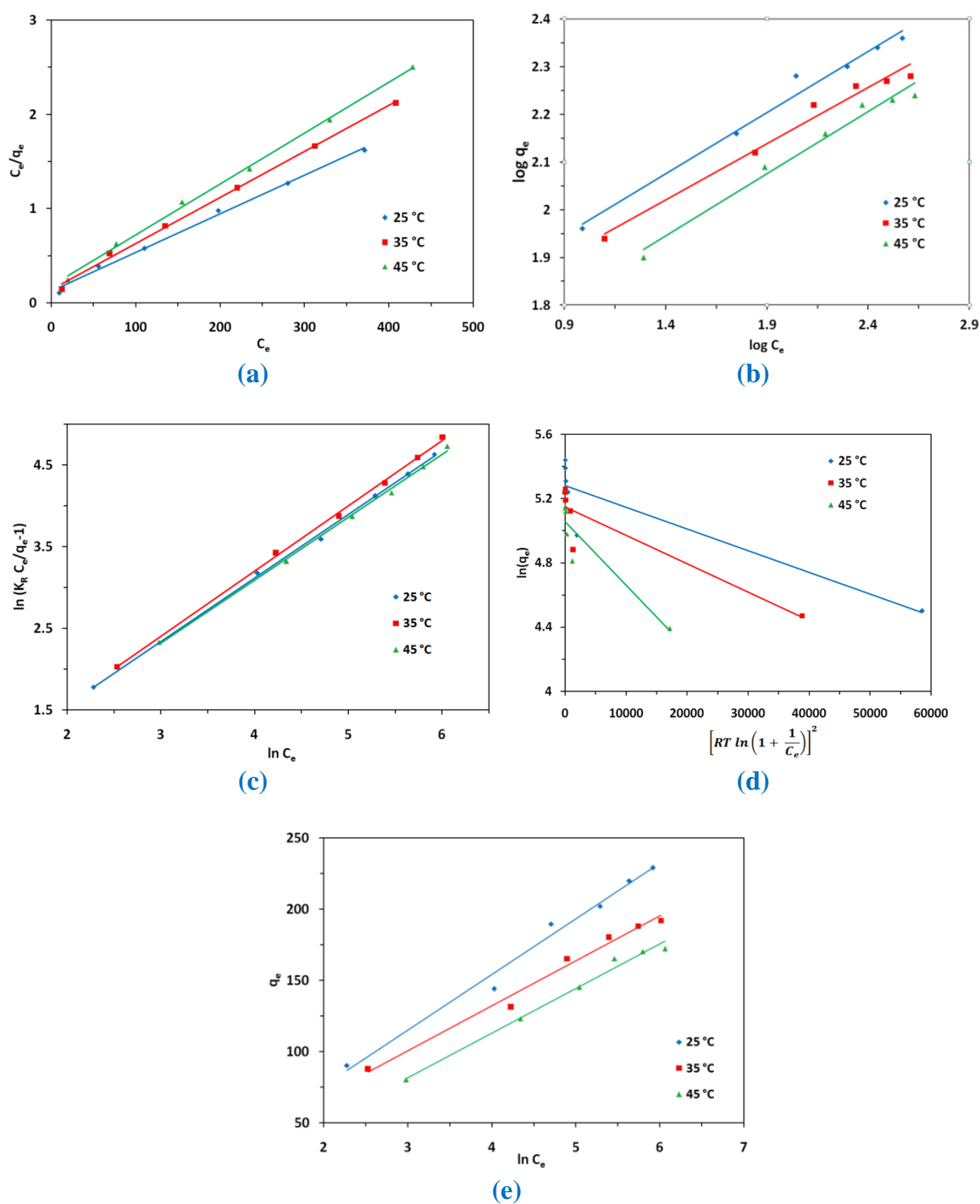


Figure 6.17: Adsorption isotherm of tannic acid adsorption on Chitosan / NaOH / fly ash composite (a) Langmuir (b) Freundlich (c) Redlich-Peterson (d) D-R and (e) Tempkin

The different isotherm parameters were evaluated from the linear plots and presented in Table 6.14 along with constants and correlation coefficients root mean square error (RMSE) and chi-square (χ^2). The RMSE and χ^2 are used to measure the goodness of fit of an isotherm defined in chapter 2.

The value of RMSE and χ^2 for the Langmuir and D-R isotherm models were high, indicating that the equilibrium adsorption of tannic acid onto Chitosan / NaOH / fly ash composite cannot be represented appropriately by these isotherm models. The values of RMSE and χ^2 for the Redlich-Peterson, Tempkin and Freundlich isotherm models were low, indicating that the equilibrium data for the adsorption of tannic acid onto Chitosan / NaOH / fly ash composite can be well represented by these three isotherm models. Langmuir isotherm model can be concluded that the adsorption of tannic acid onto Chitosan / NaOH / fly ash composite takes place as monolayer adsorption and the surface of Chitosan / NaOH / fly ash composite is homogenous in adsorption affinity. The predicted maximum monolayer tannic acid adsorption capacity for Chitosan / NaOH / fly ash composite derived from Langmuir isotherm was found to be 243.90 mg/g. The values of R_L obtained in this study were between 0.066 and 0.2304 indicating that the adsorption of tannic acid onto Chitosan / NaOH / fly ash composite is favourable.

Table 6.14: Isotherm parameters for tannic acid adsorption onto Chitosan / NaOH / fly ash composite at various temperatures

Langmuir	T (°C)	q_{max} (mg/g)	K_L (L/mg)	R²	RMSE	χ²	
	at 25	243.90	0.0334	0.9957	17.77	12.35	
	at 35	204.08	0.03538	0.9977	14.28	8.56	
	at 45	185.18	0.0299	0.9981	7.74	2.44	
Freundlich	T (°C)	K_F (mg/g)(L/mg)^{1/n}	1/n	R²	RMSE	χ²	
	at 25	51.88	0.257	0.9827	9.05	1.73	
	at 35	49.125	0.235	0.9783	7.55	1.29	
	at 45	38.03	0.261	0.9783	8.07	1.63	
Tempkin	T (°C)	K_T (mg/g)	B_T	R²	RMSE	χ²	
	at 25	1.054	39.02	0.984	7.24	1.381	
	at 35	1.201	31.57	0.985	5.52	0.844	
	at 45	1.477	31.37	0.988	4.31	0.447	
D-R	T (°C)	q_{max} (mg/g)	K_D (mg²/KJ²)	R²	RMSE	χ²	
	at 25	196.17	-1x 10 ⁻⁵	0.807	33.32	8.06	
	at 35	171.57	-2 x 10 ⁻⁵	0.822	23.22	14.86	
	at 45	156.96	-4 x 10 ⁻⁵	0.849	18.23	9.54	
Redlich Peterson	T (°C)	K_R (L/g)	α_R (L/mg)^β	β	R²	RMSE	χ²
	at 25	64	1.006	0.776	0.998	7.90	1.32
	at 35	60	1.01	0.797	0.998	6.34	0.943
	at 45	45.9	1.003	0.770	0.998	6.706	1.12

(m = 0.5 g l⁻¹, agitation rate = 200 rpm, pH = 5.5, C₀ = 50 - 300 mg l⁻¹)

6.3.6 Thermodynamic Studies

The thermodynamic parameters of standard enthalpy (ΔH°) and entropy (ΔS°) for the adsorption process were estimated from the Van't-Haff equation as described in chapter 2.

The values of K_L for Langmuir isotherm at 25 °C, 35°C and 45 °C were used to calculate thermodynamic parameters such as Gibbs free energy change (ΔG°). The values of ΔH° and ΔS° can be calculated from the intercept and the slope of the linear plot of $\ln K_L$ versus $1/T$ as shown in Figure 6.18.

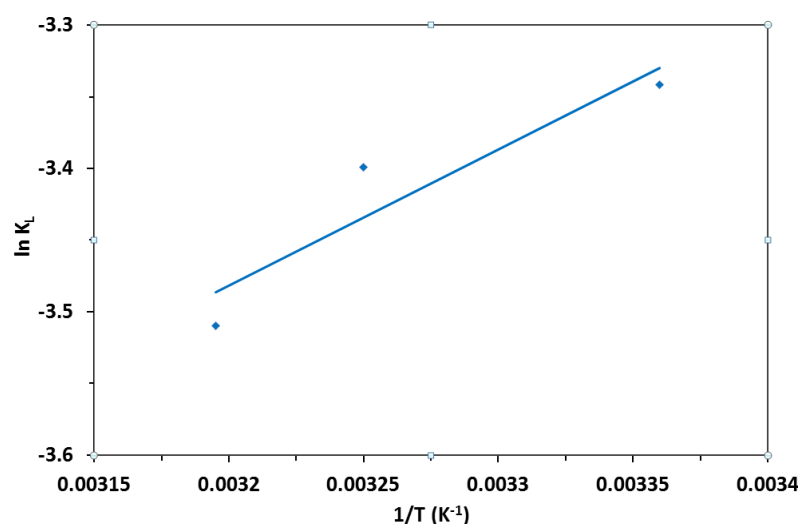


Figure 6.18: Van't Hoff plot for the adsorption of tannic acid onto Chitosan / NaOH / fly ash composite

The obtained values of the thermodynamic parameters of tannic acid adsorption onto Chitosan / NaOH / fly ash composite are given in Table 6.15. The negative values of ΔG° suggest that adsorption of tannic acid onto Chitosan / NaOH / fly ash composite is spontaneous and favourable process. In general, the value of ΔG° for physisorption is < 8.0 kJ/mol, and that chemisorption is between 20 and 40 kJ/mol [56]. The values of ΔG° obtained in this study were in the range of neither physisorption nor chemisorption, indicating that the adsorption of tannic acid onto Chitosan / NaOH / fly ash composite involves the other adsorption process such as hydrogen bonding. This conclusion confirms that the mechanisms controlling the adsorption of tannic acid onto Chitosan / NaOH / fly

ash composite at solution of pH 5.5 include hydrogen bonding and electrostatic attraction.

Table 6.15: Thermodynamic parameters for tannic acid adsorption on Chitosan / NaOH / fly ash composite

ΔH° (KJ/mol)	ΔS° (J/mol)	ΔG° (KJ/mol)			R^2
		25 °C	35 °C	45 °C	
-7.87	54.08	-8.407	-8.542	-9.118	0.868

The negative value of ΔH° indicates that the adsorption process is exothermic in nature. The absolute value of ΔH° was 7.87 kJ/mol, also indicates that hydrogen bonding and organic partitioning are important to the adsorption process in addition to electrostatic attraction. The positive value of ΔS° shows an increase in randomness at the solid/liquid interface during the adsorption process [59].

6.3.7 Adsorption performance of Chitosan / NaOH / fly ash composite

Table 6.16 lists the comparison of the maximum adsorption capacity of tannic acid onto various adsorbent obtained from adsorption experiments. The Chitosan / NaOH / fly ash composite prepared in this work has a relatively large adsorption capacity of 243.90 mg g⁻¹ compared to some other adsorbents reported in the literature. Therefore, the Chitosan / NaOH / fly ash composite prepared in this work could be used as an effective adsorbent for removing tannic acid from solution.

Table 6.16: Comparison of the maximum monolayer adsorption of tannic acid onto various adsorbents

Adsorbents	Adsorption Capacity (mg/g)	References
Activated carbon	162	[44]
Organo-clay	110	[45]
Montmorillonite	219	[9]
Clay	138	[32]
Chitosan / NaOH / fly ash composite	243.90	This work

6.4 Conclusion

After Modification with the chitosan, zeolitic material that was hydrothermally synthesized from fly ash exhibited greatly enhanced adsorptive capacity for tannic acid. Chitosan / NaOH / fly ash composite has good physical as well as chemical stability, hence it can be used for various environmental applications. N₂ adsorption isotherms of Chitosan / NaOH / fly ash composite is of combination of type II and type IV. The values of BET surface area, pore volume and pore diameter are 23.75 m²/gm, 0.103612 cm³/gm and 174.4739 Å respectively. The results show that Chitosan / NaOH / fly ash composite includes mesopores. Redlich-Peterson, Tempkin and Freundlich equation is best fitted for the description of tannic acid adsorption isotherm. Adsorption of tannic acid onto Chitosan / NaOH / fly ash composite increases with decrease in temperature indicating that the process is exothermic. The monolayer adsorption capacity for tannic acid is 243.90 mg/g. The adsorption kinetics of tannic acid onto Chitosan / NaOH / fly ash composite was found to follow a pseudo-second order model with intraparticle diffusion model. The thermodynamic parameters such as ΔH° , ΔS° and ΔG° values show an exothermic heat of adsorption, the feasibility of the adsorption process and its spontaneity, respectively. The tannic acid adsorption capacity for Chitosan / NaOH / fly ash composite slightly decreased with increasing ionic strength. The tannic acid adsorption capacity was maximum at solution pH 5.5 and decreased with increasing solution pH from 7.0-11.0. The main mechanism controlling tannic acid adsorption onto Chitosan / NaOH / fly ash composite at solution pH < 7.0 include electrostatic attraction, hydrogen bonding and organic partitioning.

6.5 References

- [1] J.H. Wang, S.R. Zheng, J.L. Liu, Z.Y. Xu, *Chem. Eng. J.*, 165 (2010) 10-16.
- [2] J.N. Wang, A.M. Li, L. Xu, Y. Zhou, *J. Hazard. Mater.*, 169 (2009) 794-800.
- [3] J.H. Wang, C.L. Zheng, S.L. Ding, H.R. Ma, Y.F. Ji, *Desalination*, 273 (2011) 285-91.
- [4] P.C. Chiang, E.E. Chang, P.C. Chang, C.P. Huang, *Sci. Total Environ.*, 407 (2009) 5735-42.
- [5] W.W. Li, X.D. Li, K.M. Zeng, *Biochem. Eng. J.*, 43 (2009) 142-48.
- [6] Y. Sun, A.M. Li, Q.X. Zhang, J.L. Chen, D.F. Fu, S.H. Wang, *Sep. Sci. Technol.*, 43 (2008) 389-402.
- [7] T.S. Anirudhan, M. Ramachandran, *J. Colloid Interface Sci.*, 299 (2006) 116-24.
- [8] J.H. Huang, Y.F. Liu, X.G. Wang, *J. Hazard. Mater.*, 160 (2008) 382-87.
- [9] J.H. An, S. Dultz, *Appl. Clay Sci.*, 36 (2007) 256-64.
- [10] T.S. Anirudhan, P.S. Suchithra, *Ind. Eng. Chem. Res.*, 46 (2007) 4606-13.
- [11] C. Sarıcı-Ozdemir, Y. Onal, *Desalination*, 251 (2010) 146-52.
- [12] F. Liu, X.G. Luo, X.Y. Lin, *J. Hazard. Mater.*, 178 (2010) 844-50.
- [13] D. Karadag, M. Turan, E. Akgul, S. Tok, A. Faki, *J. Chem. Eng. Data* 52 (2007) 1615-20.
- [14] M.K. Purkait, S. DasGupta, S. De, *J. Environ. Manage.*, 76 (2005) 135-42.
- [15] H.L. Wang, W.F. Jiang, *Ind. Eng. Chem. Res.* 46 (2007) 5405-11.
- [16] W.T. Tsai, H.C. Hsu, T.Y. Su, K.Y. Lin, C.M. Lin, *J. Colloid Interface Sci.*, 299 (2006) 513-19.
- [17] B.H. Hameed, *Colloids Surf., A* 307 (2007) 45-52.
- [18] S.H. Lin, M.J. Cheng, *Waste Manage.*, 22 (2002) 595-603.
- [19] G.M. Zeng, C. Zhang, G.H. Huang, J. Yu, Q. Wang, J.B. Li, B.D. Xi, H.L. Liu, *Chemosphere*, 65 (2006) 1490-99.

- [20] R. Baciocchi, M.R. Boni, R. Lavecchia, *J. Hazard. Mater.*, 118 (2005) 239-46.
- [21] S. Andini, R. Cioffi, F. Colangelo, F. Montagnaro, L. Santoro, *J. Hazard. Mater.*, 157 (2008) 599-604.
- [22] S.P. Kamble, P.A. Mangrulkar, A.K. Bansiwai, S.S. Rayalu, *Chem. Eng. J.*, 138 (2008) 73-83.
- [23] X. Querol, N. Moreno, J.C. Uman, A. Alastuey, E. Hernandez, A Lopez-Soler, F. Plana, *Int. J. Coal Geol.*, 50 (2002) 413-23.
- [24] D.Y. Wu, B.H. Zhang, C.J. Li, Z.J. Zhang, H.N. Kong, *J. Colloid Sci.*, 304 (2006) 300-306.
- [25] N. Moreno, X. Querol, C. Ayora, *Environ. Sci. Technol.*, 35 (2001) 3526-3534.
- [26] J.G. Chen, H.N. Kong, D.Y. Wu, Z.B. Hu, Z.S. Wang, Y.H. Wang, *J. Colloid Interface Sci.*, 300 (2006) 491-97.
- [27] X. Querol, N. Moreno, J.C. Umana, R. Juan, S. Hernandez, C. Fernandez-pereira, C. Ayora, M. Janssen, J. Garcia-Martinez, A. Linares-Solano, D. Cazorla-Amoros, *J. Chem. Technol. Biotechnol.*, 77 (2002) 292-98.
- [28] S.B. Wang, Y.L. Peng, *Chem. Eng. J.*, 156 (2010) 11-24.
- [29] Y. Dong, D.Y. Wu, X.C. Chen, Y. Lin, *J. Colloid Interface Sci.*, 348 (2010) 585-90.
- [30] C.J. Li, Y. Dong, D.Y. Wu, L.C. Peng, H.N. Kong, *Appl Clay Sci.*, 52 (2011) 353-57.
- [31] M. Darder, M. Colilla, E. Ruiz-Hitzky, *Chem. Mater.*, 15 (2003) 3774-80.
- [32] M.Y. Chang, R.S. Juang, *J. Colloid Interface Sci.*, 278 (2004) 18-25.
- [33] F.C. Wu, R.L. Tseng, R.S. Juang, *Ind. Eng. Chem. Res.*, 38 (1999) 270-75.
- [34] F.C. Wu, R.L. Tseng, R.S. Juang, 2001. *J. Hazard. Mater.*, B 81(2001) 167-77.
- [35] L. Dambies, C. Guimon, S. Yiacoumi, E. Guibal, *Colloids Surf., A Physico chem. Eng. Asp.*, 177 (2001) 203-14.
- [36] S. Agarwal, A. Rani, *J. of Environ. Chem. Eng.*, 5 (2017) 526-38.

- [37] J. Xie, W. Meng, D. Wu, Z. Zhang, H. Kong, *J. Hazard. Mater.*, 231-232 (2012) 57-63.
- [38] K.H.S. Kung, K.F. Hayes, *Langmuir*, 9 (1993) 263-67.
- [39] S.J. Gregg, K.S.W. Sing, Adsorption, in: *Surface Area and Porosity*, 2nd ed., Academic Press, London, 1982.
- [40] W.T. Tsai, H.C. Hsu, T.Y. Su, K.Y. Yu Lin, C.M. Lin, T.H. Tai, *J. of Hazard. Mater.*, 147 (2007) 1056-62.
- [41] J. Lin, Y. Zhan, Z. Zhu, Y. Xing, *J. Hazard. Mater.*, 193 (2011) 102-11.
- [42] Z.H. Wang, B. Xiang, R.M. Cheng, Y.J. Li, *J. of Hazard. Mater.*, 183 (2010) 224-32.
- [43] V. S. Mane, I. D. Mall, V. C. Srivastava, *J. of Environ. Manag.*, 84 (2007) 390-400.
- [44] C.T. Hsieh, H. Teng. *Carbon*, 38 (2000) 863-69.
- [45] S.K. Dentel, A.I. Jamrah, D.L. Sparks, *Water Res.*, 32 (1998) 3689-97.



Chapter-7

***Adsorption of 4-chloro-2-methyl
phenoxyacetic acid (MCPA) from Aqueous
Solution onto CTAB / NaOH / Fly Ash
Composites: Equilibrium, Kinetics,
Thermodynamics and Modeling***

ABSTRACT

Various technologies have been used for the treatment and remediation of areas contaminated by pesticides. In this work, a surfactant modified NaOH treated fly ash (CTAB / NaOH / fly ash composite) was investigated for its efficiency in removing 4-chloro-2-methylphenoxyacetic acid (MCPA) from aqueous solutions in a batch system. CTAB / NaOH / fly ash composite presented higher MCPA adsorption efficiency than FA and NaFA. This may be attributed to the hydrophobicity imparted by surfactant molecules on the surface of NaFA, consequently leading to organic partitioning. The effects of pH, contact time, initial solute concentration, adsorbent dose, ionic strength, and temperature on the adsorption of MCPA onto modified fly ash were investigated. The MCPA adsorption capacity slightly decreased with increasing ionic strength adjusted by NaCl. Kinetics studies indicated that the adsorption equilibrium was reached within 15 min. and followed pseudo second order kinetics. The Langmuir, Freundlich, Redlich–Peterson, D-R and Temkin models were used to evaluate the MCPA adsorption by CTAB / NaOH / fly ash composite. The Redlich-Peterson isotherm model was found to be best for MCPA removal at all concentration. The maximum monolayer adsorption capacity for MCPA was 5.65 mg/g at 30 °C. The value of ΔG° , ΔS° and ΔH° indicated spontaneous and exothermic adsorption process. From the results it can be concluded that the surfactant-modified fly ash could be a good adsorbent for treating MCPA-contaminated waters.

7.1 Introduction

Pesticides are the major input in today's intensive agriculture. Wide spread use of these agricultural inputs has caused contamination of ground and surface water due to their leaching and runoff losses. Improper disposal of the empty pesticide containers, washing of spray instruments and unregulated discharge from manufacturing units are other causes of sources of this contaminant. Many pesticides that are commonly used are resistant to natural degradation in the environment; hence, there is a concern about possible adverse human health effects and ecotoxicity [1, 2]. Chlorophenoxy herbicides, which have potential toxicity toward humans and animals [3] and are suspect mutagens and carcinogens, are used worldwide on a large scale as plant growth regulators for agricultural and non-agricultural purposes.

Among them, 4-chloro-2-methylphenoxyacetic acid (MCPA) is used in amounts exceeding 2000 tons per year in Western European countries [4]. MCPA has a relatively high water solubility (825 mg L^{-1}), low retention potential in soils ($K_d = 0.21\text{--}2.7 \text{ L kg}^{-1}$), and its intensive use are responsible for the contamination of ground and surface waters at concentrations frequently above the European threshold for drinking water, $0.1 \mu\text{g L}^{-1}$ (Environmental Agency, 2003). Indeed, MCPA was one of the most abundant pesticides in terms of frequency of detection in rivers and lakes [5] and groundwater [6]. Furthermore, this herbicide has been classified by the U.S. Environmental Protection Agency (EPA) as a potential groundwater contaminant [7]. It is used as the dimethylammonium, potassium, or sodium–potassium salt in commercial preparations, very often formulated together with other chlorophenoxy pesticides (2,4-D, dicamba, MCPB) and is widely used for controlling broad leaf weeds mainly in cereals, grasses, plants, tobacco and cotton [8]. However, when MCPA is used in the agricultural area, only a minor proportion reaches the target [9]. Most of it penetrates in the soil and enters the surface water as a result of runoff from agricultural land [10]. Hence, it has potential toxicity for humans and animals, such as irreversible damage to the nervous system after adsorption, and causing dizziness and cough after inhalation [11]. It is therefore imperative to

develop effective management practices to control water contamination by MCPA.

Number of methods used for the clean-up of water includes, oxidation with ozone, biological method, ion exchange, electrochemical oxidation, reverse osmosis, photocatalytic degradation and adsorption. Each method has its own merits and limitations in application. Despite the availability of number of clean up methods, adsorption process still remains the best method as it is not specific to only one type of contaminant and removes most of the contaminants. Activated charcoal is the most commonly used adsorbent for removing pesticide residue from contaminated water [12-14]. Other materials investigated as adsorbents for pesticides includes, charcoal from agro waste [15-17], straw [18, 19], date and olive stones [20, 21], wood chips/corn cob [19], lignocellulosic substrate from agro industry [22], bark [23], watermelon peel [24], baggasse fly ash [25, 26].

The removal of MCPA from aqueous solutions by activated spent bleaching earth (SBE) [27], organic polymer resin Lewatit VP OC 1163 [28], on layered double hydroxides (LDHs) [29], on the surface of goethite and of humic acid-coated goethite [30], Polish agricultural soils [31], on an argentine montmorillonite (MMT) and its organo-montmorillonite product (OMMT) with different dodecyl trimethyl ammonium loading [32], on Cu-Fe-NO₃-LDH [33] are reported. However, because of high cost and low abundance of these adsorbents, exploitation of newer, cheaper and indigenous waste materials for the removal of pesticides from water and waste water have been the focus of intense research.

In the present work a systematic study of the adsorption capacity of MCPA from aqueous solution by CTAB / NaOH / fly ash composite is reported. The effects of several experimental parameters such as contact time, initial adsorbate dosage, initial adsorbent concentration, temperature, ionic strength and solution pH on MCPA adsorption onto CTAB / NaOH / fly ash composite were investigated. The experimental results were analyzed by kinetic and isotherm models. Thermodynamic parameters such as Gibbs free energy change (ΔG°), enthalpy change (ΔH°) and entropy change (ΔS°) were calculated. The

mechanism for MCPA adsorption onto CTAB / NaOH / fly ash composite is also proposed.

7.2. Materials and methods

7.2.1 Adsorbate

MCPA of Sigma aldrich, NaOH, HCl were purchased from S.D. Fine Chemicals Ltd, India. Structure of MCPA is shown in [Figure 7.1](#).

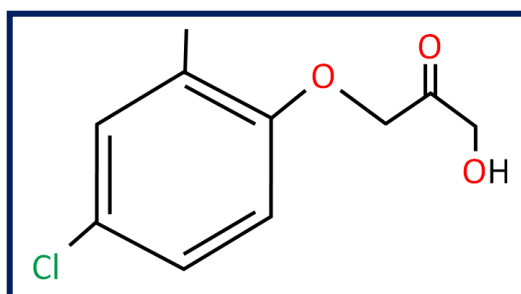


Figure 7.1: Structure of MCPA

7.2.2 Synthesis of CTAB / NaOH / fly ash composite

Synthesis of adsorbent CTAB / NaOH / fly ash composite has already discussed in chapter 5.

7.2.3 Adsorption experiments

The concentrations of MCPA was measured with Double Beam UV/Visible spectrophotometer (model Spectrascan UV 2600/02) at the wavelength of 225 nm. The experimental setup is as described in Chapter 2 and adsorbent preparation described in Chapter 5.

7.3. Result and discussion

7.3.1 Characterization of Adsorbent

Characterization of adsorbent CTAB / NaOH / fly ash composite has already discussed in chapter 5.

7.3.2 Effect of surfactant loading on NaFA

Figure 7.2 reveals the schematic representation of mechanism of adsorption of MCPA by CTAB / NaOH / fly ash composite. The effect of surfactant loading on removal of MCPA was given in Table 7.1. It was found that the MCPA adsorption efficiency was increased with increase loading amount of CTAB on NaFA. After surfactant loading with 11 mmol l^{-1} there was no further increase in adsorption efficiency due to excessive crowding of monomers of surfactant molecule on external surface of NaFA, which might have blocked the organic partitioning created by tails of long chain alkyl compound for adsorption of organics. Therefore CTAB / NaOH / fly ash composite with 11 mmol l^{-1} loading amount of CTAB was the most efficient adsorbent for the removal of MCPA from aqueous solution.

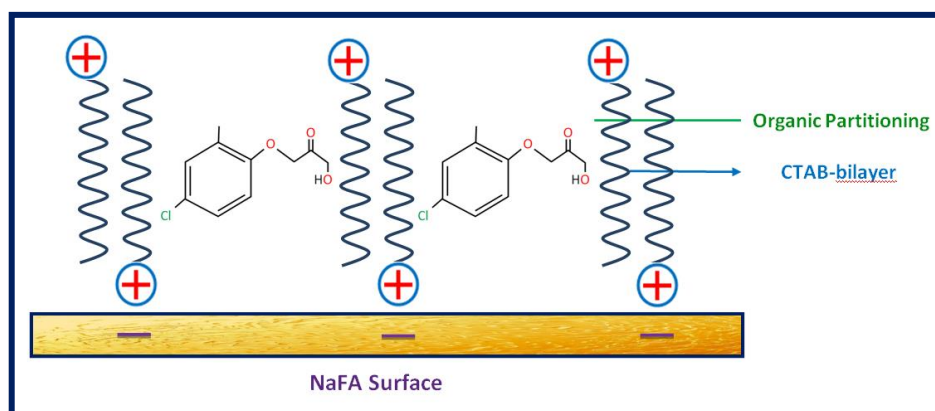


Figure 7.2: Schematic representation of adsorption of MCPA on CTAB / NaOH / fly ash composite

(Interaction mechanisms of MCPA, as an example of organic pollutants, with CTAB / NaOH / fly ash composite. In this figure, the meaning of the symbols are as follows: \oplus the head of CTAB; \sim the C-16 chain of CTAB; --- NaFA in which --- represents the negative charge and show the interaction between the hydrophobic benzene ring of MCPA and the hydrophobic C-16 chain of CTAB as a function to contribute in adsorption.)

Table 7.1: Effect of surfactant loading on NaFA on adsorption for MCPA

NaFA dose (g)	CTAB concentration (mmol l ⁻¹)	Surfactant Loading (mmol l ⁻¹)	Adsorption capacity of MCPA (mg/g)
10	2	0.032	-
10	4	0.045	-
10	6	0.062	0.5
10	8	0.096	1.4
10	11	0.141	3.9

(m = 4 g l⁻¹, agitation rate = 200 rpm, pH = 6.9, C₀ of MCPA = 50 ppm, T = 303 K, t = 24 h)

7.3.3 Effect of various parameters on adsorption of MCPA

(i) Preliminary adsorption experiments

The preliminary adsorption experiments under identical set of experimental conditions were carried out using FA, NaFA and CTAB / NaOH / fly ash composite. Removal of MCPA on FA and NaFA was not observed. Only CTAB / NaOH / fly ash composite showed adsorptive removal of MCPA. This may be attributed to the hydrophobicity imparted by surfactant leading to organic partitioning. Therefore, further experiments were carried out using CTAB / NaOH / fly ash composite for optimization of adsorption parameters.

(ii) Effect of adsorbent dosage

The adsorption of MCPA on CTAB / NaOH / fly ash composite was carried out at different adsorbent dosages by keeping other parameters constants. The relationship between adsorbent dose and contact time for MCPA removal is presented in [Table 7.2](#) and [Figure 7.3](#). It can be seen that the % removal of MCPA increased with increase in adsorbent dose due to greater surface area and availability of more adsorption site while adsorption capacity (amount of MCPA loaded per unit weight of adsorbent) gradually decreased for same. This decrease in adsorption capacity is due to availability of lower number of solutes (MCPA) per unit mass of adsorbent, i.e. lower solute/adsorbent ratio. These experiments

were performed with 40 mg L^{-1} initial concentration of MCPA, $30 \text{ }^\circ\text{C}$ temperature and 6.9 pH of the solution. It can be concluded that the rate of MCPA/ binding with adsorbent increases more rapidly in the initial stages and after some time the adsorption is marginal and becomes almost constant.

Table 7.2: Effect of adsorbent dose on adsorption capacity of CTAB / NaOH / fly ash composite for MCPA

Time (min)	Adsorption Capacity (mg/g)		
	m = 2 g/l	m = 4 g/l	m = 6 g/l
0.5	2	1.9	1.74
1	2.6	2.8	2.2
5	3.24	3.04	2.69
10	3.82	3.52	3.24
15	3.955	3.65	3.288
30	4.26	3.83	3.33
45	4.25	3.81	3.29

($T = 303 \text{ K}$, $\text{pH} = 6.9$, $C_0 = 40 \text{ mg/l}$)

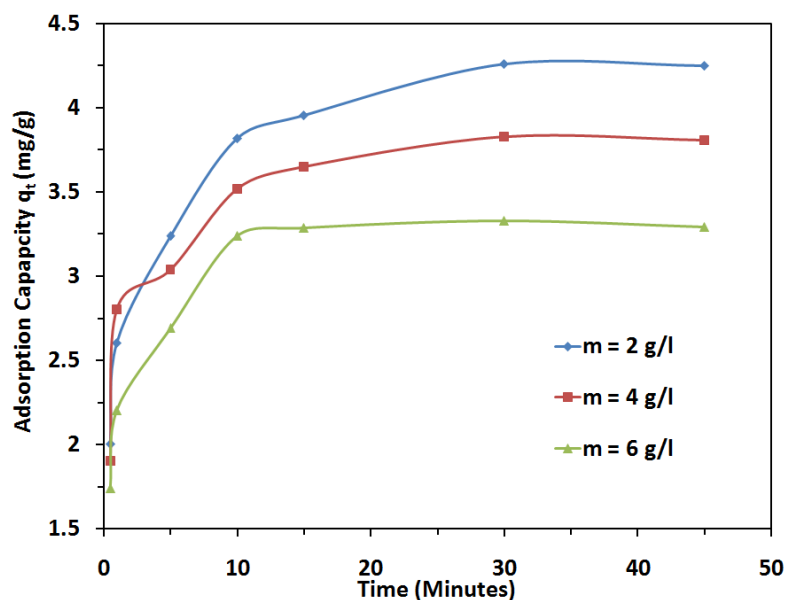


Figure 7.3: Effect of adsorbent dose on adsorption capacity of CTAB / NaOH / fly ash composite for MCPA
($T = 303 \text{ K}$, $\text{pH} = 6.9$, $C_0 = 40 \text{ mg/l}$)

(iii) *Effect of contact time and initial concentration*

The effect of contact time for removal of MCPA (Table 7.3 & Figure 7.4) showed rapid adsorption in first 10 minutes and thereafter the adsorption rate decreased gradually, equilibrium reaching in about 15 minutes. A large number of vacant surface sites are available for adsorption during the initial stage, and after a lapse of time, the remaining vacant surface sites are difficult to be occupied due to repulsive forces between the solute molecules on the solid and bulk phases.

Effect of initial concentrations on the adsorption of MCPA on CTAB / NaOH / fly ash composite was studied at different initial concentration from 20 to 60 mg L⁻¹ by keeping other parameters constant. From Figure 7.4, it was observed that with increase in initial concentration of MCPA, the adsorption capacity increases. It was possible that the initial concentration of MCPA provided the necessary driving force to overcome the resistances of mass transfer between the aqueous phases and the solid phase. The increase in initial concentration also enhances the interaction between MCPA and CTAB / NaOH / fly ash composite, resulting in increase in adsorption uptake.

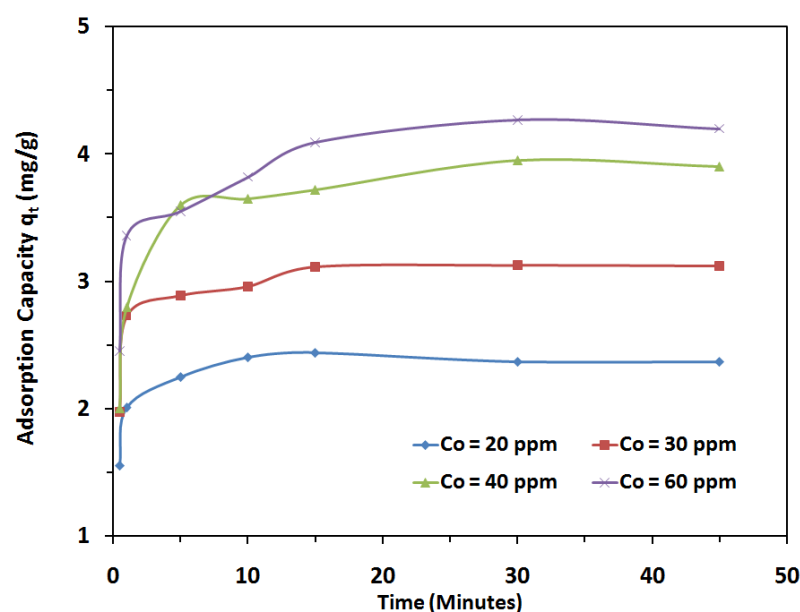


Figure 7.4: Effect of Initial Concentration of MCPA on adsorption capacity of CTAB / NaOH / fly ash composite ($m = 4.0$ gm/l, $\text{pH} = 6.9$, $T = 303$ K)

Table 7.3: Effect of Initial Concentration of MCPA on adsorption capacity of CTAB / NaOH / fly ash composite

t (min)	Co = 20 ppm		Co = 30 ppm		Co = 40 ppm		Co = 60 ppm	
	q _t (mg/g)	% removal	q _t (mg/g)	% removal	q _t (mg/g)	% removal	q _t (mg/g)	% removal
0.5	1.55	31	1.975	26.35	2	20	2.45	16.33
1	2.01	40.25	2.73	36.4	2.8	28	3.36	22.40
5	2.25	44.9	2.89	38.53	3.6	36.05	3.55	24.15
10	2.4	48.05	2.96	39.57	3.65	36.55	3.82	25.47
15	2.44	48.85	3.115	41.53	3.72	37.2	4.09	27.25
30	2.37	47.5	3.127	41.7	3.95	39.5	4.27	28.45
45	2.37	47.5	3.12	41.7	3.9	39.5	4.2	28.45

(m = 4.0 gm/l, pH = 6.9, T = 303 K)

(iv) *Effect of Temperature*

Effect of temperature on adsorption of MCPA was studied at temperature 30° to 50 °C as shown in Figure 7.5 and results given in Table 7.4. It was observed that adsorption capacity decreased with increase in temperature. Lower temperature may provide more chance for MCPA molecule to pass the external boundary layer and produce the enlargement of pore volume and surface area enabling to penetrate.

Table 7.4: Effect of Temperature of solution on adsorption capacity of CTAB / NaOH / fly ash composite for MCPA adsorption

Time (min)	Adsorption Capacity (mg/g)		
	30 °C	40 °C	50 °C
0.5	2	2.1	1.98
1	2.8	2.79	2.775
5	3.2	3.06	2.99
10	3.52	3.33	3.12
15	3.65	3.385	3.32
30	3.83	3.4425	3.38
45	3.8	3.4725	3.38

(m = 4.0gm/l, pH = 6.9, C₀ = 40 ppm)

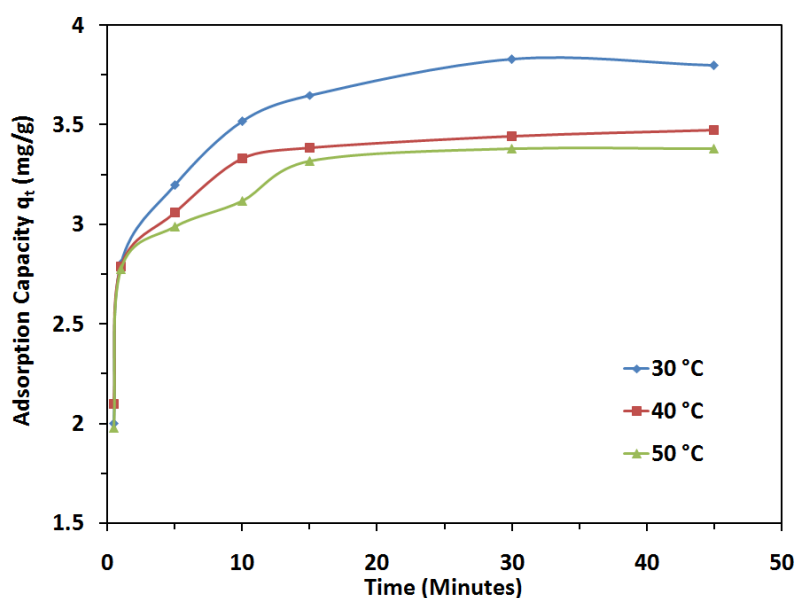


Figure 7.5: Effect of Temperature of solution on adsorption capacity of CTAB / NaOH / fly ash composite for MCPA adsorption
(m = 4.0gm/l, pH = 6.9, C₀ = 40 ppm)

(v) *Effect of pH*

The initial pH of adsorption medium is one of the most important parameters affecting the adsorption process. Effect of initial pH on adsorption of MCPA was studied with initial concentration of 40 mg l^{-1} , solution temperature $30 \text{ }^\circ\text{C}$ adsorbent dose of 4.0 g l^{-1} . The pH was adjusted by adding 0.1 mol l^{-1} or 0.01 mol l^{-1} HCl (or NaOH) to the solutions. Below pH 5.0 some zeolitic phases show dissolution so was not investigated. The adsorption of MCPA onto CTAB / NaOH / fly ash composite as a function of solution pH is shown in Figure 7.6 and results given in Table 7.5. Results showed that the MCPA adsorption capacity of CTAB / NaOH / fly ash composite was relatively high at solution pH 5.1-7.0, and decreased with increasing solution pH from 7.0 to 10.5. This observation is explained below. MCPA is a weak acid, and its ionization is strongly dependent on solution pH. The adsorption of unionized MCPA onto the positively charged surface of CTAB / NaOH / fly ash composite is unlikely to be driven by the electrostatic attraction. Therefore, the hydrogen bonding and organic partitioning are responsible for the adsorption of MCPA onto CTAB / NaOH / fly ash composite, at solution pH 5.1. MCPA molecules are ionized at solution pH above 5.1 and they are almost completely ionized at solution pH 7.0 [34]. Therefore, the electrostatic attraction together bonding with the hydrogen bonding and organic partition are responsible for the adsorption of MCPA onto CTAB / NaOH / fly ash composite at solution pH 5.1-7.0. The increase of solution pH from 5.1 to 7.0 leads to decreased hydrogen bonding between MCPA and CTAB / NaOH / fly ash composite but the increased electrostatic attraction. The former is counteracted by the later, resulting in the adsorption of MCPA on CTAB / NaOH / fly ash composite only slightly influenced by solution pH ranging 5.1-7.0. At solution pH above 7.0, completely ionized MCPA molecules cannot provide hydroxyl hydrogen atom to nitrogen atom of CTAB bilayer to form hydrogen bonding. In this case, the electrostatic attraction plays an important role in the adsorption of MCPA onto CTAB / NaOH / fly ash composite, the increase of solution pH from 7.0 to 10.5 leads to the increase in the competitions between the hydroxyl ion and the ionized MCPA molecules for the same positively

charged adsorption sites on the surface of CTAB / NaOH / fly ash composite, which causes a decrease in MCPA adsorption.

Table 7.5: Effect of pH on adsorption capacity of CTAB / NaOH / fly ash composite for MCPA adsorption

pH Initial	Adsorption Capacity (mg/g)
5.15	2.75
5.95	2.81
6.9	2.94
8.4	2.84
9.6	2.8
10.4	2.69
5.15	2.75

($m = 4.0$ gm/l, $t = 15$ min, $T = 303$ K, $C_0 = 40$ ppm)

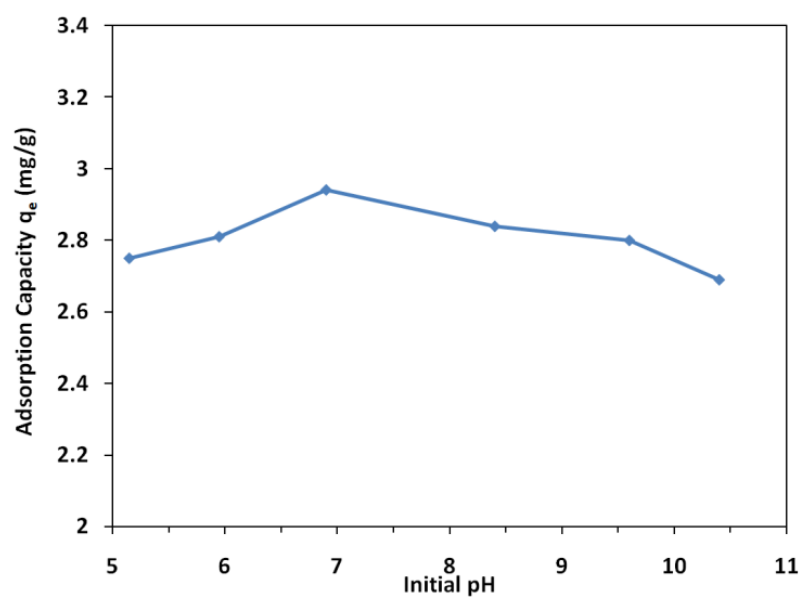


Figure 7.6: Effect of pH on adsorption capacity of CTAB / NaOH / fly ash composite for MCPA adsorption
($m = 4.0$ gm/l, $t = 15$ min, $T = 303$ K, $C_0 = 40$ ppm)

(vi) *Effect of ionic strength*

The adsorption of MCPA onto CTAB / NaOH / fly ash composite as a function of ionic strength at solution pH 6.9 is presented in Table 7.6 and Figure 7.7. The presence of electrolytes such as NaCl in aqueous solution had slightly decreased effect on MCPA adsorption onto CTAB / NaOH / fly ash composite. When the ionic strength of the aqueous solution increased from 0 to 0.1 mol/L, the MCPA adsorption remains almost constant, changed only from 3.8 to 3.9 mg/g. this result suggest that CTAB / NaOH / fly ash composite bilayer coverage is effective in removing MCPA from water or wastewater containing salt. If electrostatic attraction is the main adsorption mechanism, the ionic strength should have a significant negative effect on the adsorption process [34, 35]. The slight positive effect of ionic strength on MCPA adsorption onto CTAB / NaOH / fly ash composite at solution pH 6.9 confirms that the electrostatic attraction is not the only mechanism for the adsorption process and the electrostatic attraction together with the other mechanisms such as hydrogen bonding and organic partitioning control the adsorption process.

Table 7.6: Effect of Ionic Strength on adsorption capacity of CTAB / NaOH / fly ash composite for MCPA adsorption

Ionic Strength (mol/L)	Adsorption Capacity (mg/g)
0	153.68
0.02	150
0.04	148
0.06	146.3
0.1	145.8
0.15	145
0.2	144.8
0.3	144.7
0.5	144.6
0.7	144.6
0.8	144.6

(m = 4.0 gm/l, t = 15min, T = 303 K, C₀ = 40 ppm, pH = 6.9)

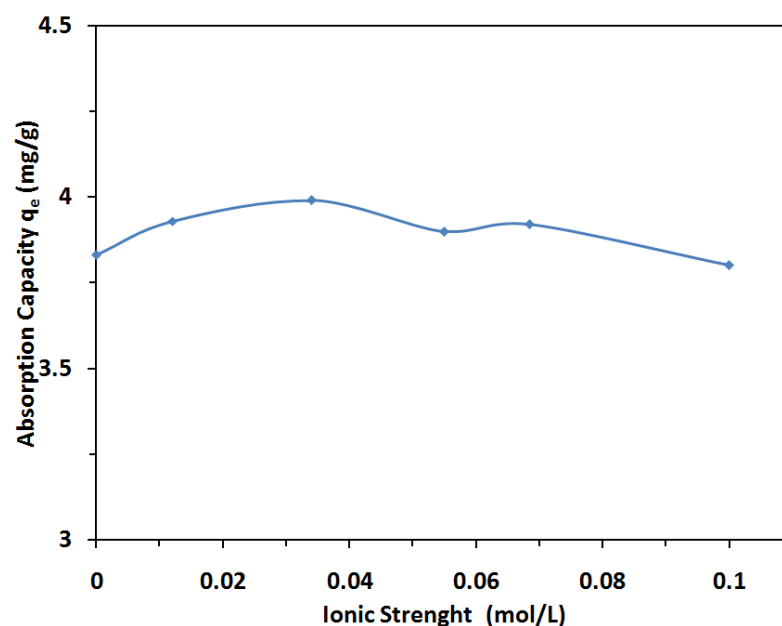


Figure 7.7: Effect of Ionic Strength on adsorption capacity of CTAB / NaOH / fly ash composite for MCPA adsorption ($m = 4.0$ gm/l, $t = 15$ min, $T = 303$ K, $C_0 = 40$ ppm, $pH = 6.9$)

7.3.4 Adsorption Kinetics

Four widely used kinetic models, pseudo-first-order, pseudo-second-order, Bangham equation and intra-particle diffusion model were employed to interpret the kinetic results. All kinetic parameters are given in [Tables 7.7, 7.8](#) and [Figure 7.9](#).

For pseudo-first-order kinetic model, the R^2 value obtained was relatively high ($R^2 = 0.9825$), but the calculated q_e value did not agree with the experimental one. This suggests that the pseudo-first-order kinetic model is not appropriate to represent the adsorption kinetics data of MCPA onto CTAB / NaOH / fly ash composite.

For pseudo-second-order kinetic model, the R^2 value obtained was very high ($R^2 > 0.9976$), and the calculated q_e value was in good agreement with the experimental one, suggesting the applicability of the pseudo-second-order kinetic model to describe the adsorption kinetics data of MCPA onto CTAB / NaOH / fly ash composite.

Linear plots of q_e and h against C_0 were regressed to obtain the value of h and q_e in terms of C_0 with high a coefficient of regression. Therefore, q_e and h can be express as a function of C_0 as follows:

$$q_e = 1.802 \ln C_0 - 2.977 \quad (7.1)$$

$$h = -1.9 \times 10^{-2} C_0^2 + 1.183 C_0 + 2.59 \quad (7.2)$$

$$q_t = \frac{t}{1/(-1.9 \times 10^{-2} C_0^2 + 1.183 C_0 + 2.59) + (1/1.802 \ln C_0 - 2.977) t} \quad (7.3)$$

A comparison of experimental data points and the surface predicted by the Eq. (7.3) is given in Figure 7.8. It can be used to derive the sorption capacity, q_t at any given C_0 and t .

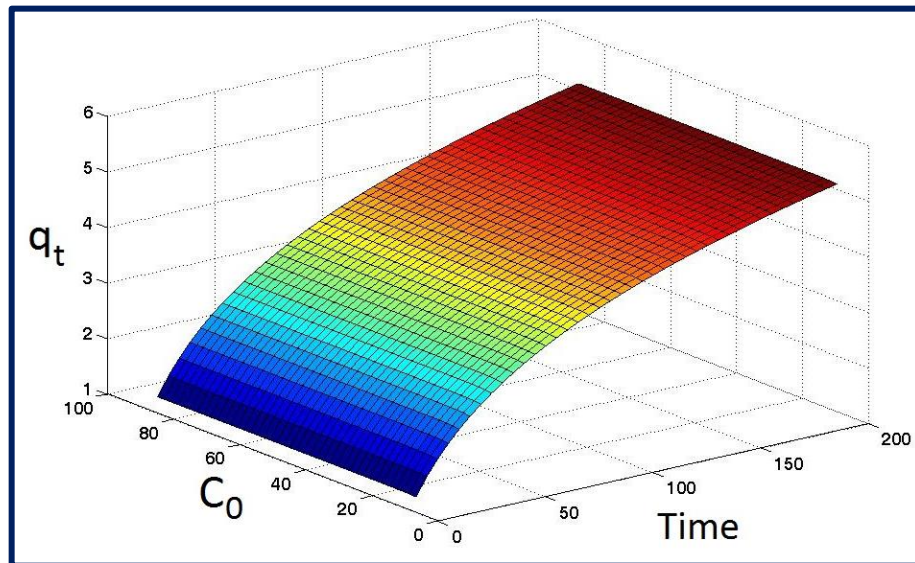


Figure 7.8: Comparison of experimental data points given by symbols and the surface predicted by the model given Eq. (7.3)

Bangham's equation show (Figure 7.9 c) linear curves for the resorcinol removal by the CTAB / NaOH / fly ash composite , signifying that the diffusion of adsorbate into the pores of the adsorbent was the only rate-controlling step. It may be that pore diffusion was important to different extents in the removal process Intra-particle diffusion model gives a straight line with a slope k_{diff} and intercept C . The term k_{diff} is indicative of an enhancement in the rate of adsorption. The value of C gives (Table 7.8) an idea about the boundary layer thickness.

Table 7.7: Details of all kinetic parameters for MCPA adsorption on CTAB / NaOH / fly ash composite

MCPA C_0	time (min.)	0.5	1	5	10	15	30
		$\sqrt{\text{time}}$	0.707	1.000	2.236	3.160	3.870
	$\log t$	-0.301	0.000	0.699	1.000	1.176	1.477
20 ppm	$\ln(q_e - qt)$	-0.116	-0.844	-1.635	-3.218	-	-
	t/qt	0.456	0.497	2.227	4.166	6.147	12.66
	qt	1.55	2.01	2.245	2.4	2.44	2.37
	$\log \log (C_0/C_0 - q_t m)$	-0.793	-0.651	-0.586	-0.547	-0.537	-0.534
30 ppm	$\ln(q_e - qt)$	0.142	-0.923	-1.439	-1.789	-4.423	-
	t/qt	0.358	0.366	1.73	3.378	4.815	9.49
	qt	1.975	2.730	2.890	2.960	3.115	3.127
	$\log \log (C_0/C_0 - q_t m)$	-0.877	-0.707	-0.675	-0.662	-0.632	-0.630
40 ppm	$\ln(q_e - qt)$	0.668	0.139	-1.049	-1.204	-1.469	-
	t/qt	0.25	0.357	1.389	2.74	4.03	7.59
	qt	2	2.8	3.6	3.65	3.72	3.95
	$\log \log (C_0/C_0 - q_t m)$	-1.014	-0.846	-0.713	-0.705	-0.695	-0.661
60 ppm	$\ln(q_e - qt)$	0.597	-0.0976	-0.3327	-0.805	-1.72	-
	t/qt	0.288	0.298	1.408	2.618	3.67	7.03
	qt	2.450	3.360	3.550	3.820	4.088	4.267
	$\log \log (C_0/C_0 - q_t m)$	-1.111	-0.958	-0.931	-0.894	-0.859	-0.837

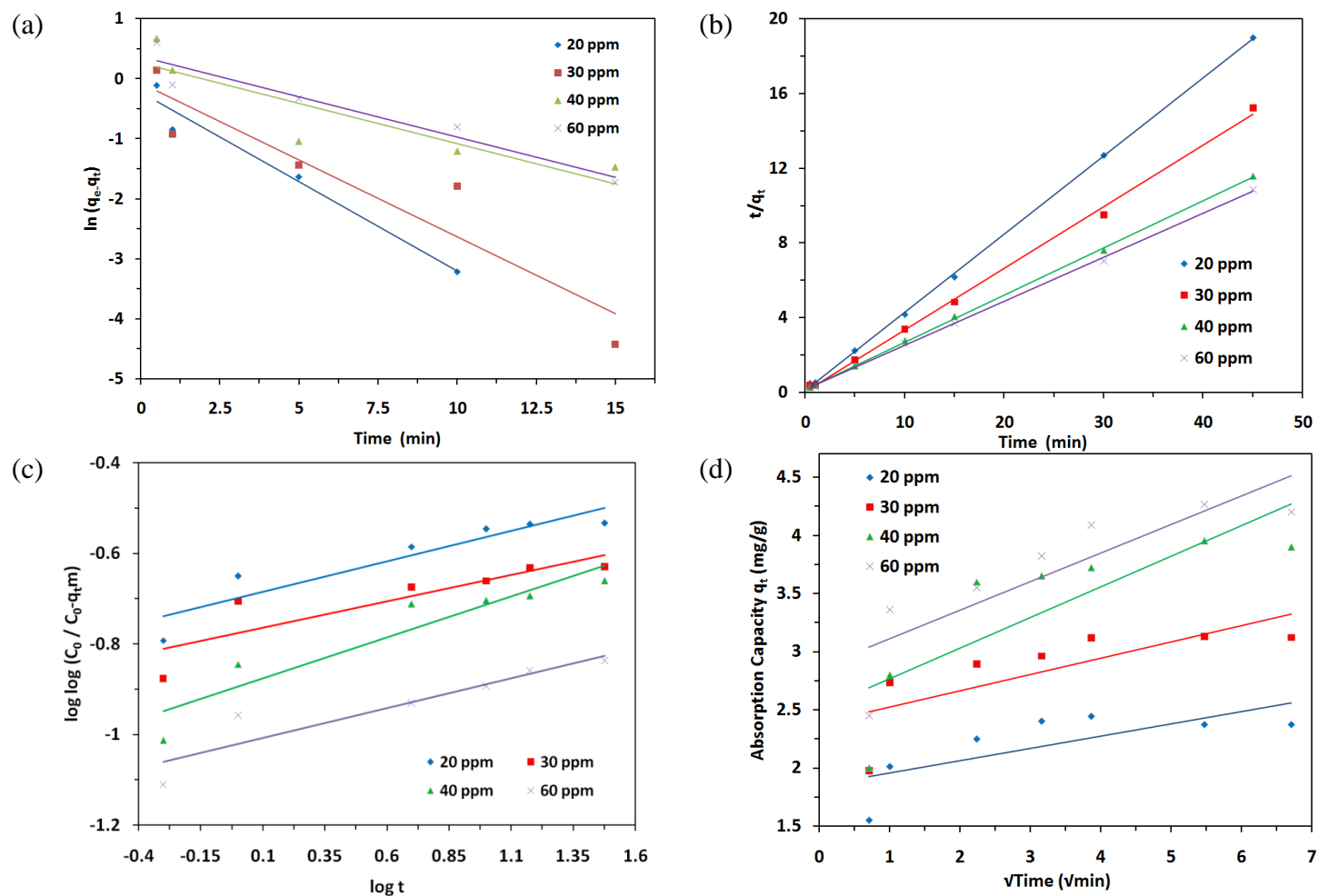


Figure 7.9: Kinetic Model of MCPA on CTAB / NaOH / fly ash composite (a) Pseudo First Order, (b) Pseudo Second Order, (c) Bangham equation and (d) intra-particle diffusion model

Table 7.8: Pseudo-first order, Pseudo-second order and Intra-particle Diffusion Models rate constants for MCPA adsorption onto CTAB / NaOH / fly ash composite at various concentrations

C_0 (mg/L)		20	30	40	60
$q_{e, \text{exp}}$ (mg/g)		2.44	3.18	3.95	4.27
Pseudo-first order model	K_1 (1/min)	0.296	0.256	0.134	0.133
	$q_{e, \text{cal}}$ (mg/g)	1.256	1.074	1.298	1.449
	R^2	0.966	0.873	0.79	0.921
Pseudo-second order	K_2 (g/mg min)	2.18	4.03	0.45	0.36
	$q_{e, \text{cal}}$ (mg/g)	2.39	3.03	3.97	4.26
	h	12.5	37.04	7.04	6.49
	R^2	0.999	0.998	0.999	0.999
Bangham's equation	K_0 (g)	5.758	4.826	3.670	2.745
	α	0.135	0.116	0.1812	0.1317
	R^2	0.8629	0.7597	0.8777	0.8621
Intra-particle Diffusion Model	K_{id} (mg/g(min ^{0.5}))	0.105	0.139	0.263	0.245
	C	1.85	2.38	2.5	2.86
	R^2	0.533	0.572	0.671	0.739

($m = 4.0 \text{ g l}^{-1}$, agitation rate = 200 rpm, pH = 6.9, T = 30 °C)

7.3.5 Adsorption isotherms

The adsorption isotherms of MCPA adsorption onto CTAB / NaOH / fly ash composite at 30°C, 40°C and 50°C and solution pH 6.8 is shown in [Figure 7.10](#) and values of isotherm parameters are given in [Table 7.9](#). Results showed that the MCPA adsorption capacity increased with increasing the MCPA concentration until equilibrium was reached. Two-parameter isotherm models Langmuir, Freundlich, Dubinin - Redushkevich (D-R), Tempkin and three-parameter isotherm model Redlich - Peterson were used to fit the experimental data.

Table 7.9: Isotherm parameters for adsorption of MCPA on CTAB / NaOH / fly ash composite

T (°C)	Parameters				
30 °C	C_e	10.23	17.49	24.2	42.93
	$\ln C_e$	2.325	2.862	3.186	3.76
	$\log C_e$	1.0098	1.2428	1.3838	1.6327
	q_e	2.44	3.127	3.95	4.267
	$\log q_e$	0.3874	0.495	0.596	0.63
	C_e / q_e	4.192	5.593	6.126	10.06
	$\ln(K_R C_e / q_e - 1)$	2.994	3.295	3.389	3.898
	$\ln q_e$	0.892	1.14	1.37	1.45
	ε^2	55199	19619	10405	3365
40 °C	C_e	10.46	19.08	25.88	46.85
	$\ln C_e$	2.347	2.9486	3.253	3.8469
	$\log C_e$	1.0195	1.2805	1.413	1.671
	q_e	2.38	2.73	3.53	3.29
	$\log q_e$	0.376	0.436	0.548	0.517
	C_e / q_e	4.395	6.989	7.33	14.24
	$\ln(K_R C_e / q_e - 1)$	3.043	3.525	3.574	4.251
	$\ln q_e$	0.867	1.004	1.26	1.19
	ε^2	56453	17671	9733	3021
50 °C	C_e	11	20.5	29	49
	$\ln C_e$	2.398	3.02	3.37	3.892
	$\log C_e$	1.041	1.312	1.462	1.69
	q_e	2.25	2.375	2.75	2.75
	$\log q_e$	0.352	0.376	0.439	0.439
	C_e / q_e	4.889	8.632	10.545	17.82
	$\ln(K_R C_e / q_e - 1)$	1.113	1.260	1.274	1.447
	$\ln q_e$	0.811	0.865	1.012	1.012
	ε^2	54598	16359	8288	2943

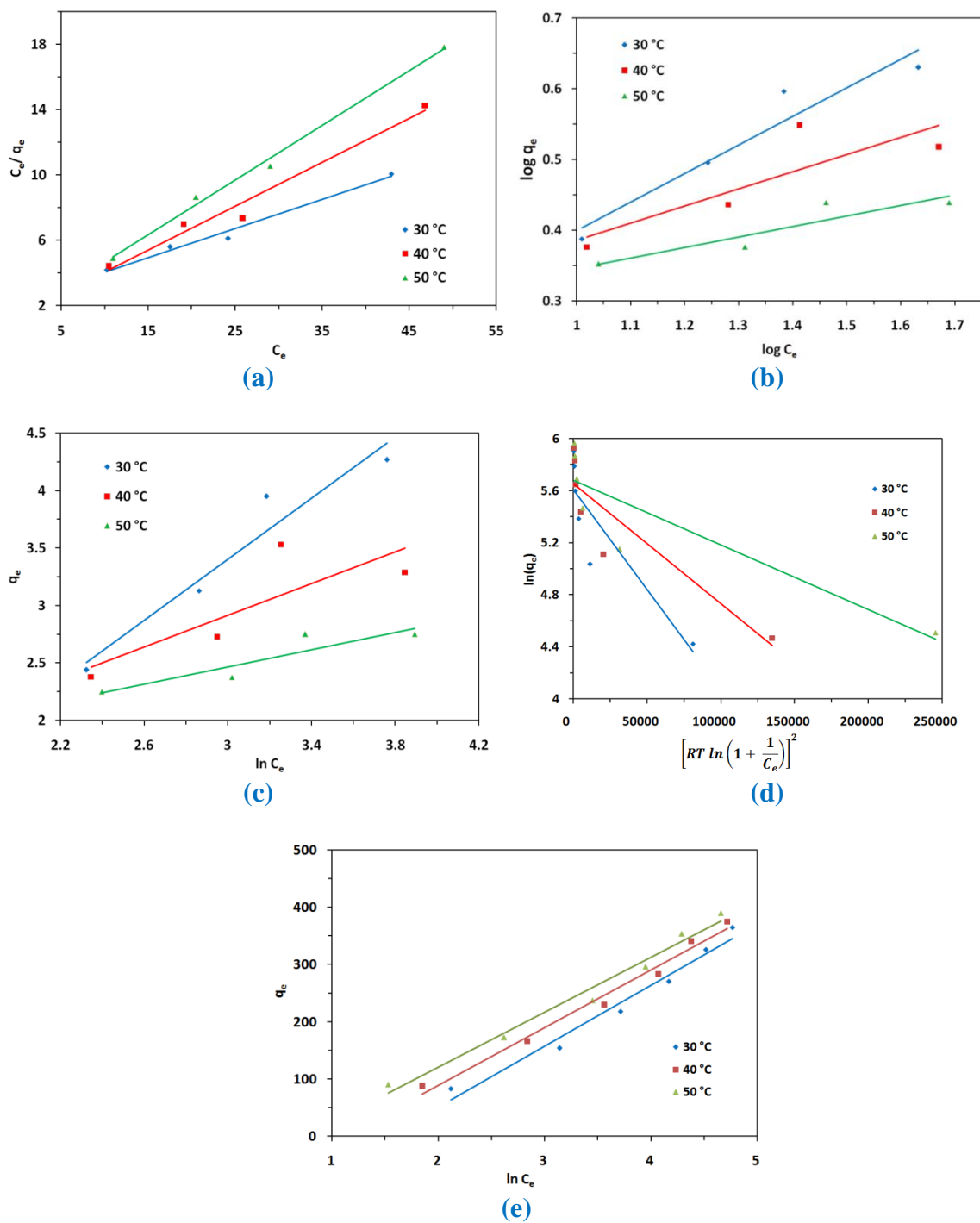


Figure 7.10: Adsorption of MCPA on CTAB / NaOH / fly ash composite
 (a) Langmuir (b) Freundlich (c) Redlich-Peterson (d) D-R and (e) Tempkin

The different isotherm parameters were evaluated from the linear plots and presented in Table 7.10 along with constants and correlation coefficients root mean square error (RMSE) and chi-square (χ^2). The RMSE and χ^2 are used to measure the goodness of fit of an isotherm defined as discussed in chapter 2. A better curve fitting is observed by smaller RMSE value. If the data obtained from the isotherm models are nearer to the experiment results the χ^2 values will be lesser digit.

Table 7.10: Isotherm parameters for MCPA adsorption onto CTAB / NaOH / fly ash composite at various temperatures

Langmuir	T (°C)	q_{max} (mg/g)	K_L (L/mg)	R²	RMSE	χ²	
	at 30	5.65	0.0779	0.985	0.2128	0.0245	
	at 40	3.74	0.1914	0.974	0.343	0.0723	
	at 50	2.99	0.2560	0.994	0.1446	0.0171	
Freundlich	T (°C)	K_F (mg/g)(L/mg)^{1/n}	1/n	R²	RMSE	χ²	
	at 30	1.009	0.403	0.927	0.3327	0.0573	
	at 40	1.389	0.241	0.706	0.3873	0.0873	
	at 50	1.567	0.149	0.839	0.1332	0.0108	
Tempkin	T (°C)	K_T (mg/g)	B_T	R²	RMSE	χ²	
	at 30	1.559	1.331	0.939	1.69	1.768	
	at 40	3.452	0.687	0.674	0.366	0.0795	
	at 50	36.16	0.374	0.832	0.129	0.0127	
D-R	T (°C)	q_{max} (mg/g)	KD (mg²/KJ²)	R²	RMSE	χ²	
	at 30	4.25	-1 × 10 ⁻⁵	0.929	0.208	0.052	
	at 40	3.40	-7 × 10 ⁻⁶	0.778	0.229	0.067	
	at 50	2.73	-4 × 10 ⁻⁶	0.746	0.113	0.020	
Redlich Peterson	T (°C)	K_R (L/g)	α_R(L/mg)^β	β	R²	RMSE	χ²
	at 30	5	4.604	0.615	0.966	0.223	0.051
	at 40	5	3.261	0.779	0.961	0.269	0.085
	at 50	5	2.924	0.869	0.993	0.497	0.377

(m = 4.0 g l⁻¹, agitation rate = 200 rpm, pH = 6.9, C₀ = 20-60 mg l⁻¹)

The value of RMSE and χ^2 for the Redlich-Peterson, Langmuir, Freundlich, Tempkin and D-R isotherm model are low, indicating that the equilibrium data for the adsorption of MCPA onto CTAB / NaOH / fly ash composite can be well represented by these five isotherm models but best fitted with Redlich-Peterson isotherm model. The predicted maximum monolayer MCPA adsorption capacity for CTAB / NaOH / fly ash composite derived from Langmuir isotherm was found to be 5.65 mg/g. The values of R_L obtained in this study were between 0.06 and 0.39 indicating that the adsorption of MCPA onto CTAB / NaOH / fly ash composite is favorable.

7.3.6 Thermodynamic Studies

The thermodynamic parameters of standard enthalpy (ΔH°) and entropy (ΔS°) for the adsorption process were estimated from the Van' t-Haff equation represented in chapter 2. The values of K_L for Langmuir isotherm at 30 °C, 40°C and 50 °C were used to calculate thermodynamic parameters such as Gibbs free energy change (ΔG°). The values of ΔH° and ΔS° can be calculated from the intercept and the slope of the linear plot of $\ln K_L$ versus $1/T$ as shown in [Figure 7.11](#).

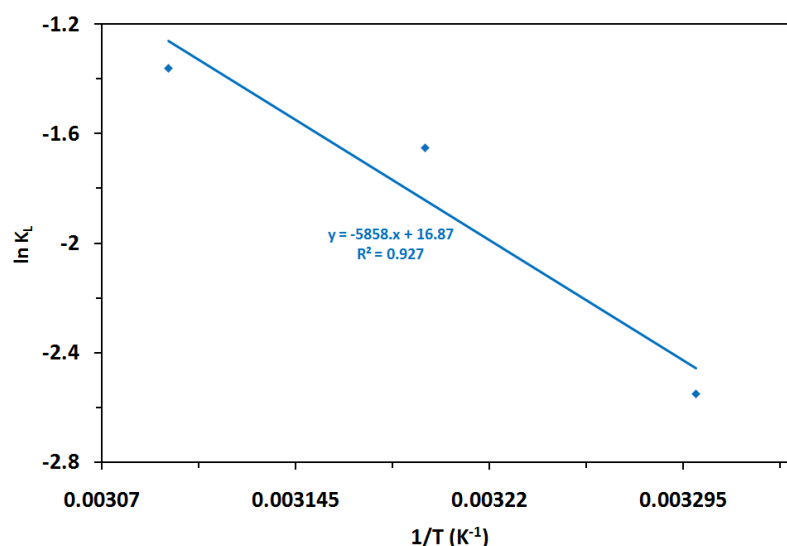


Figure 7.11: Van't Hoff plot for the adsorption of MCPA onto CTAB / NaOH / fly ash composite

The obtained values of the thermodynamic parameters of MCPA adsorption onto CTAB / NaOH / fly ash composite are given in Table 7.11. The negative values of ΔG° suggest that feasibility of the adsorption of MCPA onto CTAB / NaOH / fly ash composite in a spontaneous and favourable way. The values of ΔG° obtained in this study were in the range of neither physisorption nor chemisorption, indicating that the adsorption of MCPA onto CTAB / NaOH / fly ash composite involves the other adsorption process such as interaction mechanism. This conclusion confirms that the mechanisms controlling the adsorption of MCPA onto CTAB / NaOH / fly ash composite at solution of pH 6.9 include electrostatic attraction.

Table 7.11: Thermodynamic parameters for MCPA adsorption on CTAB / NaOH / fly ash composite

ΔH° (KJ/mol)	ΔS° (J/mol)	ΔG° (KJ/mol)			R^2
		30 °C	40 °C	50 °C	
-48.70	140.26	-6.424	-4.294	-3.652	0.927

The negative value of ΔH° indicates that the adsorption process is exothermic in nature. The absolute value of ΔH° was 48.70 kJ/mol, also indicates that hydrogen bonding and organic partitioning are important to the adsorption process in addition to electrostatic attraction. The positive value of ΔS° shows a increase in randomness at the solid/liquid interface during the adsorption process.

7.4 Conclusion

After Modification with the surfactant (CTAB, Cetyltrimethylammonium bromide), hydrothermally treated fly ash exhibited greatly enhanced adsorptive capacity for MCPA. CTAB / NaOH / fly ash composite has good physical as well as chemical stability; hence it can be used for various environmental applications. N_2 adsorption isotherms of CTAB / NaOH / fly ash composite is of combination of type II and type IV. The values of BET surface area, pore volume and pore diameter are $51.12 \text{ m}^2/\text{gm}$, $0.176996 \text{ cm}^3/\text{gm}$ and 138.4928 \AA respectively. The results show that CTAB / NaOH / fly ash composite include mesopores. Redlich-Peterson equation is best fitted for the description of MCPA adsorption. Increase in temperature, increase adsorption indicating that the process is endothermic. The monolayer adsorption capacity for MCPA is 5.65 mg/g . The adsorption kinetics was found to follow pseudo-second order model. The thermodynamic parameters such as ΔH° , ΔS° and ΔG° values show an exothermic heat of adsorption, the feasibility of the adsorption process and its spontaneity, respectively. The MCPA adsorption on CTAB / NaOH / fly ash composite slightly decreased with increasing ionic strength. The MCPA adsorption capacity was relatively high at solution pH 5.1-7.0 and decreased with increasing solution pH from 7.0-11.0. The main mechanism controlling MCPA adsorption onto CTAB / NaOH / fly ash composite at solution pH < 7.0 include electrostatic attraction and organic partitioning.

7.5 References

- [1] R. Grover, A.J. Cessna, (Eds.), 1991. Environmental Chemistry of Herbicides. CRC Press, Boca Raton, FL.
- [2] E.P. Hodgson, E. Levi, Environ. Health Perspect., 104 (1996) 97–105.
- [3] S.K., Hoar, Blair, A., Holmes, F.F., Boysen, C.B., Robel, J.R., Hoover, Fraumeni, R.H., J. Am. Med. Assoc., 256 (1986) 1141-48.

- [4] M. Fielding, D. Barcelo, A. Helweg, L. Torstenson, P. V. Zoonen, G. Angeletti, Pesticides in Ground Drinking Water. Water Pollution Research Report 27. Commission of the European Communities, Brussels, (1992) 1-136.
- [5] M. Kuster, M.J. López de Alda, M.D.Hernando, M.Petrovic, J. Martín-Alonso, D. Barceló, Journal of Hydrology, 358 (2008) 112-23.
- [6] Silva, E., Batista, S., Viana, P., Antunes, P., Serodio, L., Cardoso, A.T., Cerejeira, M.J., Intern. J. of Environ. and Analyt. Chem., 86 (2006) 955-72.
- [7] Walker, M. Mary Keith, H. Lawrence 1992. EPA's Pesticide Fact Sheet Database. Lewis Publishing, Chelsea, MI.
- [8] I.Vergili, H. Barlas, Desalination, 249 (2009) 1107-14.
- [9] A. Zertal, M. Jacquet, B. Lavedrine, T.Sehili, Chemosphere, 58 (2005) 1431-37.
- [10] P. Vizcaino, A. Pistocchi, Environ. Pollut., 158 (2010) 3017-27.
- [11] M.A.CrespIn, M. Gallego, M. Valcarcel, Environ. Sci. Technol., 35 (2001) 4265-70.
- [12] D.C. Adams, L.T. Watson, J. Environ. Eng. ASCE, 39 (1996) 327-30.
- [13] H. Jiang, C. Adams, N. Grazino, A. Roberson, M. Mac Guire, D. Khiari, Environ. Sci. Technol., 40 (2006) 3609-16.
- [14] M.V. Lopez-ramon, M.A. Fontecha-Camara, M.A. Alvarez-Merino, C. Moreno-Castilla, Water Res., 41 (2007) 2865-70.
- [15] Y. Sudhakar, A.K. Dikshit, J. Environ. Sci. Health B, 34 (1999) 97-118.
- [16] J.B. Alam, A.K. Dikshit, M. Bandyopadhyay, Global Nest: The Int. J., 2 (2000) 139-48.
- [17] R.K. Sharma, A. Kumar, P.E. Joseph, Bull. Environ. Contam. Toxicol., 8 (2008) 461-64.
- [18] M. Akhtar, S.M. Hasany, M.I. Bhangar, S. Iqbal, Chemosphere, 66 (2007) 1829-38.
- [19] N. Balkaya, Int. J. Waste Water, 2 (2002) 211-19.

- [20] H.E. Bakouri, J. Morillo, J. Usero, A. Quassini, *J. Hydrol.*, 353 (2008) 335-42.
- [21] H.E. Bakouri, J. Morillo, J. Usero, A. Quassini, *J. Hydrol.*, 364 (2009) 175-81.
- [22] S. Boudesocque, E. Guillon, M. Aplincourt, F. Martel, S. Noael, *J. Environ. Qual.*, 37 (2008) 631-38.
- [23] I.P. Bras, L. Santos, A. Alves, *Environ. Sci. Technol.*, 33 (1999) 631-34.
- [24] G.Z. Memon, M.I. Bhangar, M. Akhtar, F.N. Talpur, J.R. Memon, *Chem. Eng. J.*, 138 (2008) 616-21.
- [25] G.K. Vinod, A. Imran, *Water Res.*, 35 (2001) 33-40.
- [26] G.K. Vinod, C.K. Jain, A. Imran, S. Chandra, *Water Res.*, 36 (2002) 2483-90.
- [27] X.Querol, N. Moreno, J.C.Uman, A.Alastuey, E. Hernandez, A Lopez-Soler, F. Plana, , *Int. J. Coal Geol.*, 50 (2002) 413-23.
- [27] M. Mahramanlioglu, I. Kizilcikli , I. O. Bicer & M. Tuncay, *J. of Environ. Sci. and Health, Part B*, 38 (2003) 813-27.
- [28] I. Vergili, H. Barlas, *Desalination*, 249 (2009) 1107-14.
- [29] J. Inacio, C.T. Gueho , C. Forano, J.P Besse, *Applied Clay Science*, 18 (2001) 255–64.
- [30] A. Iglesias, R. Lopez, D. Gondar, J. Antelo, S. Fiol, F. Arce ,*Chemosphere*, 78 (2010) 1403-1408.
- [31] T. Paszko , *J. Environ. Sci. Health B*. 46(7) (2011) 569-80.
- [32] C.C. Santiago, M.A. Fernández, R.M. Torres Sanchez, *J. Environ. Sci. Health B.*, 51(4) (2016) 245-53.
- [33] K. Nejati, S.Davari, Z. Rezani, M. Dadashzadeh, *J. of chine. Chem. Soci.*, 62 (2015) 371-79
- [34] J. Lin, Y. Zhan, Z. Zhu, Y. Xing, *J. Hazard. Mater.*, 193 (2011) 102-11.
- [35] Z.H. Wang, B. Xiang, R.M. Cheng, Y.J. Li, *J.of Hazard. Mater.*, 183 (2010) 224-32.

Publications

List of Paper published: 1

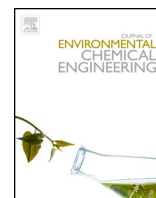
1. Adsorption of resorcinol from aqueous solution onto CTAB / NaOH / fly ash composites: Equilibrium, kinetics and thermodynamics, **Swarnima Agarwal**, Ashu Rani , Journal of Environmental Chemical Engineering, 5 (2017) 526-38.

List of Paper submitted for publication:

1. Adsorption of tannic acid from aqueous solution onto Chitosan / NaOH / fly ash composites: Equilibrium, kinetics, thermodynamics and modeling, **Swarnima Agarwal**, Priyanka Rajoria, Ashu Rani, Journal of Environmental Chemical Engineering [communicated].
2. A comparative study of removal of acidic and basic dyes on fly ash from different origin: Equilibrium, Kinetics, Thermodynamics and Modeling, **Swarnima Agarwal**, Ashu Rani, Dyes and Pigments [communicated].
3. A comparative study of removal of resorcinol from aqueous solution onto low cost Fly Ash (FA) and NaOH Treated Fly Ash (NaFA): Equilibrium, Kinetics, Thermodynamics and Modeling, **Swarnima Agarwal**, Ashu Rani, Journal of Water Process Engineering [communicated].
4. Equilibrium, kinetic and thermodynamic adsorptions of various organic pollutants from aqueous solution using the composite of CTAB and activated fly ash, **Swarnima Agarwal**, Ashu Rani, Water Research [communicated].

National and International Conferences

1. Poster presented on National Conference on “**National Symposium on Recent Advances in Chemical Sciences**” held on 7th & 8th January 2011, organized by Department of Pure and Applied Chemistry, University of Kota, Kota.
2. Participated in National Conference on “**Global Environmental changes and Disaster Management for Sustainable Life on Earth - A burning issue**” held on 21st October, 2013, organized by Maharishi Arvind College of Engineering & Technology, Ranpur, Kota.
3. Participated in 5th National Academic Workshop on “**Organic Reaction Mechanisms & Analytical Techniques used in Chemical Sciences**”, during 21st - 25th October, 2013 in the Department of Pure and Applied Chemistry, University of Kota, Kota.
4. Participated in Symposium on “**E-Resources**”, during 16th & 17th December, 2013 in the Department of Library and Information Science, University of Kota, Kota.
5. Presented research paper in National Seminar on “**Recent Advancements in Protection of Environment and its Management Issues**” held on 27th & 28th February, 2015, organized by Maharishi Arvind College of Engineering & Technology, Ranpur, Kota.
6. Presented a paper in International conference on “**Advances in Power Generation from Renewable Energy Sources**” (APGRES 2015) held on 15th & 16th June, 2015, organized by Department of Mechanical Engineering, Rajasthan Technical University, Kota.
7. Participated in “**Third Rashtriya Hindi Vigyan Sammelan**” held on 16th & 17th December, 2016, organized by Vigyan Bharti, Jaipur, Rajasthan.
8. Oral Paper presented in National Conference on “**Ground Water Quality, Water Conservation, Management and Technology**” (NCGWCMT-2017) held on 20th & 21st January, 2017, organised by Govt. R.R. (PG) Autonomous College, Alwar, Rajasthan.



Adsorption of resorcinol from aqueous solution onto CTAB/NaOH/flyash composites: Equilibrium, kinetics and thermodynamics



Swarnima Agarwal, Ashu Rani*

Department of Pure and Applied Chemistry, University of Kota, Kota 324005, Rajasthan, India

ARTICLE INFO

Article history:

Received 30 August 2016

Received in revised form 3 November 2016

Accepted 25 November 2016

Available online 19 December 2016

Keywords:

Adsorption

Resorcinol

Flyash composite

Surfactant

Kinetic modelling

ABSTRACT

The contamination of water by organic pollutant viz. phenolic compounds is a worldwide environmental problem due to their highly toxic nature. The resorcinol adsorption efficiencies for fly ash (FA), NaOH treated fly ash (NaFA) and surfactant modified NaOH treated fly ash (CTAB/NaOH/flyash composite) were compared. CTAB/NaOH/flyash composite presented higher resorcinol adsorption efficiency than FA and NaFA. This may be attributed to the hydrophobicity imparted by surfactant molecules on the surface of NaFA, consequently leading to organic partitioning. The adsorption of resorcinol onto CTAB/NaOH/flyash composite as a function of initial resorcinol concentration, contact time, temperature, ionic strength and solution pH were investigated for their optimization. The adsorbent were characterized by X-ray diffraction (XRD), field emission scanning electro-microscope (FE-SEM), surface area and porosity measurement, Fourier transform infrared (FT-IR) etc. The adsorption kinetics of resorcinol followed a pseudo-second order model. The equilibrium adsorption data were best fitted by Redlich-Peterson isotherm. The resorcinol adsorption capacity slightly decreased with increasing ionic strength adjusted by NaCl. The adsorption was relatively high at solution pH 5.0–6.8 and decreased above pH 7.0. The value of ΔG° , ΔS° and ΔH° indicated spontaneous and endothermic adsorption process.

© 2016 Elsevier Ltd. All rights reserved.

1. Introduction

Water pollution by organic chemicals is a major problem over decades. Owing to this, there is growing public concern over the contamination of groundwater by organic compounds. The removal of organic contaminants from groundwater or separation of contaminants present in polluted water has become a major focus of research and policy debate. The presence of these compounds even at low concentrations can be an obstacle for reuse of water [1,3]. These organic compounds constitute a very large group of pollutants in the wastewater. Amongst them aromatic compounds especially phenol and its derivatives such as resorcinol, catechol, and cresols are widely found in the effluent of many industries [2,3]. Phenol is present in the surface water of industrial effluents such as coal tar, gasoline, plastic, rubber-proofing, coking, pharmaceutical and steel industries, domestic wastewaters and chemical spillage [4]. Resorcinol is a 1,3-dihydroxybenzene and found in the effluents of many industries such as textile, paper and pulp, steel, petrochemical, petroleum refinery, rubber, dyes, plastics, pharmaceutical, cosmetics etc. [5].

The effluents from synthetic coal fuel conversion process may contain resorcinol and catechol concentrations ranging from 1 to 1000 mg/L [5].

Phenolic compounds are very harmful to organisms even at very low concentration due to their toxicity, foul odour and carcinogenic properties [6,8]. The health effects following repeated exposure to low levels of phenol in water include liver damage, diarrhoea, mouth ulcers, dark urine and hemolytic anemia [7,8]. Resorcinol is classified as a hazardous chemical. Inhalation can cause abdominal pain, nausea, and unconsciousness. It causes redness and pain on skin. It's also considered hazardous to the environment, as it dissolves easily and may infiltrate waterways, presenting hazards to fish and other aquatic life. According to the World Health Organization (WHO), animal studies show that resorcinol caused thyroid dysfunction, effects on the central nervous system, immune system dysfunction and red blood cell change. Ministry of Environment and Forest (MOEF), Govt. of India, New Delhi and United States Environmental Protection Agency (USEPA) has listed phenol and phenolic compound under priority pollutants list. As per the Bureau of Indian Standards, New Delhi,

* Corresponding author.

E-mail addresses: swarnima79@rediffmail.com (S. Agarwal), ashu.uok@gmail.com, ashugck@rediffmail.com (A. Rani).

India, the allowable limit of phenol in drinking water is 1 mg/L while MOEF (Govt. of India) has set a maximum concentration level of 1 mg/L of phenol in the industry effluents for safe discharge into inland surface water and 5 mg/L for safe discharge into public sewers and marine coastal areas [8]. The WHO recommended 0.001 mg/L as the permissible phenolic concentration in portable water. It is therefore necessary to reduce or to eliminate phenols from water and wastewater before discharge or reuse.

Various treatment methods are available for removal of phenolic compounds which include adsorption, ion exchange, reverse osmosis, chemical oxidation, precipitation, distillation, gas stripping, solvent extraction, complexation and even bioremediation [9]. Among them, adsorption is considered to be the cost effective method for quickly lowering the concentrations of phenol and other organic molecule in an effluent. The activated carbon (AC) is widely used for removal of a variety of organics from water, but the generation of carbon fines due to the brittle nature of carbon make it unsuitable in many cases [4]. The challenge is now to find an alternative adsorbent of comparable efficiency with lower cost. Various adsorbents such as mesoporous MCM-41 [1], parthenium based activated carbon [2], granular activated carbon [3], synthetic resin [4], coconut shell [6], agricultural waste material [7], carbonaceous adsorbents [8] and bagasse ash and wood charcoal [9] have been reported for removing resorcinol and phenolic compounds from water and wastewater.

Coal fly ash (FA) is a solid waste generated in large amounts worldwide; therefore, development of new techniques for its productive reuse is important. As a measure to recycle FA, zeolites synthesized from FA (ZFAs) have been extensively investigated in recent years. A number of zeolites have been produced from FA, including Na-P1, philipsite, chabazite, F linde, herchelite, faujasite, analcime, zeolite A, zeolite X, zeolite Y, and hydroxysodalite [10]. It is shown that ZFA is applicable for the removal of a number of pollutants from water, including ammonium [11], heavy metals [12],

as well as phosphate [13]. Very encouraging results have also been obtained for ZFA to remove some waste gases from flue [14] because zeolites are hydrated aluminosilicate minerals with a framework formed by tetrahedra of SiO_4 and AlO_4 containing water molecules, alkali and alkaline earth metals in their structural framework [15]. Since zeolites have a net permanent negative charge resulting from isomeric substitution of Si^{4+} by Al^{3+} , cationic surfactants such as hexadecyltrimethylammonium bromide (HTAB) and cetylpyridinium bromide (CPB) are suitable for surface modification of zeolites [15–27]. The positive head groups of cationic surfactants readily exchange with the exchangeable cations on the external surface of zeolites, forming surfactant monolayers [21]. In properly chosen conditions, the loaded cationic surfactants on the external surface of zeolite form bilayers, where the upper layer is bound to the lower layer by the hydrophobic interaction between the tail groups of surfactants in both layers [19]. Surfactant-modified zeolites (SMZs) have been investigated as adsorbents for removing various pollutants such as chromate [16], arsenate [17], phosphate [18], nitrate [19], phenol [20], 4-chlorophenol [20], volatile petroleum hydrocarbons [21], orange II [22], bisphenol A [23], fulvic acid (FA) [24], humic acid (HA) [25] and sodium. However, to our knowledge, the use of SMZs as adsorbents to remove resorcinol from aqueous solution has not been studied.

In the present work a systematic study of the adsorption capacity of resorcinol from aqueous solution by CTAB/NaOH/flyash composite is reported. The effects of several experimental parameters such as contact time, initial adsorbate dosage, initial adsorbent concentration, temperature, ionic strength and solution pH on resorcinol adsorption onto CTAB/NaOH/flyash composite were investigated. The experimental results were analyzed by kinetic and isotherm models. Thermodynamic parameters such as Gibbs free energy change (ΔG°), enthalpy change (ΔH°) and entropy change (ΔS°) were calculated. The mechanism for

Table 1
Chemical composition and properties of coal FA, NaFA & CTAB/NaOH/flyash composite Study.

Parameter	Coal Fly Ash (Wt%) (by XRF)	NaFA(Wt%) (by EDX)	CTAB/NaOH/flyash composite (Wt%) (by EDX)
SiO_2 (%)	60.46	13.74	12.37
Al_2O_3 (%)	21.50	5.99	7.66
Fe_2O_3 (%)	4.30	2.79	4.06
CaO (%)	7.63	2.69	2.42
MgO (%)	0.82	0.23	0.28
Na_2O (%)	0.19	9.42	7.89
K_2O (%)	1.25	0.45	0.24
Moisture (%)	1.2	4.5	5.1
TiO_2	1.53	0.69	0.67
TCEC (mmol g^{-1})	<0.03	1.02	0.815
ECEC (mmol g^{-1})	<0.02	0.068	0.051
Surface area of pores (m^2/g)			
(i) BET	1.7950	18.2875	51.1207
(ii) BJH	1.1465	15.6483	53.1196
a. Adsorption cumulative	1.7148	165528	63.6179
b. Desorption cumulative			
BJH Cumulative Pore Volume (cm^3/g)			
(i) Single Point Total	0.006714 ^a	0.102599 ^b	0.176996 ^c
(ii) BJT Adsorption	0.006264 ^d	0.100457 ^d	0.169049 ^d
(iii) BJH desorption	0.006732 ^d	0.102793 ^d	0.178586 ^d
Average pore diameter (Å)			
(i) Single Point Total	149.6238	224.4138	138.4928
(ii) BJT Adsorption	218.5352	256.7875	127.2969
(iii) BJH desorption	157.0288	248.3996	112.2868

^a Pores less than 900.1879 Å diameter.

^b Pores less than 821.9909 Å diameter.

^c Pores less than 769.8010 Å diameter.

^d Pores between 17.00 Å and 3000.00 Å diameter.

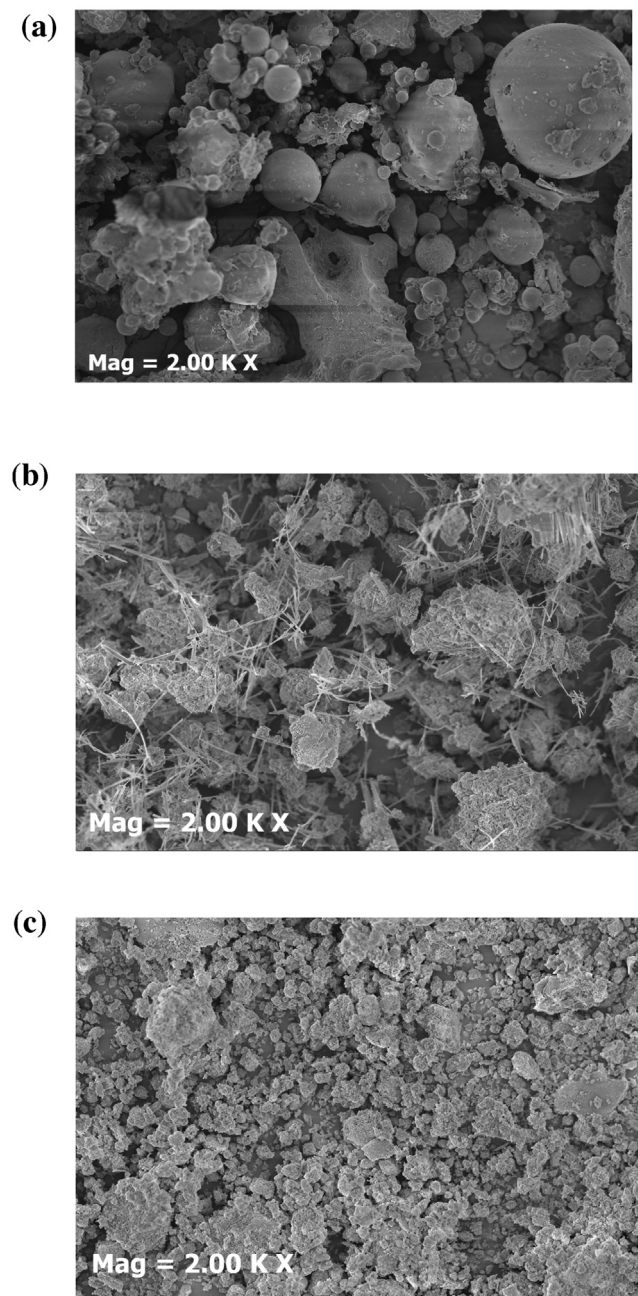


Fig. 1. Scanning electron micrographs (FE-SEM) of (a) FA (b) NaFA and (c) CTAB/NaOH/flyash composite.

resorcinol adsorption onto CTAB/NaOH/flyash composite is also proposed.

2. Materials and methods

2.1. Materials

Fly ash (Class F Type with SiO_2 and $\text{Al}_2\text{O}_3 > 70\%$) was obtained locally from Sriram Fertilisers & Chemical Ltd. (Kota, Rajasthan, India). *N*-Cetyl-*N,N,N*-Trimethyl Ammonium Bromide (CTAB) of LOBA Chemi. and resorcinol, NaOH, HCl were purchased from S.D. Fine Chemicals Ltd, India. Double distilled water was used in all adsorption experiments.

2.2. Synthesis of NaFA and CTAB/NaOH/flyash composite

NaFA was hydrothermally synthesized from FA. For NaFA synthesis, 25 g of FA, 150 mL of 2.0 M NaOH solution were mixed and heated to 96°C . The slurry was boiled with reflux for 24 h with continuous stirring. The obtained slurry was centrifuge and washed with doubly distilled water three times with repeated centrifugation followed by drying in an oven at 100°C and calcined at 380°C for 2 h in muffle furnace and ball milled in planetary ball mill for 2 h at 250 rpm. For synthesis of CTAB/NaOH/flyash composite, 500 mL of the solution of the surfactant, Cetyltrimethylammonium bromide (CTAB), with a concentration of 11 mmol L^{-1} was vigorously mixed with 10 g of NaFA at 50°C for 4 h. These reaction conditions were adopted to assure high loading of surfactant. After being cooled to room temperature, the product was centrifuged, washed with doubly distilled water, dried in an oven at 60°C and ball milled in planetary ball mill for 2 h at 250 rpm.

2.3. Instrumentation

For the chemical analysis, WD-XRF (S8 Tiger Bruker, Germany) & EDX (coupled with FE-SEM) were used. The crystalline phase(s) in the materials were identified by powder X-ray diffraction analysis on a X'Pert Pro, X-ray diffractometer using Ni filtered $\text{Cu-K}\alpha$ radiation (40 kV, 40 mA). Particle morphology was observed by SEM using a FE-SEM SUPRA 55 attached with Energy Dispersive Microanalysis. The FTIR spectra were recorded with a Bruker FT-IR spectrophotometer (Tensor-27) using the KBr method. The specific surface area and porosity measurement were made on an ASAP 2010 from Micrometrics by fitting the amount of N_2 adsorbed at -196°C for the BET equation. Organic carbon content was measured by the difference in weight loss between 105 and 750°C . The total cation exchange capacity (TCEC) was determined from the amount of retained ammonium by the ammonium acetate method [28]. The external cation exchange capacity (ECEC) was determined by adsorption of methylene blue from aqueous solution [29,30].

2.4. Adsorption experiments

Phenolic compounds resorcinol was selected to assess the decontamination performance by CTAB/NaOH/flyash composite. The experimental parameter such as pH, temperature, initial concentration, contact time and adsorbent dose on the removal of resorcinol were studied in batch reactor. For this purpose the materials were mixed with aqueous solutions containing the organic pollutants ranging in initial concentrations and then shaken continuously in a thermostatic Orbital Incubator Shaker at $30 \pm 0.1^\circ\text{C}$ for 24 h. The sample were withdrawn from the shaker at predetermined time interval and separated by centrifugation (Centrifuge machine MBL-20) at 2000 rpm for 4 min to yield a clear supernatant for analysis of the equilibrium concentrations of the solutes. The concentrations were measured with Double Beam UV/Visible spectrophotometer (model Spectrascan UV 2600/02) at the wavelength of 313 nm for resorcinol.

3. Result and discussion

3.1. Characterization of adsorbent

The primary mineralogical constituents of FA, NaFA and CTAB/NaOH/flyash composite like Silica, alumina and sodium contents are shown in Table 1. The amount of silica and alumina with NaFA and CTAB/NaOH/flyash composite were lower than FA. The FA contain higher amount of SiO_2 content which decreases in NaFA

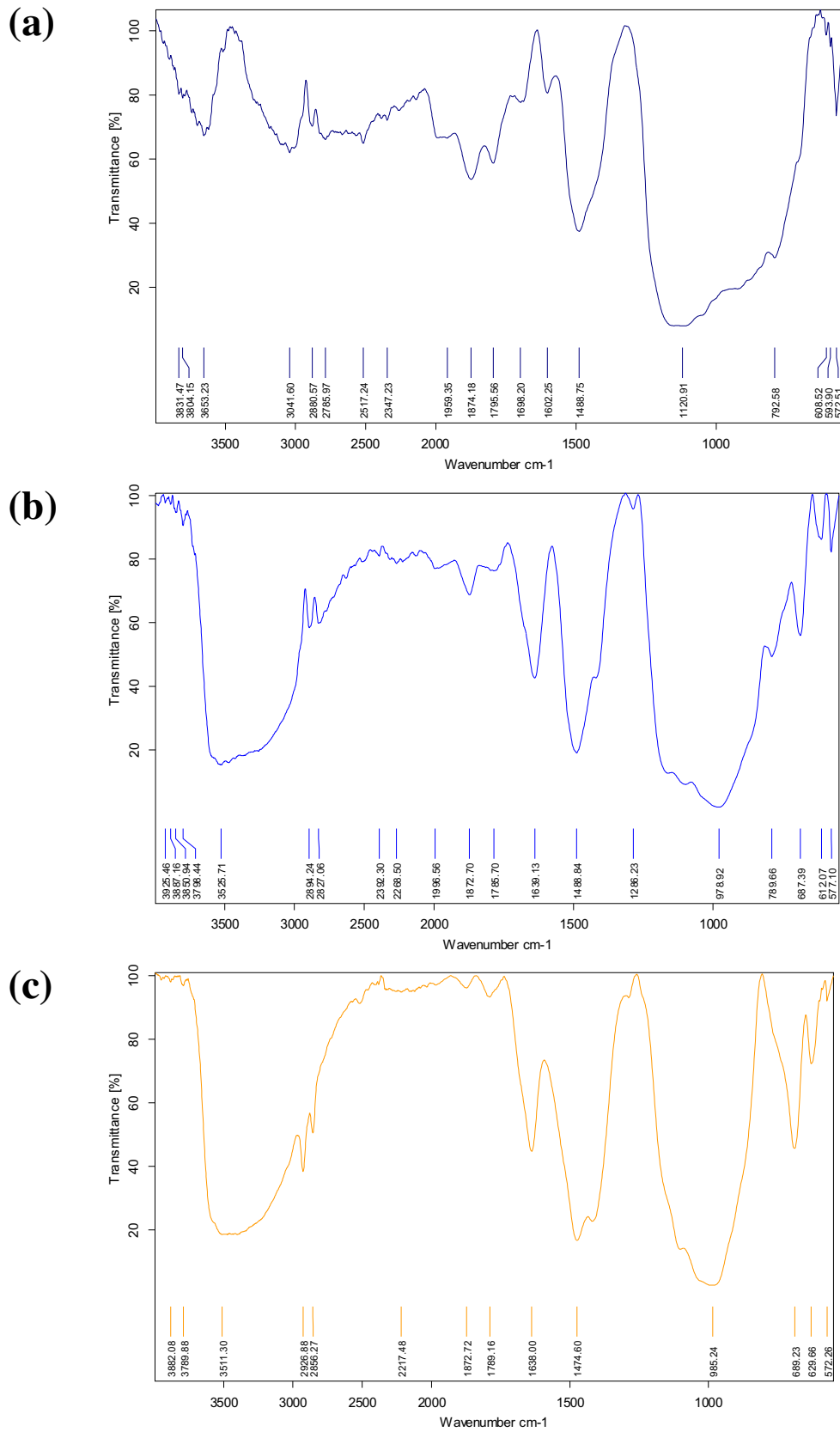


Fig. 2. The FTIR patterns for (a) FA (b) NaFA and (c) CTAB/NaOH/flyash composite.

and CTAB/NaOH/flyash composite due to the dissolution of glass phase (aluminium – silicate).

Fig. 1 a, b and c shows the field emission scanning electron microscopy (FE-SEM) images of FA, NaFA and CTAB/NaOH/flyash composite respectively. The original FA particles typically had

Table 2
Comparison and shifting of bands data for FA, NaFA and CTAB/NaOH/flyash composite in FTIR spectroscopy.

Wave number (cm ⁻¹)	Possible assignment	Observed value (cm ⁻¹)		
		FA	NaFA	CTAB/NaOH/flyash composite
3600–3300	Stretching vibration of —OH group, Silanol (Si-OH)	3653.23	3525.1	3511
1700–1400	—OH deformation & bending vibration of interstitial water	1698.20	1639.13	1638
		1602.25	1488.84	1474.60
		1488.75		
1250–850	Asymmetric stretching of internal tetrahedral TO ₄ , Si-O-Si (T=Si, Al)	1120.91	978.92	985.24
720–650	Symmetric stretching of internal tetrahedral TO ₄ (T=Si, Al)	–	687.39	689.23

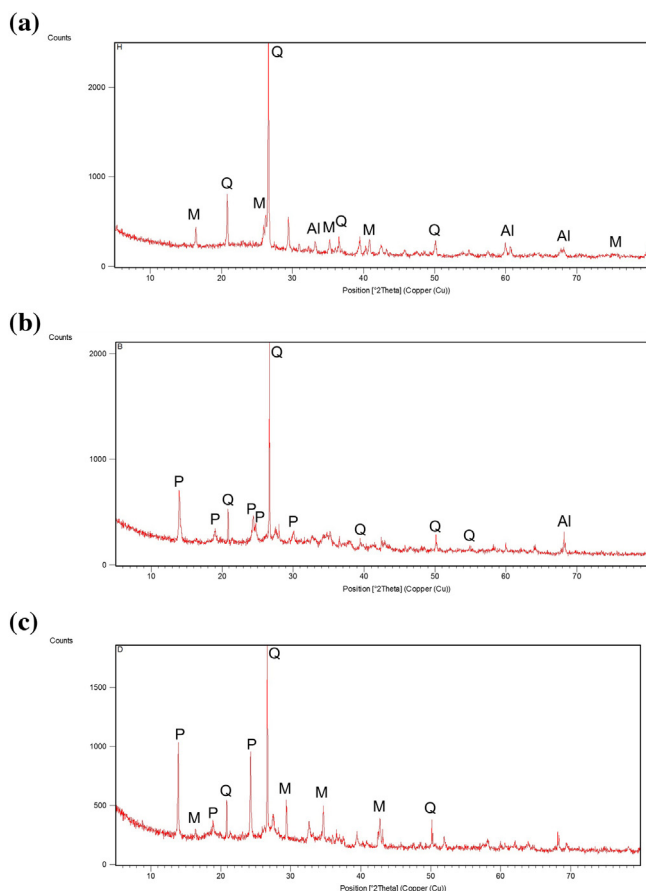


Fig. 3. The XRD patterns for (a) FA (b) NaFA and (c) CTAB/NaOH/flyash composite, in which the abbreviation was as follows: Q, quartz; M, mullite; Al, aluminium; P, zeolitic phase.

Table 3
Comparison between XRD Peak and d-spacing of NaFA and CTAB/NaOH/flyash composite.

Adsorbent	d-spacing (Å)	2θ (degree)	Intensity (Counts)
NaFA	6.33671	13.9751	24.54
CTAB/NaOH/flyash composite	6.35364	13.9271	52.97

spherical shapes and different sizes, with a smooth surface made of an aluminosilicate glass phase. Upon formation of NaFA, the surface became rough, indicating the deposition of clusters of zeolitic material and developed crystalline tubular habits. The morphological difference between CTAB/NaOH/flyash composite and NaFA was observable. After loading of CTAB on to NaFA, the surface of zeolitic crystal were covered with an organic layer and

the crystalline depositions seen in Fig b were completely disappear.

Formation of silicoaluminate crystalline material in NaFA was confirmed by the shift of the band from 1120 cm⁻¹ for FA to 978.92 cm⁻¹ for NaFA on Fourier transformed infrared (FTIR) spectra (Fig. 2b and Table 2), an increase in tetrahedral Al (formation of zeolitic phases) would induce a shift of the band within the range of 1180–950 cm⁻¹ (which is assigned to the asymmetric internal T-O stretching vibration mode of the TO₄tetrahedra, where T=Si or Al) to a lower wave number [31]. The four bands at 577, 612, 687 and 789 cm⁻¹ are confirm the formation of zeolitic material on alkali and hydrothermal treatment of fly ash [32]. The FTIR absorption bands at 2856 and 2926 cm⁻¹ (Fig. 2c), which are attributed to the symmetric and asymmetric stretching vibrations of C—C in the alkyl chain of CTAB, indicate that CTAB formed a bilayer micelle, rather than monolayer coverage [33].

The XRD pattern of the FA, NaFA and CTAB/NaOH/flyash composite was shown in Fig. 3. The very wide reflection at low 2θ values (3–16°) on XRD pattern of FA gives the evidence of the presence of amorphous material. It was observed from that the XRD of NaFA exhibited some significant peaks of reflections at 2θ of about 13, 16, 22, 23.5, 27, 28 and 32°, which were indicative of the probable formation of zeolite-P2 [(Ca_{0.6}Na_{2.6}K_{2.2})Al₆Si₁₀O₃₂·12H₂O] [34] with hydroxysodalite [Na_{1.08}Al₂Si_{1.68}O_{7.44}·1.8H₂O] in the hydrothermal synthesis. For example, the XRD peaks at about 27° and 28° 2θ suggest the presence of zeolite-P, which is topologically related to the natural zeolite called gobbinsite [35]. The Presence of CTA⁺ion on NaFA surface confirmed by first strong peak increased slightly the d-spacing of NaFA (Table 3). Mullite and quartz in FA, NaFA and CTAB/NaOH/flyash composite were also confirmed.

Due to the production of zeolitic material, NaFA exhibited a greatly enhanced total cation exchange capacity (TCEC, 1.02 mmol g⁻¹) and Brunauer–Emmett–Teller (BET) area (18.2875 m² g⁻¹) when compared to FA (<0.02 mmol g⁻¹ and 1.795 m² g⁻¹, respectively) (Table 1). It is worthy of note that NaFAs are not pure zeolite but contain some components as non zeolite fraction. The comparison of the TCEC value of a NaFA with that of a pure zeolite may provide a semiquantitative estimate of the zeolite content in the NaFA given that the NaFA contained only one kind of zeolite. The external surface was used to load CTAB because the pore size of NaFA is too small for the CTAB cation to enter. The amount of CTAB loaded was determined to be 0.141 mmol g⁻¹ based on the difference in the carbon content between CTAB/NaOH/flyash composite and NaFA. This was nearly twice as the amount of ECEC, indicating that CTAB formed a bilayer micelle on the external surface of NaFA.

Fig. 4 shows the N₂-adsorption isotherm and the pore-size distribution of the CTAB/NaOH/flyash composite. An adsorption is the source of information about properties, such as the porous structure of the adsorbent, heat of adsorption and physical and chemical characteristics. The BET surface area, pore diameter and pore volume of FA, NaFA and CTAB/NaOH/flyash composite are shown in Table 1. The combination of type II and type IV adsorption

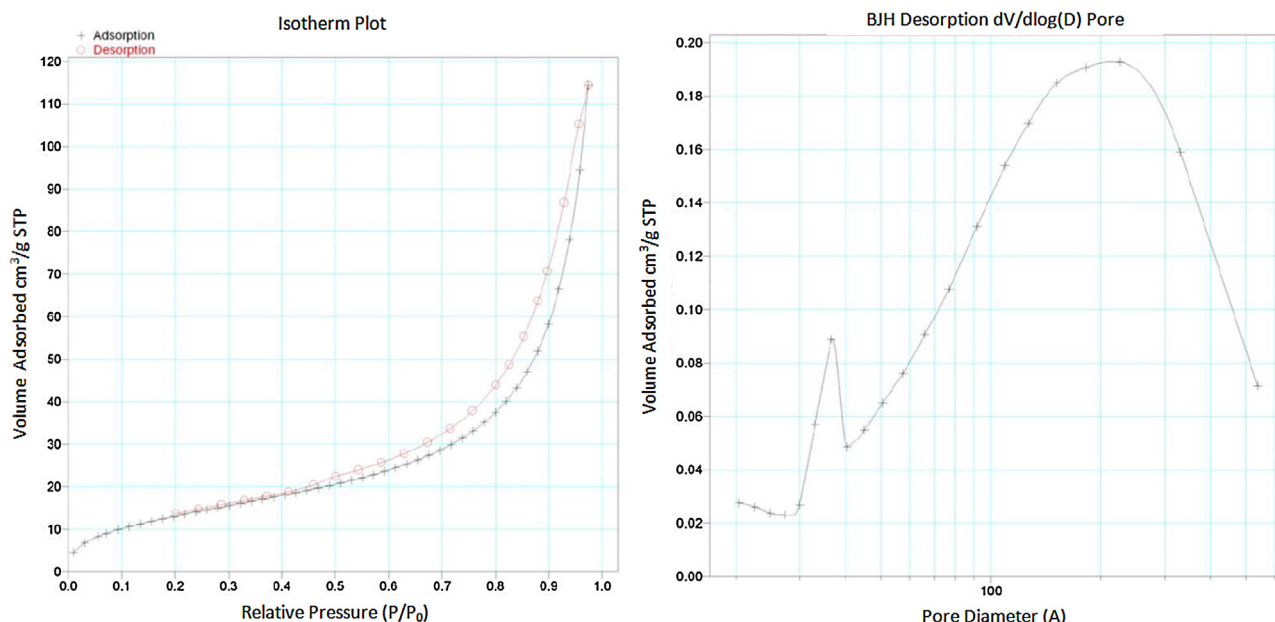


Fig. 4. Adsorption isotherm of nitrogen at 77 K and pore size distribution for CTAB/NaOH/flyash composite.

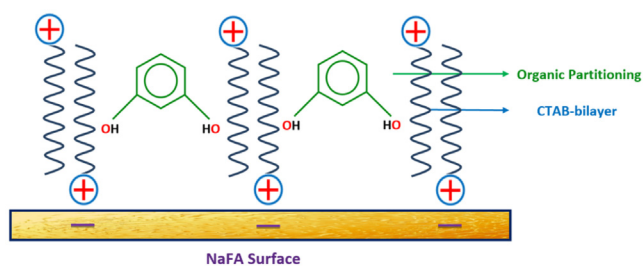


Fig. 5. Schematic representation of adsorption of resorcinol on CTAB/NaOH/flyash composite (Interaction mechanisms of resorcinol, with CTAB/NaOH/flyash composite. In this figure, the meaning of the symbols are as follows: \oplus the head of CTAB; \sim the C-16 chain of CTAB; NaFA in which represents the \ominus negative charge and show the interaction between the hydrophobic benzene ring of organic pollutants and the hydrophobic C-16 chain of CTAB as a function to contribute in adsorption.).

isotherm for CTAB/NaOH/flyash composite implies the mesoporous and micropores (with additional external surface area) structure of materials according to the IUPAC and Brunauer, Deming, Deming & Teller (BDDT) classification [36]. The pore size distribution confirms that the pore size of NaFA and CTAB/NaOH/flyash composite ranged from 20 Å (1 Å = 0.1 nm) to 500 Å.

3.2. Effect of surfactant loading on NaFA

When NaFA is mixed with the surfactant solution having concentration less than its critical micelle concentration ($9 \times 10^{-4} \text{ mmol L}^{-1}$) [37] then the surfactant molecule forms a monolayer on the external surface of NaFA via exchange. If the concentration of surfactant is increased then it forms micelle which attaches itself in a patchy layer and subsequently rear-ranges to form a second layer over the first layer via hydrophobic tail to tail interaction of surfactant due to weak Van der Waals cohesive forces. Due to this tail-to-tail interaction, an organic fraction is created over the NaFA surface, which is responsible for trapping organic hydrophobic pollutants like phenolics. Fig. 5 reveals the schematic representation of mechanism of adsorption of resorcinol by CTAB/NaOH/flyash composite. The effect of surfactant loading on removal of resorcinol was given in Table 4. It was found that the resorcinol adsorption efficiency was increased with increase loading amount of CTAB on NaFA. After surfactant loading with 11 mmol L^{-1} there was no more increase in adsorption efficiency due to excessive crowding of monomers of surfactant molecule on external surface of NaFA, which might have blocked the organic partitioning created by tails of long chain alkyl compound for adsorption of organics. There for CTAB/NaOH/flyash composite with mmol L^{-1} loading amount of CTAB was the most efficient adsorbent for the removal of resorcinol from aqueous solution.

Table 4
Effect of surfactant loading on NaFA on adsorption capacity of resorcinol.^a

NaFA dose (g)	CTAB concentration (mmol L^{-1})	Surfactant Loading (mmol L^{-1})	adsorption capacity of resorcinol (mg/g)
10	2	0.032	70.1
10	4	0.045	82.2
10	6	0.062	90.05
10	8	0.096	95.2
10	11	0.141	102.25
10	15	0.201	102.85

^a adsorption condition: adsorbent dose 0.4 g L^{-1} , agitation rate 200 rpm, pH 6.8 and initial concentration of resorcinol 50 ppm, temperature 303 K, contact time 24 h.

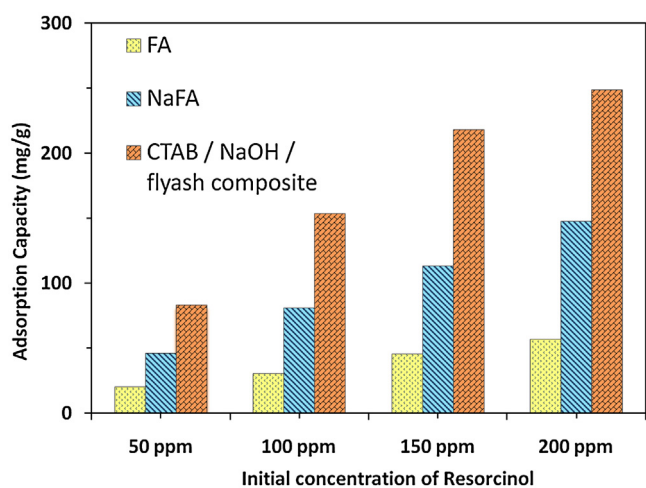


Fig. 6. Comparison of removal of resorcinol using FA, NaFA&CTAB/NaOH/flyash composite. (initial concentration = 50–200 mg/L, pH 6.8, contact time = 24 h.)

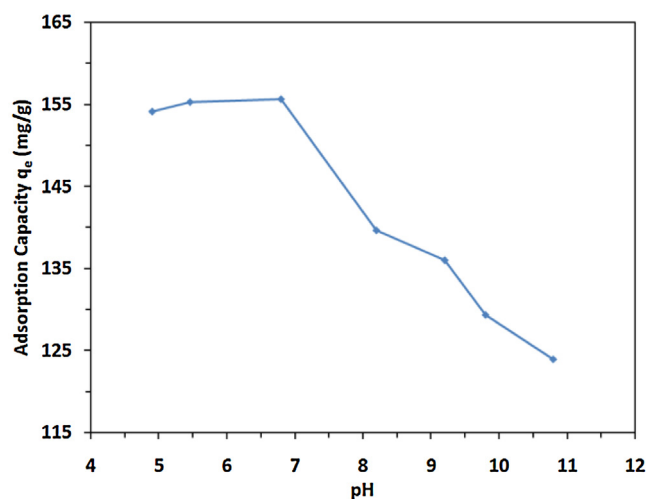


Fig. 7. Effect of pH on adsorption capacity of resorcinol on CTAB/NaOH/flyash composite. (adsorbent dose = 0.5 gm/l, contact time = 24hr, T = 303 K, initial concentration = 100 ppm.)

3.3. Effect of various adsorbent composite on adsorption of resorcinol

The preliminary adsorption experiments under identical set of experimental conditions were carried out using FA, NaFA and CTAB/NaOH/flyash composite. The adsorption capacity of resorcinol by FA, NaFA and CTAB/NaOH/flyash composite are shown in Fig. 6. It was observed that the removal efficiency of FA and NaFA is significantly less as compared to CTAB/NaOH/flyash composite. This may be attributed to the hydrophobicity imparted by surfactant leading to organic partitioning. Therefore, further experiments were carried out using CTAB/NaOH/flyash composite for optimization of adsorption parameters.

3.4. Effect of initial pH

The initial pH of adsorption medium is one of the most important parameters affecting the adsorption process. Effect of initial pH on adsorption of resorcinol was studied with initial concentration of 100 mg L⁻¹, solution temperature 30 °C adsorbent dose of 0.5 g L⁻¹. The pH was adjusted by adding 0.1 mol L⁻¹ or

0.01 mol L⁻¹ HCl (or NaOH) to the solutions. Below pH 5.0 some zeolitic phases show dissolution so was not investigated. The adsorption of resorcinol onto CTAB/NaOH/flyash composite as a function of solution pH is shown in Fig. 7. Results showed that the resorcinol adsorption capacity for CTAB/NaOH/flyash composite was relatively high at solution pH 5.0–7.0, and decreased with increasing solution pH from 7.0 to 11.0. This observation is explained below. Resorcinol is a weak acid, and its ionization is strongly dependent on solution pH. The adsorption of unionized resorcinol onto the positively charged surface of CTAB/NaOH/flyash composite is unlikely to be driven by the electrostatic attraction. Therefore, the hydrogen bonding and organic partitioning are responsible for the adsorption of resorcinol onto CTAB/NaOH/flyash composite, at solution pH 5.0. Resorcinol molecules are ionized at solution pH above 5.0 and they are almost completely ionized at solution pH 7.0 [38]. Therefore, the electrostatic attraction together bonding with the hydrogen bonding and organic partition are responsible for the adsorption of resorcinol onto CTAB/NaOH/flyash composite at solution pH 5.0–7.0. The increase of solution pH from 5.0 to 7.0 leads to decreased hydrogen bonding between resorcinol and CTAB/NaOH/flyash composite but the increased electrostatic attraction between resorcinol and CTAB/NaOH/flyash composite. The former is counteracted by the later, resulting in that the adsorption of resorcinol on CTAB/NaOH/flyash composite is slightly influenced by solution pH at 5.0–7.0. At solution pH above 7.0, completely ionized resorcinol molecules cannot provide hydroxyl hydrogen atom to nitrogen atom of CTAB bilayer to form hydrogen bonding. In this case, the electrostatic attraction plays an important role in the adsorption of resorcinol onto CTAB/NaOH/flyash composite, the increase of solution pH from 7.0 to 11.0 leads to the increased of the competitions between the hydroxyl ion and the ionized resorcinol molecules for the same positively charged adsorption sites on the surface of CTAB/NaOH/flyash composite, which causes a decreases resorcinol adsorption capacity.

3.5. Effect of ionic strength

The adsorption of resorcinol onto CTAB/NaOH/flyash composite as a function of ionic strength at solution pH 6.8 is shown in Fig. 8. The presence of electrolytes such as NaCl in aqueous solution had a slight negative effect on resorcinol adsorption onto CTAB/NaOH/flyash composite. When the ionic strength of the aqueous solution increased from 0 to 0.8 mol/L, the resorcinol adsorption capacity decreases from 153.68 to 144.6 mg/g this result suggest that CTAB/NaOH/flyash composite bilayer coverage is effective in removing resorcinol from water or wastewater containing salt. If electrostatic attraction is the main adsorption mechanism, the ionic strength should have a significant negative effect on the adsorption process [38,39]. The slight negative effect of ionic strength on resorcinol adsorption onto CTAB/NaOH/flyash composite at solution pH 6.8 confirms that the electrostatic attraction is not the only mechanism for the adsorption process and the electrostatic attraction together with the other mechanisms such as hydrogen bonding and organic partitioning control the adsorption process. The slight decrease of resorcinol adsorption capacity after NaCl addition. On one hand, resorcinol adsorption onto CTAB/NaOH/flyash composite may be reduced by chloride ions due to the competition between the chloride ions and the ionized resorcinol ions for the adsorption sites on the surface of the adsorbent. On the other hand, resorcinol adsorption onto CTAB/NaOH/flyash composite may be enhanced by the sodium ions due to the weakening of the repulsive interaction between adsorbed resorcinol molecules on the surface of the adsorbent and resorcinol molecules in solution [38]. The decreased resorcinol adsorption caused by the chloride ions may be partially counteracted by the

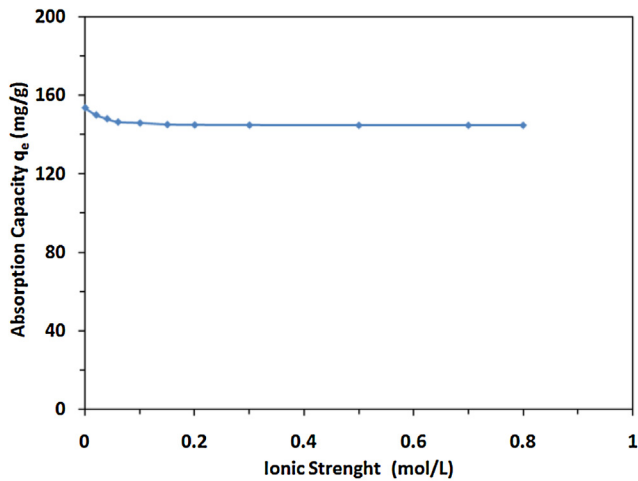


Fig. 8. Effect of Ionic Strength on adsorption capacity of resorcinol on CTAB/NaOH/flyash composite. (adsorbent dose = 0.5 gm/l, contact time = 24hr, T = 303 K, initial concentration = 100 ppm, pH = 6.8.)

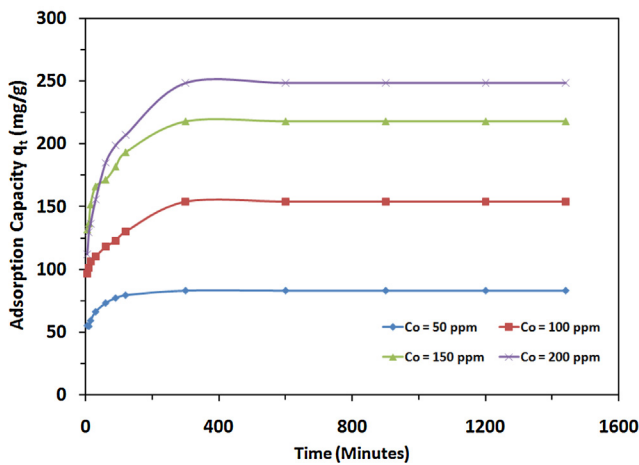


Fig. 9. Effect of Initial Concentration of adsorbate on adsorption capacity of resorcinol on CTAB/NaOH/flyash composite. (adsorbent dose = 0.5 gm/l, pH = 6.8, T = 303 K.)

increased resorcinol adsorption caused by the sodium ion, resulting in that resorcinol adsorption caused by the sodium ion, resorcinol adsorption is slightly reduced by the ionic strength of the aqueous solution.

3.6. Adsorption kinetics

The adsorption of resorcinol onto CTAB/NaOH/flyash composite as a function of contact time and initial concentration are shown in Fig. 9. Results showed that the rate of adsorption was rapid at the beginning and gradually decreased with increasing contact time until equilibrium was attained. It was observed that with increase in initial concentration of resorcinol, the adsorption capacity increases. It was possible that the initial concentration of resorcinol provided the necessary driving force to overcome the resistances of mass transfer between the aqueous phases and the solid phase [40]. The increase in initial concentration also enhance the interaction between resorcinol and onto CTAB/NaOH/flyash composite so increase in adsorption uptake. Three widely used kinetic models, pseudo-first-order, pseudo-second-order and intra-particle diffusion model were employed to interpret the

kinetic results [Fig. 10]. The linearized form of pseudo-first-order kinetic model is given as follows [41]:

$$\ln(q_e - q_t) = \ln(q_e) - k_1 t \quad (1)$$

Where q_e (mg/g) and q_t (mg/g) are the resorcinol adsorption capacities for CTAB/NaOH/flyash composite at equilibrium and at any time t (min), respectively. k_1 (1/min) is the rate constant of pseudo-first-order kinetic model. The linear plot of $\ln(q_e - q_t)$ versus t was used to calculate the rate constant k_1 , the equilibrium adsorption capacity q_e , and the determination coefficient R^2 , and the results were given in Table 5. Although the R^2 value obtained was relatively high ($R^2 = 0.9825$), the calculated q_e value did not agree with the experimental one. This suggests that the pseudo-first-order kinetic model is not appropriate to represent the adsorption kinetics data of resorcinol onto CTAB/NaOH/flyash composite.

The linearized form of pseudo-second-order kinetic model is given as follows [41]:

$$\frac{t}{q_t} = \frac{1}{k_2 q_e^2} + \frac{t}{q_e} \quad (2)$$

where k_2 (g/mg min) is the rate constant of pseudo-second-order kinetic model. The values of equilibrium adsorption capacity q_e and rate constant k_2 , calculated from the intercept and slope of the linear plot of t/q_t versus t , along with the value of determination coefficient R^2 , are listed in Table 2. The R^2 value obtained was very high ($R^2 > 0.9976$), and the calculated q_e value was in good agreement with the experimental one, suggesting the applicability of the pseudo-second-order kinetic model to describe the adsorption kinetics data of resorcinol onto CTAB/NaOH/flyash composite.

An adsorption reaction is said to be intra-particle diffusion controlled if the reaction sites are internally located in the porous adsorbents and the external resistance to diffusive transport process is much less than the internal resistance. Intra-particle diffusion given by Weber & Moris. The Intra-particle diffusion model is expressed as follows [47]:

$$q_t = k_{diff} t^{0.5} + C \quad (3)$$

Where q_t is as defined in Eq. (2), k_{diff} is the intra-particle diffusion rate constant ($\text{mg min}^{-1/2} \text{g}^{-1}$) and C is the intercept. Accordingly to Eq. (3), a plot of q_t vs. $t^{0.5}$ should be straight line with a slope k_{diff} and intercept C . The term k_{diff} is indicative of an enhancement in the rate of adsorption. The value of C gives (Table 5) an idea about the boundary layer thickness.

3.7. Adsorption isotherm

The adsorption isotherm of resorcinol onto CTAB/NaOH/flyash composite at 30 °C, 40 °C and 50 °C and solution pH 6.8 is shown in Fig. 11. Results showed that the resorcinol adsorption capacity increased with increasing the resorcinol concentration until equilibrium was reached. Two-parameter isotherm models Langmuir, Freundlich, Dubinin – Redushkevich (D-R), Tempkin and three-parameter isotherm model Redlich – Peterson were used to fit the experimental data. The linearized form of Langmuir isotherm model can be written as [41,43]:

$$\frac{C_e}{q_e} = \frac{1}{q_{max} K_L} + \frac{C_e}{q_{max}} \quad (4)$$

Where C_e (mg/L) is the equilibrium concentration of resorcinol in solution. q_e (mg/g) is the resorcinol adsorption capacity for CTAB/NaOH/flyash composite at equilibrium. q_{max} (mg/g) is the maximum monolayer resorcinol adsorption capacity for CTAB/NaOH/flyash composite. K_L (L/mg) is the Langmuir isotherm constant

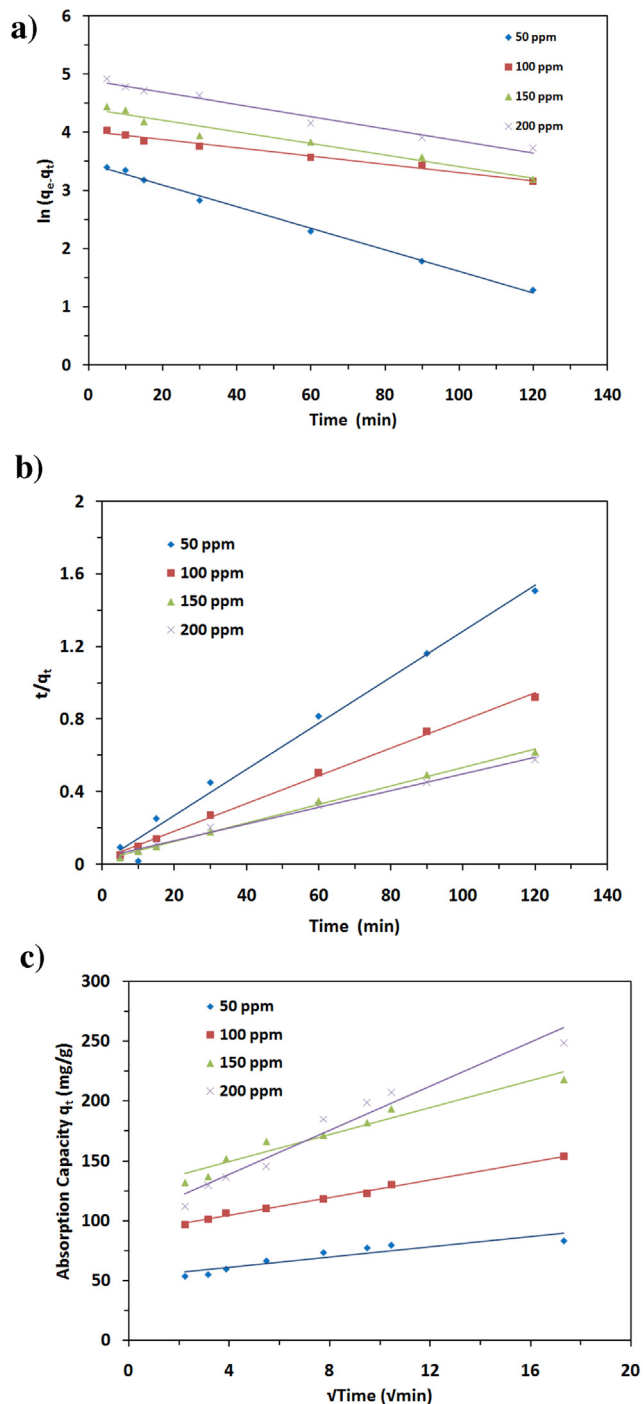


Fig. 10. Kinetic Model of Resorcinol on CTAB/NaOH/flyash composite (a) Pseudo First Order (b) Pseudo Second Order and (c) intra-particle diffusion model.

Table 5

Pseudo-first order, Pseudo-second order and Intra-particle Diffusion Model rate constant for resorcinol adsorption onto CTAB/NaOH/flyash composite at various concentration.^a

C_0 (mg/L)	$q_{e,exp}$ (mg/g)	Pseudo-first order model			Pseudo-second order			Intra-particle Diffusion Model		
		K_1 (1/min)	$q_{e,cal}$ (mg/g)	R^2	K_2 (g/mg min)	$q_{e,cal}$ (mg/g)	R^2	K_{id} (mg/g(min ^{0.5}))	C	R^2
50	83.28	0.0105	134.50	0.9764	9.83×10^{-4}	78.74	0.9878	2.167	52	0.8491
100	153.68	0.007	55.46	0.9825	1.96×10^{-4}	131.57	0.9976	3.689	89.81	0.9945
150	217.9	0.0099	82.35	0.9583	1.09×10^{-4}	196.08	0.9971	5.668	126.5	0.9487
200	248.54	0.0185	31.93	0.9957	0.52×10^{-4}	217.39	0.9944	9.213	101.5	0.9589

^a adsorption condition: adsorbent dose 0.5 g L⁻¹, agitation rate 200 rpm, pH 6.8 and temperature 30 °C.

related to the free energy of adsorption. The values of q_{max} and K_L can be calculated from the intercept and the slope of the straight line of the linearized form of Langmuir isotherm. The essential characteristics of the Langmuir isotherm can be expressed in terms of a dimensionless constant separation factor, R_L , which is defined as follows [41]:

$$R_L = \frac{1}{1 + K_L C_0} \quad (5)$$

where C_0 (mg/L) is the initial concentration of resorcinol in solution. The adsorption is considered favorable when $0 < R_L < 1$ [41].

The linearized form of Freundlich isotherm model can be written as [41,43]:

$$\ln(q_e) = \ln(K_F) + \frac{1}{n} \ln(C_e) \quad (6)$$

where K_F ((mg/g)(L/mg)^{1/n}) and $1/n$ are the Freundlich constants which are related to the adsorption capacity and adsorption intensity, respectively. The values of K_F and $1/n$ can be calculated from the intercept and the slope of the straight line of the linearized form of the Freundlich isotherm.

The Redlich-Peterson isotherm model is used as compromise between Langmuir and Freundlich isotherm models. The non-linearized form of Redlich-Peterson isotherm can be given as follows [39]:

$$q_e = \frac{K_R C_e}{1 + \alpha_R C_e^\beta} \quad (7)$$

Where K_R (L/g) and α_R (L/mg) ^{β} are Redlich-Peterson isotherm constant. β is the exponent which lies between 0 and 1 and can characterize the adsorption isotherm. If $\beta = 1$. Eq. (7) reduces to the Langmuir isotherm model, and if $\beta = 0$. Eq. (7) reduces to the linear isotherm model [34]. The values of K_R , α_R and β can be obtained by nonlinear regression method.

The value of β for the Redlich – Peterson isotherm was 0.5–0.6, which means that the isotherm confirms to the both Langmuir isotherm model and Freundlich isotherm model.

The linearized form of D-R isotherm model can be written as [39,43]:

$$\ln(q_e) = \ln(q_{max}) - K_D \left[RT \ln \left(1 + \frac{1}{C_e} \right) \right]^2 \quad (8)$$

Where C_e (mg/L) is the equilibrium concentration of resorcinol solution. q_e (mg/g) is the resorcinol adsorption capacity of CTAB/NaOH/flyash composite at equilibrium. q_{max} (mg/g) is the maximum resorcinol capacity for CTAB/NaOH/flyash composite. K_D (mg²/kJ²) is the D-R isotherm constant related to the free energy of adsorption. R (8.314 J/mol K) is the gas constant. T (K) is the absolute temperature. The value of K_D and q_{max} can be calculated from the intercept and the slope of the straight line of the linearized form if D-R isotherm.

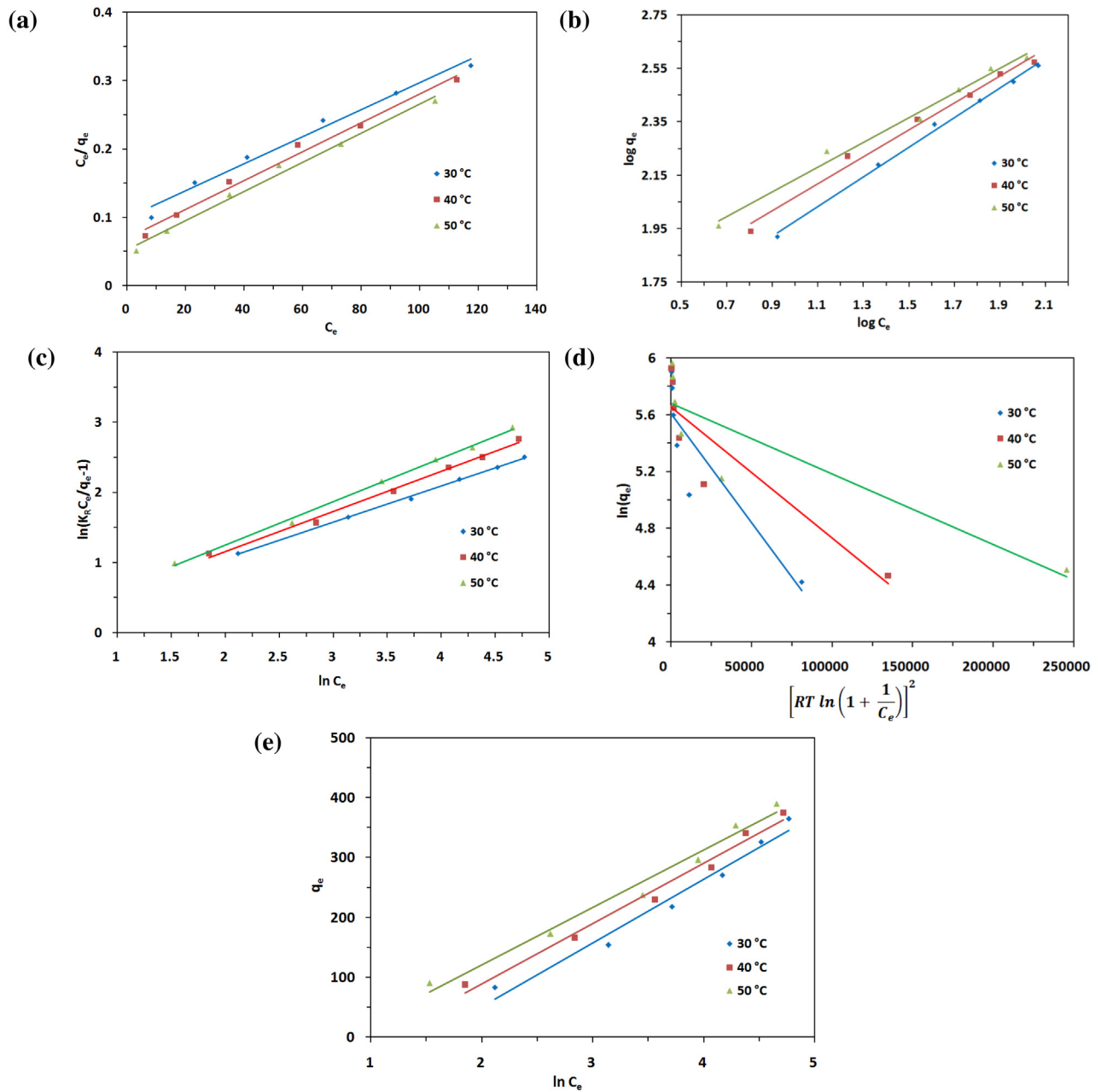


Fig. 11. Adsorption Isotherm of resorcinol on CTAB/NaOH/flyash composite (a) Langmuir (b) Freundlich (c) Redlich-Peterson (d) D-R and (e) Temkin.

The Temkin isotherm has generally been applied in the following form [41,43]:

$$q_e = B_T \ln K_T + B_T \ln C_e \quad (9)$$

where $B_T = RT/b_T$, T (K) is the absolute temperature, R (8.314 J/mol) is the universal gas constant, K_T (l/mg) is the equilibrium binding constant and b_T (J/mol) is related to the heat of adsorption. The isotherm constants K_T and b_T are calculated from the slope and intercept of the q_e versus $\ln C_e$.

The different isotherm parameters were evaluated from the linear plots and presented in Table 6 along with constants and correlation coefficients root mean square error (RMSE) and chi-square (χ^2). The RMSE and χ^2 are used to measure the goodness of

fit of an isotherm defined as below.

$$RMSE = \sqrt{\left(\frac{1}{m-2}\right) \sum_{i=1}^m (q_{i,exp} - q_{i,cal})^2} \quad (10)$$

$$\chi^2 = \sum_{i=1}^m \frac{(q_{i,exp} - q_{i,cal})^2}{q_{i,exp}} \quad (11)$$

Where m is the number of observation in the experimental isotherm $q_{i,exp}$ is the calculated capacity observed from the experiment's value and $q_{i,cal}$ is the calculated capacity observed from the isotherm for the corresponding $q_{i,exp}$ value. A better curve fitting is observed by smaller RMSE value. If the data obtained from

Table 6
Isotherm parameters for resorcinol adsorption onto CTAB/NaOH/flyash composite at various temperature.^a

Langmuir	Temperature	q_{\max} (mg/g)	K_L (L/mg)	R^2	RMSE	χ^2
	at 30 °C	500	0.0202	0.984	12.98	3.5
	at 40 °C	500	0.02898	0.988	20.53	7.67
	at 50 °C	500	0.03846	0.999	28.95	3.22
Freundlich	Temperature	K_F (mg/g)(L/mg) ^{1/n}	1/n	R^2	RMSE	χ^2
	at 30 °C	26.54	0.553	0.996	10.63	1.649
	at 40 °C	36.73	0.503	0.988	14.13	3.187
	at 50 °C	47.10	0.46	0.987	13.0	2.785
Tempkin	Temperature	K_T (mg/g)	B_T	R^2	RMSE	χ^2
	at 30 °C	1.52	106.4	0.973	251.88	1356
	at 40 °C	1.11	100.4	0.983	121.06	180.05
	at 50 °C	0.738	95.77	0.979	190.42	483
D-R	Temperature	q_{\max} (mg/g)	K_D (mg ² /KJ ²)	R ²	RMSE	χ^2
	at 30 °C	272.33	-2×10^{-5}	0.791	68.03	77.28
	at 40 °C	285.72	-9×10^{-6}	0.818	67.86	70.42
	at 50 °C	292.66	-5×10^{-6}	0.799	73.76	80.27
Redlich Peterson	Temperature	K_R (L/g)	α_R (L/mg) ^a	R^2	RMSE	χ^2
at 30 °C	41	1.025	0.515	0.998	5.512	0.497
at 40 °C	56	1.008	0.572	0.993	11.61	1.95
at 50 °C	72.5	1.008	0.619	0.997	9.04	1.19

^a adsorption condition: adsorbent dose 0.5 g L⁻¹, agitation rate 200 rpm, pH 6.8 and initial concentration range 50–300 mg l⁻¹.

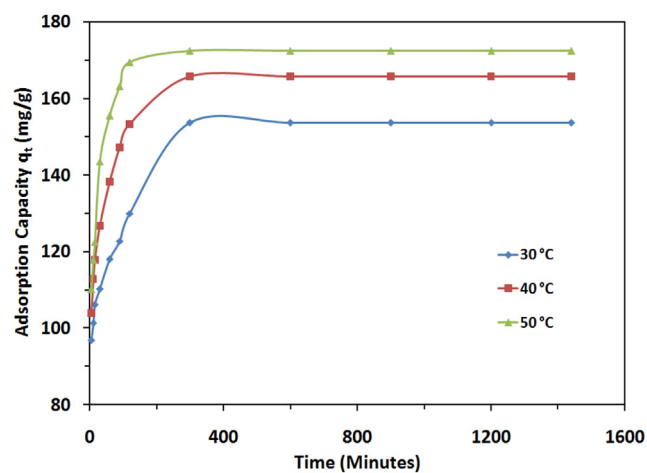


Fig. 12. Effect of Temperature of solution on adsorption capacity of resorcinol on CTAB/NaOH/flyash composite. (adsorbent dose = 0.5 gm/l, pH = 6.8, initial concentration = 100 ppm.)

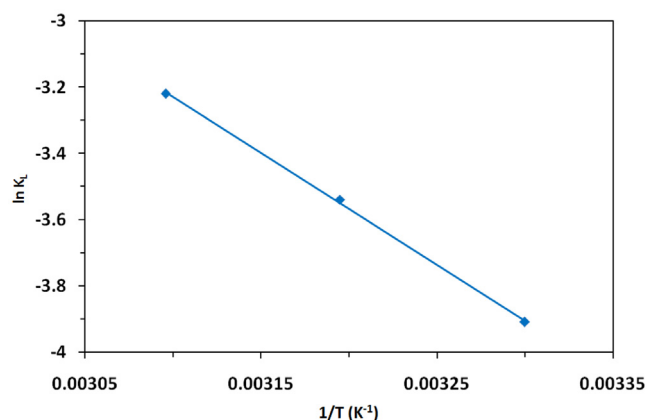


Fig. 13. Van't Hoff plot for the adsorption of resorcinol onto CTAB/NaOH/flyash composite.

the isotherm model are nearer to the experiment results the χ^2 values will be lesser digit [42,43].

The value of RMSE and χ^2 for the Tempkin and D-R isotherm model were high, indicating that the equilibrium adsorption of resorcinol onto CTAB/NaOH/flyash composite cannot be represented appropriately by these isotherm models. The value of RMSE and χ^2 for the Redlich-Peterson, Langmuir and Freundlich isotherm models were low, indicating that the equilibrium data for the adsorption of resorcinol onto CTAB/NaOH/flyash composite can be well represented by these three isotherm models but best fitted with Redlich-Peterson isotherm model. The predicted maximum monolayer resorcinol adsorption capacity for CTAB/NaOH/flyash composite derived from Langmuir isotherm was found to be 500 mg/g. The values of R_L obtained in this study were between 0.07968 and 0.5 indicating that the adsorption of resorcinol onto CTAB/NaOH/flyash composite favorable.

3.8. Thermodynamic studies

The adsorption of resorcinol onto CTAB/NaOH/flyash composite as a function of temperature is shown in Fig. 12. It was observed that adsorption capacity increased with increase in temperature. Higher temperature may provide more chance for phenolic compound molecule to pass the external boundary layer and produce the enlargement of pore volume and surface area enabling phenolic compound to penetrate. The thermodynamic parameters of standard enthalpy (ΔH°) and entropy (ΔS°) for the adsorption process were estimated from the Van't-Haff equation represented as

$$\ln K_L = \frac{\Delta S^\circ}{R} - \frac{\Delta H^\circ_{ads}}{RT} \quad (12)$$

$$\Delta G^\circ = -RT \ln K_L \quad (13)$$

Where K_L (L/mol) is Langmuir constant. R (8.314 J/mol K) is the gas constant. T (K) is absolute temperature. The values of K_L for Langmuir isotherm at 30 °C, 40 °C and 50 °C were used to calculate thermodynamic parameters such as Gibbs free energy change (ΔG°). The values of ΔH° and ΔS° can be calculated from the intercept and the slope of the linear plot of $\ln K_L$ versus $1/T$ as shown in Fig. 13.

The obtained values of the thermodynamic parameters of resorcinol adsorption onto CTAB/NaOH/flyash composite are given

Table 7

Thermodynamic parameters for resorcinol adsorption on CTAB/NaOH/flyash composite.

ΔH° (KJ/mol)	ΔS° (J/mol)	ΔG° (KJ/mol)			R^2
		30 °C	40 °C	50 °C	
26.189	-54.332	-9.83	-9.22	-8.75	0.997

Table 8

Energy of adsorption for different type of forces.

Type of forces	Energy of adsorption (kJ/mol)
Van der Waals	4–10
Hydrophobic bond	≈5
Hydrogen bond	2–40
Coordination exchange	≈40
Dipole bond	2–29
Chemical bond	>60

in Table 7. The negative values of ΔG° suggest that feasibility of the adsorption of resorcinol onto CTAB/NaOH/flyash composite is a spontaneous and a favourable process. In general, the value of ΔG° for physisorption is < 8.0 kJ/mol, and that chemisorption is between 20 and 40 kJ/mol [43]. The values of ΔG° obtained in this study were in the range of neither physisorption nor chemisorption, indicating that the adsorption of resorcinol onto CTAB/NaOH/flyash composite involves the other adsorption process such as interaction mechanism. This conclusion confirms that the mechanisms controlling the adsorption of resorcinol onto CTAB/NaOH/flyash composite at solution of pH 6.8 include electrostatic attraction.

The positive value of ΔH° indicates that the adsorption process is endothermic in nature. The energy of adsorption for different forces shown in Table 8 [44]. The absolute value of ΔH° was 26.189 kJ/mol, also indicates that hydrogen bonding and organic partitioning are important to the adsorption process in addition to electrostatic attraction. The negative value of ΔS° shows a decrease in randomness at the solid/liquid interface during the adsorption process [45].

3.9. Adsorption performance of CTAB/NaOH/flyash composite

Table 9 lists the comparison of the maximum adsorption capacity of resorcinol onto various adsorbent obtained from adsorption experiments. The CTAB/NaOH/flyash composite prepared in this work has a relatively large adsorption capacity of 500 mg g^{-1} compared to some other adsorbents reported in the literature. Therefore, the CTAB/NaOH/flyash composite prepared in this work could be used as an effective adsorbent for removing resorcinol from solution.

Table 9

Comparison of the maximum monolayer adsorption of resorcinol onto various adsorbents.

Adsorbents	Adsorption Capacity (mg g^{-1})	References
Activated carbon	142.82	[5]
Granular activated carbon	209	[3]
Carbonaceous material	< 1.5	[8]
High area activated carbon cloth	82% from activated carbon (AC), 72% from wood charcoal (WC), 79% from rice husk (RHA)	[46]
CTAB/NaOH/flyash composite	232.1 ($2.11 \times 10^{-3} \text{ mol/g}$) 500	This work

4. Conclusion

After Modification with the Surfactant (CTAB, Cetyltrimethylammonium bromide), hydrothermally treated fly ash exhibited greatly enhanced adsorptive capacity for resorcinol. CTAB/NaOH/flyash composite has good physical as well as chemical stability; hence it can be used for various environmental applications. N_2 adsorption isotherms of CTAB/NaOH/flyash composite is of combination of type II and type IV. The values of BET surface area, pore volume and pore diameter are $51.12 \text{ m}^2/\text{gm}$, $0.176996 \text{ cm}^3/\text{gm}$ and 138.4928 \AA respectively. The results show that CTAB/NaOH/flyash composite includes mesopores. Redlich-Peterson equation is best fitted for the description of resorcinol adsorption isotherm. Adsorption of resorcinol onto CTAB/NaOH/flyash composite increase with an increase in temperature indicating that the process is endothermic. The monolayer adsorption capacity for resorcinol is 500 mg/g . The adsorption kinetics of resorcinol onto CTAB/NaOH/flyash composite was found to follow a pseudo-second order model. The thermodynamic parameters such as ΔH° , ΔS° and ΔG° values of resorcinol adsorption onto CTAB/NaOH/flyash composite show an endothermic heat of adsorption, the feasibility of the adsorption process and its spontaneity, respectively. The resorcinol adsorption capacity for CTAB/NaOH/flyash composite slightly decreased with increasing ionic strength. The resorcinol adsorption capacity was relatively high at solution pH 5.0–7.0 and decreased with increasing solution pH from 7.0–11.0. The main mechanism controlling resorcinol adsorption onto CTAB/NaOH/flyash composite at solution pH < 7.0 include electrostatic attraction, hydrogen bonding and organic partitioning.

Acknowledgement

The authors are thankful to CSMCRI, Bhavnagar, Gujarat for Surface area & Porosimetry analysis, ISM, Dhanbad for SEM (EDX) and SAIF, Chandigarh for XRF & XRD. The financial support was provided under JRF Scheme of University Grants Commission (UGC) and Fly ash Mission of Department of Science & Technology (DST), New Delhi, India.

References

- [1] P.A. Mangrulkar, S.P. Kamble, J. Meshram, S.S. Rayalu, Adsorption of phenol and o-chlorophenol by mesoporous MCM-41, *J. Hazard. Mater.* 160 (2008) 414–421.
- [2] R.K. Singh, S. Kumar, S. Kumar, A. Kumar, Development of parthenium based activated carbon and its utilization for adsorptive removal of p-cresol from aqueous solution, *J. Hazard. Mater.* 155 (2008) 523–535.
- [3] S. Kumar, M. Zafar, J.K. Prajapati, S. Kumar, S. Kannepalli, Modeling studies on simultaneous adsorption of phenol and resorcinol onto granular activated carbon from simulated aqueous solution, *J. Hazard. Mater.* 185 (2011) 287–294.
- [4] S.H. Lin, R.S. Juang, Adsorption of phenol and its derivatives from water using synthetic resin and low cost natural adsorbents: a review, *J. Environ. Manag.* 90 (2009) 1336–1349.
- [5] A. Kumar, S. Kumar, S. Kumar, Adsorption of resorcinol and catechol on granular activated carbon: equilibrium and kinetics, *Carbon* 41 (2003) 3015–3025.

- [6] A.T.M. Din, B.H. Hameed, A.L. Ahmad, Batch adsorption of phenol onto physicochemical-activated coconut shell, *J. Hazard. Mater.* 161 (2009) 1522–1529.
- [7] K.P. Singh, A. Malik, S. Sinha, P. Ojha, Liquid-phase adsorption of phenols using activated carbons derived from agricultural waste material, *J. Hazard. Mater.* 150 (2008) 626–641.
- [8] R.M. Aghav, S. Kumar, S.N. Mukherjee, Artificial neural network modeling in competitive adsorption of phenol and resorcinol from water environment using some carbonaceous adsorbents, *J. Hazard. Mater.* 188 (2011) 67–77.
- [9] S.N. Mukherjee, S. Kumar, A.K. Mishra, F. Maohong, Removal of phenol from water environment by activated carbon, bagasse ash and wood charcoal, *Chem. Eng. J.* 129 (2007) 133–142.
- [10] X. Querol, N. Moreno, J.C. Uman, A. Alastuey, E. Hernandez, A. Lopez-Soler, F. Plana, Synthesis of zeolites from coal fly ash: an overview, *Int. J. Coal Geol.* 50 (2002) 413–423.
- [11] D.Y. Wu, B.H. Zhang, C.J. Li, Z.J. Zhang, H.N. Kong, Simultaneous removal of ammonium and phosphate from aqueous solution by zeolite synthesized from fly ash as influenced by salt treatment, *J. Colloid Sci.* 304 (2006) 300–306.
- [12] N. Moreno, X. Querol, C. Ayora, Utilization of zeolites synthesized from coal fly ash for the purification of acid mine waters, *Environ. Sci. Technol.* 35 (2001) 3526–3534.
- [13] J.G. Chen, H.N. Kong, D.Y. Wu, Z.B. Hu, Z.S. Wang, Y.H. Wang, Removal of phosphate from aqueous solution by zeolite synthesized from fly ash, *J. Colloid Interface Sci.* 300 (2006) 491–497.
- [14] P. X. Querol, J.C. Umana Moreno, R. Juan, S. Hernandez, C. Fernandez-pereira, C. Ayora M.Janssen, J. Garcia-Martinez, A. Linares-Solano, D. Cazorla-Amoros, Application of zeolitic material synthesized from fly ash to decontamination of waste water and flue gas, *J. Chem. Technol. Biotechnol.* 77 (2002) 292–298.
- [15] S.B. Wang, Y.L. Peng, natural zeolites as effective adsorbents in water and waste water treatment, *Chem. Eng. J.* 156 (2010) 11–24.
- [16] Y. Zeng, H. Woo, G. Lee, J. Park, adsorption of Cr(VI) on hexadecylpyridinium bromide (HDPB) modified natural zeolites, *Microporous Mesoporous Mater.* 130 (2010) 83–91.
- [17] P. Chutia, S. Kato, T. Kojima, S. Satokawa, Adsorption of AS(V) on of surfactant-modified natural zeolite, *J. Hazard. Mater.* 162 (2009) 204–211.
- [18] J. Hrenovic, M. Rozic, L. Sekovanic, A. Anic-Vucinic, Interaction of surfactant-modified zeolite and phosphate accumulating bacteria, *J. Hazard. Mater.* 156 (2008) 576–582.
- [19] H. Guan, E. Bestland, C.Y. Zhu, H.L. Zhu, D. Albertsdottir, J. Hutson, C.T. Simmons, M. Ginic-Markovic, X. Tao, A.V. Ellis, Variation in performance of surfactant loading and resulting nitrate removal among four selected natural zeolites, *J. Hazard. Mater.* 183 (2010) 616–621.
- [20] A. Kuleyin, Removal of phenol and 4-chlorophenol by surfactant-modified natural zeolite, *J. Hazard. Mater.* 144 (2007) 307–315.
- [21] J.A. Simpson, R.S. Bowman, Nonequilibrium adsorption and transport of volatile petroleum hydrocarbons in surfactant-modified zeolite, *J. Contam. Hydrol.* 108 (2009) 1–11.
- [22] X.Y. Jin, M.Q. Jiang, X.Q. Shan, Z.G. Pei, Z.L. Chen, Adsorption of methylene blue and orange II onto unmodified and surfactant-modified zeolite, *J. Colloid Interface Sci.* 328 (2008) 243–247.
- [23] Y. Dong, D.Y. Wu, X.C. Chen, Y. Lin, Adsorption of bisphenol A from water by surfactant-modified zeolite, *J. Colloid Interface Sci.* 348 (2010) 585–590.
- [24] S.G. Wang, W.X. Gong, X.W. Liu, B.Y. Gao, Q.Y. Yue, Removal of fulvic acid using the surfactant-modified zeolite in a fixed bed reactor, *Sep. Purif. Technol.* 51 (2006) 367–373.
- [25] Y.H. Zhan, J.W. Lin, Y.L. Qiu, N.Y. Gao, Z.L. Zhu, Adsorption of humic acid from aqueous solution on bilayer hexadecyltrimethyl ammonium bromide modified zeolite, *Front. Environ. Sci. Eng. China* 5 (2011) 65–75.
- [26] S.R. Taffarel, J. Rubio, Adsorption of sodium dodecyl benzene sulfonate from aqueous solution using a modified natural zeolite with CTAB, *Miner. Eng.* 186 (2011) 771–779.
- [27] P. Roy, N.K. Mondal, S. Bhattacharya, B. Das, K. Das, Removal of arsenic(III) and arsenic(V) on chemically modified low-cost adsorbent: batch and column operations, *Appl. Water. Sci.* 3 (2013) 293–309.
- [28] ISRIC, in: L.P. van Reeuwijk (Ed.), *Procedures for Soil Analysis*, International Soil Reference and Information Centre, Wageningen, 1992 (p. 91).
- [29] Y. Yukselen, A. Kaya, Suitability of the methylene blue test for surface area, cation exchange capacity and swell potential determination of clayey soils, *Eng. Geol.* 102 (2008) 38–45.
- [30] S.M. Mak, B.T. Tey, K.Y. Cheah, W.L. Siew, K.K. Tan, The effect of mechanical grinding on the mesoporosity of steam-activated palm kernel shell activated carbon, *J. Chem. Technol. Biotechnol.* 84 (2009) 1405–1411.
- [31] J. Xie, W. Meng, D. Wu, Z. Zhang, H. Kong, Removal of organic pollutants by surfactant modified zeolite: comparison between ionizable phenolic compounds and non-ionizable organic compounds, *J. Hazard. Mater.* 231–232 (2012) 57–63.
- [32] M. Sougazeh, J.C. Buhl, Synthesis and characterization of zeolite A by hydrothermal transformation of natural Jordanian kaolin, *J. Assoc. Arab Univ. Basic Appl. Sci.* 15 (2014) 35–42.
- [33] K.H.S. Kung, K.F. Hayes, Fourier transform infrared spectroscopic study of the adsorption of cetyltrimethylammonium bromide and cetylpyridinium chloride on silica, *Langmuir* 9 (1993) 263–267.
- [34] C. Covarrubias, R. Garcia, R. Arriagada, J. Yanez, M.T. Garland, Ce(III) exchange in zeolite obtained from kaolin and natural mordenite, *Microporous Mesoporous Mater.* 88 (2006) 220–231.
- [35] L.B. McCusker, Ch. Baerlocher, Rab Nawaz, Rietveld refinement of the crystal structure of the new zeolite mineral gobbinsite, *Z. Kristallogr.* 171 (1985) 281–289.
- [36] S.J. Gregg, K.S.W. Sing, *Adsorption, Surface Area and Porosity*, 2nd ed., Academic Press, London, 1982.
- [37] W. Li, M. Zhang, J. Zhang, Y. Han, Self-assembly of cetyltrimethylammonium bromide in ethanol-ware mixtures, *Front. Chem. China* 1 (2006) 438–442.
- [38] J. Lin, Y. Zhan, Z. Zhu, Y. Xing, Adsorption of tannic acid from aqueous solution on surfactant-modified zeolite, *J. Hazard. Mater.* 193 (2011) 102–111.
- [39] Z.H. Wang, B. Xiang, R.M. Cheng, Y.J. Li, Behaviors and mechanism of acid dyes sorption onto diethylenetriamine-modified native and enzymatic hydrolysis starch, *J. Hazard. Mater.* 183 (2010) 224–232.
- [40] W.T. Tsai, H.C. Hsu, T.Y. Su, K.Y. Yu Lin, C.M. Lin, T.H. Tai, The adsorption of cationic dye from aqueous solution onto acid-activated andesite, *J. Hazard. Mater.* 147 (2007) 1056–1062.
- [41] A. Achmad, J. Kassim, T.K. Suan, R.C. Amat, T.L. Seey, Equilibrium, kinetic and thermodynamic studies on the adsorption of direct dye onto a novel green adsorbent developed from *Uncaria gambir* extract, *J. Phys. Sci.* 23 (1) (2012) 1–13.
- [42] K. Vijayraghvan, T.V. Padmesh, K. Palanivelu, M. Velan, Biosorption of nickel (II) ions onto *Sargassum wightii*: application of two-parameter and three-parameter isotherm model, *J. Hazard. Mater. B* 33 (2006) 304–308.
- [43] B.A. Shah, C.B. Mistry, A.V. Shah, Sequestration of Cu(II) and Ni(II) from wastewater by synthesized zeolitic materials: Equilibrium, kinetics and column dynamics, *Chem. Eng. J.* 220 (2013) 172–184.
- [44] J.H. Huang, Y.F. Liu, X.G. Wang, Selective adsorption of tannin from flavonoids by organically modified attapulgite clay, *J. Hazard. Mater.* 160 (2008) 382–387.
- [45] S.C.D.A. Fernanda, F.S.V. Eunice, R.C. Antini, Interaction of Indigo Carmine Dye with Chitosan Evaluated by Adsorption and Thermochemical Data, *J. Colloid Interface Sci.* 253 (2002) 243–246.
- [46] E. Bayram, N. Hoda, E. Ayranci, Adsorption/electrosorption of catechol and resorcinol onto high area activated carbon cloth, *J. Hazard. Mater.* 168 (2009) 1459–1466.
- [47] D. Rameshraj, V.C. Srivastava, J.P. Kushwaha, I.D. Mall, Quinoline adsorption onto granular activated carbon and bagasse fly ash, *Chem. Eng. J.* 181–182 (2012) 343–351.